A Computer Simulation of Polar Sunrise Ozone Depletion in the Planetary Boundary Layer

Apollo Teck Choon Tang

A
Thesis Submitted to The Faculty of Graduate Studies
in
Partial Fulfillment of the Requirements
for
The Degree of

Master of Science

Graduate Programme in Physics and Astronomy
York University
Toronto, Ontario
Canada

May 2000

A Computer Simulation of Polar Sunrise Ozone Depletion in the Planetary Boundary Layer

by Apollo Teck Choon Tang

a thesis submitted to the Faculty of Graduate Studies of York University in partial fulfillment of the requirements for the degree of

Master of Science

Abstract

This work attempts to relate the polar spring time O_3 depletion in the boundary-layer to the annual geochemical cycle of reactive bromine in the Arctic. The cycle appears to have three stages: (1) the winter build up of Br^- in the snow pack, (2) spring time bromine release to the boundary layer, and (3) the dissipation of bromine into the free troposphere at the end of spring. Using a box model, the proposed mechanism for the spring time release of bromine is demonstrated. The model highlights the feature of this mechanism — the auto-catalytic release of bromine from snow pack, initiated by a bromine seed. It is pointed out here that the bromine seed can be any active bromine that leads to HOBr(aq) formation. In the aqueous phase, HOBr(aq) can react with Br^- and results in the release of Br_2 into the gas phase. Once bromine is in the atmosphere, an O_3 destructive catalytic cycle can be sustained by recycling HBr, HOBr and $BrONO_2$. In this manner O_3 can be depleted within a day. From observations it is known that the geochemical cycle for chlorine in the Arctic does not exhibit the seasonal variation shown for bromine. For this, the seasonally independent geochemical cycle proposed previously for Cl_2 in the marine boundary layer is adopted to recycle HCl in the model. The simulations show that the presence of chlorine in the model slows down the release of bromine from snow pack. With slower release, the bromine content in the atmosphere takes a longer time to build up and the rate of O_3 depletion slows down. The bromine release is slower because NO_x is tied up in $ClONO_2$. In the proposed mechanism, the rate for bromine release depends on the amount of NO_x present. Moreover, the model shows that Cl atom density increases after O_3 depletion. This happens because $BrONO_2$ formed in the presence of BrO diffuses to the aqueous phase to undergo hydrolysis. In this manner, atmospheric nitrogen is lost to NO_3^-(aq) during O_3 depletion. And with less nitrogen in the atmosphere, the amount of ClO_x inactivated in the form of $ClONO_2$ is reduced. The increase of Cl atom density after O_3 depletion increases the oxidation rate for CH_4, which, in turn, increases HCHO production. The elevated HCHO acts to convert bromine in the Br atom 'explosion' into HBr which is then returned to the snow pack or scavenged by aerosols or ice crystals. Given the setup in the model, the Br atom 'explosion' is fueled by HOBr(aq) instead BrO.

Acknowledgments

I wish to express my appreciation to my supervisor, Dr. Jack McConnell who introduced me to the field of modeling. I am grateful for his patience and for his many insightful discussions. I am thankful for the freedom and financial support he gave to me in allowing me to pursue my own research and interests. Thanks also to Dr. Rolf Sander, Dr. Mike Mozurkewich, Dr. Leonard Barrie, Dr. Jan Bottenheim, Dr. Paul Shepson, Dr. Don Hastie, and Dr. Geoffrey Harris for their helpful suggestions. I would like to thank Dr. David Plummer and Ka-Hing Yau for helping me with NCAR graphics and many thanks to Edna Templeton and Dr. Stephen Beagley for keeping our computer systems running. I would also like to thank the department administrators, Marlene Caplan and Karen Cunningham for their help. I thank the staff at Department of Physics and Astronomy, Department of Earth and Atmospheric Science, Centre for Atmospheric Chemistry and York University for the use of their facilities. And finally, many thanks to my family and friends for their support.

Table of Contents

List of Tables

List of Figures

List of Diagrams

Chapter I
Introduction

The presence of O_3 in the stratosphere makes life on Earth possible. Twenty kilometers above the Earth's surface, O_3 screens the ultraviolet radiation which is harmful to biological activities. Although 90% of the O_3 is in the stratosphere, the 10% in the troposphere is important since O_3 drives the chemistry in the troposphere. The photodissociation of O_3 in the troposphere produces O^1D which reacts with H_2O resulting in OH formation. The OH plays a role in the oxidation of a wide variety of atmospheric trace constituents. However, in the making of environmental policies that concern air quality, regulating the concentration of O_3 is a central issue, since high levels of O_3 near ground level cause respiratory problems. Economically, elevated O_3 levels can damage crops resulting in financial loss as agricultural output decreases. Globally, as O_3 is a greenhouse gas, its amount in the atmosphere is an important factor in determining the state of the global climate system. Being of such importance, the study of O_3 is a critical element in the study of the Earth system.

This work concerns the depletion of ground level O_3 that occurs in the polar regions. The chemistry in the polar regions takes a different form because physically, the environment is cold (for instance, $\sim$ 240 K in the early spring). As a result of the cold temperature, many reactions which are sensitive to temperature can slow down or become negligible. Also, in this region, the period of dark and light changes every half a year. This means photo-chemical activities are interrupted for a lot longer period than at lower latitudes.

It is during spring time that the ground level O_3 depletion is observed. This event was first reported in 1986 by *Oltmans & Komhyr* [1986] in Point Barrow (Alaska) and *Bottenheim et al.* [1986] in Alert (Canada). The depletion usually happens in the planetary boundary layer where the temperature increases with height. Since then, similar observations have been discovered at different Arctic locations. For example : Ice camp over the ocean NW of Ellesmere Island [*Hopper et al.*, 1994]: Observations over the Arctic ocean from aircraft [*Leaitch et al.*, 1994]; Ny-Ålesund, Spitsbergen, Norwegian Arctic [*Solberg et al.*, 1996]: Kangerlussuaq, Greenland [*Miller et al.*, 1997]. Later, evidence of such depletion has also been found in the Antarctic, Neumayer-Station (*Wessel et al.*, [1997]). With observations at different locations, it is now believed this phenomenon is widespread over the polar regions during spring time.

In the O_3 depleted air masses, it was found that the level of bromine in aerosol rises dramatically. This lead to the hypothesis by *Barrie et al.* [1988] that the bromine catalytic cycle was responsible for the destruction of O_3. Later, based on non methane hydrocarbon (NMHC) measurements, *McConnell & Henderson* [1993] surmised that chlorine chemistry was also active and may have been involved in the destruction of O_3. The qualitative evidence that supported this hypothesis for the presence of bromine and chlorine was provided by *Hausmann et al.* [1992] and *Jobson et al.* [1994]. The former provided the spectroscopic measurement of BrO, the product formed when Br atom and O_3 react; the latter noted that the depletion of (NMHC) points to the presence of

Br and Cl atoms. Several modeling studies on this subject have been done :

- *Barrie et al.* [1988] attempted to simulate the first bromine catalytic destruction of O_3.
- *McConnell et al.* [1992] pointed out that a mechanism is required to recycle inactive bromine species. They also suggested the source for bromine — sea-salt accumulates in the snow pack surface during the winter.
- *Fan and Jacobs* [1992] proposed a mechanism to recycle inactive bromine.
- *McConnell & Henderson* [1993] are the first to include chlorine chemistry.
- *Tang & McConnell* [1996a] demonstrated the possibility of an auto catalytic release of bromine from the snow pack similar to that proposed by *Mozurkewich* [1995]
- *Tang & McConnell* [1996b] investigated the synergistic effect of chlorine and bromine chemistry.
- *Sander et al.* [1997] included complex aqueous phase chemistry and added iodine chemistry to their model.

This thesis is a continuation of the work of *Tang & McConnell* [1996a,b]. The detailed interaction of bromine and chlorine in O_3 destruction not presented previously is shown here. Also, some updated (1999) information is included. Chapter II describes the role of bromine chemistry in the destruction of O_3. With this knowledge as a base, Chapter III proceeds to describe the chemistry of chlorine — its interaction with bromine and methane. Following the description of the model set up (Chapter IV), the results of simulations are then presented. These are divided into two parts. Part I (Chapter V) highlights the activities of bromine chemistry in the model, and Part II (Chapter VI) describes the behavior of chemistry attributed to the presence of chlorine. Within this context, some thoughts on the chemical cycle of bromine and chlorine, and the role of NO_x in the remote troposphere are discussed. The conclusions are presented in Chapter VII.

Chapter II
Ozone Depletion and Bromine Chemistry

Section 2.1 Ground Level Ozone Depletion in the Arctic Troposphere

The mixing ratio of O_3 measured at Alert (82.5°N, 62.3°W) during 1992 from Julian Day (JD) 0 to 120 is shown in Figure 2.1.1. The variation of solar radiation intensity is also shown in the figure. It can be seen that sunlight begins to appear at about JD 60. Before that the O_3 mixing ratio is at its typical winter level. During the twilight period (JD 60 to 90), an increase in the variability in O_3 mixing ratio is apparent. With the onset of twenty four hour sunlight (after JD 90) episodes of O_3 depletion can be seen. Figure 2.1.2 shows the detail of O_3 for the period from JD 91 to 111. It can be seen, the mixing ratio of O_3 dropped abruptly from its typical 40 ppbv to less than few ppbv; and for the case in JD 108 it disappeared (< 0.5 ppbv, detection limit). A vertical profile of O_3 showing depletion, taken in Ny-Ålesund (78°54'N, 11°53'E) is presented in Figure 2.1.3. The figure also shows a potential temperature profile that is typical of those during early spring in Arctic, i.e., increase of

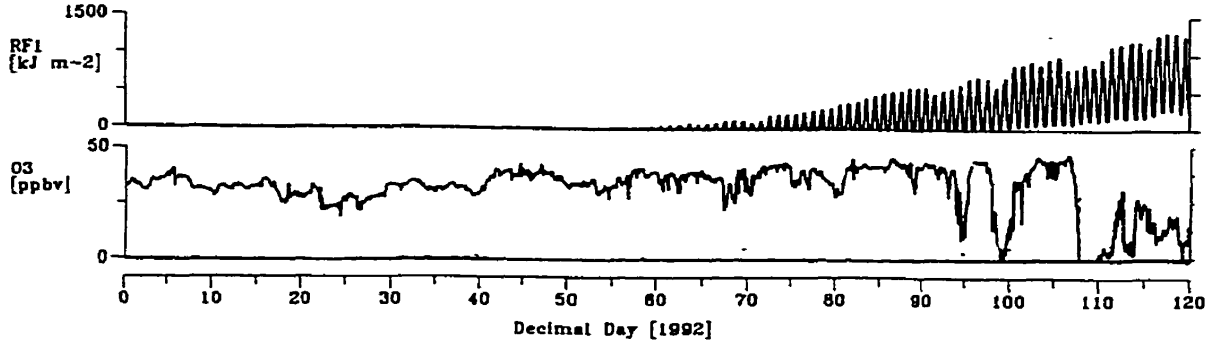

Figure 2.1.1
Solar radiation and ozone from JD 0 to 120, (1 Jan. – 29 Mar.) 1992. Measured at Alert (82.5°N, 62.3°W), BAPMoN laboratory during polar sunrise experiment II. [*Hopper & Hart*, p.25,319, 1994].

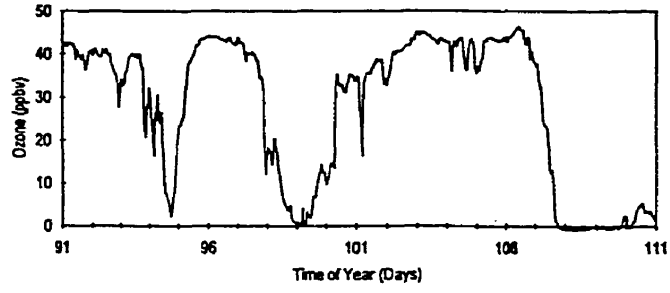

Figure 2.1.2
Surface level ozone measured at Baseline Observatory site from March 31 to April 20, 1992. [*Anlauf at el.*, p.25,346, 1994].

temperature with height from the surface. In this temperature inverted layer vertical mixing is inhibited. Thus, the surface layer is dynamically isolated from short term influences of the free troposphere aloft. It can be seen in this layer, that O_3 is close to being completely depleted. The exact spatial extent of the depletion is not known. However, it is believed to be large. Aircraft

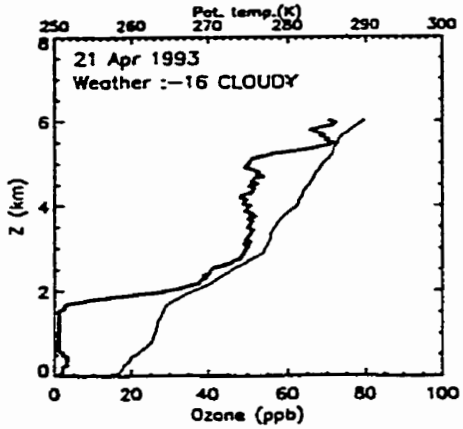

Figure 2.1.3

Measure of ozone and potential temperature by ozone sounding at Ny-Ålesund (78°54′N, 11°53′E). Thick line is ozone mixing ratio (ppbv), thin line is the potential temperature. [*Solbeerg at el.*, p.327, 1996].

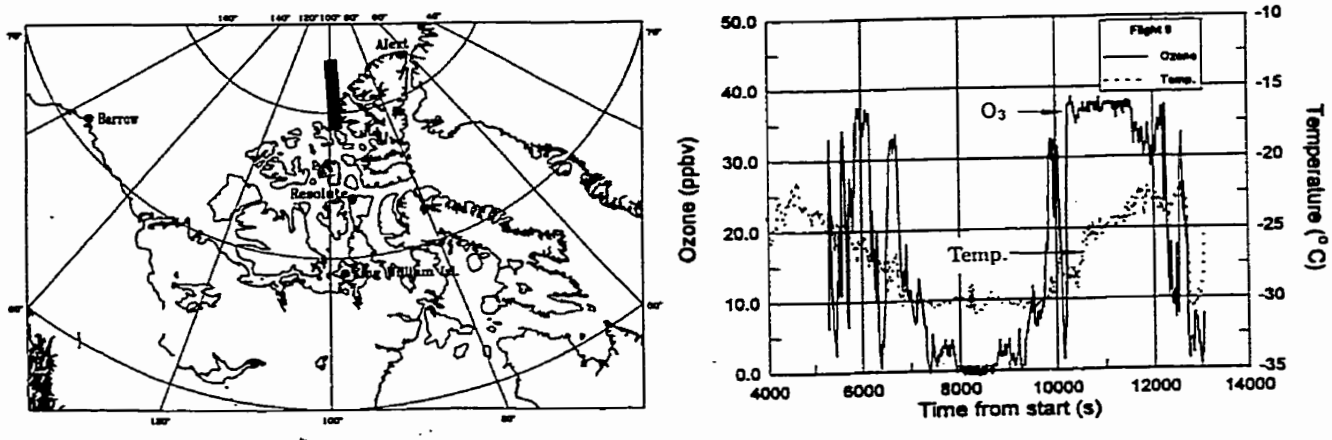

Figure 2.1.4

Airborne observation of temperature and ozone along a north-south lines over the region shaded in the map. Observations are made with level flight at pressure altitude of several hundred meters. A flight track along a north-south line is about 480 km long. The observations was conducted during April, 1992 [*Leaitch at el.*, p.25,200 & p.25,509, 1996].

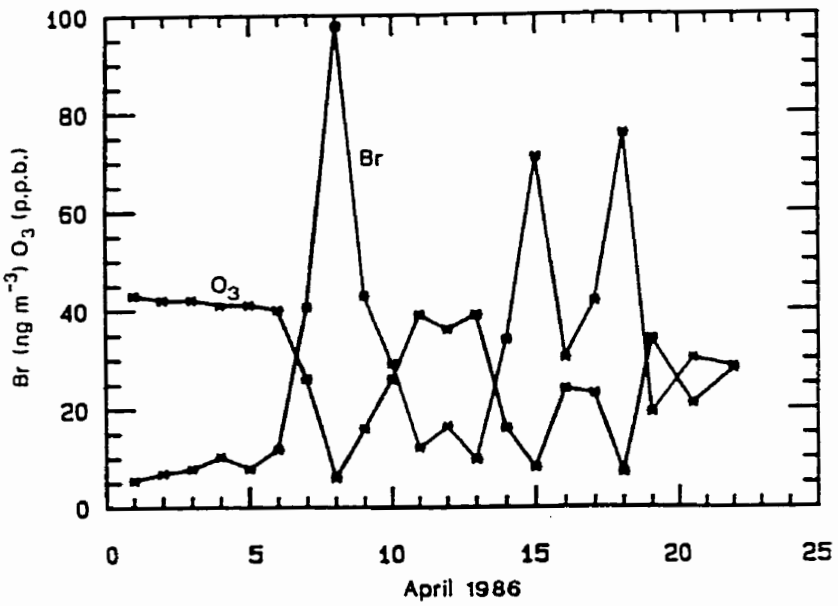

Figure 2.2.1
A comparison of daily mean ground level ozone and filterable bromine at Alert, Canada in April 1986. [*Barrie et al.*, p.138, 1989].

observations conducted by *Leaitch et al.* [1994] show a cross section of the depletion region over Arctic ocean as large as 100 km (see Figure 2.1.4).

Section 2.2 Ozone Depletion and the Bromine Catalytic Cycle

The variability of O_3 and filterable bromine (f-Br) at ground level during the Arctic spring (April 1986) is shown in Figure 2.2.1. Note the negative correlation between the two. For this measurement, the composition of f-Br was not measured. Nevertheless, the relationship between the two indicates the

presence of bromine activity in the O_3 depleted air mass. The explaination for the observed event of *Barrie et al.* [1988] is as follows : During spring, the source begins to release reactive bromine into the atmosphere. The amount of bromine involved is unusually high. Reactive bromine, if present can rapidly destroy O_3 in the inversion layer. One of the products from bromine reactions is HBr which can be absorbed onto aerosol and may be caught on the filter as f-Br. From the existing chemical knowledge, it is known that the gas phase bromine catalytic cycle involving Br atom and BrO can destroy O_3, viz.

$$2(Br + O_3 \rightarrow BrO + O_2) \tag{2.2.1a}$$

$$BrO + BrO \rightarrow 2Br + O_2 \tag{2.2.1b}$$

$$\text{net} : 2O_3 \rightarrow 3O_2 \tag{2.2.1c}$$

To explain the idea of catalytic cycle : O_3 and Br atom reacts to form BrO. During this, an O_3 is destroyed, and the bromine is converted from O_3-potent (Br atom) to O_3-impotent (BrO). Since the total amount of O_3 is much greater than amount of Br available, O_3-impotent bromine must be coverted back to O_3-potent bromine, so that more O_3 can be destroyed. In the above, it is the self-reaction of BrO that returns the necessary Br atoms. Photo-dissociation of BrO also converts bromine in BrO to Br atom,

$$BrO + h\nu \rightarrow Br + O(^3P). \tag{2.2.2}$$

However, this path does not result in O_3 loss since the $O(^3P)$ produced is immediately combined with O_2 to return the O_3 just destroyed. The net result is heating,

$$Br + O_3 \rightarrow BrO + O_2 \tag{2.2.3a}$$

$$BrO + h\nu \rightarrow Br + O(^3P) \tag{2.2.3b}$$

$$O(^3P) + O_2 \xrightarrow{M} O_3 \tag{2.2.3c}$$

$$\text{net : heating.}$$

Thus, this null cycle reduces the efficiency of the O_3 catalytic destruction of Cycle 2.2.1

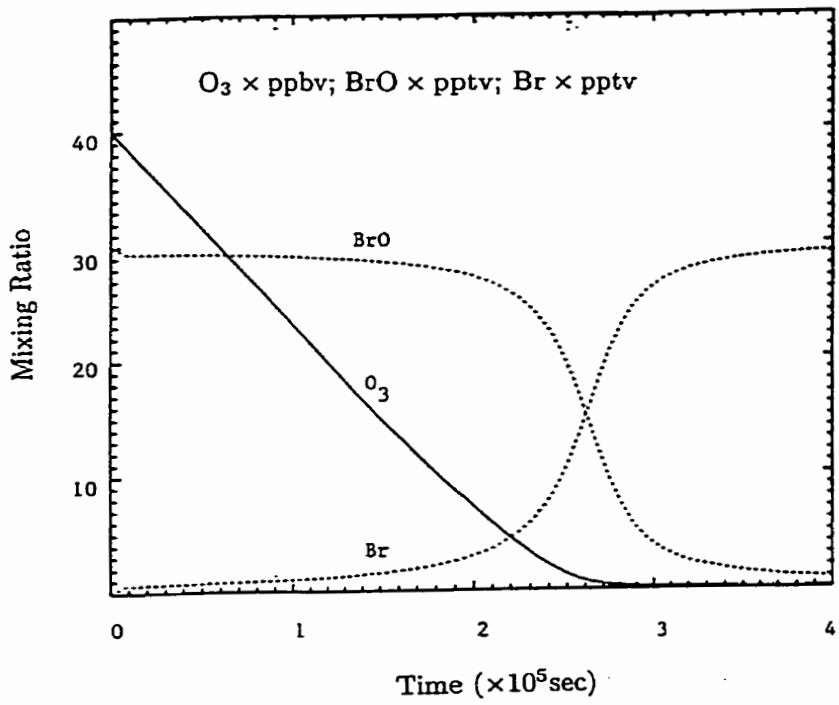

Figure 2.3.1
The mixing ratio of O_3, BrO and Br atom from the results of a simulation to illustrate the effect of bromine catalytic cycle on O_3.

Section 2.3 Time Scale of Ozone Depletion

How fast the Arctic ground level O_3 is destroyed is not known. A Lagrangian measurement has never made. The measured time series of O_3 decreasing with increasing f-Br is the result of physical process that happens when the airmass of rich O_3 and poor f-Br at the observation site is displaced by an airmass with poor O_3 but rich in f-Br. To address the question how fast bromine catalytic

cycle could destroy O_3, a simple numerical calculation is performed. Consider the simplfied† reaction scheme of bromine catalytic cycle:

$$Br + O_3 \rightarrow BrO + O_2 \qquad k_1 = 6.49\times10^{-13}cm^3molec.^{-1}s^{-1} \qquad (2.3.1a)$$

$$BrO + BrO \rightarrow 2Br + O_2 \qquad k_2 = 3.28\times10^{-12}cm^3molec.^{-1}s^{-1} \qquad (2.3.1b)$$

$$BrO + h\nu \xrightarrow{O_2} Br + O_3 \qquad Jv = 1.\times10^{-2}s^{-1} \qquad (2.3.1c)$$

The result of the calculation with the initial $[O_3]$ at 40 pptv and [BrO] at 30 pptv is shown in Figure 2.3.1. In the results, three stages of development can be seen :

(1) From t = 0s to 2×10^5s. Rate of O_3 depletion is almost constant. Most of the O_3 (> 95%) is destroyed in this stage. Almost all the bromine is in the form of BrO. Levels of both BrO and Br atoms are relatively constant.

(2) Between t = 2×10^5s and 3×10^5s. O_3 is almost depleted. The depletion rate is slowing down (no longer a constant rate). A conversion of bromine from the form of BrO to the form of Br atom occurs rapidly.

(3) After t = 3×10^5s. O_3 has been destroyed and all the bromine is in the form of Br atoms.

During stage (1), large amounts of O_3 are present to react with Br atoms. And there are immediately converted to BrO, few Br atoms can accumulate. The opposite of stage (1) is stage (3) where O_3 has depleted. Without O_3, Br atom cannot be converted to BrO. Stage (2) is the transitional stage, during which, level of O_3 are an order of magnitude smaller. And the rate at which Br atom being converted to BrO begins to slow down.

The duration of stage (1) characterizes the time scale of O_3 loss since it is during this stage that most O_3 is destroyed. The rate O_3 depletion is *limited*

† Simplifications are: (1) The reaction $Br_2 + h\nu \rightarrow 2Br$ is included in Eq 2.3.1b; (2) reaction $O(^3P) + O_2 \xrightarrow{M} O_3$ is included in Eq 2.3.1c. (3) The average photolysis rate constant is used (see Appendix B).

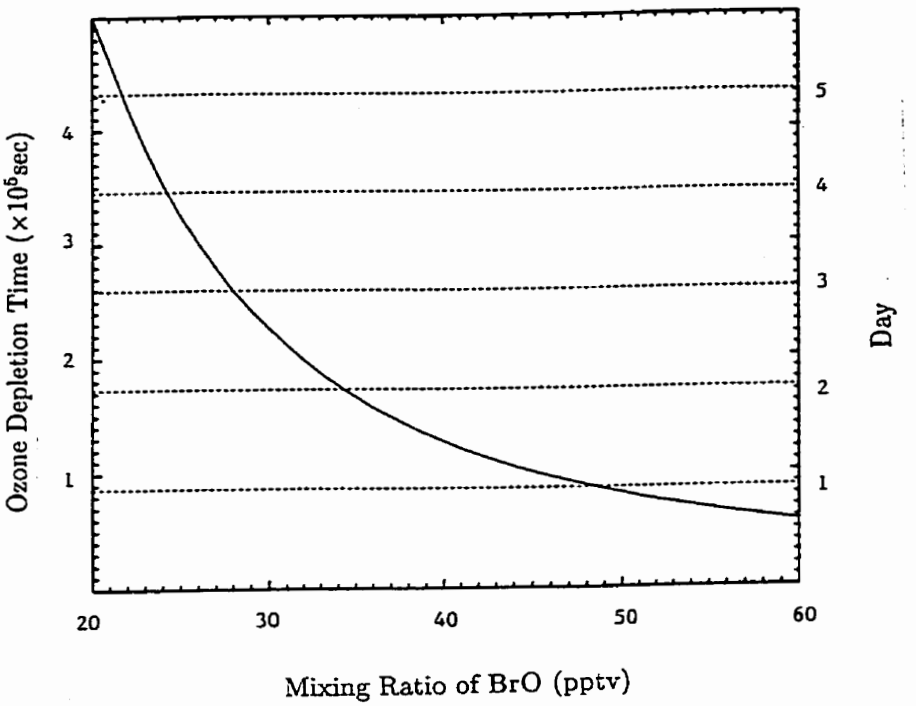

Figure 2.3.2

The characteristic destruction time of O_3 as a function of BrO. The initial O_3 is 40 ppbv. The graph is plotted using Equation 2.3.4.

by the rate at which Br atoms are supplied — that is, the rate at which BrO reacts with another BrO,

$$\frac{d[O_3]}{dt} = -2k_2[BrO]^2. \tag{2.3.2}$$

In the above, the square bracket denote concentration. Equation 2.3.2 can be integrated to give the expression for the total amount of ozone being destroyed in a period of time Δt

$$\Delta[O_3] = -2k_2 \int^{\Delta t} [BrO]^2 dt. \tag{2.3.3}$$

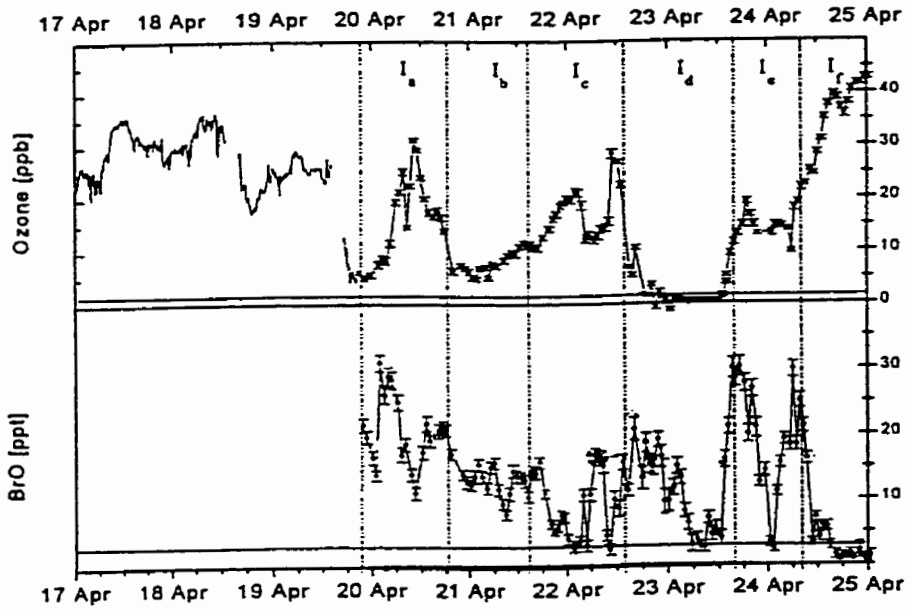

Figure 2.3.3
Time series of O_3 and BrO during the 1995 ozone depletion event (19-25 April) at Ny-Ålesund, Svalbard (78.9°N, 11.8°E) [*Tuckermann et al.*, p.542, 1997].

To first order, [BrO] in the above equation can be taken out of the integral since levels of BrO are relatively stable during stage (1). Solving for $\int^{\Delta t} dt$ and defines the characteristic life time of ozone depletion due to bromine catalytic cycle:

$$\tau_{O_3} = \frac{[O_3]_o}{2k_2[BrO]^2}. \tag{2.3.4}$$

In the above, $\Delta[O_3]$ has been replaced with $[O_3]_o$, the initial O_3 concentration (since the final level is essentially zero). The above expression with $[O_3]_o$ = 40 ppbv is plotted in Figure 2.3.2 as a function of [BrO]. Both *Hausmann &*

Platt [1994] and *Tuckermann et al.* [1997] have measured in-situ BrO using differential optical absorption spectrographic (DOAS) technique. Figure 2.3.3 show some of the results from *Tuckermann et al.* [1997]. The mixing ratio of BrO at a level up to 30 pptv can be seen. Although O_3 depletion probably had commenced along the trajectory before the air mass arrived at the measurement site, the amount of BrO at 30 pptv (if it is maintained at this level) implies a O_3 depletion characteristic time of 2.3 days. Note that since Eq 2.3.4 is inversely quadratic, a doubling of BrO (i.e., 60 pptv) would quarter the characteristic time (i.e. about 14 hours). It is not known at this point the upper limit of BrO present in the tropospheric inversion layer. Satellite observations [*Chance*, 1998] and airborne survey [*McElroy et al.*, 1999] indicate a spring time tropospheric BrO vertical column density $\sim 10^{14}\text{cm}^{-2}$. If this BrO was contained in a layer of 1 km thickness, the equivalent BrO mixing ratio would be in the range of 50 to 100 pptv.

Section 2.4 Recycling of Inactive Bromine

In the real atmosphere, Br atoms and BrO in the bromine catalytic cycle can react with other species. For BrO, it can react with HO_2 and NO_2 to form HOBr and $BrONO_2$:

$$BrO + HO_2 \rightarrow HOBr + O_2 \tag{2.4.1}$$

$$BrO + NO_2 \rightarrow BrONO_2. \tag{2.4.2}$$

Br atoms can react, for example, with HO_2 and HCHO to form HBr :

$$Br + HO_2 \rightarrow HBr + O_2 \tag{2.4.3}$$

$$Br + HCHO \rightarrow HBr + HO_2 + CO. \tag{2.4.4}$$

With the formation of HOBr, $BrONO_2$ and HBr, the amount of bromine available for BrO and Br atom is reduced, this slows down and even shuts down O_3

depletion. *McConnell et al.* [1992] have shown this effect in their simulation. They pointed out that inactive bromine must be converted back (or "recycled") to BrO, Br atom or Br_2 by a mechanism. They speculated that the recycling mechanism involved is multi-phased since the known gas phase mechanisms,

$$BrONO_2 + h\nu \rightarrow Br + NO_3 \qquad \tau_{(ave)} \sim 3 \times 10^3 sec \tag{2.4.5}$$

$$HOBr + h\nu \rightarrow Br + OH \qquad \tau_{(ave)} \sim 5 \times 10^3 sec. \tag{2.4.6}$$

$$HBr + OH \rightarrow Br + H_2O \qquad 1.1 \times 10^{-11} cm^3 molec^{-1} s^{-1} \tag{2.4.7}$$

are too slow in the Arctic which is weak in solar radiation and low in OH concentration. The most promising heterogeneous mechanism at this point is that suggested by *Fan & Jacob* [1992] who based their mechanism on the known aqueous phase chemistry of *Eigen & Kustin* [1962]. In this mechanism, HBr, $BrONO_2$ and HOBr are scavenged onto the aqueous phase to become HBr(aq), $BrONO_2$(aq) and HOBr(aq):

$$HBr \rightarrow HBr(aq) \tag{2.4.8}$$

$$BrONO_2 \rightarrow BrONO_2(aq) \tag{2.4.9}$$

$$HOBr \rightarrow HOBr(aq). \tag{2.4.10}$$

Once in the aqueous phase, HBr can dissociate into ionic form and $BrONO_2$(aq) can be hydrolyzed to HOBr(aq) :

$$HBr(aq) \rightarrow Br^- + H^+ \tag{2.4.11}$$

$$BrONO_2(aq) \xrightarrow{H_2O} HOBr(aq) + HNO_3(aq). \tag{2.4.12}$$

The HOBr(aq) from direct HOBr diffusion and from $BrONO_2$(aq) hydrolysis can react with Br^- to form Br_2(aq) which volatilizes into the gas phase :

$$HOBr(aq) + Br^- \xrightarrow{H^+} Br_2(aq) + H_2O \tag{2.4.13}$$

$$Br_2(aq) \rightarrow Br_2. \tag{2.4.14}$$

Fan & Jacob [1992] noted that the speed of Br_2 liberated is limited by the uptake of HBr, $BrONO_3$ and HOBr. Evidence for this mechanism has been seen by *Abbatt* [1994] in the laboratory. The drawback of this mechanism is that it converts nitrogen in $BrONO_2$ to $HNO_3(aq)$, this results in the loss of atmospheric odd nitrogen to the aqueous phase.

The recycling mechanism described above offer an alternative route to convert bromine in BrO to Br atom. This path is long and indirect compared to the self-reaction of BrO :

$$BrO \xrightarrow{HO_2} HOBr \xrightarrow{diffu.} HOBr(aq) \xrightarrow{Br^-} {}_{1/2}Br_2(aq) \xrightarrow{volat.} {}_{1/2}Br_2 \xrightarrow{h\nu} Br.$$

$$BrO \xrightarrow{NO_2} BrONO_2 \xrightarrow{diffu.} BrONO_2(aq) \xrightarrow{hydro.} HOBr(aq) \xrightarrow{Br^-} {}_{1/2}Br_2(aq) \xrightarrow{volat.} {}_{1/2}Br_2 \xrightarrow{h\nu} Br.$$

Section 2.5 Sources of Bromine

With regard to the source of bromine, *Barrie et al.* [1988] proposed bromoform ($CHBr_3$) produced by the decay of marine algae [*Dryssen & Fogelqvist*, 1981]. Upon photodissociation $CHBr_3$ can release Br atom for O_3 destruction. Example of the supporting evidence for $CHBr_3$ as the bromine source includes : (1) the airborne observations of *Leaitch et al.* [1994] which show an especially high concentration of $CHBr_3$ in the inversion layer (Figure 2.5.1): (2) spring time inverse correlation between O_3 and $CHBr_3$ by *Yokouchi et al.* [1994] (Figure 2.5.2). However, The idea of *Barrie et al.* [1988] was ruled out for two reasons. First, the amount of $CHBr_3$ available is insufficient and, second, the photolysis rate of $CHBr_3$ is too slow. *Li et al.* [1994] measured $CHBr_3$ with the range between 7 and 60 $ng(Br)m^{-3}$. This amounts to 2 pptv to 17 pptv of bromine†.

On the bases of laboratory measurements, *Finlayson-Pitts et al.* [1990] suggested that the reaction of N_2O_5 with NaBr on air-borne sea-salt would

† 1 pptv(Br) = 3.365 $ng(Br)m^{-3}$.

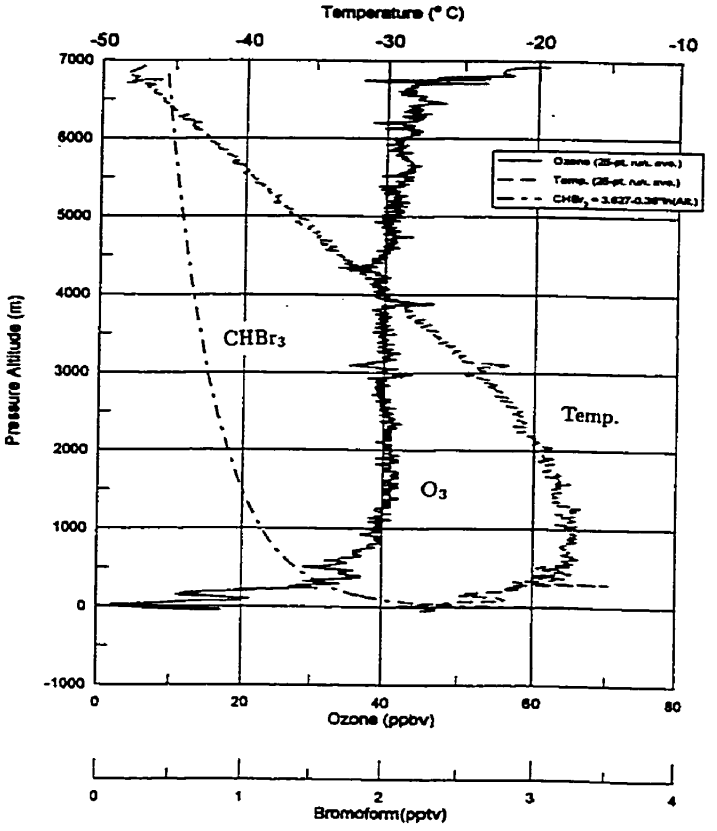

Figure 2.5.1

Running averaged profiles of ozone, temperature and bromoform collected in the high Arctic during April 6 to 16, 1992. Survey area was bounded by 79°N and 83°N latitude and 19°W and 100°W longitude. Bromoform also includes data from ice camp SWAN (83.94°N, 63.09°W), April 9 to 25, 1992 [*Hopper et al*, 1994] and from Alert, April 1 to 15, 1992 [*Yokouchi et al*, 1994]. Note that bromoform exhibited a well-defined logarithmic decrease with increasing altitude, indicative of a strong surface source [*Leaitch et al.*, p. 25,515, 1994].

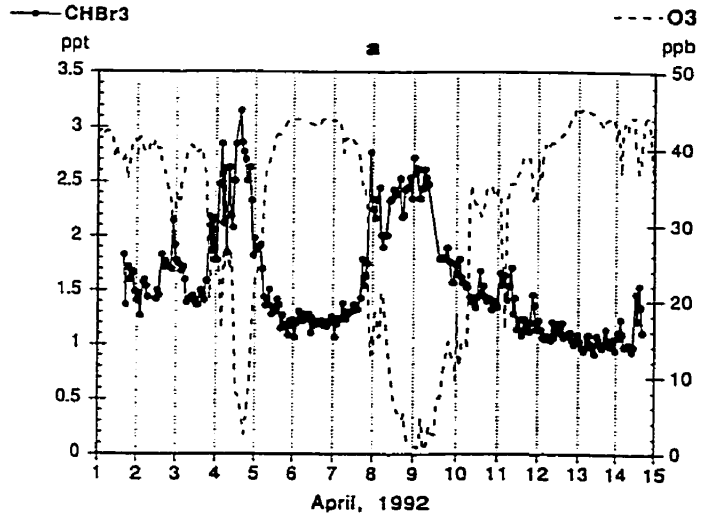

Figure 2.5.2

Variation of bromoform with O_3 at Alert, April 1 to 14, 1992 [*Yokouchi et al.*, p. 25,381, 1994].

release BrONO:

$$N_2O_5 + NaBr \rightarrow BrONO + NaNO_3. \quad (2.5.1)$$

BrONO would photolyze rapidly at polar sunrise to give the bromine required by the catalytic cycle. They speculated that N_2O_5 is readily available during the polar winter since the loss of its precursor, NO_3, is low with the absence of solar radiation. Suppose if there were sufficient NO_x in the Arctic to provide the necessary amount of N_2O_5 to drive the above reaction, it is questionable the amount of sea-salt present is sufficient to provide the amount of bromine necessary for O_3 depletion. Using the measurement of airborne sodium conducted by *Berg et al.* [1983] ($\sim 10^3$ ng(Na)m^{-3}) and considering that NaBr is of oceanic origin‡, the bromine content in newly formed sea-salt particles is calculated* to be $\sim$ 6.2 ng(Br)m^{-3} ($\sim$ 1.8pptv). This is much less than the amount of BrO observed.

The results of four years sampling of Arctic (Barrow, Alaska) bromine content in aerosol by *Berg et al.* [1983] is shown in Figure 2.5.3. Notice the presence of a seasonal maximum in their data. The bromine content in the aerosol averages 6 ● 4 ng(Br)m^{-3} (1.7 $\pm$ 1.1 pptv) begining in the end of spring for nine months of every year. This amount is similar to that from the sea-salt calculated above. However, beginning every mid-February and continuing for a period of three months, aerosol bromine content increases an order of magnitude, reaching over 100 ng(Br)m^{-3} (30 pptv) with typical values ranging near 65 ng(Br)m^{-3} (19.6 pptv). Interestingly, the enrichment reaches a maxima at the end of March or beginning of April which appears to coincide with the periods of maximum ozone depletion. The coincidence suggests that the

---

‡ *Berg et al.* [1983] noted that the content of chlorine and sodium in aerosol collected in Arctic (Barrow, Alaska) are very closely coupled and the average chlorine and sodium ratios agree to that of sea water within 95%. They concluded that sodium in the Arctic aerosol is very likely to be of marine origin.

* Using $[\frac{Br^-}{Na^+}] \sim 6.2 \times 10^{-3}$ for bulk sea water by mass [*Berg et al.* , 1983].

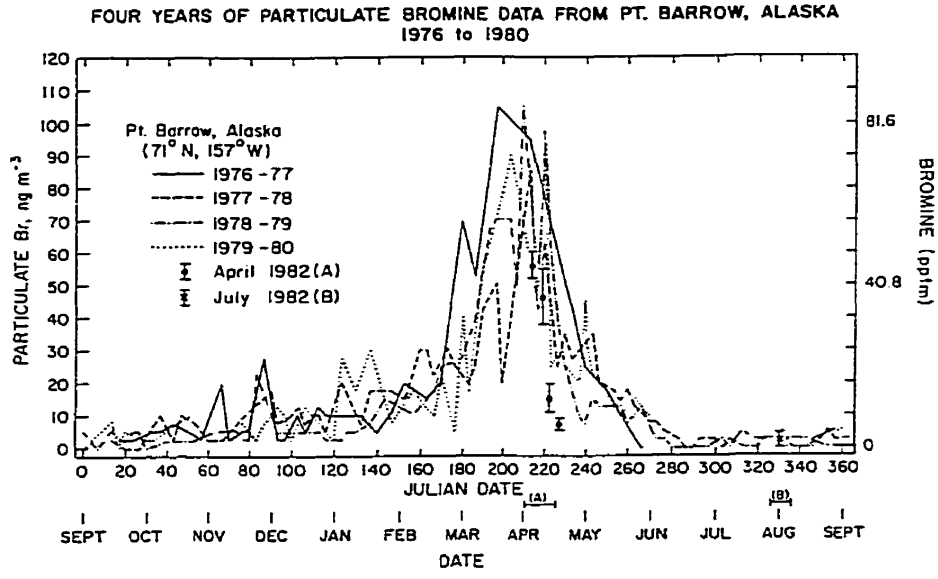

Figure 2.5.3

Bromine content of the Arctic aerosol at Barrow, Alaska, 1976–1980. The 4 years data record represents a compilation of over 200 single bromine analysis. A clear seasonal pattern is evident with bromine maxima occurring annually during the February 15 to May 15 period. The conversion factor used on the right scale is 1 ngBr/SCM = 0.8163pptm Br (part per trillion by mass) [*Berg et al.*, p. 6726, 1983]

source of the bromine that enriches the bromine in aerosol and the source of the bromine that fuels the catalytic cycle which destroys O_3 are related. *Berg et al.* [1983] pointed out that enrichment of bromine in aerosol in the Arctic region is unique. The bromine content in marine aerosol at lower latitudes has shown signs of enrichment only on rare occasions [e.g., *Duce et al.*, 1963; *Duce et al.*, 1965; *Duce et al.*, 1967; *Moyers & Duce* , 1972]. The general trend has been towards a bromine deficit.

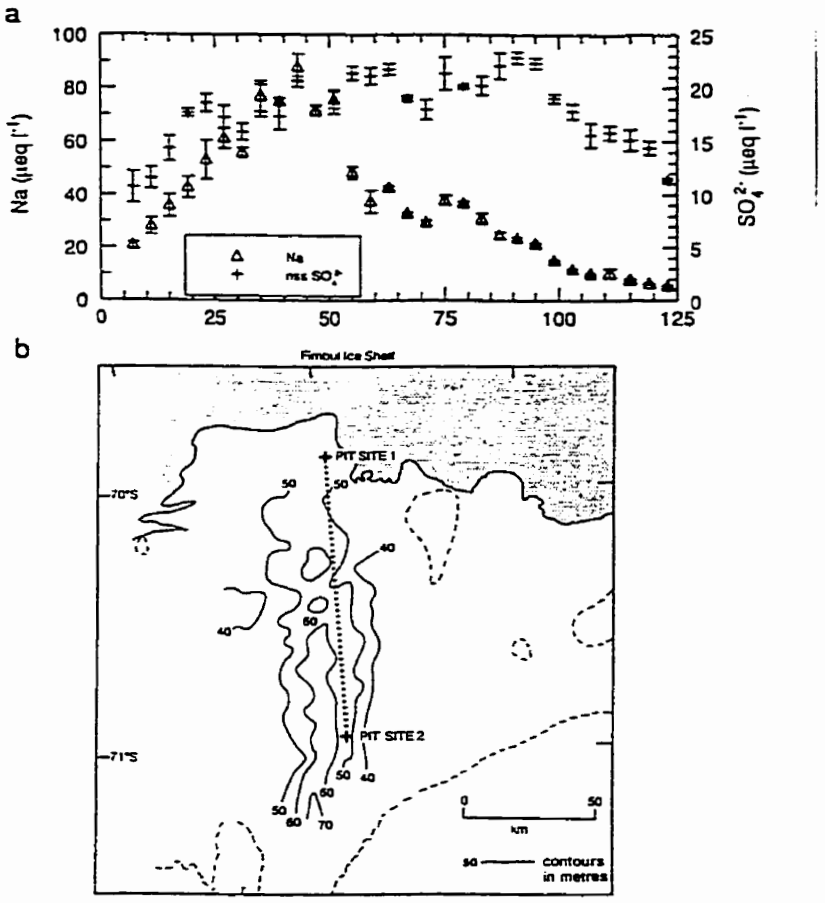

Figure 2.5.4

Panel (a) shows sodium (denoted Δ) and non sea-salt sulphate (denoted +) in the surface snow samples collected at Fibulisen ice shelf, Antarctic during January 1990. During the sampling shallow pits were dug to allow sampling through about 10 to 55 mm of snowfall every 4km. The map (panel b) shows the route taken by the 116 km surface snow sampling traverse approximately along the 50m contour. Note that a maximum in sodium concentration at $\sim$ 43 km from ice shelf front. This maximum happens because larger particles are progressively removed from the aerosol, leaving smaller particles with less sea-salt further away from the shelf front [*Mulvaney et al.*, p.185 & p.180, 1992].

McConnell et al. [1992] proposed that sea-salt particles originating from the ocean could be carried by the wind and be deposited on the snowpack throughout the polar night. In this manner, the bromine content of in the snowpack can be augmented to acquire the necessary level. Up to the preparation of this work (1999), pre-sunrise measurements of bromine in the Arctic snow had not been found in the literature. However, a report of surface snow samples along a traverse of the Antarctic ice shelf by *Mulvaney et al.* [1993] showed that sodium ion concentration in snow samples increases from the coast going inland, reaching a maximum at ~ 43 km from the ice shelf front (Figure 2.5.4). The measured snow content of sodium ion is ~ 60 μeq/l, which is equivalent to a concentration of bromine ion at ~ $3 \times 10^{13} \mathrm{cm}^{-3}$†. This concentration of bromine ion in 30 cm of snow would yield ~ 300 pptv of bromine in an atmospheric layer 1 km thick. It is likely that bromine amounts in the Arctic snowpack are even larger than that in Antarctic since there are other routes to the snowpack such as through cracks and leads (polynyas) over the ice covered Arctic Ocean. Leads and cracks are formed as the result of ice deformation under wind forcing [*Schnell et al.*, 1989]. These openings rapidly re-freeze, forming new ices. *Wolff & Martine* [1998] pointed out that when sea water evaporates from brine, frost flowers can grow. These frost flowers have enhanced salinity and they are easily broken off and become airborne. Furthermore, the heat lost from the leads can generate energy to create buoyant plumes 1 to 2 km high [*Kahl & Andreas*, 1992] which can result in salty flower 'petal' ejected into the atmosphere aloft. The air plumes rich in sea-salt can then be advected by wind and deposit their content over snow surfaces downwind of leads.

Sea-salt deposited in the snowpack in the manner described above can be readily accessed by atmospheric air as the specific surface area and poros-

---

† Using $[\frac{Br^-}{Na^+}] \sim 1.8 \times 10^{-3}$ for bulk sea water by volume [*Well*, 1986] and assuming a conservative snow to liquid volume ratio of 2.

ity for snow is high ($\sim 10^7 cm^2 cm^{-3}$, *Waddington et al.* [1996]). Assuming the penetration of air is limited by the molecular diffusion time constant, atmospheric air can diffuse $\sim$ 18 cm into the snowpack in $\sim$ 1 hr. This process can be even more rapid since the ventilation of snow-pack by pressure oscillations associated with turbulence generated by small scale topography can enhance the exchange of air and thus species between the air and the snowpack [*Waddington et al.*, 1996].

Section 2.6 Release of Bromine from the Snowpack

To transfer Br^- in the snow pack to bromine in the form that can be volatilized to the gaseous phase (e.g., BrO or Br_2) requires a chemical mechanism. For this, the mechanism of *Finlayson-Pitts et al.* [1990] can be used. *McConnell et al.* [1992] and *Mozurkewich* [1995] also proposed mechanisms for this purpose. The mechanism of *McConnell et al.* [1992] follows the suggestion of *Duce et el.* [1965] in their efforts to explain the chlorine deficit in marine aerosols. The mechanism requires photoinduced conversion of halogen ion (X^-) to gas-phase halogen gas (X_2), for X = Br :

$$4Br^- + O_2 + 4H^+ + h\nu \rightarrow 2Br_2 + 2H_2O. \tag{2.6.1}$$

Mozurkewich noted that the mechanism of *Fan & Jacob* [1992],

$$HOBr(aq) + Br^- \xrightarrow{H^+} Br_2(aq) + H_2O, \tag{2.6.2}$$

proposed for the recycling of bromine can also be used for Br^- release. His mechanism has the advantage of being autocatalytic. This means the release of Br^- can be initiated with a bromine seed. This bromine seed can be bromine of any form (Br_2, Br atom, BrO, $BrONO_2$, HOBr, $BrONO_2$(aq), $CHBr_3$ and other) as long as it provide a react-able bromine leading to the formation of HOBr(aq). The concept of autocatalytic cycle is illustrated in Diagram 2.6.1. It can be

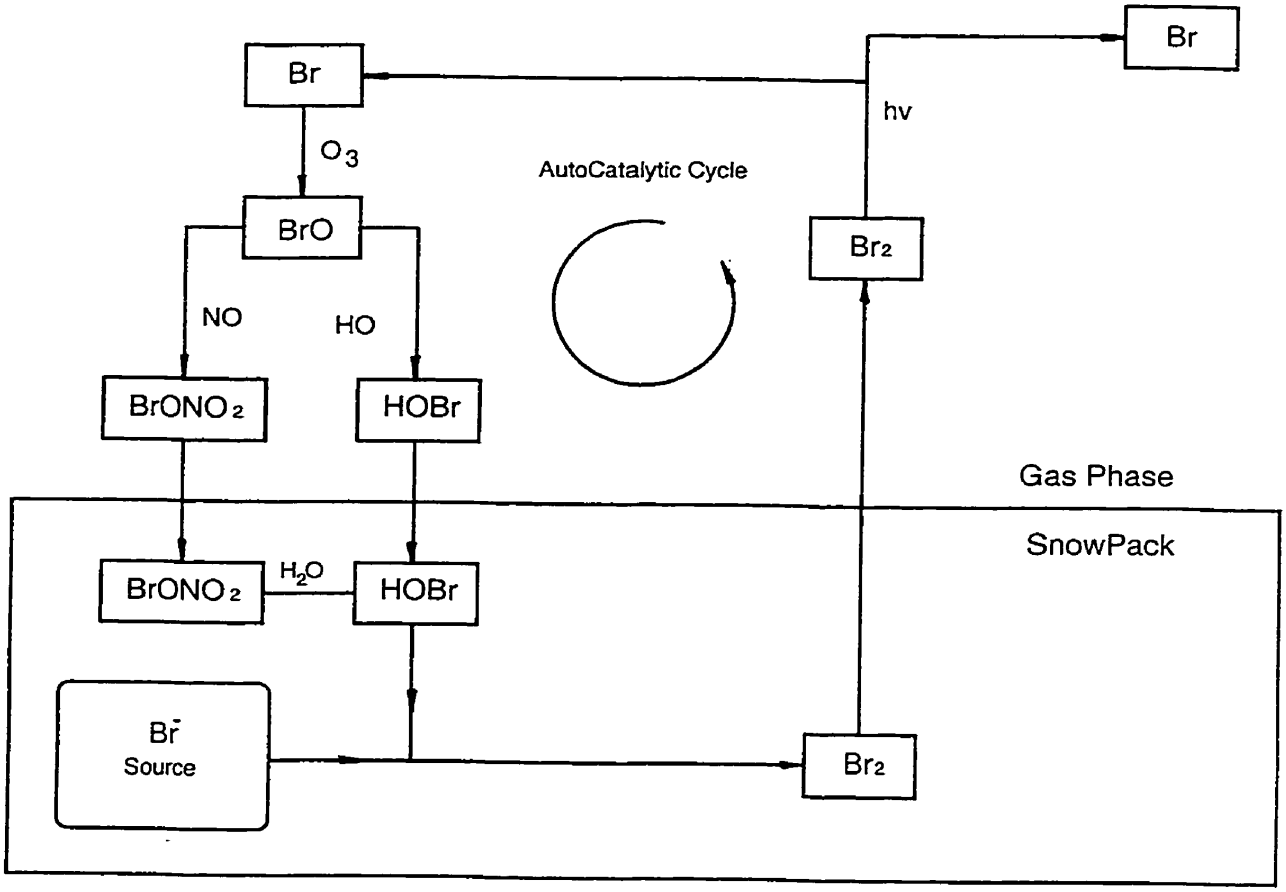

Diagram 2.6.1
Illustration of the bromine reactions chain that autocatalytically release bromine from the source (Br^-).

seen that a single HOBr(aq) can react with Br^- in the bromine source to form two bromine seeds, Br_2. This initiates the second chain, and so on. The mechanism has an amplifying factor of 2. Once initiated, the amount of bromine involved grows exponentially, and the rate of bromine from Br^- being transfered into the atmosphere increases exponentially. Note, this is not a dark mechanism, as solar radiation is required to photolyze Br_2.

Section 2.7 The Source of the Bromine Seed

The seed required to initiate the release of bromine from Br^- in the snow-pack is readily available from $CHBr_3$. One can envisage a scenario where an air parcel rich in bromoform with its origin due to biochemical activity in the ocean is accumulated in the marine boundary layer (MBL). When spring comes $CHBr_3$ photo-dissociates to provide the bromine seed to initiate the autocatalytic release of Br^- from the snowpack. As was discussed in Section 2.5, although the total amount of bromine from $CHBr_3$ is insufficient for rapid O_3 depletion, it is more than sufficient to provide the seed required for initiating the autocatalytic releasing mechanism. In addition, although the mechanisms by *Finlayson-Pitts et al.* [1990] and *McConnell et al.* [1992] are not autocatalytic, they can provide the seed for the initiation of autocatalytic release mechanism. *Mozurkewich* [1995] suggested that the autocatalytic releasing mechanism is initiated when Caro's acid (HSO_5^-) is produced. Caro's acid is produced by free radical chain oxidation of S(IV). The process begins with the uptake of gaseous SO_2, and with its subsequent dissociation, speciation and reactions:

$$SO_2(aq) \rightleftharpoons H^+ + HSO_3^- \tag{2.7.1}$$

$$HSO_3^- \rightleftharpoons H^+ + SO_3^{2-} \tag{2.7.2}$$

$$SO_3^{2-} + OH \rightarrow OH^- + SO_3^- \tag{2.7.3}$$

$$SO_3^- + O_2 \rightarrow SO_5^- \tag{2.7.4}$$

$$SO_5^- + SO_3^{2-} \rightarrow SO_3^- + SO_5^{2-} \tag{2.7.5}$$

$$SO_5^{2-} + H^+ \rightleftharpoons HSO_5^- . \quad (2.7.6)$$

Caro's acid is able to react with Br^- and results in seed formation:

$$HSO_5^- + Br^- \rightarrow SO_4^{2-} + HOBr(aq). \quad (2.7.7)$$

The source of OH in Reaction 2.7.3 is thought to be supplied by gas phase HO_2 which in the aqueous phase, undergo dissociation and further reactions to yield OH :

$$HO_2 \rightleftharpoons H^+ + O_2^- \quad (2.7.8)$$

$$O_2^- + O_3 \rightarrow O_3^- + O_2 \quad (2.7.9)$$

$$O_3^- + H^+ \rightarrow OH + O_2 \quad (2.7.10)$$

Mozurkewich [1995] noted the production of Caro's acid requires a low temperature and high SO_2 environment. Also this mechanism may require the presence of solar radiation since a source of dark production of HO_2 is not known.

During the Polar Sunrise Experiment 1995, *Impey et al.* [1997a] detected $\sim$ 10 pptv photolyzable bromine in the Arctic prior to the sunrise. Their technique did not permit them to distinguish among various bromine species. This photolyzable bromine could be equal to $\sim$ 10 pptv of Br_2, or $\sim$ 34 pptv of HOBr, or $\sim$ 20 pptv of BrNO, or $\sim$ 20 pptv of BrONO, or $\sim$ 31 pptv of $BrONO_2$, or $\sim$ 1 ppbv of $CHBr_3$[†]. The finding of *Impey et al.* [1997a] can possibility validate the dark mechanism of *Finlayson-Pitts et al.* [1990]. Moreover, if their measured dark production of photolyzable bromine included HOBr or $BrONO_2$ then bromine in Br^- can be converted into Br_2 via mechanism of *Fan & Jacob* [1992]. However, auto-catalytic release of bromine cannot begin until the sun rises to photolyze Br_2.

[†] For the explanation of equivalent factor for various bromine species on each photolyzable bromine detects see *Impey et al.* [1997b]

Chapter III
Chlorine Chemistry During Ozone Depletion

Section 3.1 Evidence for non-Br Atom Oxidation

The Mixing ratios for O_3, ethane (C_2H_6), ethyne† (C_2H_2), propane (C_3H_8) and propene (C_3H_6) measured by *Kieser et al.* [1993] are shown in Figure 3.1.1. With the exception of propene, all non-methane hydro-carbon (NMHC) species exhibit positive correlation with O_3. The preliminary rational for this is that Br atoms in the catalytic cycle which destroy O_3 also destroy NMHC. However, the calculations in Table 3.1.1 show that while the lifetimes of ethyne and propene against Br atom are comparable to that for O_3 depletion, the life times for alkanes (ethane and propane) against Br atom are too long. By comparing the rate constant of reaction for Br atom and Cl atom reacting with NMHC, *McConnell & Henderson* [1993] suggested that Cl atoms could be participating in the event of O_3 depletion.

---

† Also known as acetylene and ethine.

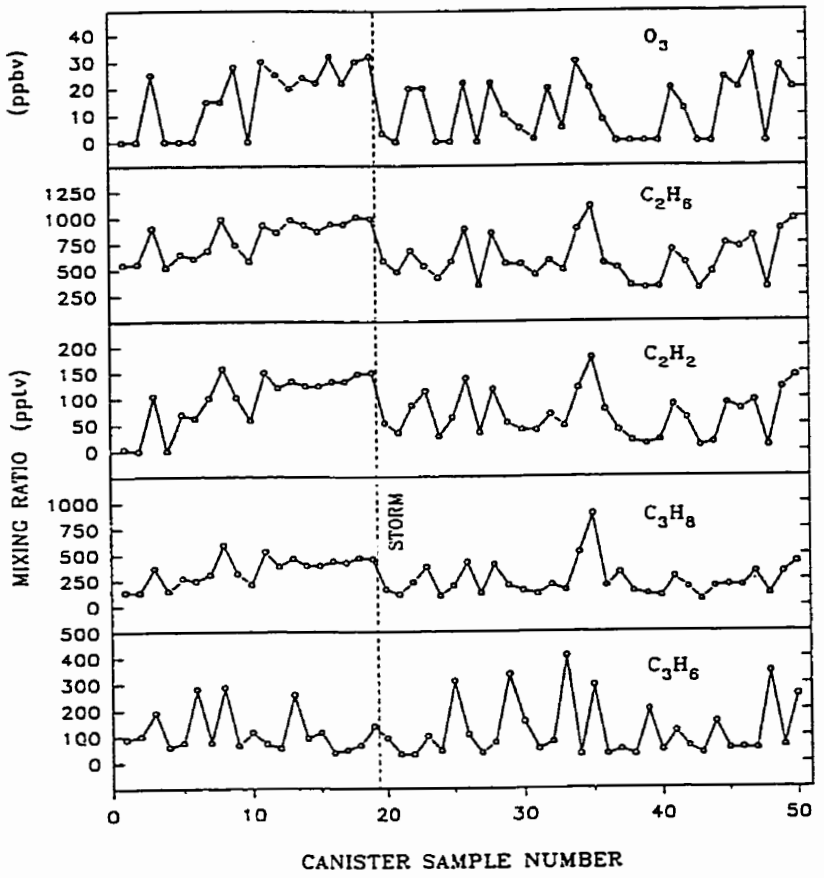

Figure 3.1.1

The observed mixing ratios for ozone, ethane, acetylene, propane and propene from 50 samples taken between 1 and 13 may, 1989, in the Alert survey area [*Kieser at el.*, p.2984, 1993].

Table 3.1.1

Lifetime for NMHC against Br atom loss. The Br atom's levels are chosen according to the amount in the simulation in Section 2.3 for the period during and after the depletion of O_3. The calculations indicate while the lifetimes of ethyne and propene against Br atom are comparable to that of O_3 depletion, the life times for ethane and propane against Br atom are too long.

NMHC	k, Rate Constant* HMHC + Br	Lifetime with 1 pptv of Br atom ?	Lifetime with 30 pptv of Br atom?
Ethane	$2.32\times10^{-21\dagger}$	4×10^{5} yrs	14 yrs
Propane	$1.31\times10^{-18\dagger}$	817 yrs	25 yrs
Ethyne	$1.54\times10^{-13\dagger}$	2.3 day	1.8 hrs
Propene	$2.70\times10^{-12\ddagger}$	3.3 hrs	6.8 min

* $cm^3molec.^{-1}s^{-1}$; † at 243K, *Ariya et al.* [1998]; ‡ at 298K, *Ramacher et al.* [1999]

? Calculated with $\tau = \frac{1}{k[Br]}$

Table 3.2.1

A comparison of reaction rate constant for various oxidant

NMHC	NMHC + Br	NMHC + Cl	NMHC + OH
Ethane	$2.32\times10^{-21\dagger*}$	$5.32\times10^{-11\dagger*}$	$1.18\times10^{-13\dagger*}$
Propane	$1.31\times10^{-18\dagger*}$	$1.27\times10^{-10\dagger*}$	$7.45\times10^{-13\dagger*}$
Ethyne	$1.54\times10^{-13\dagger*}$	$8.44\times10^{-11\dagger*}$	$4.93\times10^{-13\dagger*}$
Propene	$2.70\times10^{-12\ddagger*}$	$3.22\times10^{-10\ddagger*}$	$3.00\times10^{-11\ddagger*}$

* $cm^3molec.^{-1}s^{-1}$; † at 243K, *Ariya et al.* [1998];

‡ at 250K, *Ramacher et al.* [1999]; ? $cm^3molc.^{-1}$

Table 3.2.2

Amount of hydroxyl radical required for NMHC's life time of 1 day and 10 days

NMHC	k, rate constant* NMHC + OH	τ_{NMHC} = 1 day $[OH]^{\gamma\alpha}$	τ_{NMHC} = 10 days $[OH]^{\gamma\beta}$
Ethane	$1.18\times10^{-13\dagger}$	9.85×10^{7}	9.85×10^{6}
Propane	$7.45\times10^{-13\dagger}$	2.36×10^{7}	2.36×10^{6}
Ethyne	$4.93\times10^{-13\dagger}$	2.36×10^{7}	2.36×10^{6}
Propene	$3.00\times10^{-11\ddagger}$	3.63×10^{5}	3.63×10^{4}

*$cm^3molec.^{-1}s^{-1}$; †at 243K, *Ariya et al.* [1998]; ‡at 250K, *Ramacher et al.* [1999]; $^{\gamma}cm^3molec.^{-1}$; $^{\alpha}$ calculated with $(8.6 \times 10^{4}s \times k)^{-1}$; $^{\beta}$ calculated with $(8.6 \times 10^{5}s \times k)^{-1}$.

Section 3.2 The Possible OH and Cl Atom Associated With O_3 Depletion

The rate constants for the reactions of OH, Cl and Br atom with NMHC shown in Figure 3.1.1 are tabulated in Table 3.2.1. OH and Cl atoms are included in addition to Br atoms because they are common oxidants in the remote environment especially in marine atmosphere [*Singh & Kasting*, 1988]. Note that the rate coefficients for ethane and propane with Br atoms are several orders of magnitude less than other rate constants in the table. Thus, Br atom can not be responsible for the decay of ethane and propane. The observed correlation for ethane and propane with O_3 suggests the possibility of elevated concentrations of Cl atoms and OH.

For an estimate of how much OH or Cl atom are present in association with O_3 depletion, the amount of OH or Cl atom required for NMHC's lifetime of 1 day and 10 days are calculated (see Table 3.2.2 and Table 3.2.3). The results show that the amounts of OH and Cl atom required are in the range

Table 3.2.3

Amount of chlorine required for NMHC's life time of 1 day and 10 days

NMHC	k, rate constant* NMHC + Cl	τ_{NMHC} = 1 day $[Cl]^{\gamma\alpha}$	τ_{NMHC} = 10 days $[Cl]^{\gamma\beta}$
Ethane	$5.32\times10^{-11\dagger}$	2.18×10^{5}	2.18×10^{4}
Propane	$1.27\times10^{-10\dagger}$	9.16×10^{4}	9.16×10^{3}
Ethyne	$8.44\times10^{-11\dagger}$	1.38×10^{5}	9.16×10^{4}
Propene	$3.22\times10^{-10\ddagger}$	3.63×10^{4}	3.63×10^{3}

*$cm^3molec.^{-1}s^{-1}$; †at 243K, *Ariya et al.* [1998]; ‡at 250K, *Ramacher et al.* [1999]; $^{\gamma}cm^3molec.^{-1}$; $^{\alpha}$ calculated with $(8.6\times10^4s\times k)^{-1}$; $^{\beta}$ calculated with $(8.6\times10^5s\times k)^{-1}$.

of $10^4 - 10^7$ and $10^3 - 10^5$ $cm^3molec.^{-1}$ respectively. These can be compared with the estimates for the remote tropical and mid-latitude marine boundary layer (MBL). For example : the concentration of OH and Cl atom based on the decay of airborne hydrocarbon measurements in the morning over North Atlantic east of Azores, mid-June by *Wingenter et al.* [1996] are of $\sim 10^6$ and $10^4 molec.cm^{-3}$, respectively.

Section 3.3 Evidence of Chlorine Chemistry

The evidence of Cl atom reacting with NMHC concomitant with the O_3 depletion event was provided by *Jobson et al.* [1994]. To understand their result, consider a particular NMHC, RH_i, being oxidized by oxidant X. Assume that the reaction between X and RH_i is the only significant loss and that there are no sources. The expression for the rate of which RH_i decays is

$$\frac{d}{dt}[RH_i]_t = -k_i[RH_i]_t[X]_t. \qquad (3.1.1)$$

In the above, k_i is the reaction rate constant for the reaction $RH_i + X$, $[RH_i]_t$ and $[X]_t$ is the number density. The subscript, i in the expression represents the

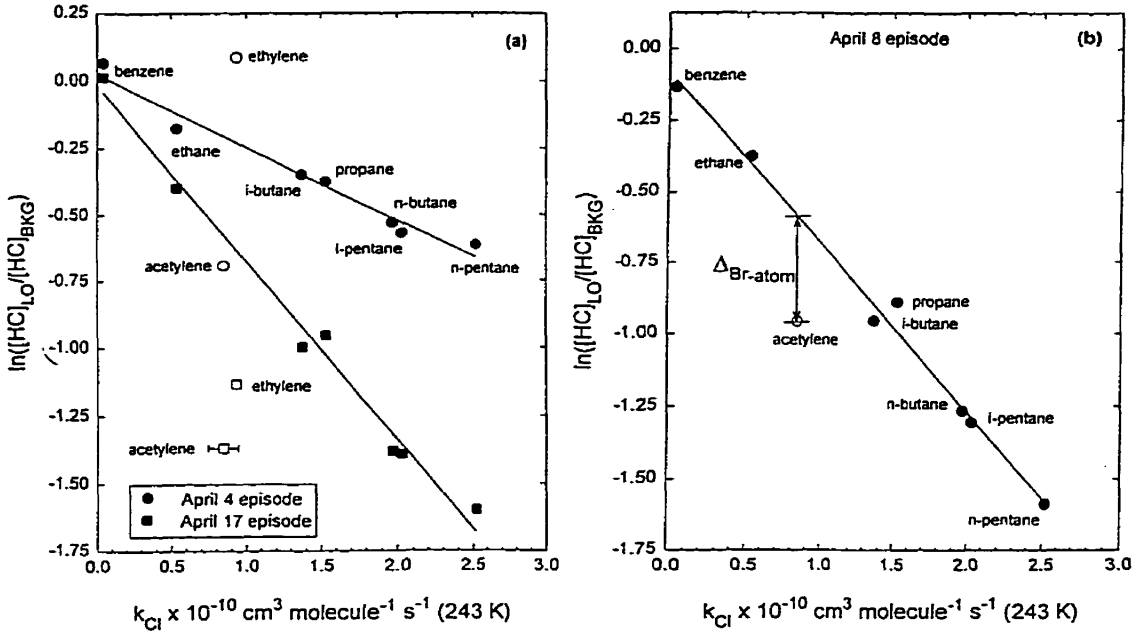

Figure 3.3.1

Correlation between hydrocarbon concentration change in ozone depleted air ($[HC]_{LO}$) from normal ozone days ($[HC]_{BKG}$) against Cl atom rate constant during the ozone depletion episodes on April 4,17 (panel a) and 8 (panel b) 1992, at Alert. Least squares fit lines have been drawn through the alkane and benzene data. Acetylene and ethylene are excluded in the line fitting. The deviation of acetylene from the $C_2 - C_5$ alkane trend is attributed to additional removal by Br atoms. The slopes (i.e., $\int[Cl]dt$) in the plots are -2.7 ± 0.2, -5.9 ± 0.3 and $-6.6 \pm 0.3 \times 10^{-9}$ molec.cm^{-3}s for April 4, 17 and 8 respectively. [*Jobson et al.*, p. 25,362, 1994]

particular species of NMHC. The solution for the above differential equation is

$$[RH_i]_t = [RH_i]_{t_o} e^{-k_i \int_{t_o}^{t} [X]_t dt}. \qquad (3.1.2)$$

Where $[RH_i]_{t_o}$ is the initial number density at initial time t_o. Taking the natural

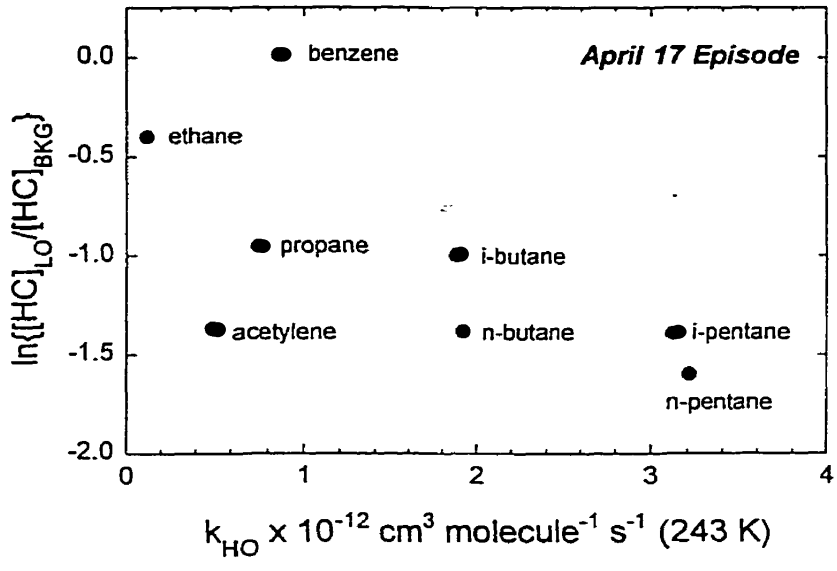

Figure 3.3.2

Correlation between the concentration change in O_3 depleted air from normal O_3 days against HO reaction rate coefficients for the April 17, 1992, O_3 depletion episode, at Alert. [p. 25,363, *Jobson et al.*, 1994]

logarithm of the above,

$$\ln\left([RH_i]_t/[RH_i]_{t_o}\right) = -k_i \int_{t_o}^{t} [X]_t dt, \tag{3.1.3}$$

the expression becomes linear with a slope $-\int_{t_o}^{t}[X]_{t_o}dt$ if $\ln\left([RH_i]_t/[RH_i]_{t_o}\right)$ is plotted as a function of increment of rate constant for various NMHC, k_i.

Applying the above to an air parcel in the Arctic troposphere inversion layer where both levels of O_3 and NMHC are initially at their free tropospheric background concentration (i.e., $[O_3]_{t_o}$ and $[RH_i]_{t_o}$). After a period of time, Δt, this air parcel is advected to the measuring site where levels of O_3 and NMHC have decreased to $[O_3]_{t_o+\Delta t}$ and $[RH_i]_{t_o+\Delta t}$. During this passage, it is assumed that Cl atoms have reacted with the NMHC. The plot of $\ln\left([RH_i]_{t_o+\Delta t}/[RH_i]_{t_o}\right)$ against their corresponding rate constant $k_{i,Cl}$ is presented in Figure 3.3.1. The

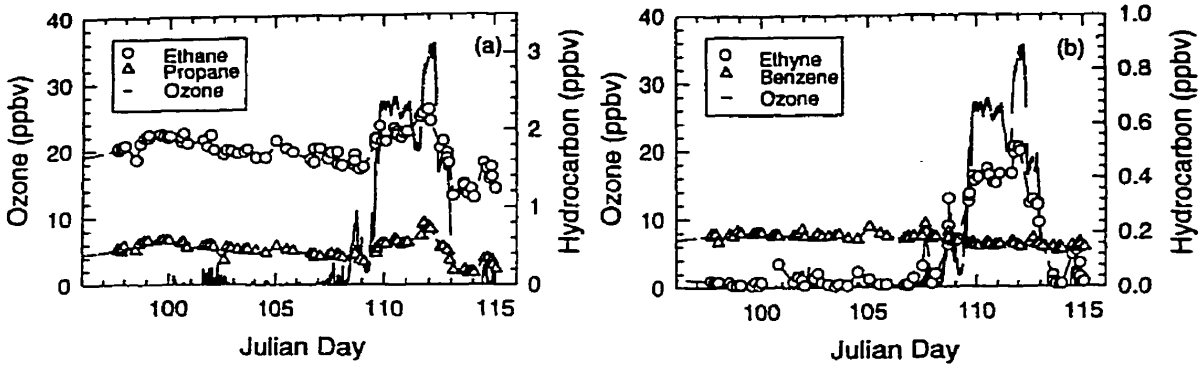

Figure 3.4.1

The time series for ozone, ethane and propane (panel a) and ozone , ethyne and benzene (panel b) at Narwhal ice camp, an ice floe 140km northwest of Alert during the period from JD 97 to 115, 1994. [*Ariya et al.*, p 13,173, 1998]

linear alignment of data points for alkane and benzene is remarkable. The well fitted data with $k_{i,Cl}$ imply that the decay of alkane and benzene in O_3 depleted airmass is chiefly due to oxidation by Cl atoms. Figure 3.3.2 shows the same data plotted using rate constants for reaction between NMHC and OH, $k_{i,OH}$. The scatter of data points imply an insignificant role for OH.

Section 3.4 Time Integrated Chlorine Density

The least squares fit line through the $C_2 - C_5$ alkane and benzene with the measurements made by *Jobson et al.* [1994] in Figure 3.3.1 gives the slopes of the order of magnitude of 10^9 molec.cm^{-3}s. This slope is referred to as the time integrated chlorine density (i.e., $\int$[Cl]dt). Note that the time integrated chlorine density does not provide information when and how much Cl atom was present. If one assumed the interaction with Cl atom lasts 1 day, the calculated average

Cl atom density is $\sim 10^4$ molec.cm^{-3}; if 10 days are assumed, $\sim 10^3$ molec.cm^{-3} of Cl atoms would be present.

Ariya et al. [1998] later observed the decay of NMHCs in O_3 depleted air mass, lasting as long as 7 days at the Narwhal ice camp (an ice floe 140 km northwest of Alert). The O_3 had already been depleted prior to their first air sample collection. This scenario provides a condition for post O_3 depletion chemistry study. Some of their NMHC measurements are presented in Figure 3.4.1. Note that after a minor increase at about JD 100, NMHC decayed gradually for about 8 days. The time integrated chlorine density based on the period for this gradual decay gives the average Cl atom density of 10^3 molec.cm^{-3}. Calculation of average Cl atom density with different time intervals within this period yield similar results. This result is the same as that calculated by *Jobson et al.* [1994] when 10 days is assumed for the decay time for NMHC. The meteorological conditions in this boundary layer are very stagnant [*Hopper et al.* 1998], therefore vertical mixing is not important. Under this meteorological condition, the average Cl atom density can be interpreted as an in-situ Cl atom density. If these observations represent a typical post O_3 depletion scenario, then this suggests that typical Cl atom densities in the O_3 free air mass is one order of magnitude less than that calculated for lower latitudes in MBL (cf. Section 3.2). It should be borne in mind that *Ariya et al.* [1998] did not encounter an in-situ O_3 depletion episode: Cl atom density *during* the depletion of O_3 is not known.

Section 3.5 Decay of Ethyne and the Density of Br and Cl Atoms

In Figure 3.3.1 it can be seen the data points for ethyne (C_2H_2) and ethene† (C_2H_4) lie outside of the linear slope fitted to alkane and benzene data points. These data points can form a line because alkane and benzene are only sensitive to Cl atom. Ethyne and ethene lie outside this line because in addition to Cl atom they are also sensitive to Br atom. *Jobson et al* [1994] have calculated time integrated bromine density (i.e., $\int$[Br]dt) based on decay of ethyne. Consider ethyne being oxidized by both Cl atom and Br atom under minimum influence from the free troposphere. If there are no other significant sources, its rate of change is

$$\frac{d}{dt}[C_2H_2]_t = -\left(k_{C_2H_2.Cl}[Cl]_t + k_{C_2H_2.Br}[Br]_t\right)[C_2H_2]_t. \qquad (3.5.1)$$

In the above, $k_{C_2H_2.Cl} = 8.4 \times 10^{-11}$ [*Ariya et al.*, 1998] and $k_{C_2H_2.Br} = 1.6 \times 10^{-13}$ $cm^3 molec.^{-1} s^{-1}$ [*Ramacher et al.*, 1999] are the reaction rate constants for the reaction $C_2H_2 + Cl$ and $C_2H_2 + Br$, respectively; $[C_2H_2]_t$, $[Cl]_t$ and $[Br]_t$ are the number density for the respective species. The solution for the above differential equation with the initial condition is

$$\ln\left\{\frac{[C_2H_2]_{t_o+\Delta t}}{[C_2H_2]_{t_o}}\right\} = -k_{C_2H_2.Cl}\int_{t_o}^{t_o+\Delta t}[Cl]_t dt - k_{C_2H_2.Br}\int_{t_o}^{t_o+\Delta t}[Br]_t dt. \qquad (3.5.2)$$

In the above, $[C_2H_2]_{t_o}$ is the number density for ethyne at time t_o, that is, ethyne at its free tropospheric background concentration in an O_3 rich air mass. And $[C_2H_2]_{t_o+\Delta t}$ is number density for ethyne after a period of time Δt in an O_3 reduced air mass. Using the integrated chlorine density calculated in the previous section, the calculated integrated bromine density is of order

† Also known as ethylene

of magnitude of 10^{12} molec.cm^{-3}s. Assuming 1 day and 10 days of integration time, the average Br atom density is $\sim 10^7$ and $\sim 10^6$ molec.cm^{-3} respectively.

As noted in the previous section, the Cl atom density estimated by *Ariya et al.* [1998] could be viewed as an in-situ value. This is possible because they have observed a gradual decay of alkane and benzene. However, *Ariya et al.* [1998] were not able to estimate Br atom density since ethyne had been depleted long before the measurement began (see Figure 3.4.1b). In spite of this, one can still make an estimate, using the life time for ethyne decay in Equation 3.5.1. The rate of change for ethyne in Equation 3.5.1 gives a characteristic decay time of

$$\tau_{C_2H_2} = \frac{1}{k_{C_2H_2,Cl}[Cl]_t + k_{C_2H_2,Br}[Br]_t}. \tag{3.5.3}$$

To estimate the density of Br atoms using the above equation, two assumptions are needed: (1) Cl atoms density during ethyne depletion, and (2) life time for the ethyne depletion ($\tau_{C_2H_2}$). Assuming [Cl] is the same as the 'in-situ' Cl atom density of *Ariya et al.* [1998] (4.5×10^3molec.cm^{-3}), and assuming that the life time of ethyne is one day (this choice will be understood later), [Br] estimated from Eq 3.5.3 is 7.03×10^7molec.cm^{-3}.

With the level of Cl and Br atom density above, it is interesting to determine which oxidant is more important in destroying ethyne. To see this, consider the case with only Cl atoms present; the lifetime of ethyne with 4.5×10^3molec.cm^3 of Cl atom is :

$$\tau_{C_2H_2} = \frac{1}{k_{C_2H_2,Cl}[Cl]} \sim 1 \text{ month}. \tag{3.5.4}$$

Now consider the case with only Br atoms (7.0×10^7molec.cm^3) present :

$$\tau_{C_2H_2} = \frac{1}{k_{C_2H_2,Br}[Br]} \sim 1.03 \text{ day}. \tag{3.5.5}$$

Thus, the absence of Cl atom does not increase the lifetime of ethyne very much, but the absence of Br atom increases the life time of ethyne dramatically.

As a matter of fact the lifetime of ethyne depends weakly on the amount of Cl atom present. If the assumed Cl number density were to increase by two orders of magnitude (to 10^5molec.cm^{-3}) while holding $\tau_{C_2H_2}$ at 1 day, the resultant Br atom density calculated from Eq 3.5.3 remains at the same order of magnitude (2.02×10^7molec.cm^3). For these Cl and Br atom desities, the lifetime of ethyne with only Cl atom present is shortened to 1.3 days; and the lifetime of ethyne with only Br present is lengthened to 3.7 day.

The Cl atom density in previous case is more likely to occur since the Cl atom density in the later scenario would imply alkane being depleted long before the air mass arrived to the observation site. The lifetime of ethane with 10^5molec.cm^{-3} of Cl atom is

$$\tau_{C_2H_6} = \frac{1}{k_{C_2H_6,Cl}[Cl]} = \frac{1}{(5.3 \times 10^{-11})(10^5)} \sim 2 \text{ days.} \tag{3.5.6}$$

From this, it can be concluded that chlorine chemistry play a minor or even no role during the depletion of ethyne.

Furthermore, it should not be a problem to assume both ethyne and O_3 are present prior to bromine release. A storm could easily break the temperature inversion layer, mixing the free tropospheric air (which is rich in both O_3 and NMHC) into the boundary layer. Therefore, O_3 and ethyne depletion could occur simultaneously. Given the above scenario, one can proceed to assume the possibility that the presence of chorine chemistry is not necessary during the depletion of O_3.

Moreover, for consistency, the Br density estimated from Eq 3.5.3, should yield the life time of O_3 assumed previously — about one day (recall Section 2.3). To estimate the O_3 chemical lifetime from a known Br atom density, the time constant for linear first order O.D.E. is used:

$$\tau_{O_3} = \frac{1}{k_a[Br]_t} \tag{3.5.7}$$

With the rate constant for reaction between O_3 and Br atom as $k_a = 6 \times 10^{-13}$ cm^{3}molec.$^{-1}$s^{-1} and Br atom density of 7.0×10^7molec.cm^3, the result in Equation 3.5.7 is 2.37×10^4sec ($\approx$ 6.6 hours). This is faster than the time scale of

O_3 depletion previously assumed. However, the life time of O_3 given in Equation 3.5.6 is the lower limit. It does not take into consideration that BrO can be photolyzed and contributes to O_3 production (see Section 2.2). The equation for the rate of change for O_3,

$$\frac{d}{dt}[O_3] = -k_a[Br][O_3] + J[BrO], \tag{3.5.8}$$

is non-linear† and the exact expression for life time of O_3 depletion in terms of [Br] is impossible to determine in this manner. In writing Equation 3.5.6, it is considered that BrO photolysis is unimportant. This is not accurate since depending on the intensity of photolysis rate, this production term can become comparable in magnitude to the loss term. To illustrate this, consider $[Br] \sim 10^7 molec.cm^3$, $[O_3] \sim 40ppbv$, $J \sim 10^{-2}s^{-1}$ and $[BrO] \sim 10pptv$

$$k_a[Br][O_3] \sim 7 \times 10^6 molec.cm^{-3}s^{-1} \tag{3.5.9}$$

$$J[BrO] \sim 3 \times 10^6 molec.cm^{-3}s^{-1}. \tag{3.5.10}$$

Thus, taking into account the photolysis of BrO, the lifetime of O_3 calculated by Eq 3.5.6 can increase by a factor of 3 to 5 .

Section 3.6 Spring Time OH in the Arctic

Time series of methane (CH_4) and ethane from the dark period to early spring of 1992 in Alert are shown in Figure 3.6.1. Note that the fluctuations for methane and ethane are in step with each other until the end of dark period (~JD 84, March 25). After sunrise, the mixing ratio of methane continues

---

† Non-linear because BrO is related to O_3 by

$$\frac{d}{dt}[BrO] = k_a[Br][O_3] - J[BrO] - k_b[BrO]^2.$$

Table 3.6.1

A

OH	$k_{Butane(n)} = 1.92^a$	$k_{Propane} = 0.745^a$
$k_{Butane(i)} = 1.88^a$	2%	60%

$^a \times 10^{-12}$ $cm^3 molecule^{-1} s^{-1}$

B

Cl	$k_{Butane(n)} = 1.97^3$	$k_{Propane} = 1.53^3$
$k_{Butane(i)} = 1.37^3$	43%	11%

$^3 \times 10^{-10}$ $cm^3 molecule^{-1} s^{-1}$

Table A tabulates the percentage differences between the rate constant for the reaction of OH with both n-butane and i-butane, and between that for the reaction of OH with propane and i-butane. i.e.,

$$\frac{|k(\text{butane(n)} + OH) - k(\text{butane(i)} + OH)|}{k(\text{butane(i)} + OH)} \times 100\%$$

and

$$\frac{|k(\text{propane} + OH) - k(\text{butane(i)} + OH)|}{k(\text{butane(i)} + OH)} \times 100\%$$

Items in Table B is the same but with Cl atom as the oxidant.

to represent that of the free troposphere while the mixing ratio of ethane deviates from the free tropospheric trend. The three prominent dips at JD 95, 99 and 108 (April 4, 8 and 17) occur concomitant with the arrival of air mass depleted in O_3. As was discussed previously, these are attributed to the presence of Cl atoms. Excluding these three dips, the deviation of ethane from tropospheric trend is due to its reaction with OH radical. The fact that OH is the chief oxidant in the non O_3 depleted air mass can be illustrated by plotting the ratios of [i-butane] to [n-butane] versus the ratio of [i-butane] to [propane]. This is shown in Figure 3.6.2. One can see that data of normal O_3

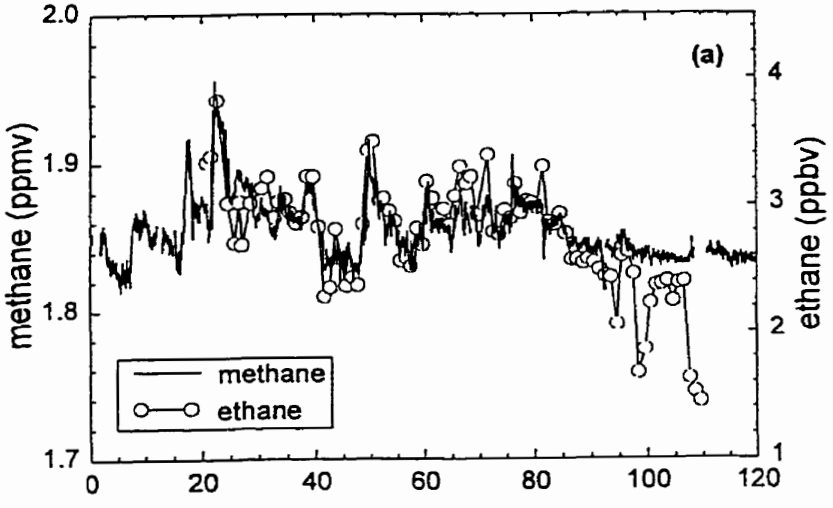

Figure 3.6.1

Methane (solid line) and ethane (circles) time series profiles showing deviation after the onset of 24-hour daylight at Alert. [*Jobson et al.*, p.25,358, 1994].

align themselves horizontally at a constant [i-butane]:[n-butane] to indicate HO kinetics while data associate with low O_3 air mass align themselves vertically at a constant [i-butane]:[propane] to indicate Cl kinetics. This identification method is based of the fact that the rate constants of OH reacting with n-butane and i-butane are very similar. Thus, if OH is the dominant oxidant, n-butane and i-butane will decay in step with each other, i.e., their ratio would be a constant. On other hand the rate constant of Cl atom reacting with propane and i-butane is very similar. If the Cl atom is the dominant oxidant, propane and i-butane would decay in step with each other resulting in a constant ratio. If both Cl and OH are equally important, the data points would be scattered. Table 3.6.1A, tabulated the percentage differences between the rate constant

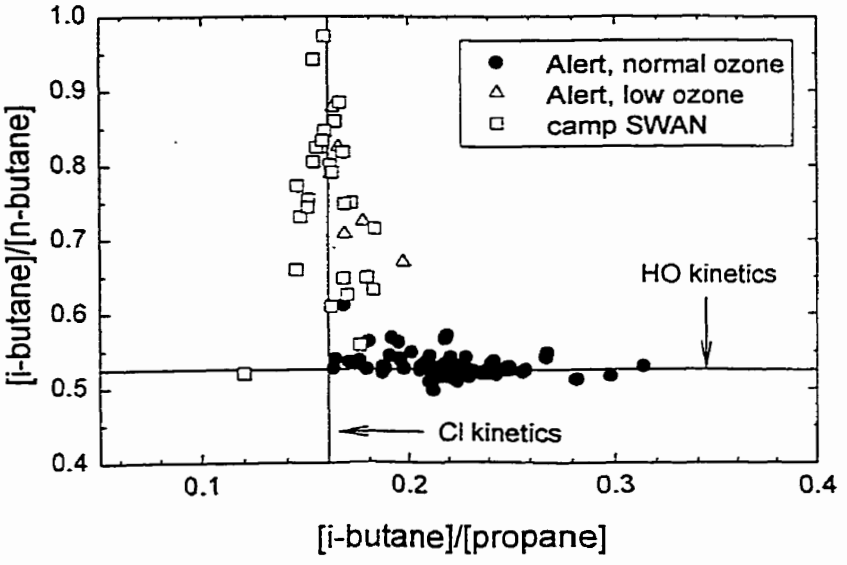

Figure 3.6.2
Plot of $\frac{[i-butane]}{[n-butane]}$ versus $\frac{[i-butane]}{[propane]}$ for Alert and camp Swan. Solid line indicate approximately how data would align under OH oxidation (horizontally) and Cl atom oxidation (vertically) kinetics. The plot illustrates that OH oxidation was driving the hydrocarbon concentration change in the ozone rich air masses. See text. [*Jobson et al.*, p.25,367, 1994].

for the reaction of OH reacting with n-butane and i-butane, and between that for OH reacting propane and i-butane. A similar tabulation is also made for Cl atom in Table 3.6.1B.

The average OH concentration can be found by applying the analysis technique described in Section 3.3 — by plotting data points associated with normal O_3 versus the reaction rate constant between NMHC and OH. The time integrated hydroxyl density, $\int$[OH]dt, is calculated to be 1.84×10^{11} molec.cm^{-3}s over a period of 18.5 days [*Jobson*, 1994]. The average hydroxyl density over this period is 1.1×10^{5} molec.cm^{-3}. This value is an order of magnitude less

than that of *Wingenter et al.*, [1996] (cf. Section 3.2). Considering the weak solar radiation of early spring in the polar environment, the lower value calculation by *Jobson* [1994] is not a surprise (The estimated average daytime global hydroxyl radicals in the troposphere during winter are of the order of 10^6 molec.cm^{-3} [*Spivakovsky et al.*, 1990; p.137 *Stainfield* ,1986]).

Section 3.7 Chlorine Catalytic Cycle

In the lower stratosphere where levels of O^3P are low, the chlorine catalytic destruction of O_3 with Polar Stratospheric Clouds (PSCs) has been well studied (eg., [*Molina and Molina*, 1987]). This catalytic cycle,

$$2(Cl + O_3 \rightarrow ClO + O_2) \tag{3.7.1a}$$

$$ClO + ClO \xrightarrow{M} ClOOCl \tag{3.7.1b}$$

$$ClOOCl + h\nu \rightarrow Cl + ClOO \tag{3.7.1c}$$

$$ClOO \xrightarrow{M} Cl + O_2 \tag{3.7.1d}$$

$$\text{net} : 2(O_3 \rightarrow 3O_2), \tag{3.7.1e}$$

can be applied to the MBL. As was pointed out early, in the bromine catalytic cycle, the rate of O_3 destruction is limited by the rate at which bromine in the BrO is being converted into the free radical form. Similarly, in the case of chlorine, the rate of O_3 destruction is limited by the self-reaction of ClO which converts its chlorine into Cl atoms[†]. Thus, the rate of O_3 depletion due to the

[†] Note that the self-reaction of BrO (cf. Section 2.2) is different from the self-reaction of ClO above in that, the former is a bimolecular reaction, the later is a termolecular reaction. The rate for bimolecular self-reaction of ClO is slow. At 245 K, the bimolecular reaction rate constants for ClO + ClO is 4.3×10^{-15} cm^{3}molec.$^{-1}$s^{-1} and for BrO + BrO is 3.8×10^{-12} cm^{3}molec.$^{-1}$s^{-1} [*DeMore et al.*, 1992]. The termolecular self-reaction of BrO does not appear to be important for atmospheric conditions.

chlorine catalytic cycle is,

$$\frac{d[O_3]}{dt} = -2k_{eff.}[ClO]^2. \tag{3.7.2}$$

Assuming a constant [ClO], the above can be integrated to give an expression for the amount of time required in destroying an initial amount of ozone ($[O_3]_o$).

$$\tau_{O_3} = \frac{[O_3]_o}{2k_{eff}[ClO]^2}. \tag{3.7.3}$$

The effective rate constant for self reaction of ClO is estimate to be around $k_{eff.} = 7.6 \times 10^{-14}$ $cm^3 molec^{-1}.s^{-1}$‡. The above estimate has taken into consideration the thermal decomposition of the dimer,

$$ClOOCl \rightarrow ClO + ClO. \tag{3.7.4}$$

which is important. At the cold temperature of the lower stratosphere (< 210 K) the dimer can survive to undergo photolysis, yielding Cl atoms. In the warmer troposphere, however, the dimer decomposes rapidly to ClO and the conversion rate of ClO to Cl atom is reduced to about 10% of that in the lower stratosphere.

Tuckermann et al. [1997] have measured a peak level of ClO of ~ 40 pptv during the 1995 ozone depletion event (19-25 April) at Ny-Ålesund, Svalbard (78.9°N, 11.8°E) (see Figure 3.7.1). However, the level of ClO measured has a very large uncertainty (≈ 20 pptv) due to poor signal to noise ratio in the ClO absorptions. Comparing their measured time series of BrO to that of ClO, BrO

---

‡ Based on $ClO + ClO \overset{k^{\pm}}{\rightleftharpoons} ClOOCl \xrightarrow{h\nu} 2Cl + O_2$ at 245°K:

$$k_{eff.} = k^{+}\frac{jv}{jv + k^{-}[M]} = 7.6 \times 10^{-14} cm^3 molec.^{-1} s^{-1}.$$

Where $k^{+} = 7.6 \times 10^{-13}$ $cm^3 molec^{-1}.s^{-1}$ is the effective three body reaction rate constants; $k^{-} = 2.6 \times 10^{-1}$ s^{-1} is the thermal dissociation of ClOOCl; $Jv = 3 \times 10^{-2} s^{-1}$ (estimated); $[M] = 2.99 \times 10^{19} molec.cm^{-3}$. Rate coefficients are taken from [*DeMore et al.*, 1992].

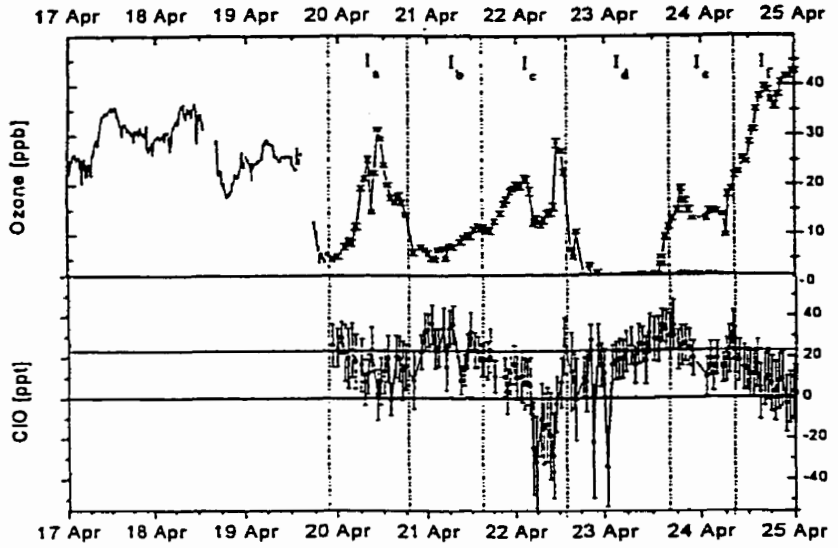

Figure 3.7.1

Time series of O_3 and ClO during the 1995 ozone depletion event (19-25 April) at Ny-Ålesund, Svalbard (78.9°N, 11.8°E). Note that the detection limit for ClO is about 20 pptv. [*Tuckermann et al.*, p.542, [1997].

shows distinctive and discernable variation (Figure 2.3.3) while ClO exhibits a gradual variation resembling a background level. The reliability of this ClO measurement is questionable. Notwithstanding, even with 40 pptv of ClO, it would take the chlorine catalytic cycle more than a month to destroy 40 ppbv of O_3. Considering the length of this time scale, the likelihood of O_3 depletion due to the chlorine catalytic cycle (Eq 3.7.1) is very small. There are other channels by which chlorine in ClO can be released to Cl atoms. The most

important of these channels are:
(1) The reaction between ClO and NO_2, giving rise to $ClONO_2$ from which chlorine can be released after photo-dissociation,

$$ClO + NO_2 \xrightarrow{M} ClONO_2 \tag{3.7.5a}$$

$$ClONO_3 + h\nu \rightarrow Cl + NO_3. \tag{3.7.5b}$$

(2) The reaction between ClO and NO. This directly converts chlorine in ClO to fresh Cl atoms,

$$ClO + NO \rightarrow Cl + NO_2. \tag{3.7.6}$$

(3) The reaction between ClO and HO_2, resulting in HOCl production which can be photo-dissociated yielding Cl atoms,

$$ClO + HO_2 \rightarrow HOCl \tag{3.7.7a}$$

$$HOCl + h\nu \rightarrow Cl + OH. \tag{3.7.7b}$$

These channels are summarized together with the channel of ClO self-reaction in Table 3.7.1. Note that the ClO self-reaction is the least effective in converting chlorine in ClO into free Cl atom in the PBL. The rate of O_3 depletion due to reaction of ClO with Z ($= NO_2, NO$ and HO_2) is

$$\frac{d[O_3]}{dt} = -2k_{Z+ClO}[ClO][Z]. \tag{3.7.8}$$

Assuming a constant [ClO] and [Z], the above can be integrated to give an expression for the amount of time required in destroying an initial amount of ozone ($[O_3]_o$),

$$\tau_{O_3} = \frac{[O_3]_o}{2k_{Z+ClO}[ClO][Z]}. \tag{3.7.9}$$

Consider an average mixing ratio for ClO at 10 pptv, the amount of NO_2, NO and HO_2 required to deplete 40 ppbv of O_3 in one day is 344 pptv, 72 pptv and 184 pptv respectively. These amounts are unlikely in the Arctic environment.

It should be pointed out that, since NO_3 and NO_2 are actually the precursors of O_3, the above are not concerned with the *net* loss of O_3.

Section 3.8 Interaction Between ClO and BrO

As was seen in the previous section, the chlorine catalytic destruction rate for O_3 is limited by the rate at which chlorine in the ClO being converted into Cl atom. Table 3.7.1 has tabulated these conversion channels. Another important channel that shall be added to this is the interaction between ClO and BrO (see *McElroy et al.* [1986]). The reaction between ClO and BrO has three channels:

$$ClO + BrO \rightarrow Cl + Br + O_2 \tag{3.8.1a}$$

$$\rightarrow BrCl + O_2 \tag{3.8.1b}$$

$$\rightarrow OClO + Br. \tag{3.8.1c}$$

The BrCl produced in the second channel above can be photolyzed rapidly (53 to 250 sec). Therefore, the first two channels (Eq. 3.8.1a & b) have the effect of converting halogen oxides into halogen atoms:

$$ClO + BrO \xrightarrow{net} Cl + Br + O_2. \tag{3.8.2}$$

At 245 K, 47% of the reaction proceeds in this fashion and the resulting O_3 destuction catalytic cycle is:

$$Cl + O_3 \rightarrow ClO + O_2 \tag{3.8.4a}$$

$$Br + O_3 \rightarrow BrO + O_2 \tag{3.8.4b}$$

$$ClO + BrO \xrightarrow{net} Br + Cl + O_2 \tag{3.8.4c}$$

$$\text{net} : 2(O_3 \rightarrow 3O_2). \tag{3.8.4d}$$

The reaction channel between BrO and ClO that results in OClO formation (Eq. 3.8.1c) does not leads to O_3 destuction since photolysis of OClO leads to

Table 3.7.1 Important channels in the model that convert chlorine in the form of ClO to Cl atom.

Channels	Effective rate$^{\alpha}$($cm^3 molec^{-1}.s^{-1}$)	
$ClO + ClO \rightarrow 2Cl + O_2$	$k_a = 7.6\times10^{-14}$	β
$ClO + NO_2 \rightarrow Cl + NO_3$	$k_b = 4.5\times10^{-12}$	γ
$ClO + NO \rightarrow Cl + NO_2$	$k_c = 2.1\times10^{-11}$	(1)
$ClO + HO_2 \rightarrow Cl + OH$	$k_d = 8.4\times10^{-12}$	δ

$^{\alpha}$ at 245K

$^{\beta}$ see footnote‡.

$^{\gamma}$ Based on the chain of reaction for

$$ClO + NO_2 \rightarrow ClONO_2 \xrightarrow{h\nu} Cl + NO_3.$$

Under steady state condition,

$$\frac{d}{dt}[ClONO_2] = k_a[ClO][NO_2] - h\nu[ClONO_2] = 0.$$

The formation rate of Cl atom from this chian is therefore,

$$\frac{d}{dt}[Cl] = h\nu[ClONO_2] = k_a[ClO][NO_2].$$

k_a is the reaction rate coefficients for $ClO + NO_2$[(1)].

$^{\delta}$ Based on the chain of reaction for

$$ClO + HO_2 \rightarrow HOCl \xrightarrow{h\nu} Cl + OH.$$

With same argument as $^{\gamma}$, the formation rate for Cl atom for this chain is same as the rate of the rate of reaction $ClO + HO_2$.

(1) *DeMore et al.* [1992].

formation of $O(^3P)$ which immediately yields an O_3 in the presence of O_2.

$$ClO + BrO \rightarrow OClO + Br \quad (3.8.5a)$$

$$OClO + h\nu \rightarrow O(^3P) + ClO \quad (3.8.5b)$$

$$O(^3P) + O_2 \xrightarrow{M} O_3 \quad (3.8.5c)$$

$$\text{net} : ClO + BrO + O_2 \xrightarrow{h\nu,M} ClO + Br + O_3. \quad (3.8.5g)$$

Thus, the effect of a third channel in Eq 3.8.1 is to enhance BrO to Br atom conversion while generating an O_3. After combining the above with the reactions that produce ClO and BrO :

$$Cl + O_3 \rightarrow ClO + O_2 \quad (3.8.6a)$$

$$Br + O_3 \rightarrow BrO + O_2 \quad (3.8.6b)$$

$$ClO + BrO + O_2 \xrightarrow{net} ClO + Br + O_3 \quad (3.8.6c)$$

$$\text{net} : Cl + O_3 \rightarrow ClO + O_2. \quad (3.8.6d)$$

The resulting effect is a repartitioning of chlorine from Cl atom to ClO while O_3 is being depleted. Combining both cycles (Eq 3.8.4 and Eq 3.8.6) the efficiency of O_3 depletion for the interaction between ClO and BrO is:

$$2O_3 \times 0.47 + O_3 \times 0.53 = 1.47.$$

Interaction of ClO and BrO has been well studied in the mid-stratospheric O_3 depletion for some time before *Le Bras & Platt* [1995] first considered its effect in the context of troprospheric O_3 depletion. Again, with the conversion of halogen oxide to halogen radical being the rate limiting step, the rate of O_3 destruction due to the presence of BrO and ClO catalytic cycle is :

$$\frac{d[O_3]}{dt} = -2\ \{k_{BrO^2}[BrO]^2 + 1.47\ k_{BrO-ClO}[BrO][ClO]\}. \quad (3.8.7)$$

$$k_{BrO^2} = 3.2 \times 10^{-12} cm^3 molec^{-1}.s^{-1}$$

$$k_{BrO-ClO} = 7.3 \times 10^{-12} cm^3 molec^{-1}.s^{-1}$$

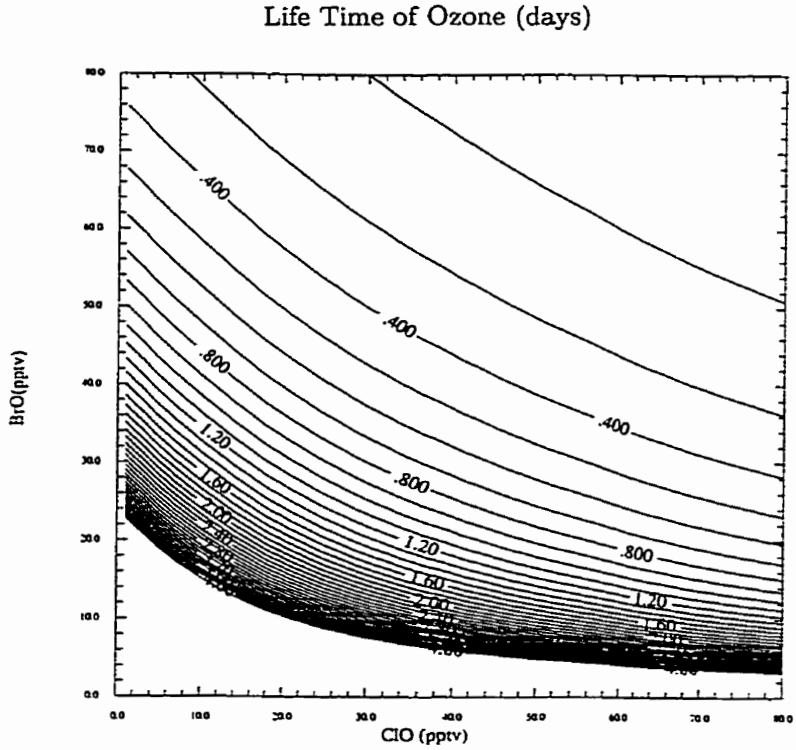

Figure 3.8.1
Life time of ozone as a function of ClO and BrO.

Notice that rapid O_3 depletion can only occur if BrO is present. Without BrO, ClO is handicapped, its self-reaction and its reaction with NO_2, NO and HO_2 is slow (see previous section).

Assuming constant [ClO] and [BrO], Eq 3.8.7 can be integrated to give the time constant for O_3 destruction,

$$\tau_{O_3} = \frac{[O_3]_o}{2\ \{k_{BrO^2}[BrO]^2 + 1.47\ k_{BrO-ClO}[BrO][ClO]\}}. \tag{3.8.8}$$

Note that, in Section 2.3, the expression of characteristic life time of O_3 de-

pletion due to the bromine catalytic cycle (Eq 2.3.4) is a special case in the above where [ClO] = 0. Figure 3.8.1 shows the contour plot of Eq 3.8.8. From the plot it can be seen that although the reaction rate constant for interaction between ClO and BrO is twice as large as that for BrO selfreaction, it is BrO which carries most of the work in the depletion of O_3 (more contour lines are crossed by varying BrO alone than by varying ClO alone). Given 20 pptv of ClO, about 30 pptv of BrO is required to deplete O_3 within one day. With ClO absent, the amount of BrO required to result in the same life time is about 48 pptv. ClO is an enhancement for the depletion of O_3, it is not a necessity.

Section 3.9 Sources of Chlorine in the Arctic Environment

The most abundant form of natural occurence chlorine in the atmosphere is HCl. Its yearly input has been estimated at about a thousand Tg(HCl). The average mixing ratio of HCl is of several hundred pptv [*Graedel & Keene*, 1995]. The most important source for HCl is believed to be the deliquescent seasalt. As much as 6000 Tg of chloride ion in the form of seasalt are injected into the marine boundary layer through wave generation processes [*Graedel & Keene*, 1995]. The release mechanism for HCl from seasalt has been generally believed to be the acid and base desorption mechanism. In this mechanism, HCl production occurs when HNO_3 and/or H_2SO_4 are incorporated into the seasalt aerosol. Both of these lower the pH of the seasalt aerosol and disrupt the equilibrium between aqueous HCl and gaseous HCl and HCl is liberated :

$$HNO_3(aq) + NaCl(p/aq) \rightarrow NaNO_3(aq) + HCl(aq) \tag{3.9.1}$$

$$H_2SO_4(aq) + NaCl(p/aq) \rightarrow Na_2SO_4(ap) + HCl(aq) \tag{3.9.2}$$

$$HCl(aq) \rightarrow HCl(g). \tag{3.9.3}$$

Robbins et al. [1959] are credited for the mechanism involving HNO_3 and *Eriksson* [1960] for the mechanism involving H_2SO_4. Although these processess

have been verified (e.g., *Keene et al.*, [1990]), it is still unclear how much of the HCl is accounted for by these processes. Even if it does provide the path for all the chloride necessary in forming HCl, it is not clear how chlorine in HCl can be released to provide the Cl atom's level measured in the marine or the Arctic environment. To convert HCl in the atmosphere into active Cl atom, the conversion process is thought to be via oxidation with hydroxyl radical

$$HCl + OH \rightarrow Cl + H_2O \qquad 6.23 \times 10^{-13} cm^3 molec^{-1}.s^{-s} \tag{3.9.4}$$

With [OH] $\sim 10^5$ molec.cm^{-3} in the Arctic's early spring (see Section 3.6), Eq 3.9.4 can yield several hundred Cl atoms per second. This amount is clearly too small since the reaction between 1.7 ppmv of CH_4 and 10^3molec.cm^{-3} of Cl atom (estimation of *Ariya et al.* [1998], see Section 3.4) would consume $\sim 10^5$ of Cl atom per second.

There are alternative mechanisms which release chlorine without involving HCl. *Schroeder* [1974] identified Nitrosyl chloride, NOCl, from the reaction of NO_2 with large salt particles. This event suggests

$$NO_2(g) + NaCl(p) \rightarrow NOCl + NaNO_3(p). \tag{3.9.5}$$

Finlayson-Pitts et al., [1989] and *Livingston & Finlayson-Pitts* [1991] had presented the process involving N_2O_5

$$N_2O_5(g) + NaCl(p) \rightarrow ClNO_2 + NaNO_3(p). \tag{3.9.6}$$

In the above, both NOCl and $ClNO_2$ are readily photolyzed, yielding Cl atoms. However, these mechanisms are probably of minor importance in the Arctic or remote oceanic environment considering the low level of odd nitrogen.

An interesting proposal of *Behnke & Zetzsch* [1989] involves free radical reactions in sea-salt aerosol. The overall stoichiometry appears to be

$$2Cl^- + O_3(g) \rightarrow Cl_2 + 2OH^- \tag{3.9.7}$$

as implied by the laboratory experiments of *Behnke & Zetzshe* [1994]. Although the above may account for release of Cl atom in the marine boundary layer, it is unlikely the mechanism that results in the Cl atom in Arctic environment because O_3 is required for this process. *Ariya et al.* [1998] have provided the evidence of Cl atom activity in air mass with little O_3 (see Section 3.4).

Vogt et al. [1996] have proposed a chloride releasing mechanism from sea-salt with HOBr(aq) as the releasing agent:

$$HOBr(aq) + Cl^- + H^+ \rightleftharpoons BrCl(aq) + H_2O \tag{3.9.8a}$$

$$BrCl(aq) \rightarrow BrCl. \tag{3.9.8b}$$

The flow chamber observation for this has been provided by *Kirchner et al.* [1997]. This mechanism is similar to the one in the releasing of bromide proposed by *Mozurkewich* [1995] (see Section 2.6):

$$HOBr(aq) + Br^- + H^+ \rightleftharpoons Br_2(aq) + H_2O, \tag{3.9.9a}$$

$$Br_2(aq) \rightarrow Br_2. \tag{3.9.9b}$$

Vogt et al. [1996] noted their proposed chlorine releasing mechanism has a slower reaction rate constant than the bromine releasing mechanism of *Mozurkewich* [1995] ($k^+_{3.9.8a} \geq 5.6 \times 10^9$ versus $k^+_{3.9.9} = 1.6 \times 10^{10}$ $M^{-2}s^{-1}$ [*Vogt et al.*, 1996]). However, this can be ameliorated since Cl^- is more abundant than Br^- in nascent sea salt aerosol ($[Cl^-]/[Br^-] \sim 700$). *Vogt et al.* [1996] also provided a computer simulation of a marine boundary layer photochemical box model to illustrate the release of active chlorine with their proposed mechanism. It is not clear, however, if their results can be extrapolated to be the chloride releasing mechanism in the Arctic environment. This mechanism, like that of *Behnke & Zetzsch* [1989], requires O_3 for the generation of HOBr(aq), As as discussed earlier, *Ariya et al.* [1998] have observed evidence of Cl atom in the absence of O_3. Although, alternative sources of HOBr(aq) can be supplied by reaction of Caro's acid with sea-salt bromine [*Mozurkewich*, 1995], this is probably too slow.

It is also noted that the mechanism of *Vogt et al.* [1996] may enhance the mechanism of *Fan & Jacob* [1992] in the initial autocatalytic transfer of bromine content of sea-salt into the atmosphere. Note that although BrCl(aq) formed in Eq 3.9.8a is highly volatile, not all of it escapes into the atmosphere, instead some undergoes hydrolysis:

$$BrCl(aq) + H_2O \rightarrow HOBr(aq) + H^+ + Cl^-, \tag{3.9.10}$$

and some reacts with Br^- to generate $Br_2(aq)$:

$$BrCl(aq) + Br^- \rightleftharpoons Br_2Cl^- \tag{3.9.11a}$$

$$Br_2Cl^- \rightleftharpoons Br_2(aq) + Cl^- \tag{3.9.11b}$$

$$Br_2(aq) \rightarrow Br_2. \tag{3.9.11c}$$

Kirchner et al. [1997] noted that hydrolysis is a very fast process. In their analysis, they noted that the probability of $Br_2(g)$ and BrCl(g) formation per HOBr(g) uptake is about 48% and 42% respectively. Thus, the bromine catalytic amplifying factor is 1.38†. It is not clear in their experiment the fraction of the Br_2 contributed by the mechanism of *Fan & Jacob* [1992] (Eq 3.9.9) and of that by *Vogt et al.* [1996] (Eq 3.9.11). Also, since the fate of BrCl(aq) is to react with Br^- or to volatilize into the gaseous phase, depletion of Br^- can increase the yield of gaseous BrCl, and thus increase the rate of chlorine transferring from the snowpack into the atmosphere.

According to the hypothesis of *McConnell et el.* [1992] sea-salt is deposited on the snowpack during the polar night. This can result in bromine and chlorine enrichment in the snowpack. If the high levels of Na^+ such as that found in the Antarctica ice shelf by *Mulvaney et al* [1993] occurs in the Arctic, and if these Na^+ are of oceanic origin, a spring time amount of potential chlorine 700 times more than that calculated for bromine in Section 2.5 is

† 0.48 × 2 Bromines (in a Br_2) + 0.42 × 1 Bromine (in a BrCl)

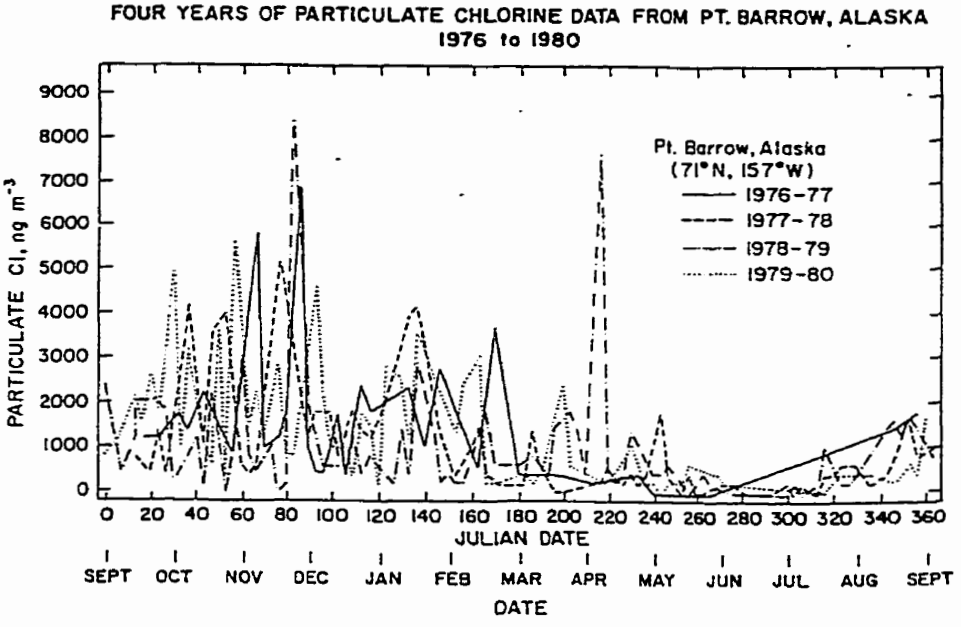

Figure 3.9.1

Chlorine content of the Arctic aerosol at Barrow, Alaska, 1976–1980. No seasonal pattern similar to that for bromine (Figure 2.5.3) is evident from these plots [*Berg et al.* p. 6726, 1983].

expected. However, the chlorine content of Arctic aerosol measured by *Berg et al.* [1983] (see Figure 3.9.1) does not show the seasonal enrichment similar to that of bromine (see Figure 2.5.3). This absence of seasonal enrichment for chlorine is inconsistent with the hypothesis of *McConnell et el.* [1992] unless the mechanism that releases chlorine into the atmosphere is different from that for the bromine release. In other words, the mechanism of *Vogt et al.* [1996] might not apply to the Arctic scenario.

Measurements of chlorine content in the aerosols for remote environments are generally in deficit throughout the year. The amount of chlorine loss relative to nascent sea salt can be as high as 80% [*Graedel & Keene*, 1995]. This is different from that of bromine in the Arctic environment which shows

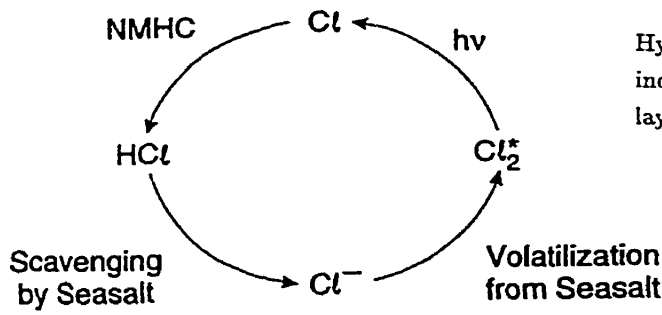

Diagram 3.9.1

Hypothesized geochemical cycle of reactive inorganic chlorine in the marine boundary layer by *Keene et al.*, [1990].

no deficit (see Section 2.5). It is possible that chlorine in sea-salt has already been released prior to its deposition on the snowpack. *Mulvaney et al* [1993] note that within 200 Km of the ocean, the Cl^- to Na^+ ratio in the snowpack is close to that in seawater. However, further inland the chlorine content in the snowpack becomes significantly depleted. They argued that the increasing NaCl fractionation with distance from the coast occurs as the larger particles are progressively removed from the aerosol, leaving smaller particles more prone to fractionation. If their argument obtains, then the chloride deposited in the snowpack is not readily released since it is contained in the aged larger size sea-salt particles. On the other hand the chlorine associated with the smaller sea-salt particles is released into the gaseous phase while the particle is still airborne. After the release, gaseous chlorine is then rapidly recycled on the airborne aerosol. A cycle of reactive chlorine has been proposed by *Keene et al* [1990]. The life time of this cycle is short, and therfore it is seasonally independent. Although this cycle was proposed for the marine boundary layer, it is the hypothesis of this work to apply it to the polar environment. Their cycle consists of photolyzable chlorine in the form of Cl_2 volatilized from the sea-salt aerosol (by an as yet unknown mechanism). After photodissociation, Cl atoms are released to oxidize NMHC resulting in HCl production. HCl can

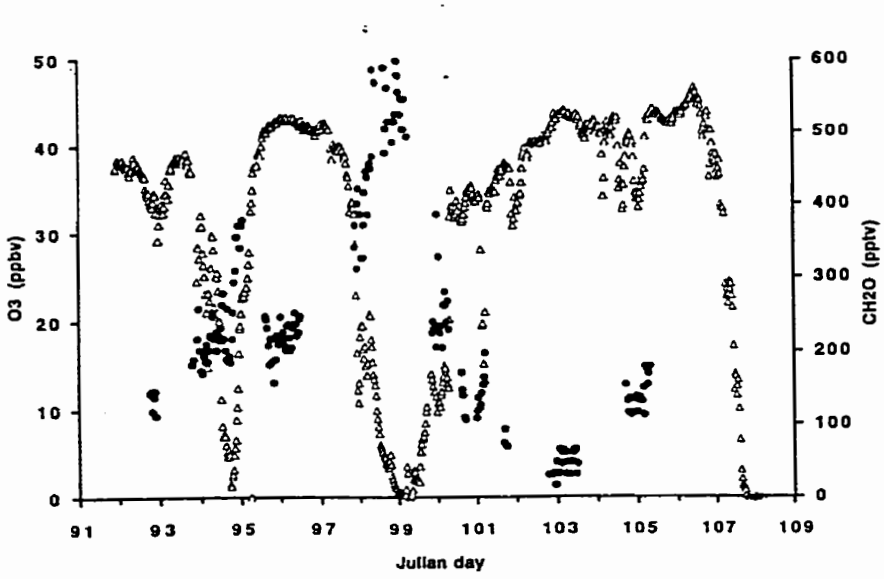

Figure 3.10.1
Ozone (triangles) and formaldehyde (dots) during Polar Sunrise II [p.25,396 *De Serves*, 1994].

be scavenged by sea-salt aerosol where it is dissociated into Cl^- which can be released again to complete the chlorine cycle (see Diagram 3.9.1).

Section 3.10 Formaldehyde in the Arctic

Figure 3.10.1 shows the measurements of O_3 and formaldehyde (HCHO) during spring time at Alert by *De Serves* [1994]. Note the formaldehyde appears to be anti-correlated with the of O_3. For the episode of O_3 depletion at JD 99, HCHO reaches as high as 600 pptv. The mixing ratios of HCHO at 100s pptv level do exist in the remote tropical marine air, for example *Lowe and Schmidt* [1994] observed HCHO on the order of 200 pptv over the Atlantic ocean (35°S and 55°N, October and November 1980). However, because of the lower tem-

perature and weaker sunlight, the level of HCHO seen in the O_3 free air mass in the Arctic is unusual. High formaldehyde is usually associated with polluted environment. In urban areas such as Los Angeles, formaldehyde has been reported with mixing ratio as high as 150ppbv [*Altshuller and McPerson*, 1961]. In polluted areas, high levels of formaldehyde are produced because of the large sources of hydrocarbons. It is not uncommon that a polluted air mass of anthropogenic origin is transported to the Arctic. An example of this effect is the Arctic Haze problem [*Barrie & Bottenheim*, 1991]. However, it is unlikely that the observed formaldehyde in the Arctic is imported. Back trajectories shows that it take about five days for continental air mass to reach Alert [*Hopper and Hart*, 1995]. This travel time is too long since Formaldehyde, with photolysis life time of one day (see Figure A.2.20 and A.2.21), would have been dissociated before its arrival at Alert. The observed formaldehyde is more likely produced within 1000 km[†]; that can be reached by observation site with advection time scale of less than one day.

Oxidation of hydrocarbons are known to be a source for HCHO. Consider the simplest, and the most abundance and ubiquitous hydrocarbon in the remote atmosphere — methane (CH_4). First of all, it is interesting to note that Br atom does not attack CH_4 (this reaction is endothermic). When OH or Cl atoms attack CH_4 in the presence of O_2, methyl peroxy radical (CH_3O_2) is formed instantly. From this point, the successful production of HCHO depends on relative amount of HO_2 and NO to react with CH_3O_2. The former reaction form the long lived methyl hydroperoxide, CH_3OOH. The later reaction forms the methoxy radicals (CH_3O). Methoxy radicals react exclusively with O_2 to form HCHO. Since the attack of CH_4 by OH and Cl atom are the rate limiting step to HCHO formation, the production rate of HCHO can be written as :

$$P = \alpha[CH_4]\{k_1[Cl] + k_2[OH]\}. \qquad (3.10.1)$$

[†] Assuming the air mass is advected at the speed of 10 m/s

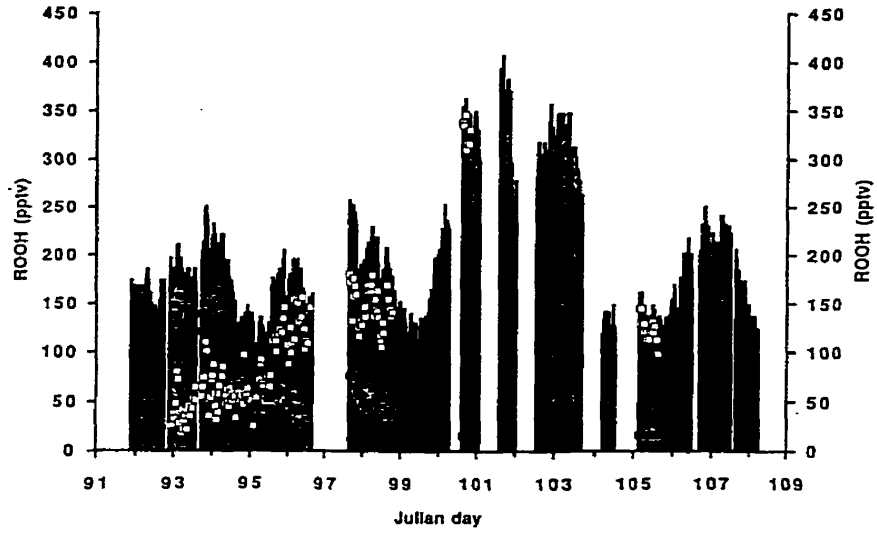

Figure 3.10.2

Sunlit period peroxide during Polar Sunrise II. The total peroxide concentrations are represented as shaded area, organic peroxide (solid squares), and H_2O_2 (open squares) [p.25,396 *De Serves*, 1994].

k_1 and k_2 are the rate coefficients with which Cl atom and OH react with CH_4 respectively. The branching ratio, α, depends on the relative amount of NO and HO_2 :

$$\alpha = \frac{k_3[NO]}{k_4[HO_2] + k_3[NO]}. \tag{3.10.2}$$

It determines the amount of peroxy radical forming HCHO. In the above, k_3 and k_4 are the rate coefficients for HO_2 and NO reacting with CH_3O_2 respectively. The chemical loss of HCHO includes photo-dissociation and oxidation by OH, Br and Cl atom. For this, the loss rate can be written as :

$$L = [HCHO]\{J + k_5[Cl] + k_6[Br]\} \tag{3.10.3}$$

If the above production and loss of HCHO is balanced, an analytic expression

for HCHO can be derived :

$$[\mathrm{HCHO}] = \alpha \frac{\mathrm{P}}{\mathrm{L}}, \tag{3.10.4}$$

The formation of HCHO has an important consequence — each HCHO can give two HO_2 which is the precursor of HOBr. As a source of HO_2, an increase in HCHO can restrict its own production by reducing α in Eq 3.10.2. Instead of producing HCHO, the peroxy radicals are directed into CH_3OOH production. Thus, it is not surprising that high levels of ROOH are observed during the spring time Arctic PBL (see Figure 3.10.2). The formation of CH_3OOH indicates a catalytic destruction of HO_x.

$$CH_3O_2 + HO_2 \rightarrow CH_3OOH + O_2 \tag{3.10.5a}$$

$$CH_3OOH + OH \rightarrow CH_3O_2 + H_2O \tag{3.10.5b}$$

$$\text{net} : HO_2 + OH \rightarrow O_2 + H_2O. \tag{3.10.5c}$$

This HO_x destruction can be minimized if more NO is present to convert CH_3O_2 to HCHO.

Chapter IV
Model Description

Section 4.1 Model Setup

A computer zero-dimensional chemical model is employed as a tool for the study of O_3 depletion in the Arctic environment. The chemical scheme used represents the chemistry of HO_x, NO_x, CH_4, bromine and chlorine with solar radiation as the external energy source. The chemistry of HO_x and NO_x forms a set of chemical reaction which describes the unperturbed mixing ratio of baseline O_3 in the atmosphere. For a detailed description of these see *Seinfeld* [1986, pp. 111–128]. The chemistry of CH_4 describes its oxidation to HCHO which is further oxidized to CO and finally to CO_2. For an excellent description of CH_4 chemistry in the natural troposphere see *Finlayson-Pitts & Pitt* [1986, pp. 974–977]. A useful summary of bromine and chlorine chemistry can be found in *Orlando & Schauffler* [1999]. The chemical reactions used in the

model are tabulated in Appendix A. They are organized into :

(1) Reactions of HO_x and NO_x chemistry (Table A.1)
(2) Reactions of bromine chemistry (Table A.2)
(3) Reactions of chlorine chemistry (Table A.3)
(4) Reactions for ClO and BrO interaction (Table A.4)
(5) Reactions of methane oxidation. (Table A.5)

In the tables, the reaction rate coefficients are included. Notice that in the table, pressure dependent third order reactions, $A + B + M \rightarrow$ products + M, are treated as second order reactions, $A + B \xrightarrow{M}$ products (i.e. with the third body, [M] ($= 2.99 \times 10^{19}$molec.cm^{-3}) included in the rate coefficients). Reactions involving photodissociation and thermal decomposition : $AB + h\nu \rightarrow A + B$ and $AB + \Delta H \rightarrow A + B$ are treated as first order reactions : $AB \xrightarrow{h\nu} A + B$ and $AB \rightarrow A + B$. The temperature is held fixed for the simulations at 245 K.

The mechanism of *Fan & Jacobs* [1992] is adopted to recycle inactive bromine ($BrONO_2$, HOBr and HBr). As was pointed out in Section 2.4, this mechanism can result in the rapid loss of gaseous nitrogen to HNO_3(aq). Although the level of NO_x in the Arctic is low, it is not zero. The small amount of NO_x ($\sim$ 30-40 pptv [*Beine et al.*, 1997]), does contribute to the ozone budget [*Jaffe*, 1994]. To conserve gaseous nitrogen, the model recycles nitrogen in HNO_3(aq) back into the atmosphere. Observations of *Honrath et al.* [1999] and *Jones et al.* [2000] appear to confirm this. The exit pathway for nitrogen from aqueous phase to gaseous phase is chosen to be HONO,

$$HNO_3(aq) \rightarrow HONO(g), \tag{4.1.1}$$

since *Li* [1994] has observed HONO(g) at concentrations of up to $\sim$ 5-10 pptv after polar sunrise. To reactivate chlorine in HCl, the recycling 'path' proposed by *Keene et al* [1990] is used (see Section 3.9). These heterogeneous recycling mechanisms are tabulated in Table A.6. The model does not have the detailed aqueous chemistry (such as that found in the work of *Lelieveld & Crutzen*

[1991]). The uptake of gaseous species, say $Y_i(g)$,

$$Y_i(g) \rightarrow Y_i(aq), \tag{4.1.2}$$

is represented in the model by the first order differential equation :

$$\frac{d[Y_i(aq)]}{dt} = D_i[Y_i(g)]. \tag{4.1.3}$$

In the above, $[Y_i(aq)]$ is the number of molecules of Y_i in the aqueous phase per unit volume of air (such as Y_i dissolved in an airborne deliquescent aerosol). D_i is the assigned first order rate coefficient for gas to liquid transfer. For the uptake of (Y_i = HBr, HOBr and $BrONO_2$), the time scales, $\tau_i = \frac{1}{D_i}$, suggested by *Fan & Jacob* [1992] are used (tabulated in Table A.6). Lacking other information, the uptake coefficient of HCl in the model is assumed to be similar to that of HBr. Once in the aqueous phase $Y_i(aq)$ (= $Br^-(aq)$, HOBr(aq), $BrONO_2(aq)$ or $Cl^-(aq)$) can undergo chemical transformation to $Z_i(aq)$,

$$Y_1(aq) + Y_2(aq) \rightarrow Z_1(aq) + Z_2(aq), \tag{4.1.4}$$

which subsequently can be liberated into the gaseous phase $Z_i(g)$.

$$Z_i(aq) \rightarrow Z_i(g). \tag{4.1.5}$$

In the model, chemical transformation in the aqueous phase is treated as a second order reaction and gaseous to liquid phase liberation is treated as a first order reaction. According to *Fan & Jacob* [1992] the effective rate of recycling is limited by the gaseous uptake ($Y_i(g) \rightarrow Y_i(aq)$), not by the chemical conversion in the aqueous phase ($Y_i(aq) \rightarrow Z_i(aq)$). Thus, the rate coefficients for Equation 4.1.4 and 4.1.5 are assigned such that their rate of reaction are faster than the supply rate of their reactants from gaseous uptake.

Due to the simplicity of this model, the simulation does not distinguish differences between species in snowpack, aerosol and liquid droplet. It assumes

Table 4.1.1 Species in the Model

O_3 O^1D H_2 O_2 H_2O CO_2 CO	OH HO_2 H_2O_2	NO NO_2 NO_3 N_2O_5 HONO HNO_3 HNO_4	CH_4 CH_2O_2 CH_3OOH CH_3ONO_2 $HOCH_2O_2$ HCHO	Br BrO Br_2 HBr $BRONO_2$ HOBr	Cl ClO Cl_2 HCl $ClONO_2$ HOCl OClO ClO_2 Cl_2O_2
			$CHBr_3$		
				BrCl	
		HNO_3(aq)		BrONO2(aq) HOBr(aq) Br^-	Cl^-

species in these three phases undergo the same aqueous phase reaction processes. The model simulates the Lagrangian time evolution of a surface air parcel, starting at local midnight, Julian Day (JD) 90 and ends before JD 115.

The species in the model are shown in Table 4.1.1. Except for those listed in Table 4.1.2, their initial mixing ratios are initialized to 10^{-30} which signifies zero. The initial O_3 mixing ratio is assigned to its pre-depletion value of 40 ppbv [*Barrie et al.* 1988]. CO and CH_4 are assigned with their globally averaged value of 150 ppbv and 1.7 ppmv respectively [*Khalil & Rasmussen*, 1995]. The nitrogen in the model is initialized to NO_x at a typical value of the Arctic, 50 pptv, [*Bottenheim et al.*, 1990; *Jaffe*, 1993; *Beine et al.*, 1997] with

Table 4.1.2 Initialization

O_3	40 ppbv	*Barrie et al.* [1988]
NO	20 pptv	*Bottenheim et al.* [1990]; *Jaffe* [1993]
NO_2	30 pptv	*Bottenheim et al.* [1990]; *Jaffe* [1993]
CO	150 pptv	*Khalil & Rasmussen* [1995]
CH_4	1.7 ppmv	*Khalil & Rasmussen* [1995]
HCHO	50 pptv	*Bottenheim et al.* [1990]
Br^-	100 pptv	see text
Cl^-	10 pptv	see text
$CHBr_3$	3.5 pptv	*Yokouchi et al.* [1994]
H_2O	2×10^{-4}	see text

Note : All species are initialized at model time JD 90 except $CHBr_3$, which is introduced in JD 93. All other species are set to to small value 10^{-30}, which represent zero physically.

20 pptv in the form of NO and 30 pptv in the form of NO_2. This partitioning of nitrogen is arbitrary and not important since NO and NO_2 in the model rapidly equilibrate. For HCHO a value of 50 pptv is assigned. This level is similar to that measured by *Bottenheim et al.* [1990]. The mixing ratio for water vapor is calculated using the Clausius-Clapeyron equation [*Rogers & Yau*, 1989] at 245 K with 50% relative humidity for water over ice. The calculation gives a water vapor mixing ratio of 2.06×10^{-4}.

The model adopted the hypothesis of *McConnell et al.* [1993] for the source of bromine. Thus, 100 pptv bromine is initialized as Br^- prior to beginning of the simulation. This is meant to represent bromine accumulated during the polar night on the snow-pack as discussed in Section 2.5. The required level of bromine in the model is based on modeling necessities in simulating

the depletion of O_3 with a time scale on the order of one day. This requires at least 60 pptv of bromine as BrO (see Section 2.3). To initiate the release of bromine from Br^-, 3.5 pptv of $CHBr_3$ is introduced three days after the simulation begins (i.e., JD 93). $CHBr_3$ is chosen to be the seed even though there are several alternates available (see Section 2.7). The amount of $CHBr_3$ is based on the measurements of *Yokouchi et al.* [1994] who measured $CHBr_3 \sim 3$ pptv in the ozone depleted air parcel (see Section 2.5).

As pointed out above, in the initialization of bromine in the model, the entry point is chosen to be Br^- in the aqueous phase. This is done with the intention that Br^- is the source of bromine. The initialization of chlorine to Cl^-, however, has less physical meaning. This entry point is chosen arbitrarily. Unlike bromine in the Arctic environment which exhibits a seasonal cycle, the cycle of chlorine is proposed to be faster and occurs through out the year (see the end of Section 3.9). For this, the proposal of *Keene et al.* [1990] for the recycling of reactive chlorine is adopted in this model. The total amount of chlorine given to the model (10 pptv) is assigned such that the run time Cl atom concentration is similar to the observation $\sim 10^4$ molec.cm^{-3} (see Section 3.4). Due to the simplicity of the scheme, it is unlikely that the amount of chlorine is a realistic representation of that in the polar atmosphere.

The Nicolet diagrams for the bromine, chlorine and methane chemistry in the model are shown in Diagrams 4.1.1, 4.1.2 and 4.1.3 attached to next three pages.

Summary of Bromine Chemistry

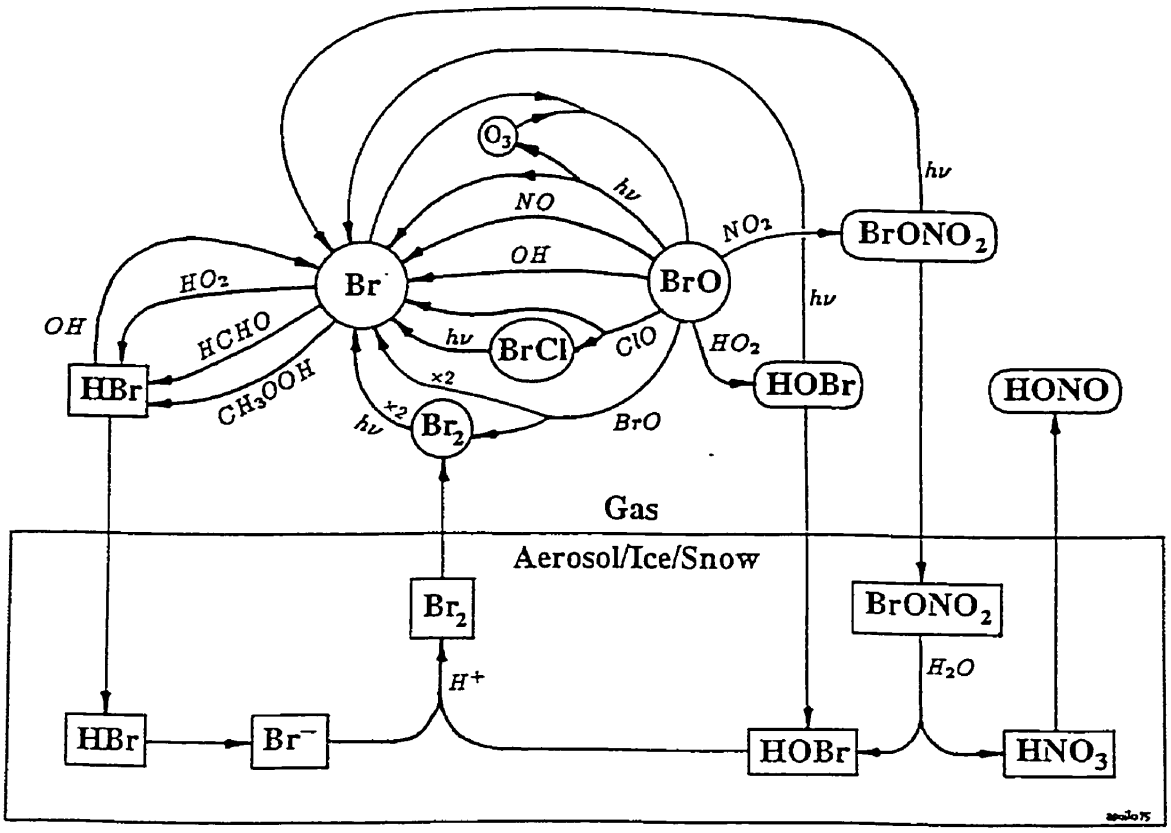

Diagram 4.1.1
Summary of Bromine Chemistry

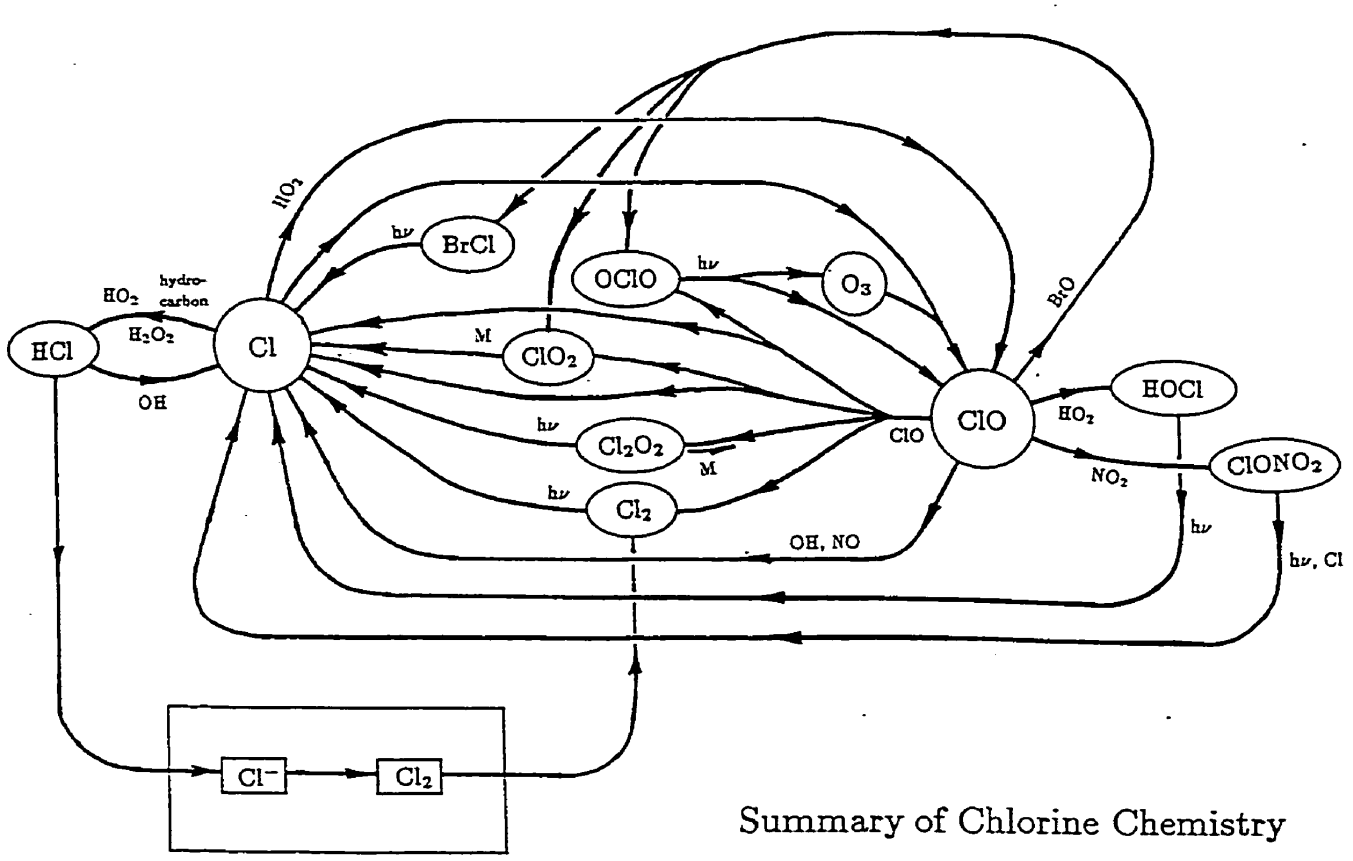

Summary of Chlorine Chemistry

Diagram 4.1.2
Summary of Chlorine Chemistry

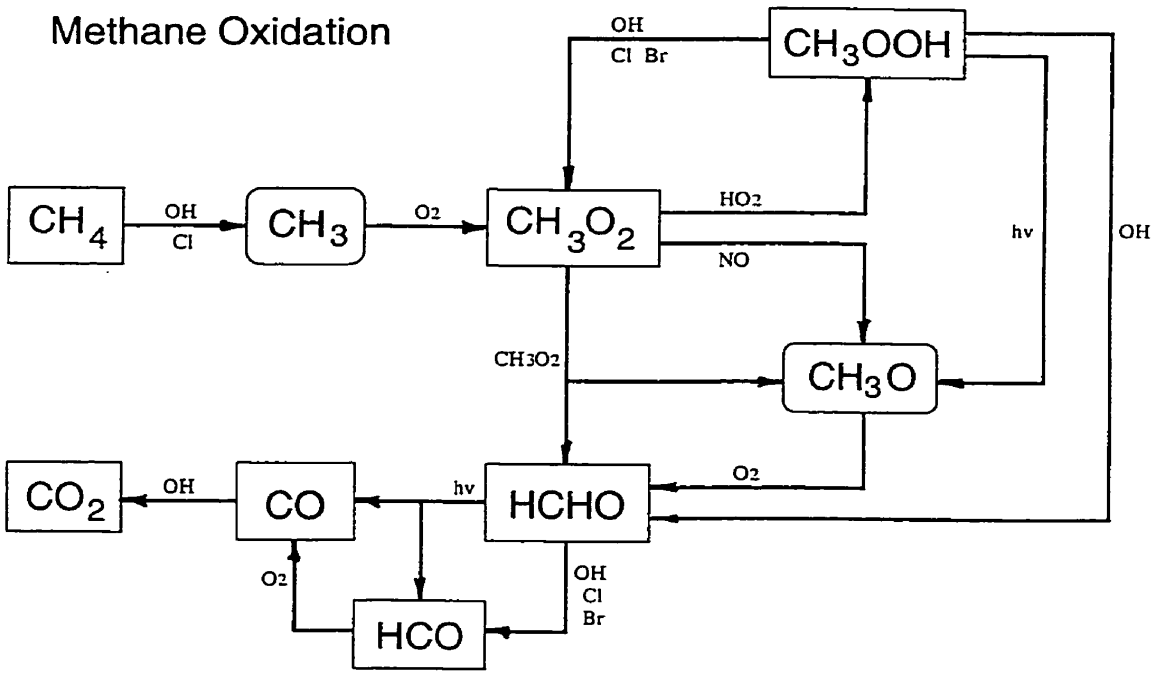

Diagram 4.1.3
Summary of Methane Chemistry

Section 4.2 Description of Chemical Solver

The rate of change of concentration for a chemical species x_i, without considering the effect of transport in its continuity equation can be written as

$$\frac{d}{dt}[x_i] = \frac{d}{dt}mf_i = P_i - L_i m f_i. \tag{4.2.1}$$

In the above, f_i is the mixing ratio for x_i while m and t are the total number density (molec.cm^{-3}) and time (sec), respective. P_i and L_i are the production rate (molec.cm^{-3}sec^{-1}) and loss frequency (sec^{-1}) for x_i, respectively.

In a system with N species and mixing ratios $f_1, f_2, ...f_N$, the above equation represents a system of non-linear differential equations with P_i and L_i both functions of $f_1, f_2, ...f_N$:

$$P_i = P_i(f_1, f_2, ...f_N); \tag{4.2.2}$$

$$L_i = L_i(f_1, f_2, ...f_N). \tag{4.2.3}$$

In such a system, Equation 4.2.1 can be written in the vector-valued differential equation :

$$\frac{d}{dt}\vec{f} = \vec{S}. \tag{4.2.4}$$

with

$$\vec{f} = [f_1, f_2, ...f_N]^T \tag{4.2.5}$$

and

$$\vec{S}(\vec{f}) = [S_1(\vec{f}), S_2(\vec{f})...S_N(\vec{f})]^T. \tag{4.2.6}$$

which is a forcing vector-value function,

$$\vec{S} = \frac{1}{m}\vec{P} - [L]\vec{f}. \tag{4.2.7}$$

In the above $\vec{P} = [P_1, P_2...P_N]^T$ is the production vector and [L] is a loss frequency diagonal square matrix such that

$$[L]\vec{f} = [L_1 f_1, L_2 f_2 ... L_N f_N]^T \tag{4.2.8}.$$

To ensure numerical stability in computation, Equation 4.2.4 is approximated in Euler backward or fully implicitly where $\vec{S}$ or the RHS of Equation 4.2.2 is expressed in terms of unknown quantities at $t+1$, i.e.,

$$\frac{\vec{f}_{t+1} - \vec{f}_t}{\Delta t} = \vec{S}_{t+1}. \tag{4.2.4}$$

The above can be expressed as a multi-valued, nonlinear vector function.

$$\vec{G}_{(\vec{f}_{t+1})} = \vec{f}_{t+1} - \vec{f}_t - \vec{S}_{t+1}\Delta t = 0 \tag{4.2.5}$$

which can be solved by Newton method of iteration [*Burden & Faires*, 1989, pp. 537 – 539]

$$\vec{f}_{t+1}^{(n+1)} = \vec{f}_{t+1}^{(n)} - [J]^{-1}\vec{G}, \qquad n = 0, 1, 2 \cdots \tag{4.2.6}$$

$\vec{f}_{t+1}^{(n=0)}$ is the first guess or approximation of the root. And $[J] = [J]_{(\vec{f}_{t+1})}$ in the above is the Jacobian matrix whose elements $J_{ij} = \partial G_i / \partial f_j$. In the model, the inverse of the Jacobian matrix, $[J]^{-1}$, is not computed but the linearized equation are solved using the method of Gaussian elimination with back substitution [*Press et al.*, 1986, pp. 24 – 31]. The iteration is terminated when

$$\frac{\vec{f}_{t+1}^{(n+1)} - \vec{f}_{t+1}^{(n)}}{\vec{f}_{t+1}^{(n)}} < 10^{-6}. \tag{4.2.7}$$

During the computation, Δt is set to 1 hour. Test runs indicated that this gave adequate accuracy while shortening the time required to run the simulation.

Section 4.3 Description of Photodissociation Rate Calculation

The photodissociation rate, J_i for a given photochemical reaction i, at position z for a local solar zenith angle χ can be written as [*Tyndall & Orlando*, 1999]

$$J_i(\vec{z},\chi) = \int_\lambda Q_i(\lambda)\Phi_i(\lambda)E(\vec{z},\chi,\lambda)d\lambda \tag{4.3.1}$$

where $Q_i(\lambda)$ is the cross-section of the species photolyzed; $\Phi_i(\lambda)$ is the quantum yield for the particular process; and

$$E(\vec{z},\chi,\lambda) = \int_{\text{sphere}} I(\vec{z},\chi,\lambda,\hat{\Omega})d\hat{\Omega}\cdot\hat{a} \tag{4.3.2}$$

is the solar actinic flux or mean radiance at position for a local solar zenith angle (photons·cm^{-2}s^{-1}nm^{-1}). It quantifies the rate at which photons at a specific wavelength are available to a infinite small sphere. $I(\vec{z},\chi,\lambda,\hat{\Omega})$ is the radiance [*Brasseur & Solomon* 1984, p.108] which is defined as the rate of photons crossing a unit area, $\hat{a}$, normal to the beam direction, per unit solid angle $\hat{\Omega}$, per wavelength interval (photons·cm^{-2}s^{-1}steradian^{-1}nm^{-1}). For box model simulation, the atmosphere can be simplified by treating it a laterally homogeneous so that the only spatially variation of the radiance is in the vertical direction. Thus the position vector in above equations represents altitude, z ($= |\vec{z}|$). Mean radiance flux can be described by the extraterrestrial flux E_∞ being attenuated by an effective transmission function, T_r, and enhanced by a term A representing scattering, i.e.,

$$E(z,\chi,\lambda) = E_\infty(\lambda)(T_r(z,\chi,\lambda) + A(z,\chi)). \tag{4.3.3}$$

The transmission is expressed by the simple Beer-Lambert law,

$$T_r(z,\chi,\lambda) = e^{-\tau(z,\chi,\lambda)}, \tag{4.3.4}$$

which describes the attenuation of solar radiation due to absorption by gas molecules in the atmosphere. The term A allows for Rayleigh scattering of the

solar beam due to N_2 and O_2, and for reflection off a Lambertian surface. A detailed description of this effective scattering function can be found in *Yung* [1976], and its solutions is available in *Templeton & McConnell* [1989]. The term τ in Equation 4.3.4 is the slant optical depth,

$$\tau(z, \chi, \lambda) = \frac{1}{\cos\chi} \sum_{\text{attenuator}} \int_z^\infty Q_i(\lambda) n_i(z') dz'. \tag{4.3.5}$$

In the above, Q_i is the total absorption cross section of species i, and $n_i(z)$ is the number density of species i at altitude z.

For this box model the radiation transfer is applied only for the atmosphere below 20 km. It is assumed that extraterrestrial flux E_∞ is attenuated by 90% of the O_3 column ($\approx 10^{19}$molec.cm^{-2}) which is in the stratosphere. Below this, a full radiation solution for the mean radiance with scattering and absorption is calculated as described above. The integral in Equation 4.3.1 is integrated starting from 300 nm since the radiation with wavelength less than 300 nm does not penetrate into the lower troposphere. Also, with the exception of NO_3, wavelength greater than 400 nm is unimportant for all the species involved. Thus, the integration stops at 400 nm†. For NO_3, the photolysis rate is assign a value of 2.20×10^{-2}sec^{-1} when χ is greater than zero. Moreover, because absorption due to O_2 in this region is not important, the summation in Equation 4.16 only involves the O_3 term. The wavelength integration is performed at 5 nm interval, this is satisfactory since O_3 cross section in this region does not exhibit fine structure. Since Rayleigh scattering is important in the lower troposphere where the air density is greatest, the evaluation of the effective scattering function, A, required the first 15 km of the atmosphere in the model is divided into 10 layers. This allows photons be scattered several times as they propagate through the atmosphere. The Lambert surface albedo is set at 0.7 to simulate photolysis rate enhancement due to reflection above snow surface [*Kondratyev*, 1972]. The local zenith angle χ, is calculated for

† The threshold for NO_2.

82.5 °N (i.e., latitude of Alert) from Julian Day (JD) 90 and ends before JD 115. The results of photolysis rate constants calculated for the first kilometer above ground are used in the chemical solver. The results of these calculation can be found in Appendix B.

Chapter V
Discussion of Simulation, Part I
Bromine Chemistry & Ozone Destruction

Section 5.1 Autocatalytic Release of Bromine

During the first three days of the simulation (JD 90 to JD 93), the simulated air parcel is bromine free. All the bromine in the model (100 pptv) resides on the snow pack in the form of Br^- (Figure 5.1.1c). As suggested by *McConnell et al.* [1993] (Section 2.5), this Br^- represents bromine of oceanic origin accumulated over the period of dark winter. In this model, the release of bromine from the snow pack into the atmosphere requires a seed. For this, 3.5 pptv of $CHBr_3$ is added to the model at JD 93 (Figure 5.1.1b). In the presence of solar radiation, $CHBr_3$ photo-dissociates yielding Br atoms with a rate about 0.3 pptv per day. Clearly, at this rate the amount of bromine added to the atmosphere is small

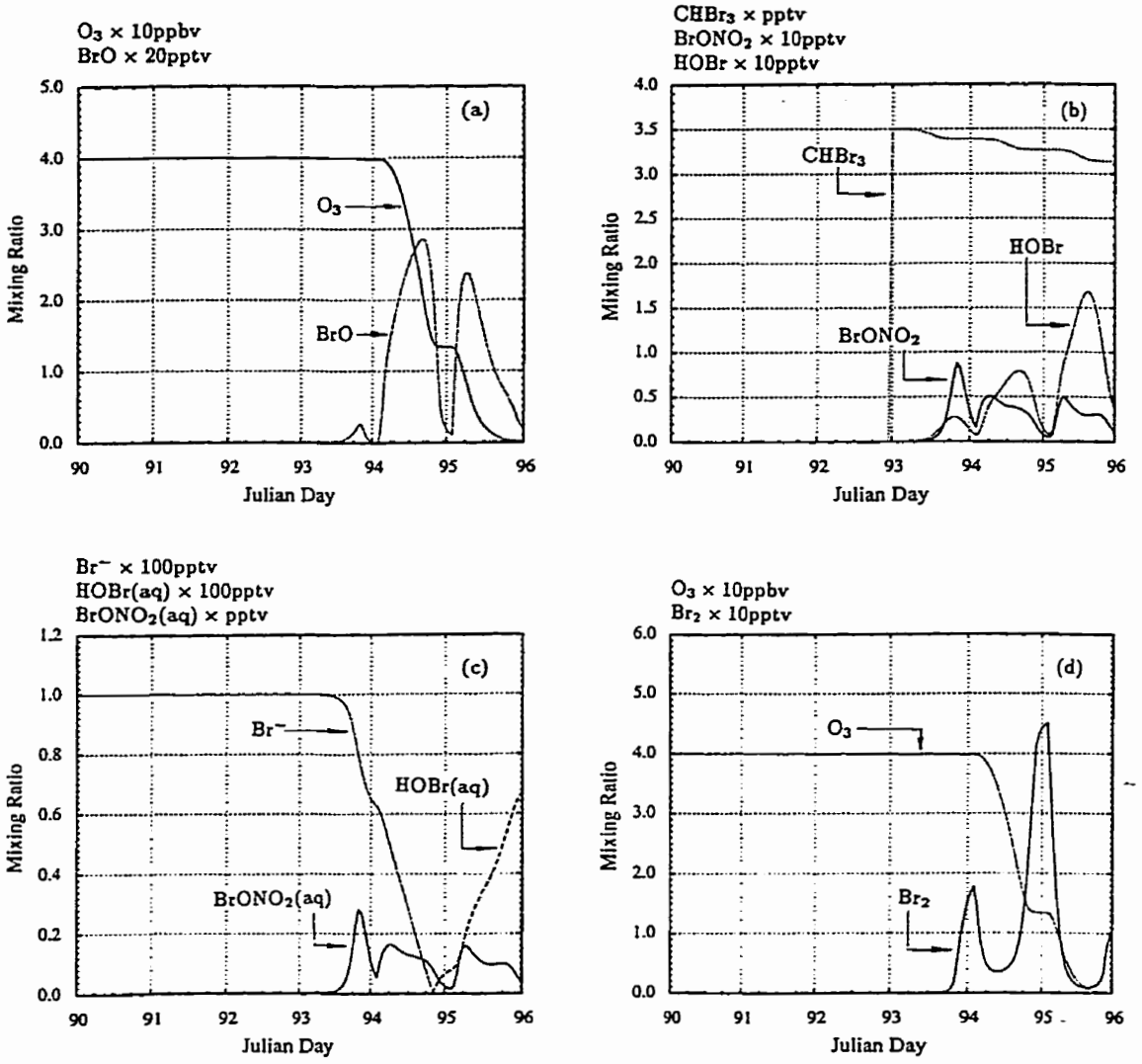

Figure 5.1.1

Plots of mixing ratio of various species (scaled) during the autocatalytic release of bromine. See text for description.

and will have little impact on the level of O_3. Figure 5.1.1a shows that after the addition of $CHBr_3$, the O_3 level remains at its typical early spring value of 40 ppbv. In order to deplete O_3 at a noticeable rate, for example: one to two ppbv a day, mixing ratios of bromine of about 10 pptv must be present in the form of BrO. The time series of BrO is shown together with that of O_3 in Figure 5.1.1a. BrO is not visible until about JD 93.5, half a day after $CHBr_3$ initiation. The sequence of bromine release from Br^- begins when the first Br atom reacts with O_3 to form BrO. Then, in the presence of HO_2 and NO_2, BrO reacts to yield HOBr and $BrONO_2$. The time series for HOBr and $BrONO_2$ are plotted in Figure 5.1.1b. Note that HOBr and $BrONO_2$ are not visible in the plot until their precursor, BrO, becomes available. Both HOBr and $BrONO_2$ can directly diffuse into the aqueous phase resulting in the formation of HOBr(aq). As was discussed in Section 2.6, this HOBr(aq) reacts with Br^- to release *another* bromine into the atmosphere. Thus, as proposed by *Mozurkewich* [1995], a chain reaction begins and the transfer of bromine from the snow pack into the atmosphere speeds up rapidly. This rapid transfer of bromine can be seen in Figure 5.1.1c (after JD 93.5) where levels of Br^- rapidly decline. And in less than two days (at JD 94.8) Br^- is exhausted.

The rates at which HOBr and $BrONO_2$ transfer into the aqueous phase are shown in Figure 5.1.2a and Figure 5.1.2b, respectively. Their time series have profiles similar to the mixing ratio of their respective gaseous precursors shown in Figure 5.1.1b. This is expected since their gas to liquid transfer rate are parameterized as first order reaction rates (see Chapter IV). The uptake of HOBr can directly supply HOBr(aq). To supply HOBr(aq) from $BrONO_2$, however, $BrONO_2$ must first diffuse into the aqueous phase and then hydrolyzes to HOBr(aq). This hydrolysis rate is plotted in Figure 5.1.2c. In this model, the hydrolysis reaction for $BrONO_2$ is also parameterized as a first order reaction rate. Thus, under quasi-steady-state conditions, the rate at which $BrONO_2$(aq) converts to HOBr(aq) is the same as the rate at which $BrONO_2$ diffuses into the

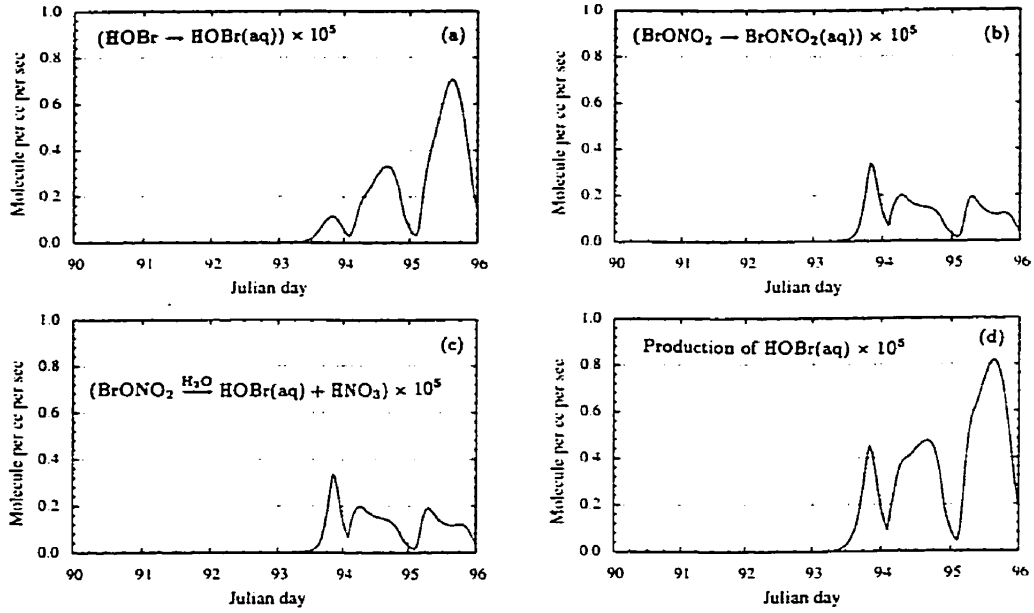

Figure 5.1.2

The time series for the rate of reaction involved in heterogeneous reactions during the release of bromine from Br^-. Panel (a) and (b) shows the rates at which HOBr and $BrONO_2$ diffuse into the aqueous phase respectively. Panel (c) is the rate at which $BrONO_2$ hydrolyzes to HOBr(aq). Panel (d) is the total HOBr(aq) production rate (i.e., (a) + (c)). (continue to next page)

aqueous phase* (compare Figure 5.1.2b to Figure 5.1.2c). It can be seen during the first 30 hours of Br^- release (JD 93–94.25), $BrONO_2$ plays a more important role in supplying HOBr(aq). This is because there is more NO_2 available initially to form $BrONO_2$. The relative abundance of $BrONO_2$ and HOBr in this model

* The rate equation for $BrONO_2(aq)$ is

$$d/dt[BrONO_2(aq)] = -k_{hydrolysis}[BrONO_2(aq)] + D_{gas \rightarrow liquid}[BrONO_2].$$

Under quasi-steady-state the above is close to zero. and loss term equals the production term.

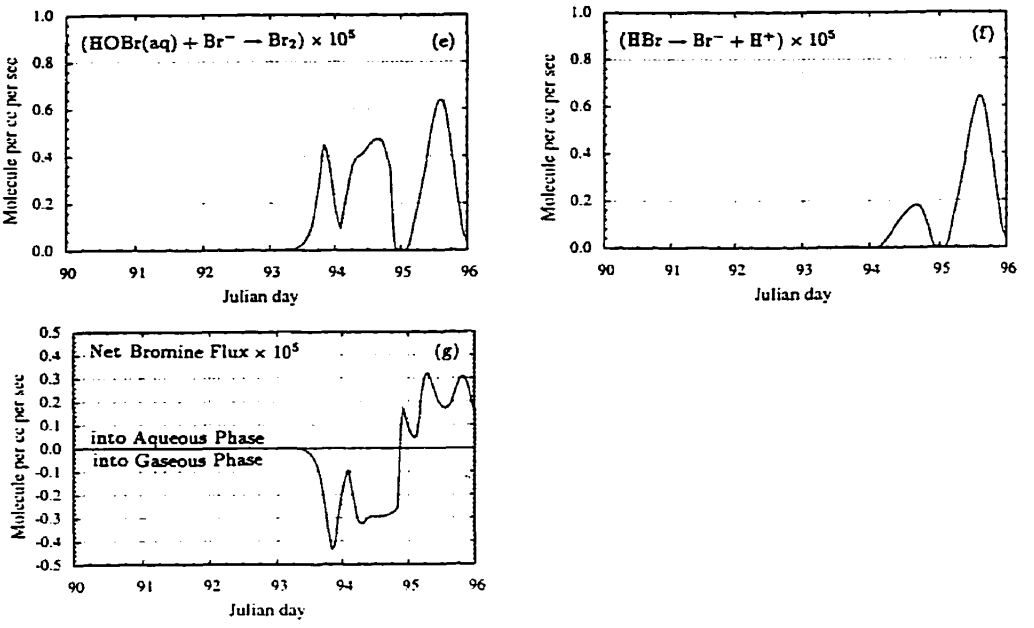

Figure 5.1.2 (continue from previous page)
The time series for the rate of reaction involved in heterogeneous reactions during the release of bromine from Br^-. Panel (e) is the rate for the reaction between Br^- and HOBr(aq). The rate at which HBr diffuses into the aqueous phase to form Br^- is plotted in Panel (f). Panel (g) illustrates the net flux of bromine transfer between gaseous phase and aqueous phase. Positive rate indicates that bromines flux is from the atmosphere to the aqueous phase.

depends on the relative availability of NO_2 and HO_2. The behavior of $BrONO_2$ and HOBr shall be discussed in Section 5.4. Figure 5.1.2d shows the total production rate of HOBr(aq) due to the contributions of both $BrONO_2$ hydrolysis and HOBr diffusion.

With the mechanism of *Fan & Jacobs* [1992] in the model, HOBr(aq) reacts with Br^- to form Br_2 which is then directly released into the atmosphere. The rate of which Br_2 is released from the aqueous phase is shown in Figure 5.1.2e. As pointed out in Chapter IV, the reaction rate of *Fan & Jacobs*

[1992] in the model is limited by uptake of $BrONO_2$, HOBr and HBr. Therefore, the sum of Fig 5.1.2d and Fig 5.1.2f is equal to Figure 5.1.2e. It can be seen, the release of Br_2 increases exponentially and reaches about $4.4 \times 10^4 molec.cm^{-3}s^{-1}$ (or 5.3 pptv per hour, see Figure 5.1.2e) at JD 93.75. Since Br_2 contains two Br atoms, this is equivalent to $8.8 \times 10^4 molec.cm^{-3}s^{-1}$ (10.6 pptv per hour) of bromine liberated into the atmosphere. This magnitude is *twice* as much as the sum of all the channels in the model by which bromine can be transfered into the aqueous phase. This is in agreement with the amplifying factor of 2 for the the autocatalytic release of bromine proposed by *Mozurkewich* [1995] (see Section 2.6). With the rate of bromine out of aqueous phase greater than that going into the aqueous phase, a net transfer of bromine into the atmosphere occurs. This is shown in Figure.5.1.2g. Negative rates imply bromine is lost from the aqueous phase to the atmosphere.

Toward the end of the day bromine activity slows down (see Figure 5.1.1 and 5.1.2, around JD 93, JD 94, JD 95 and JD 96), all bromine species except Br_2 (Figures 5.1.1d), reach a minimum. This occurs because solar radiation has declined. When solar radiation is high, Br_2 produced by rapid BrO self-reaction or by the aqueous reaction between Br^- and HOBr(aq) photolyzes rapidly to yield Br atoms. As the sun sets, however, this path is broken and bromine in the model accumulates as Br_2.

Section 5.2 Destruction of Ozone

It can be seen in Figure 5.1.1c, the release of Br^- begins in day 93. However, the depletion of O_3 lags behind the Br^- release. It begins a day later (day 94, Figure 5.1.1a). Before O_3 depletion begins, about 30 pptv of bromine has been released into the gaseous phase (this can be seen by the Br^- decrease in Figure 5.1.1c before JD 94). However, of this 30 pptv only about 3 pptv of BrO can form (see Figure 5.1.1a, from JD 93.5 to 94). This amount is too

low to cause any discernible amount of O_3 loss[§]. The amount of bromine as BrO is small at this time because by the time the release of Br^- picks up its momentum, the sun begins to set, this results in gaseous bromine accumulating as Br_2 (Figure 5.1.1d, JD 94). Note that although solar radiation is at a minimum during midnight, the release of bromine is not interrupted, (see Figure 5.1.2g, JD 94). This is because the remaining $BrONO_2$ and HOBr continue to supply HOBr(aq) to keep the mechanism of *Fan & Jacobs* [1992] in continuous operation.

As the sun rises the next morning, bromine in Br_2 is reactivated. With fresh Br atoms, the Br^- release speeds up, and in less than a day, all the aqueous bromine is released into the gas phase (Figure 5.1.1c, JD 94.74). During this period of rapid bromine transfer, BrO's level is greater than 50 pptv (Figure 5.1.1a, JD 94–95). With so much BrO, O_3 declines dramatically (Figure 5.1.1a, JD 94–95). By the time of the next sunset (end of JD 94) with all the bromine as Br_2, O_3 has reduced to one third of its initial amount. During the end of JD 94, the build up of Br_2 is the highest (about 45 pptv see Figure 5.1.1d, JD 95). This is equivalent to about 80% of total bromine in the model. The following morning, 90 pptv of bromine as Br_2 is released to reform the active bromine species. The bromine catalytic cycle regains its intensity and within half a day, the remaining 12 ppbv of O_3 is destroyed[†].

[§] Using $\frac{d[O_3]}{dt} = -2k[BrO]^2$, where $k = 3.28 \times 10^{-12} cm^3 molec^{-1} s^{-1}$, reaction rate coefficient of BrO + BrO. With 3 pptv of BrO, the rate of O_3 depletion is about 0.1 ppbv a day.

[†] Note, the term 'ozone destruction' does not imply zero O_3. It implies O_3 mixing ratio has dropped below its instrumentation detection limit – usually about half ppbv. The lowest O_3 level in this simulation is of the magnitude of 10^{-12} (i.e., pptv).

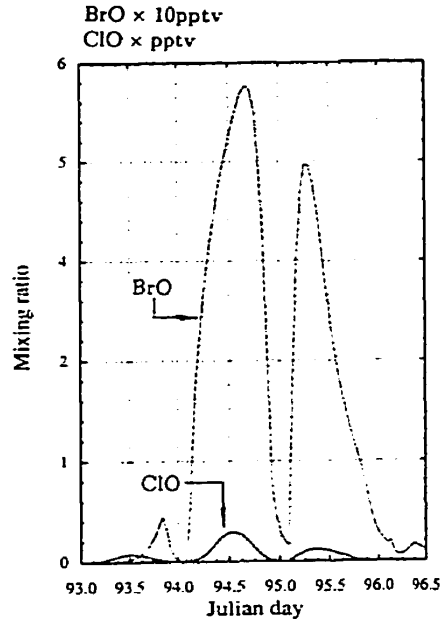

Figure 5.2.1

Plots of mixing ratios for BrO and ClO over the period when ozone is declining . To fit both species in the plot the mixing ratio of BrO is scaled by a factor of 0.1.

As was pointed out in Section 2.2, a catalytic cycle is needed for the bromine destruction of O_3 because the amounts of O_3 are so much greater than the amounts of Br atoms. After the destruction of O_3 by Br atoms, BrO is formed. To destroy more O_3, the bromine in BrO must converted back to Br atoms. This conversion of BrO to Br atoms is the slowest link in the chain. And thus, the rate of which O_3 can be destroyed is limited by this link. There are several channels that can convert BrO to Br atoms. The fastest one is the self-reaction of BrO (cf. Section 2.2). To estimate how much O_3 is destroyed due to this channel, Eq 2.3.3 is used. After the initialization, this equation becomes:

$$\Delta[O_3]_{BrO}(t) = 2k_\alpha \int_{JD90}^{t} [BrO(t)]^2 dt. \qquad (5.2.2)$$

The above is plotted in Figure 5.2.2, denoted (i). The figure shows the amount of O_3 lost up to 39 ppbv.

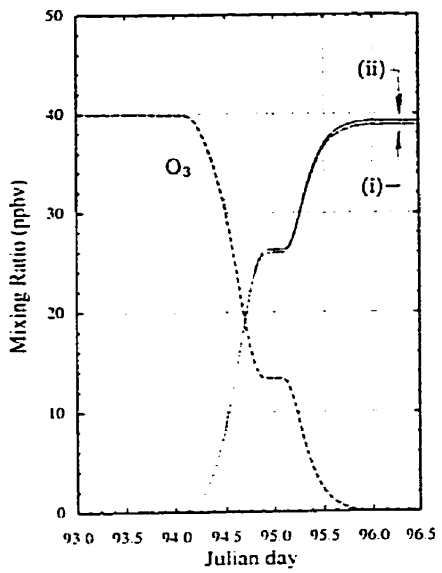

Figure 5.2.2

Mixing ratio of O_3 (dotted line) with theoretical estimation of O_3 destroyed (small doted lines). Plot (*i*) is the contribution of O_3 lost due its reaction with Br atoms form as BrO self reacts; and plot (*ii*) is O_3 lost due to (*i*) plus reaction of O_3 with Br and Cl atoms form when BrO and ClO react.

As was pointed out in Section 3.8, the synergistic reaction between ClO and BrO can also covert bromine in BrO to Br atoms. However, given the amount of ClO in the model (less than 1 pptv, see Figure 5.2.1), the contribution of O_3 loss due to this channel is insignificant. To see this, the expression Eq 3.8.7 is integrated to reveal the amount of O_3 destroyed:

$$\Delta[O_3]_{BrO.ClO}(t) = -\int_{JD90}^{t} (2\ k_a[BrO(t)]^2 + 1.47\ k_3[BrO(t)][ClO(t)])\ dt. \qquad (5.2.2)$$

The result of this is plotted in Figure 5.2.2 (denoted by ii). It can be seen that the additional O_3 destruction due to Br and Cl atoms release when ClO and BrO react (i.e., $1.47\ k_3 \int_{JD90}^{t}[ClO][BrO]dt$) is only about 0.2 ppbv.

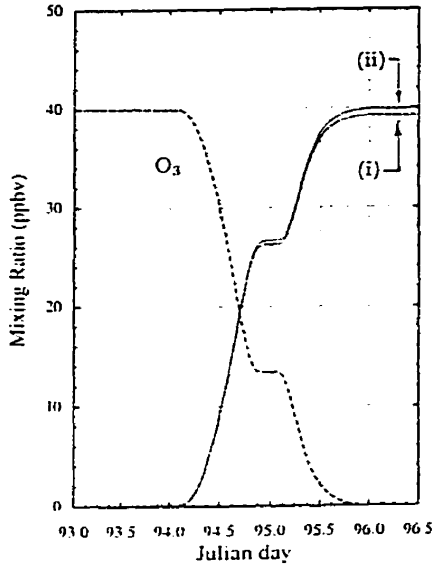

Figure 5.2.3

Mixing ratio of O_3 (dotted line) with theoretical estimation of O_3 destroyed (small dotted line). Plot (*i*) is the contribution of O_3 lost due to its reactions with Br and Cl atoms formed when BrO self-reacts and when BrO and ClO react (same as plot (*ii*) in Figure 5.2.2); and plot (*ii*) is O_3 lost due to (*i*) plus its reactions with Br atoms formed when $BrONO_2$ and HOBr are photolyzed and recycled, and when BrO reacts with NO.

The reaction of BrO with HO_2, NO_2 and NO followed by photo-dissociation or recycling by the mechanism of *Fan & Jacobs* [1992] also transforms bromine in BrO to Br atom (cf., Section 2.4). The rate of O_3 depletion contributed by these paths is:

$$\frac{d}{dt}[O_3(t)] = -\left(k_1[NO(t)][BrO(t)] + J_1(t)[HOBr(t)] + J_2(t)[BrONO_2(t)] + 2k_2[HOBr(aq)(t)][Br^-(t)]\right) \quad (5.2.3)$$

In this expression, k_1 is the reaction rate constant for NO + BrO; $J_1(t)$ and $J_2(t)$ are the time dependent photolysis rate of HOBr and $BrONO_2$, respectively. The last term in the expression is the contribution from heterogeneous recycling of *Fan & Jacobs* [1992] (which is Figure 5.1.2e ×2). The amount of O_3 destroyed due to these reactions is very small. The integrand of the above was calculated and superposed on the calculated result of Equation 5.2.2. The results of this are plotted in Figure 5.2.3, denoted (ii). It can be seen that the total amount

of ozone destroyed sum up to the initial amount of O_3 in the model – 40 pptv. For the setup of this model, self-reaction of BrO accounts for about 98% of the O_3 destroyed; interaction of BrO with ClO accounts for 0.5% ; and the interaction of BrO with NO_x and HO_2 accounts for 1.5% .

Section 5.3 Partitioning of Bromine

In Figure 5.3, the time series of bromine containing species are superposed on one another to form a partition map for the period around O_3 depletion (from JD 93 to JD 97). Thus, the distribution of bromine in various bromine containing species can be understood at a glance. This gives an overview of bromine chemistry in this modeling exercise; it displays how bromine partitioning changes as the model evolves. The following highlights some of the noticeable features.

- The plot begins at JD 93, when seeding occurs. At this time there is 100 pptv of bromine in the aqueous phase (Br^-) and 10.5 pptv of bromine in the gaseous phase ($CHBr_3$).
- The sum of inorganic bromine is 100 pptv at JD 93. Over the period of four days (JD 93 to JD 97), this sum increases slightly by about 2 pptv. This increase occurs because $CHBr_3$ (the only organic bromine in the model) has photo-dissociated to release Br atoms which form part of the inorganic bromine family.
- Bromine is transfered back and forth between the aqueous phase and gaseous phase:
  JD 93.5 to 94.8: transfers out of aqueous phase (Br^- decreases);
  JD 94.8 to 96.2: transfers into aqueous phase (HOBr(aq) increases);
  JD 96.2 to 96.4: transfers out again (HOBr(aq) declines);
  JD 96.4 to 96.7: returns to aqueous phase (Br^- increases);
  JD 96.7 to 97.0: transfers out into gaseous phase (Br^- decreases).
- Notice that HOBr(aq) and Br^- are never present simultaneously.

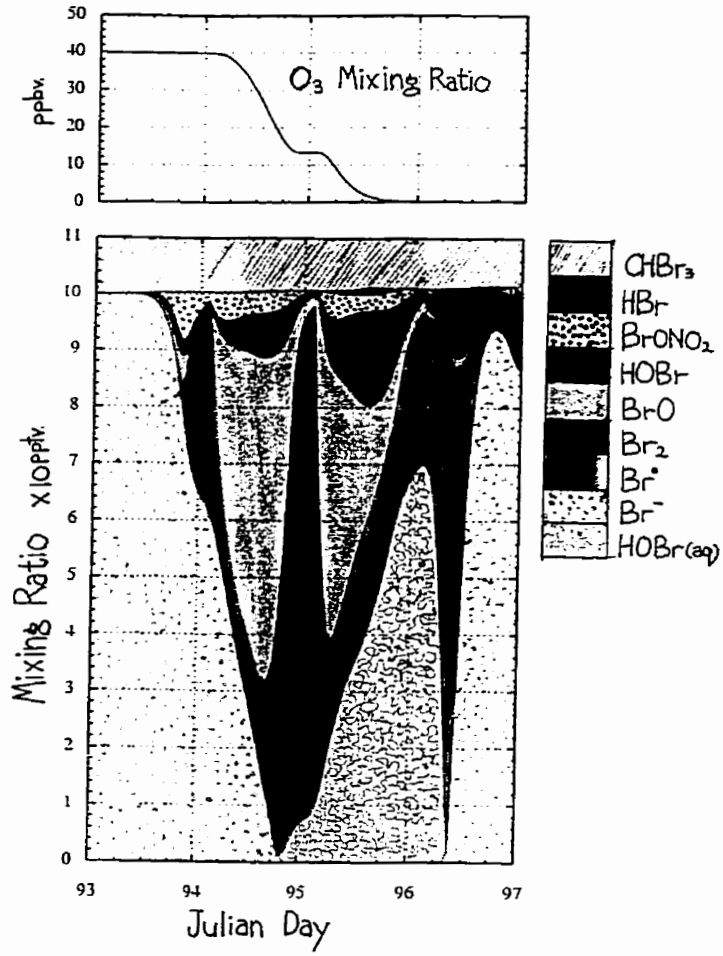

Figure 5.3.1
Bromine partition map. See text.

- During the period of O_3 depletion (JD 94 to JD 96) and immediately after the depletion (JD 96 to 96.5), bromine in the model is mostly gaseous.
- After O_3 depletion (after JD 96) almost all the bromine in the model is in the form of Br atoms.
- When solar radiation is low, gaseous inorganic bromine accumulates as Br_2. This effect is especially noticeable at around JD 95 where almost all the bromine is in the form of Br_2.

- When solar radiation is high, gaseous inorganic bromine is in various forms. If O_3 is present, then BrO dominates. If O_3 is absent, then Br atom dominates.
- Both HOBr and $BrONO_3$ are present after the initial release of bromine from Br^-. However, there is more $BrONO_3$ in the beginning of the O_3 depletion period, but more HOBr in the end of O_3 depletion period. Both of them are modulated by the variation of solar radiation.
- Two bromine containing species, BrCl and $BrONO_2$(aq) do not appear in the partitioning map. This is due to their low concentration in the model. They never exceed 0.3 pptv.

Section 5.4 $BrONO_2$ and HOBr in the Atmosphere During O_3 Depletion

In the model, HOBr and $BrONO_2$ are necessary for the release of Br^- residing in the snowpack (cf., Section 2.7). Because of this, they play an important role in O_3 depletion. Figure 5.4.1 shows the time series for HOBr and $BrONO_2$. HOBr is formed by the reaction between BrO and HO_2 and $BrONO_2$ is formed by the reaction between BrO and NO_2. The loss of both are via diffusion and by photo-dissociation. It can be seen in Figure 5.4.1 that both HOBr and $BrONO_2$ cannot appear until their common precursor BrO appears. Precursors of HOBr and $BrONO_2$ are shown in Figure 5.4.2a and Figure 5.4.2b, respectively. It can be seen, the levels of both HO_2 and NO_2 are reduced as the result of increased loss due to the presence of BrO.

It is of interest to note that the ratio of HO_2 to NO_2 can be related to the ratio of HOBr to $BrONO_2$,

$$\frac{[HO_2]}{[NO_2]} \propto \frac{[HOBr]}{[BrONO_2]}. \tag{5.4.1}$$

This is possible because the reaction rate equations for both HOBr and $BrONO_2$

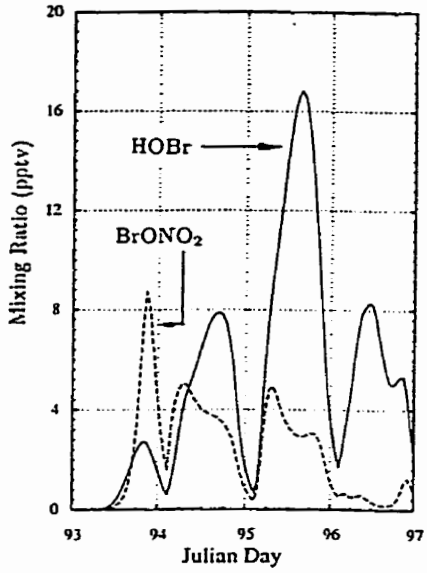

Figure 5.4.1

HOBr and $BrONO_2$ during O_3 depletion period. It can be seen both of them appear at the same time and both are modulated by the diurnal cycle of solar radiation. They differ from each other in their change in daily peaks levels.

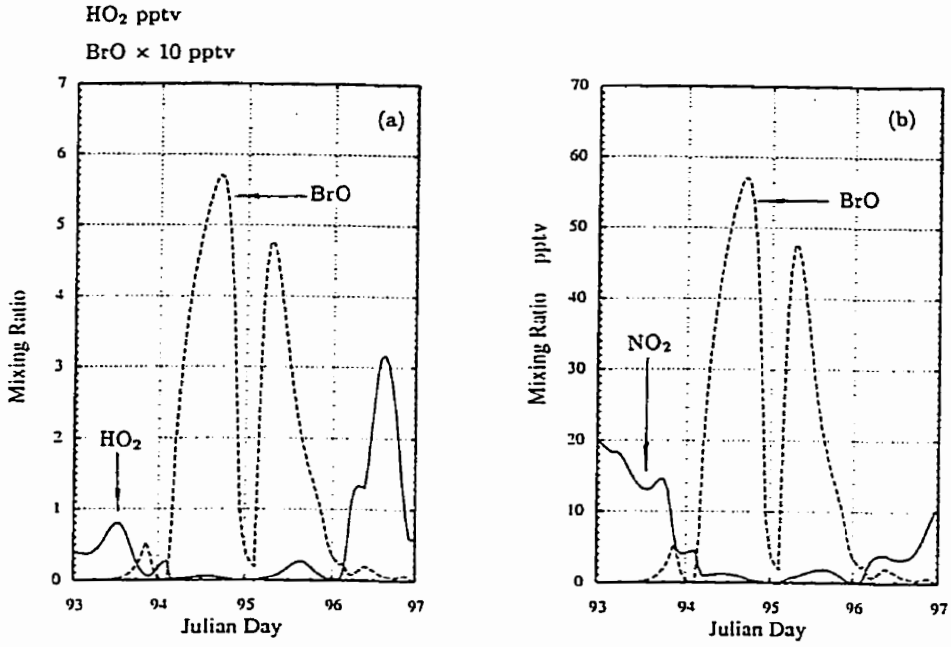

Figure 5.4.2

The figure shows precursors of HOBr (panel a) and $BrONO_2$ (panel b).

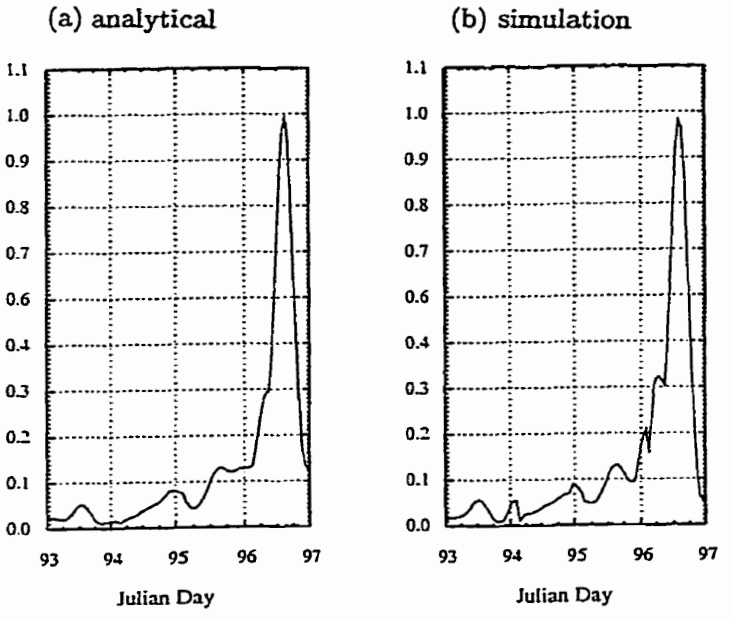

Figure 5.4.3
Plot of the ratio of HO_2 to NO_2. Panel (a) is the analytical results (i.e., Eq 5.4.3) and Panel (b) is the results of the simulation.

are relatively simple†. The above is plotted in Figure 5.4.3a. It can be

† The reaction rate equations for both HOBr and $BrONO_2$ are

$$\frac{d}{dt}[HOBr] = -(D_{HOBr} + J_{HOBr})[HOBr] + k_1[HO_2][BrO]$$

$$\frac{d}{dt}[BrONO_2] = -(D_{BrONO_2} + J_{BrONO_2})[BrONO_2] + k_2[NO_2][BrO]$$

where, D_{HOBr} and D_{BrONO_2} are first order diffusion rate coefficients; J_{HOBr} and J_{BrONO_2} are photolysis rate coefficients; k_1 and k_2 are the reaction rate coefficients for BrO reacting with HO_2 and NO_2 respectively. Set the above to zero and eliminate common term, [BrO], then

$$\frac{[HO_2]}{[NO_2]} = \frac{[HOBr]}{[BrONO_2]}\left(\frac{(D_{HOBr} + J_{HOBr})k_{x2}}{(D_{BrONO_2} + J_{BrONO_2})k_{x1}}\right)$$

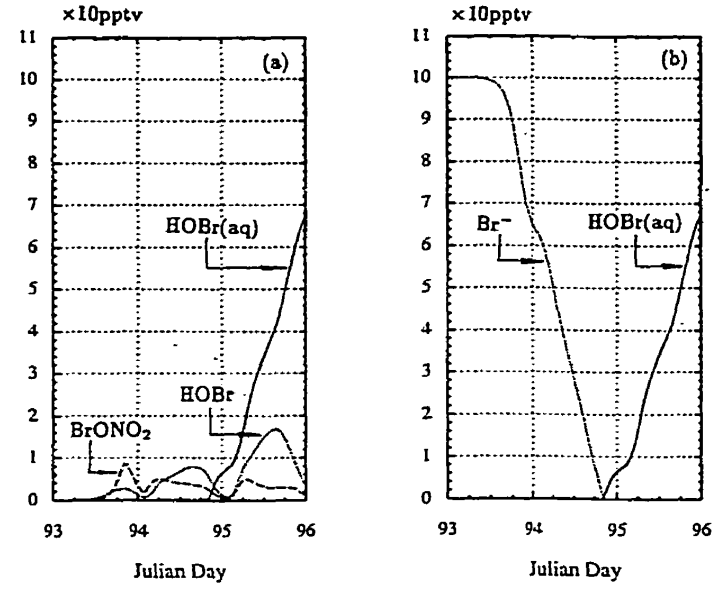

Figure 5.5.1

Panel (a) shows the mixing ratio of HOBr, $BrONO_2$ and HOBr(aq). Panel (b) shows the mixing ratio of Br^- and HOBr(aq). Notice that although HOBr and $BrONO_2$ are the precursors of HOBr(aq), their presence do not result in immediate accumulation of HOBr(aq). It can be seen in Panel (b) that HOBr(aq) only begins to appear after Br^- has depleted.

seen that the analytical result is comparable with the modeling result (Figure 5.4.3b).

Section 5.5 HOBr(aq) and Br^- in the Aqueous Phase

The precursors of HOBr(aq) are HOBr and $BrONO_2$. However, Figure 5.5.1a shows that the presence of HOBr or $BrONO_2$ does not result in immediate increase in HOBr(aq)'s level. HOBr(aq) appears only after Br^- has depleted (Figure 5.5.1b, JD 94.8). During the initialization of this model, there was no HOBr(aq). All of the bromine was initialized in the form of Br^-. When $CHBr_3$ is introduced to initiate the autocatalytic release of bromine, HOBr(aq) begins to appear in small quantities. This initial HOBr(aq) is less than Br^-. Under this condition

of excess Br^-, this newly formed HOBr(aq) is completely reacted, none is left in the aqueous phase. For this reason, no HOBr(aq) is present until Br^- depletes†.

With HOBr(aq) being available to react with Br^-, Br_2 forms and bromine from Br^- can be evolved into the atmosphere. However, a reverse process exists which works against this release — atmospheric bromine can return to the aqueous phase by HBr diffusion to replenish Br^-. Thus, for a net transfer of bromine from the snowpack to the atmosphere, HOBr(aq) must react with Br^- at a rate faster than Br^- is replenished. This condition is met as long as O_3 is present. With O_3 present, atmospheric bromine forms more HOBr and $BrONO_2$ than HBr, this ensures a transfer of bromine into the atmosphere. Figure 5.5.2 compares the supply rate of HOBr(aq) to that of Br^-, it can be seen, throughout the O_3 depleting period, the former is greater. From this one can see that *the presence of* O_3 *necessitates the release of* Br^-.

Once Br^- has been depleted (JD 94.8), HOBr, $BrONO_2$ and HBr continue to diffuse into the aqueous phase to supply HOBr(aq) and Br^-. With the supply rate of HOBr(aq) being greater (Figure 5.5.2)

$$P(HOBr(aq))^{\ddagger} > P(Br^-), \tag{5.5.1}$$

HOBr(aq) accumulates more rapidly than Br^-. This result in HOBr(aq) in excess of Br^- and the reaction between Br^- and HOBr(aq) is now limited by the supply rate of Br^-. And since this reaction is the loss for both Br^- and

---

† One can also understand this by noting that with Br^- in excess of HOBr(aq), the rate of reaction : $HOBr(aq)+Br^- \xrightarrow{H^+} Br_2+H_2O$, is limited by the rate of HOBr(aq) being supplied. Since this reaction is also the loss reaction for HOBr(aq), limiting it by the rate of which HOBr(aq) is produced, a zero net production of HOBr(aq) results.

‡ P(X) denoted the supply or production rate of X.

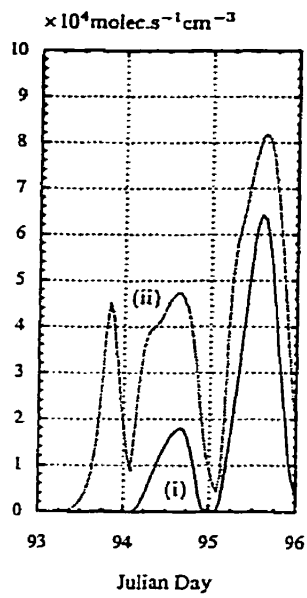

Figure 5.5.2

In this figure, the rate of formation for Br^- (i) is compared to the rate of formation for HOBr(aq) (ii). For the period shown, the rate of which HOBr(aq) can form is always greater then that of Br^-.

HOBr(aq),

$$L(Br^-)^{\S} = L(HOBr(aq)) = P(Br^-). \tag{5.5.2}$$

A zero net production for Br^- occurs. Br^- remains absent after its depletion (Figure 5.5.1b, after JD 94.8).

Section 5.6 BrO and Br Atom Levels Toward the End of O_3 Depletion

In Section 2.4, a mechanism for O_3 destruction with the bromine catalytic cycle was demonstrated. It was found that, before O_3 depletion, almost all the bromine in the catalytic cycle was in the form of BrO, with only a small amount in the form of Br atoms. This partitioning between BrO and Br atom remains until the level of O_3 is low. At low O_3, partitioning of bromine changes, with

§ L(X) denoted the loss rate of X.

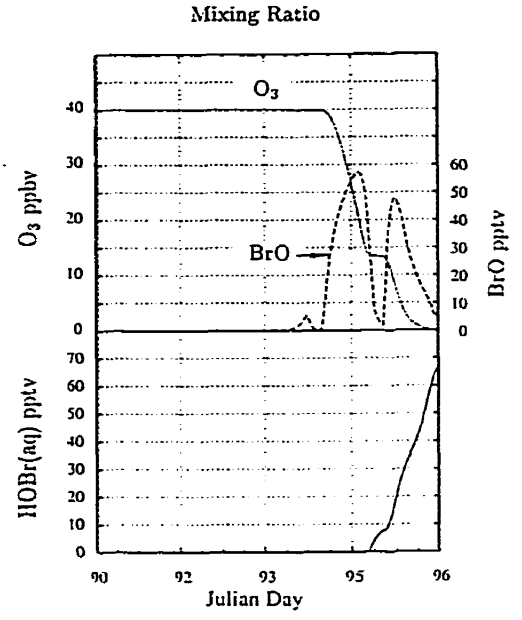

Figure 5.6.1

The upper plot shows time series of O_3 and BrO. The lower plot shows the time series of HOBr(aq). While O_3 is depleting, bromine in BrO is lost to form HOBr(aq). This conversion of bromine occurs in the period from JD 95.25 to 95.75. During this period, BrO decline from about 48 pptv to about 15 pptv (ΔBrO ≈ -33 pptv), while HOBr(aq) increase from about 16 pptv to about 50 pptv. (ΔHOBr(aq) $\approx +34$ pptv).

Br atom being the major form. As pointed out in Section 2.4, this is because there is no O_3 to react with the Br atoms.

In this simulation, other species are allowed to form. Therefore, when O_3 is depleting, the bromine in BrO can be transformed to HOBr and $BrONO_2$, both of which diffuse into solution to form HOBr(aq) (see Figure 5.6.1). With bromine in BrO diverted from Br atom formation into HOBr(aq) formation, the sudden rise of Br atoms such as that shown in Section 2.4 during the end of O_3 depletion is buffered (see Figure 5.6.2).

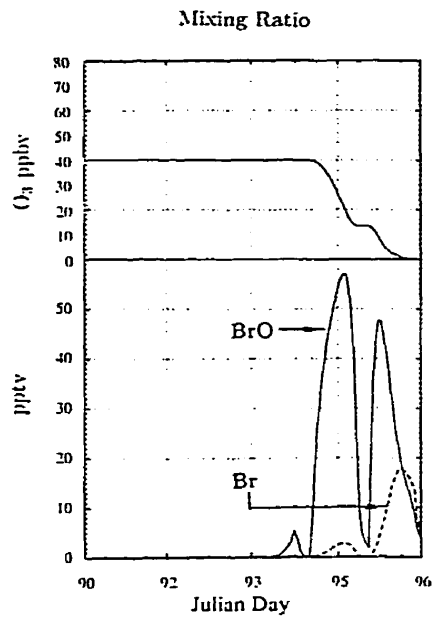

Figure 5.6.2

The mixing ratio of BrO and Br atom is plotted in the lower half of the figure. The mixing ratio of O_3 is plotted in the upper half of the figure. The sudden rise of Br atom like that in Section 2.4 (A pure bromine catalytic cycle model without interaction with NO_x and HO_x) does not occurs in this simulation. Previously in Figure 2.3.1, the magnitude of the Br atom increase mirrored the declining magnitude of BrO because all the bromines lost from BrO was converted to form Br atoms. In this simulation, however, while O_3 is depleting, bromine in BrO is diverted from Br atom formation to HOBr(aq) formation.

Section 5.7 Bromine Atom "Explosion"

In the previous section, it was seen that while O_3 is being destroyed, bromine in the atmosphere can transfer into the aqueous phase to form HOBr(aq). If HOBr(aq) were to increase continuously, all the bromine in the model would return to the aqueous phase‡. However, this does not occur because the level of HOBr(aq) changes from increasing to decreasing, and the bromine in HOBr(aq) is returned to the atmosphere in the form of Br atoms (Figure 5.7.1 after JD 96.6). Note the unusual amounts of Br atom – 80 pptv. The trigger for this shall

‡ This scenario does happen when chlorine level in the model increases. This shall be discussed in Section 6.5.

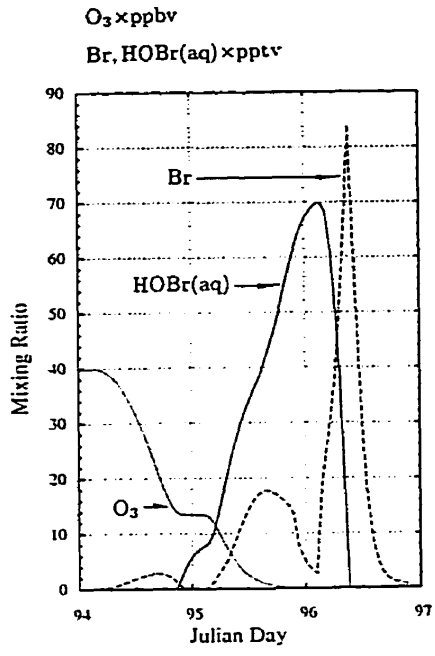

Figure 5.7.1

During JD 96 day, with the rapid release of bromine from HOBr(aq) into the atmosphere, a surge of Br atom (Br atom 'explosion') occurs. At the time this happens, O_3 has already been depleted, thus large amounts of Br atom can not be removed rapidly. As a result Br atom accumulates as high as 80 pptv.

Br atom sensitive species	Rate reaction coeficient ($cm^3 molec.^{-1} s^{-1}$)	Typical mixing ratio of Br atom sesitive species	Lifetime of Br atom (sec)
O_3	6.5×10^{-13}	10 ppbv	5
HO_2	1.3×10^{-12}	1 pptv	25×10^3
H_2O_2	5×10^{-17}	1 pptv	7×10^8
HCHO	6.5×10^{-13}	10 pptv	5×10^3

Table 5.7.1 Life time of Br atom against various species

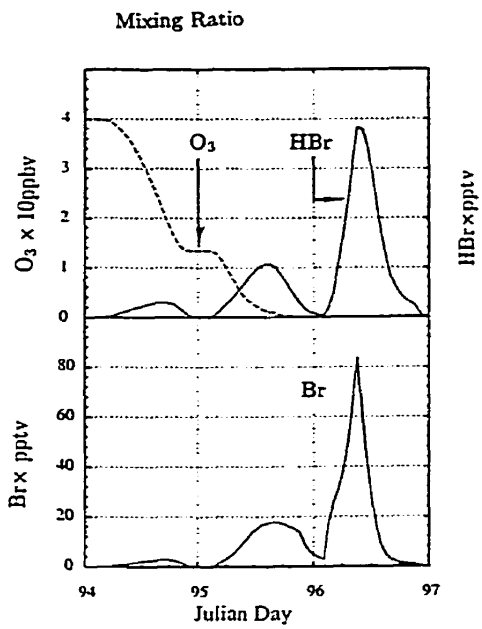

Figure 5.7.2

The figure shows the changes in HBr's level follow the changes of Br atom's level.

be discussed later. Had O_3 been present at this time, it could have rapidly reacted with Br atoms to form BrO. However, since O_3 is absent, Br atoms are channeled into HBr formation by reacting with HCHO, HO_2, and H_2O_2. The life time of Br atoms against the bromine sensitive species are tabulated in Table 5.7.1. It can be seen, compared to O_3, these species are inefficient in removing Br atoms. With a slow removal rate, Br atoms in the atmosphere rapidly accumulate and result in a Br atom 'explosion'. The time series of HBr is plotted with that of Br atom in Figure 5.7.2. The fact that the time series of HBr follows that of Br atom indicates that HBr is the product when Br atoms react. The amounts of HBr in the atmosphere is small (HBr peaks only at 3.8 pptv) because it is rapidly lost to the aqueous phase. The bromine in HBr lost to the aqueous phase is necessary to provide continuous Br^- to react with HOBr(aq) to fuel the bromine required for Br atom 'explosion'. It can be noted that this Br^- from HBr induces the release of another bromine in HOBr(aq)

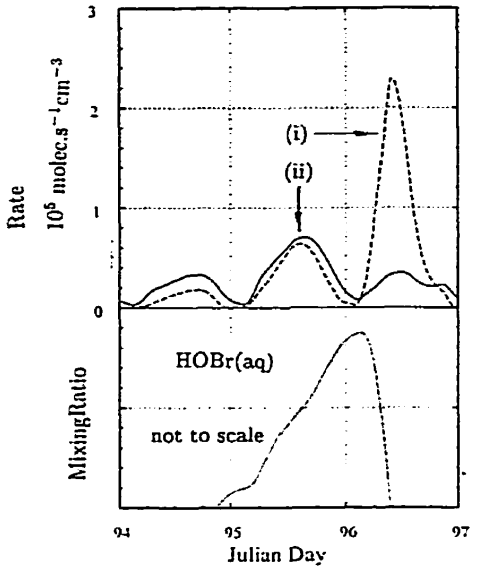

Figure 5.7.3

The upper plots compare the rate of Br^- being supplied (dotted line (i)) to the rate of HOBr(aq) being supplied (solid line (ii)). The lower plot is mixing ratio of HOBr(aq). At JD 96.2, the relative magnitude of the supply rate for Br^- changes from less to greater than that of HOBr(aq). This results in a change the direction of growth in HOBr(aq) from positive to negative.

into the atmosphere, with this new Br atom, another chain of bromine release begins. It is interesting to note that this process is the same as the initial release of bromine from the aqueous phase (before JD 94.8) — both processes are autocatalytic with amplification factor of 2. Their differences are, for the later case, the source of bromine is HOBr(aq) and the releasing agent is Br^-. For the earlier case, it was the reverse situation with the source being Br^- and the release agent being HOBr(aq).

The rapid release of HOBr(aq) resulting in the Br atom 'explosion' is triggered by O_3 depletion. While O_3 depletes, HOBr(aq) is in excess of Br^- (cf. Section 5.5). With this condition, the reaction for HOBr(aq) loss is limited by supply of Br^-.

$$L(HOBr(aq)) = P(Br^-) \tag{5.7.1}$$

However, with the absence of O_3, supply of Br^- is greater than the supply of

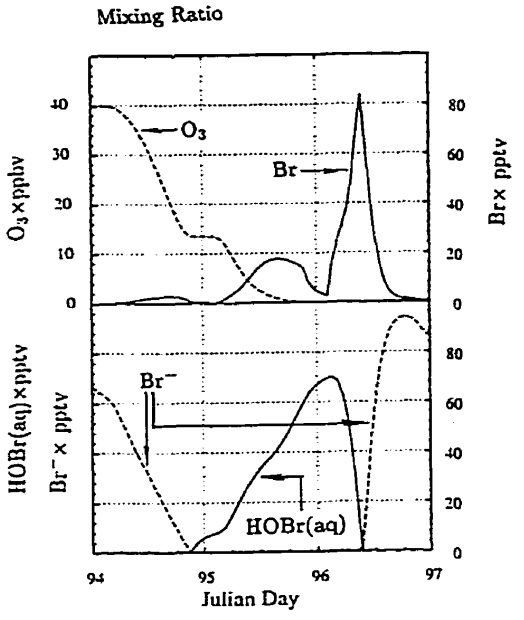

Figure 5.7.4

Time series of O_3 and Br^- are shown in upper plot. The lower plot shows time series for Br^- and HOBr(aq). The plot illustrates the rapid conversion of bromine in the Br atom 'explosion' to Br^- at about JD 96.35.

HOBr(aq)[†] (see Figure 5.7.3)

$$P(Br^-) > P(HOBr(aq)). \tag{5.7.2}$$

Thus, the loss of HOBr(aq) is greater than formation of HOBr(aq) — a net HOBr(aq) loss results. In this simulation, the cause and effect for Br atom 'explosion' being triggered by O_3 depletion is not obvious (the 'explosion' is delayed until the next morning). This is because O_3 depletion occurs immediately before the sun set. For this, bromine is tied up as Br_2 until the next morning. When solar radiation intensifies to release Br atom from Br_2 in the absence of O_3, HOBr cannot from. Instead, HBr is formed to allow the condition in Eq 5.7.2 which triggers the release of HOBr(aq).

[†] O_3 are required for BrO formation. Without BrO, no HOBr can form in the model.

The 'explosion' of Br atoms is short lived because the amount of HOBr(aq) is not unlimited. After HOBr(aq) depletes, Br^- cannot react and it accumulates — atmospheric bromine return to the aqueous phase. This is illustrated in Figure 5.7.4. As seen in the figure, before JD 96.6, the level of HOBr(aq) declines to sustain the rapid increase of Br atoms. After HOBr(aq) depletion, the rise of Br^- mirrors the decline of Br atoms.

Section 5.8 Activities After Ozone Depletion

Figure 5.8.1 shows results of O_3 and the bromine in the aqueous phase extended into the period after O_3 has depleted (from JD 97 to 105). It can be seen that O_3 is replenished slowly shortly after it is destroyed by the BrO catalytic cycle. Regeneration of O_3 is due to photolysis of NO_2[†]. However, this new O_3 can only reach 2 ppbv (at JD 100) before it is destroyed again. This second depletion can occur because BrO chemistry has been reactivated (see Figure 5.8.2). It is interesting to find that the reactivation is triggered by reformation of O_3. This O_3 reacts with Br atoms photo-dissociated from $CHBr_3$ to supply new HOBr(aq), and thus reactivate the autocatalytic release of bromine from Br^-. Unlike the first bromine release, the amount of O_3 to be destroyed is only 2 ppbv. This requires less time, and the auto catalytic cycle shuts off before all the Br^- is released.

[†] Note: One might have expected that O_3 level can be expressed in terms of the ratio of NO and NO_2. This relationship, however, is invalid here because chlorine chemistry is present.

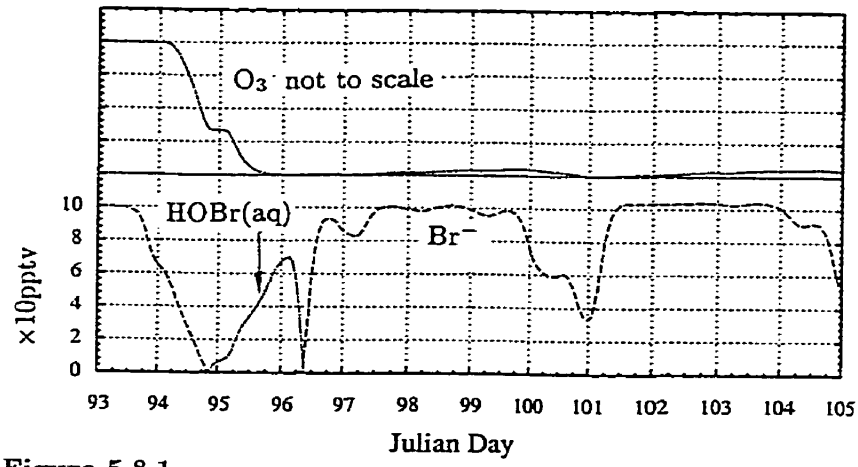

Figure 5.8.1

Extended plot of O_3 and aqueous bromine (i.e., Br^- and HOBr(aq)).

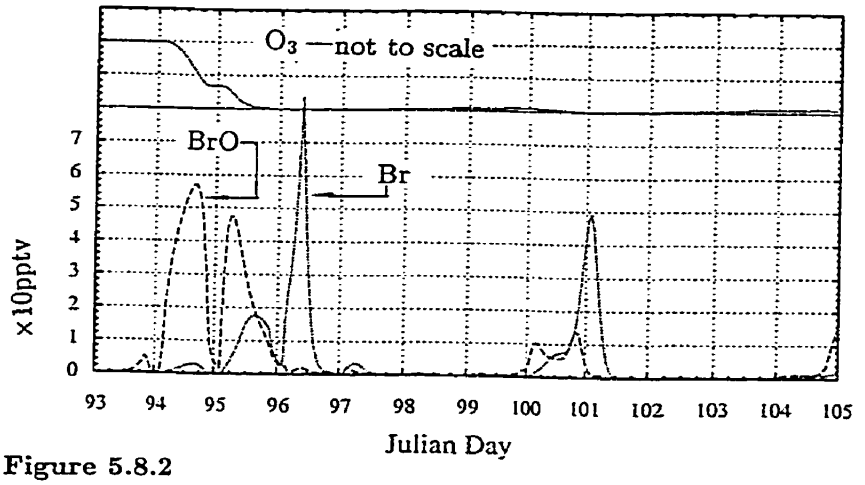

Figure 5.8.2

Extended plot of O_3, BrO and Br atom.

Chapter VI
Results of Simulation, Part II
The Effect of Chlorine Chemistry

Section 6.1 Chemistry of Chlorine Before Ozone Depletion

Once the simulation commences, the initial 10 pptv of Cl^- is converted into 5 pptv of Cl_2 (see Figure 6.1.1). This conversion is done by a hypothetical reaction in accord with the cycle of reactive chlorine in the marine boundary layer proposed by *Keene et al.* [1990] (Section 3.9). With the increasing solar radiation, Cl_2 photodissociates in a few hours, producing Cl atoms. In the presence of O_3, Cl atoms rapidly react to form ClO (Figure 6.1.1). ClO can undergo several reactions (see Table 3.7.1) to return its chlorine to Cl atoms, which react with more O_3. Thus, a chlorine catalytic cycle of O_3 destruction may be formed. However, since the amount of ClO present in this simulation is only 0.2 pptv (Figure 6.1.1), little O_3 destruction takes place. At this level,

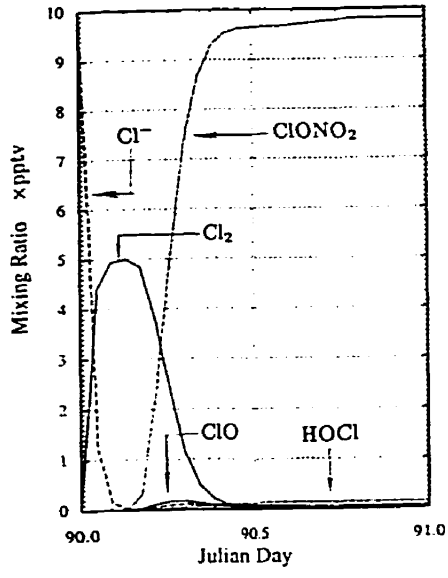

Figure 6.1.1

Activities of chlorine in the model, during the first day of model run. See text for description.

the rate of O_3 destruction by the ClO catalytic cycle is about 13 pptv a day†. Notice that 0.2 pptv of ClO amounts to only ~ 2% of the total chlorine in the model. This fraction of active chlorine is extremely small compared to that for bromine. In the bromine chemistry, BrO can take up more than 50% of the total bromine (see Section 5.3). This is a surprise since, thermodynamically, ClO is easier to produce than BrO (see Table 6.1.1). The reactions set up in

† Calculated using the channels given in Table 3.7.1, the rate at which the O_3 is destroyed

$$\frac{d[O_3]}{dt} = -(2k_a[ClO] + k_b[NO_2] + k_c[NO] + k_d[HO_2]) \times [ClO].$$

Using the daytime mixing ratio before JD 93 from the results of simulation : ClO ~ 0.2 pptv ; NO_2 ~ 15 pptv; NO ~ 9 pptv; HO_2 ~ 0.6 pptv (see Appendix A.3). $\frac{d[O_3]}{dt} \approx$ 13 pptv a day

Table 6.1.1

This table tabulates the important reactions and rate coefficients for the production and loses of ClO and BrO. γ denotes the reactions that are potentially faster compared to the similar reaction in the other halogen group. Note that for the reactions $NO_2 + XlO$ and $X + O_3$, the reactions for bromine are faster than that for chlorine.

ClO Losses		BrO Losses	
$ClO + ClO^a$	7.6×10^{-14}	$BrO + BrO$	$\gamma 3.1\times10^{-12}$
$ClO + NO_2$	$\gamma 4.5\times10^{-12}$	$BrO + NO_2$	1.9×10^{-12}
$ClO + NO$	2.1×10^{-11}	$BrO + NO$	$\gamma 2.5\times10^{-11}$
$ClO + HO_2$	8.4×10^{-12}	$BrO + HO_2$	$\gamma 4.8\times10^{-11}$
ClO Production		BrO Production	
$Cl + O_3$	$\gamma 1.0\times10^{-11}$	$Br + O_3$	6.5×10^{-13}

Note:

(1) Unit for the rates in the table are in $cm^3molec^{-1}.s^{-1}$.

(2) All rates, unless indicated otherwise, are from *DeMore et al.* [1992].

(3) ^{a} see Table 3.7.1.

the model to recycle inactive species are different for bromine and for chlorine chemistry. In bromine chemistry $BrONO_2$ and HOBr are recycled. In chlorine chemistry, however, HOCl and $ClONO_2$, are not. The release of chlorine from HOCl and $ClONO_2$ relies on their slow photo-dissociation‡. With Cl atom being slowly released, over 90% (9 pptv) of chlorine is tied up in HOCl and $ClONO_2$

‡ Photodissociation rates for HOCl and $ClONO_2$ during spring in Arctic are about $10^{-5}sec^{-1}$ and $4 \times 10^{-5}sec^{-1}$ (i.e., $\tau \sim 1.2$ day and $\tau \sim 6$ hrs) respectively (see Appendix A.2).

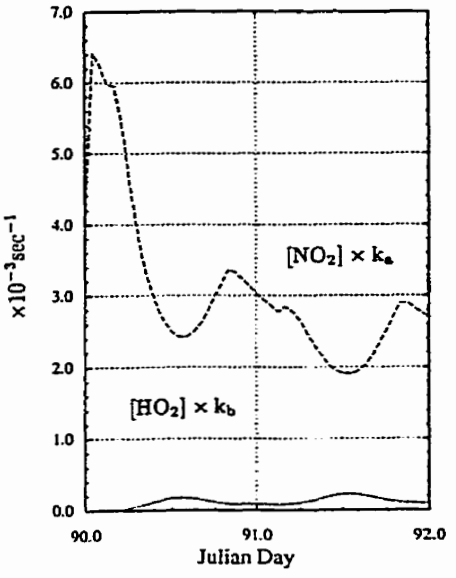

Figure 6.1.2

This figure compares the rate of $ClONO_2$ produced per ClO consumed (dashed line).

$$\frac{\frac{d}{dt}[ClONO_2]}{[ClO]} = k_a[NO_2]$$

to the rate of HOCl produced per ClO consumed (small dotted line).

$$\frac{\frac{d}{dt}[HOCl]}{[ClO]} = k_b[HO_2]$$

With rate coefficient for ClO reacting with NO_2, $k_a = 4.5 \times 10^{-12}$ $cm^3 molec.^{-1} s^{-1}$ and the rate coefficient for ClO reacting with HO_2 $k_b = 8.5 \times 10^{-12}$.

(Figure.6.1.1). Notice that $ClONO_2$ is favored over HOCl as a chlorine reservoir despite the fact that the later can be produced with greater ease*. This is because initially, the precursor of $ClONO_2$ (i.e., NO_2) is present in relatively large quantities (50 pptv of NO_x was assigned to the model initially). The precursor of HOCl (i.e., HO_2) is low due to weak sunlight. To illustrate this, Figure 6.1.2 compares the rate of HOCl and $ClONO_2$ produced for each ClO consumed.

---

* Reaction rate coefficient for HOCl generation ($HO_2 + ClO \rightarrow HOCl + O_2$) is greater than that for $ClONO_2$ ($NO_2 + ClO + M \rightarrow ClONO_2 + M$) (see Table 6.1.1); and the loss for HOCl (due to photo dissociation) is less than that for ($ClONO_2$)

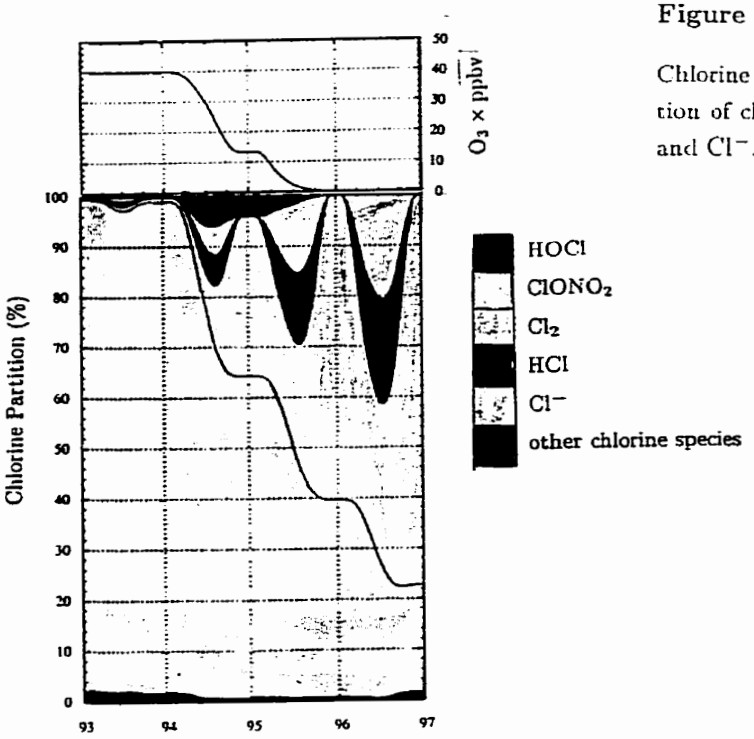

Figure 6.2.1

Chlorine partition map, showing transformation of chlorine from $ClONO_2$ to Cl_2, HCl and Cl^-.

Section 6.2 Releasing Chlorine and Nitrogen From $ClONO_2$

Bromine is released into the atmosphere after JD 94 resulting in O_3 depletion (see Section 5.1). And while O_3 is being depleted, chlorine in $ClONO_2$ is released. This can be seen in the changes in the chlorine partitioning map (Figure 6.2.1). Note that the partition fraction of $ClONO_2$ shrinks while the partitioning of chlorine in Cl_2, HCl and Cl^- increases. When bromine chemistry is active, BrO competes with ClO for NO_2. Although the rate coefficient

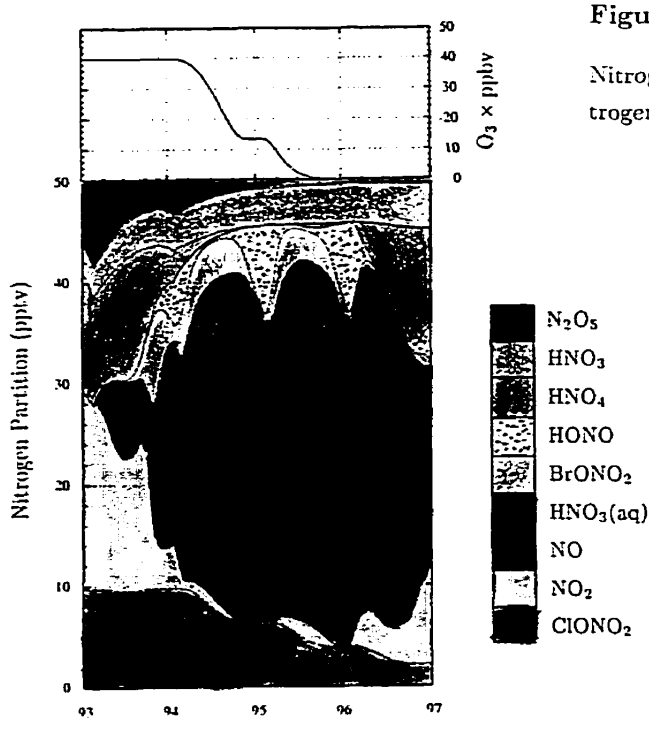

Figure 6.2.2

Nitrogen partition map. showing loss of nitrogen to HNO3(aq).

for reaction between ClO and NO_2 is about twice that for reaction between BrO and NO_2 (see Table 6.1.1), the amounts of BrO present are two orders of magnitude greater than that for ClO (see Section 6.1). As a result, the reaction between BrO and NO_2 diverts odd nitrogen consumption from $ClONO_2$ formation to $BrONO_2$ formation. With odd nitrogen channeled into $BrONO_2$ formation, the total odd nitrogen in the atmosphere is reduced since $BrONO_2$ can diffuse into the aqueous phase and hydrolyze to HNO_3(aq) (see Chapter IV). Although, according to the model setup, the nitrogen in HNO_3(aq) is returned to the gaseous phase in the form of HONO (see Chapter IV), its rate is slow. Figure 6.2.2 shows the partitioning of odd nitrogen in the model during this period. The amount of odd nitrogen lost from the gas phase is more than

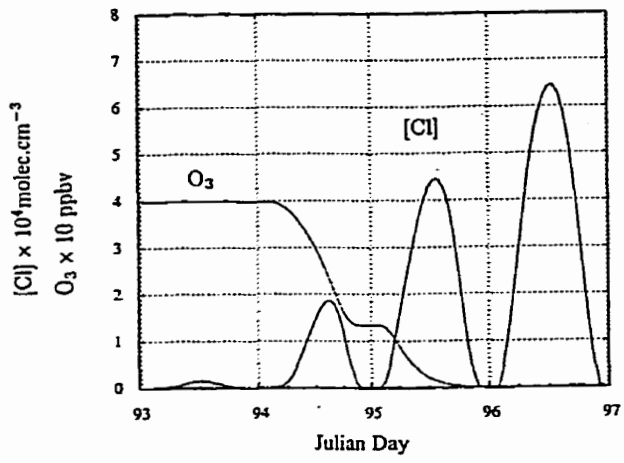

Figure 6.2.3

Number density of Cl atom with O_3 mixing ratio.

35 pptv, which is about 70% of the total odd nitrogen in the model. With gaseous odd nitrogen lost to the aqueous phase, the Cl atoms released following the photolysis of $ClONO_2$ do not reform $ClONO_2$. Instead, they form HCl via :

$$Cl + H_2O_2 \rightarrow HCl + HO_2 \quad (6.2.1)$$

$$Cl + HCHO \rightarrow HCl + HO_2 + CO \quad (6.2.2)$$

$$Cl + HO_2 \rightarrow HCl + O_2 \quad (6.2.3)$$

$$Cl + CH_3OOH \rightarrow HCl + CH_3O_2 \quad (6.2.4)$$

With the given reaction set in the model, this HCl is recycled back to Cl_2. Thus, the chlorine cycle, composed of HCl, Cl^- Cl_2 and Cl atoms, is intensified. This effect has been seen in Figure 6.2.1 which shows the repartitioning of chlorine from $ClONO_3$ into Cl^-, HCl and Cl_2. The density of Cl atom too small to be seen in the partition map and it is shown separately in Figure 6.2.3. The resultant Cl atom density in this model is of the order of magnitude of that calculated

from the observed decay of NMHC (see Section 3.4). However, it should be noted that the model result is somewhat artificial since the exact mechanism for the reactive chlorine cycle for *Keene et al.* [1990] is not available.

To summarize the above — the presence of bromine chemistry not only destroys O_3, it can change the path of NO_x reactions and intensify the reactive chlorine cycle of *Keene et al.* [1990]. Diagram 6.2.1 illustrates this change in chlorine and nitrogen cycle in the presence of bromine.

Section 6.3 ClO and its Interaction with BrO

As pointed out earlier, the presence of bromine results in the release of chlorine from $ClONO_2$. With this, more Cl atoms can react with O_3 to form ClO. During the day of JD 94, 3 pptv of chlorine is released from $ClONO_2$, however. ClO only increases by about 0.2 pptv (see Figure 6.3.1). The ClO increase is small because the amount of Cl atom lost by reaction with O_3 is less than that lost by reaction with HCHO, CH_3OOH, H_2O_2 and HO_2. Most of the chlorine released from $ClONO_2$ is channeled to HCl rather than ClO formation. Also, it can be noted in Figure 6.3.1, after JD 95, the decline of O_3 levels reduces the amount of ClO.

As was pointed out in Section 3.8, the ClO reacting with BrO may enhance O_3 destruction. The degree of enhancement can be calculated :

$$\begin{aligned}
\epsilon &= \frac{\text{ozone depletion rate enhanced by ClO - BrO interaction}}{\text{ozone depletion rate without enhancment}} \\
&= \frac{-2k_{BrO^2}[BrO]^2 - 1.47k_{BrO-ClO}[BrO][ClO])}{-2k_{BrO^2}[BrO]^2} \\
&= 1 + \zeta\frac{[ClO]}{[BrO]}; \qquad \zeta = \frac{1.47k_{BrO-ClO}}{2k_{BrO^2}} = 1.019.
\end{aligned} \tag{6.3.1}$$

In the above, k_{BrO^2} $(= 3.2 \times 10^{-12} cm^3 molec^{-1} s^{-1})$ is the reaction rate coefficient for BrO self-reaction. And $k_{BrO-ClO}$ $(= 8.2 \times 10^{-12} cm^3 molec^{-1} s^{-1})$ is the reaction rate coefficient for reaction between BrO and ClO excluding the channel leading

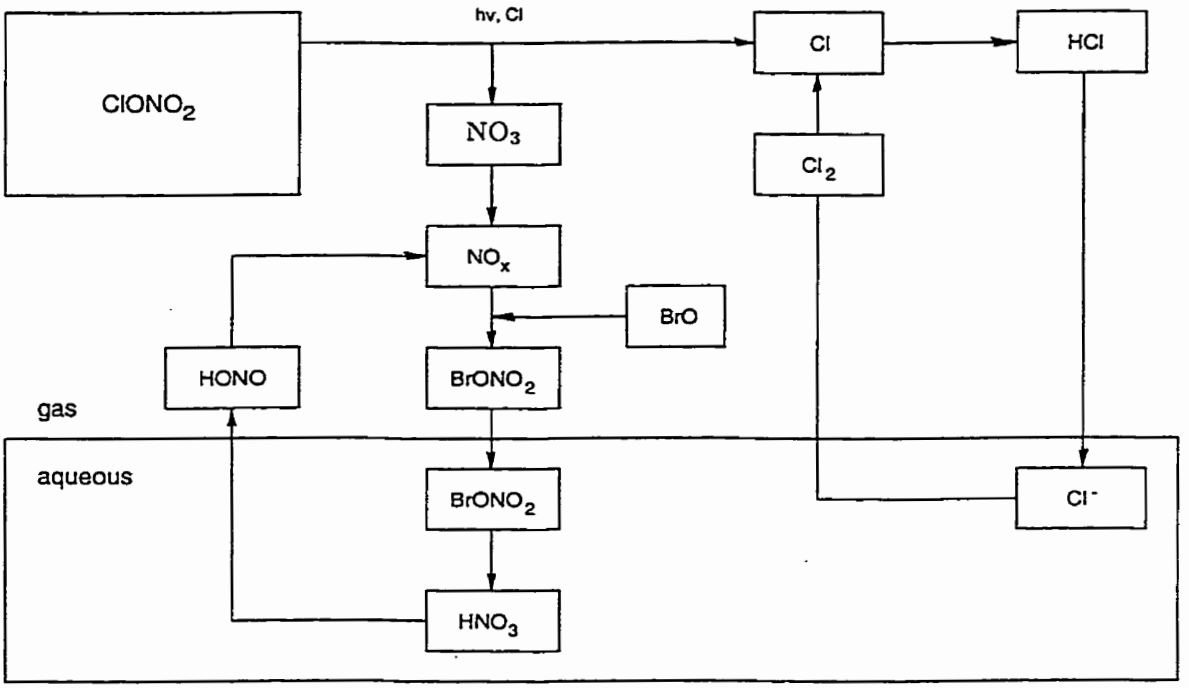

Diagram 6.2.1

Schematic diagram to illustrate the transfer of chlorine in $ClONO_2$ to a system of chlorine cycle composed of HCl Cl^-, Cl_2 and Cl atom. It also illustrates the transfer of its nitrogen to a system of nitrogen cycle composed of $BrONO_2$ HNO_3(aq) and HONO.

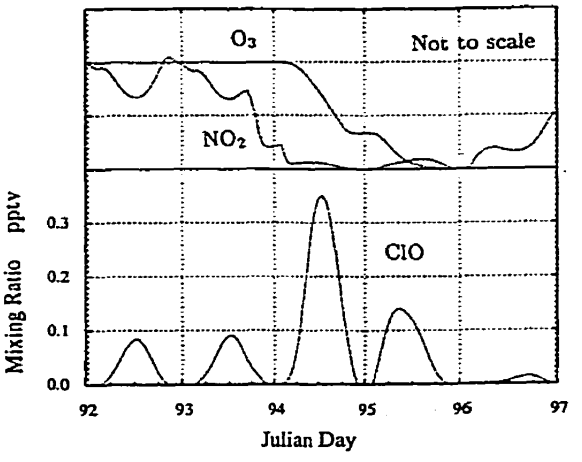

Figure 6.3.1
Mixing ratio of O_3, NO_2 and ClO.

to OClO production. The resulting ClO to BrO ratio in this simulation is $\sim \frac{1}{100}$. With this, $\epsilon = 1.019$. This amounts to about a 2% increase in O_3 destruction rate. With only 2% of total chlorine in the model as ClO, the enhancement is small.

The interaction between ClO and BrO produces several intermediate species – ClOOCl, ClO_2, OClO and BrCl. These intermediate species are shown with ClO and BrO in Figure 6.3.2. It can be seen that the level of OClO and BrCl are low – at sub pptv level – due to their rapid photolysis rate ($\sim 10^2$s and $\sim 10^3$s respectively). The levels of ClO_2 and ClOOCl are even lower, their mixing ratios are less then $\sim 10^{-18}$. Both ClO_2 and ClOOCl decomposition proceeds very rapidly ($\sim 10^{-5}$ s and ~ 3 s, respectively).

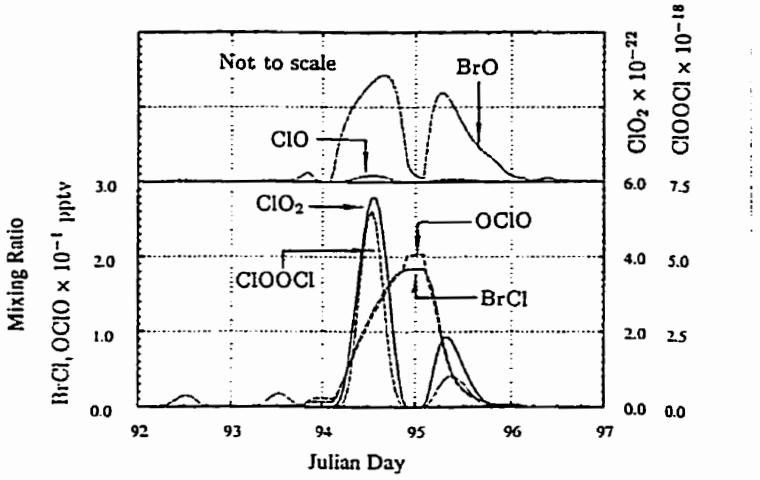

Figure 6.3.2
Upper figure shows the mixing ratio of BrO and ClO while lower figure shows the mixing ratio of ClO_2, ClOOCl, OClO and BrCl.

Section 6.4 Chlorine Chemistry and Formaldehyde production

As was pointed out in Section 3.10, the level of HCHO can be approximated analytically in the form of:

$$[\text{HCHO}] = \alpha \frac{P}{L}, \tag{6.4.1}$$

where, P is the production term attributed to the oxidation of CH_4 by OH and Cl atoms; and L is the destruction term which includes the destruction by photo-dissociation and by reaction with OH, Cl and Br atom. α is the HCHO production efficiency which depends on the amount of NO and HO_2 present. Using modeled results for OH, Cl atom, Br atom, CH_4 and J-value, the analytical results for HCHO are shown in Eq 6.4.1. In the same figure,

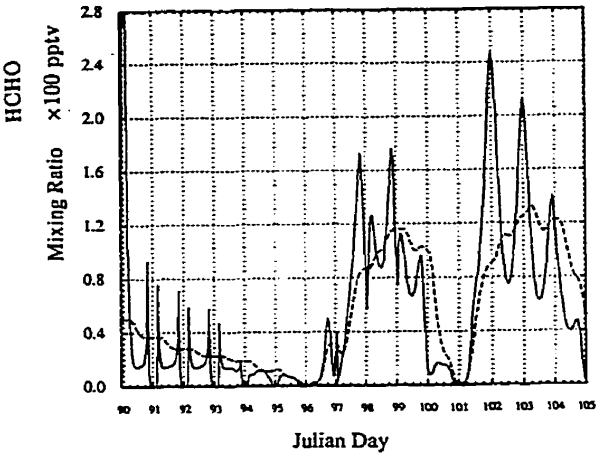

Figure 6.4.1

HCHO mixing ratios: dashed curve is from model simulation; solid curve is the steady state analytical estimate.

HCHO in the model is also plotted. It can be seen that the modeled results and analytical results would be more comparable if the analytical plot was smoothed to get rid of the spikes that occur around the periods of low solar radiation. This difference is expected since the calculation for the analytical result is based on the assumption that $\frac{d[HCHO]}{dt}$ is zero or very small. This is different from the computer simulation that $\frac{d[HCHO]}{dt}$ may not be small enough or zero. Thus, Eq 6.4.1 is useful only for illuminating the understanding of the mechanism which produces formaldehyde, it should not be used for quantitative prediction. Another disagreement between the analytical and modeled result is that before O_3 depletion (before JD 94), the amount of HCHO is underestimated by the analytical solution. HCHO in the model is greater since the model has been initialized with HCHO (see Chapter IV).

The mixing ratio of HCHO and O_3 in the simulation is shown in Figure 6.4.2. Before O_3 depletion, the mixing ratio of HCHO declines slowly from

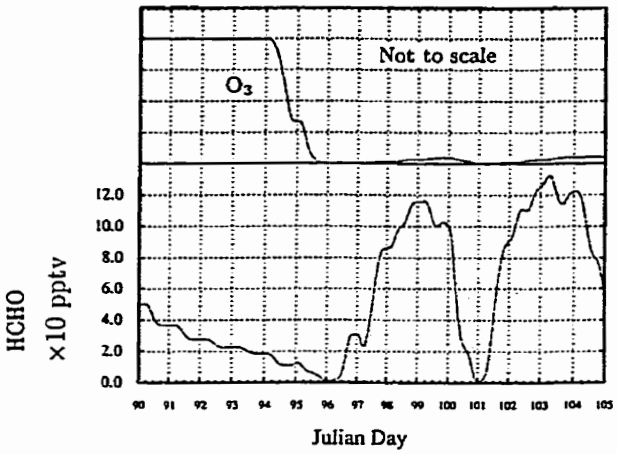

Figure 6.4.2

Lower figure is the plot of HCHO (modeling result) and the upper figure is the plot of O_3.

its initial 50 pptv and depletes at ~JD 96. After this, there are two HCHO rich periods where the mixing ratio rises over 100 pptv (JD 96 to 101 and JD 101 to 105). Note that depletion of O_3 coincides with the depletion of HCHO (JD 96 and JD 101).

In the model, the production of HCHO begins when CH_4 is oxidized by OH or Cl atoms. Figure 6.4.3b shows the production term, P, in Eq 6.4.1. The plot indicates an increase of daily HCHO production after JD 94, the day which also marks the beginning of O_3 depletion (Figure 6.4.3a). The reason for this becomes clear when one observes the time series for Cl atoms (Figure 6.4.3c). The time series for both HCHO production, P, and Cl atom exhibit similar profiles. HCHO production increases since Cl atom densities have increased which oxidizes more CH_4. As was pointed out earlier in Section 6.2, the activation of bromine chemistry changes the partitioning of chlorine from $ClONO_2$ to the reactive chlorine cycle of *Keene et al.* [1990]. Intensification of

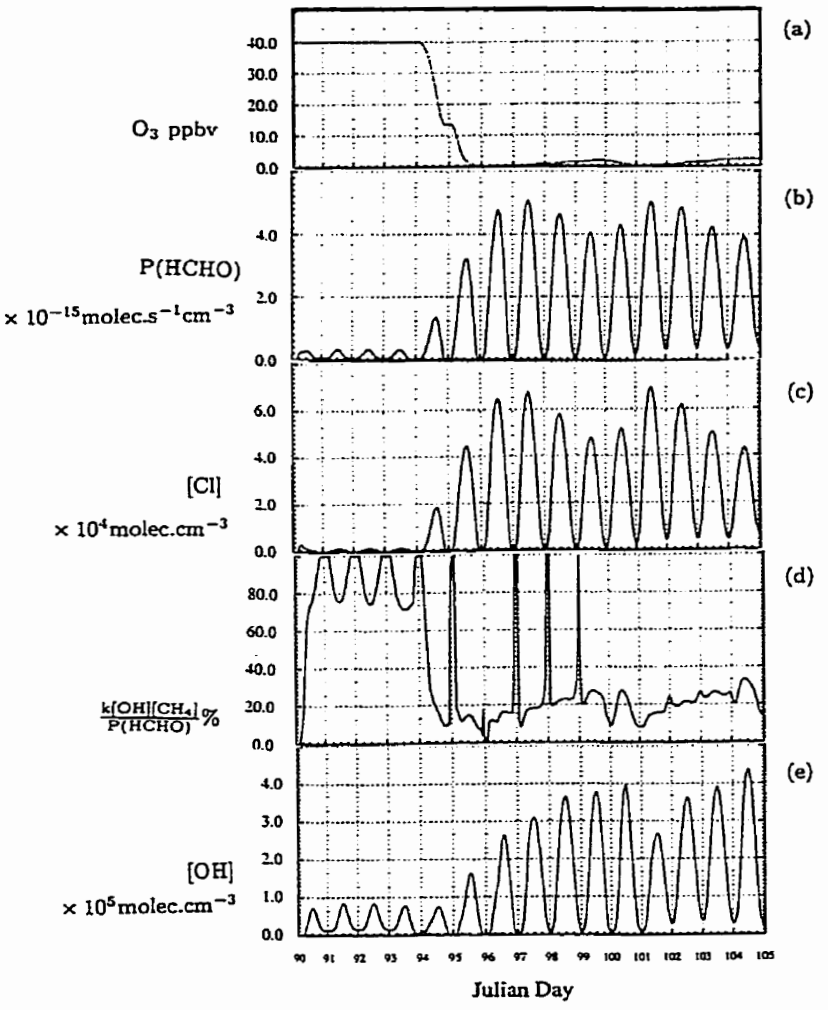

Figure 6.4.3

Panel (a) shows mixing ratio of O_3. Panel (b) shows the HCHO production term $P = (k[OH] + k[Cl])[CH_4]$ in Eq 6.4.1. Panel (c) is the chlorine number density. Panel (d) is the fraction of methane oxidized by Cl atom, $f = k[OH][CH_4]/P(HCHO)$. And Panel (e) is number density for OH.

this cycle increases the level of Cl atoms. Other than Cl atoms, OH also oxidizes CH_4 to produce HCHO. Figure 6.4.3d shows the fraction of CH_4 oxidized by the OH radical. The plot indicates that prior to O_3 depletion, OH is the chief oxidant of CH_4. However, the rate coefficient for the reaction between OH and CH_4 is a factor of $\sim$ 20 less than that for Cl atom and CH_4 (see Table A.5) and HO plays only a small role in HCHO production. As for Cl atoms, OH also increases after O_3 depletion (Figure 6.4.3f). However, this is for a different reason. The increase of Cl atoms occurs because chlorine in the model is undergoing repartitioning. The increase of OH occurs because its immediate precursor (i.e., HO_2) has increased. As pointed out in Section 3.10, each HCHO is a source for two HO_2.

The loss term, L, in Equation 6.4.1. is shown in Figure 6.4.4a. Figure 6.4.4b shows the Br atom component in L. The similarity between these two figures points out that the Br atom 'explosion' (see Section 5.7) which follows immediately after O_3 depletion also results in HCHO destruction. The HCHO reacts with the excess Br atom in the 'explosion' and returns them to the aqueous phase.

It was pointed out in Section 3.10 that HCHO production efficiency from CH_4 is

$$\alpha = \frac{k_3[NO]}{k_4[HO_2] + k_3[NO]}. \tag{6.4.2}$$

The amount of CH_3O_2 that can form HCHO is regulated by this coefficient. The time series of α is shown in Figure 6.4.5b. The average daytime efficiency for HCHO production is about 90% before O_3 depletion. As pointed out in Section 3.10, increasing HCHO can restrict its own production by reducing α. This can be seen in the model where, after O_3 depletion, the HCHO level rises to increase the supply for HO_2 (see Figure 6.4.5d). The additional HO_2 lowers α to about 70% (Figure 6.4.5b, after JD 94). It should be pointed out that for α (Eq 6.4.1) to be meaningful, the amount of HO_2 and NO must be comparable to or in excess of the amount of CH_3O_2 present. When HO_2 and NO

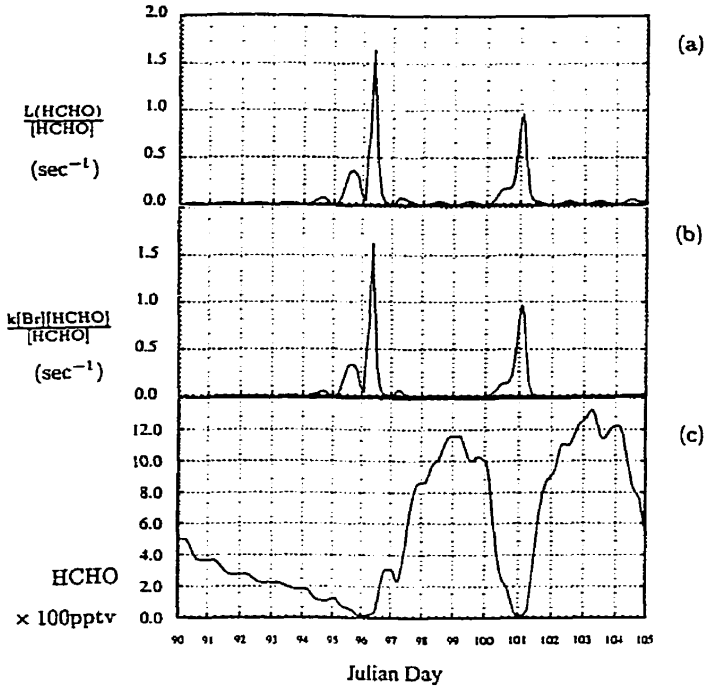

Figure 6.4.4
Panel (a) shows the HCHO loss term in Eq 6.4.1:

$$L = k[OH] + k[Br] + k[Cl] + jv.$$

Panel (b) is the k[Br] term in L. And panel (c) shows the mixing ratio of HCHO.

are scarce, the level of CH_3O_2 rises and the path for HCHO production is via CH_3O_2 self-reaction. This situation can happen when the O_3 is being depleted (Figure 6.4.5e, JD 94 to 96 and JD 100 to 101). During this time, the large quantities of BrO suppresses the level of HO_x and NO_x (Figure 6.4.5c and d; cf. Section 5.4).

There is another effect due to the increasing HO_2. The increase of HO_2 increases of CH_3OOH production. Figure 6.4.6 illustrates this effect. Note that

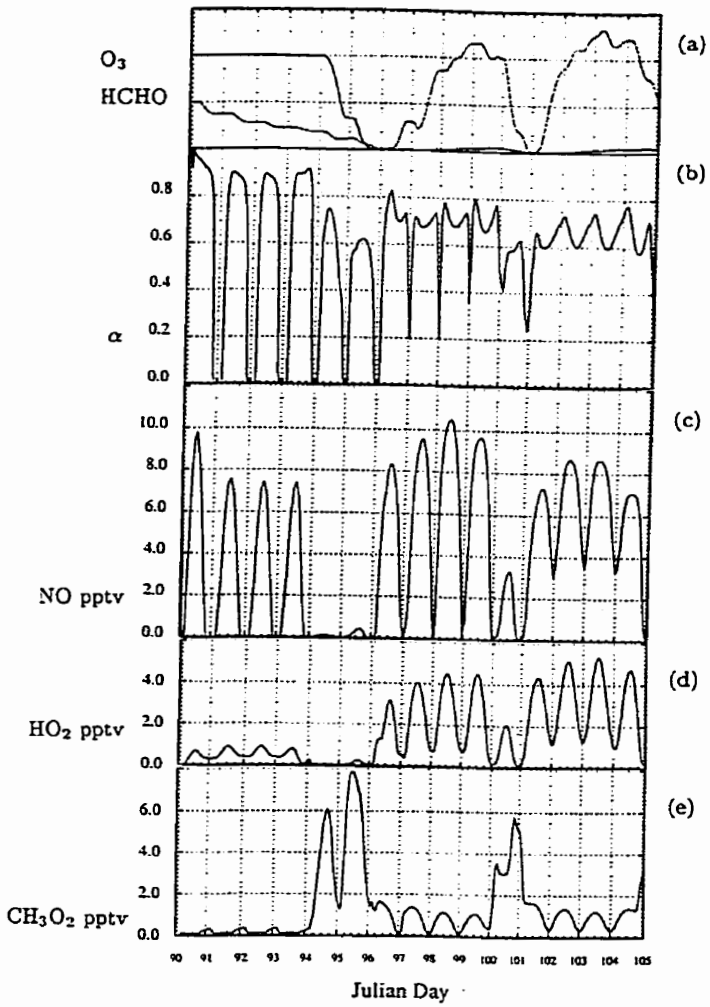

Figure 6.4.5

Panel (a) shows O_3 and HCHO (not to scale). Panel (b) is the HCHO production efficiency α (i.e., Eq 6.4.2). Panel (c), (d) and (e) are mixing ratio for NO, HO_2 and CH_3O_2 respectively.

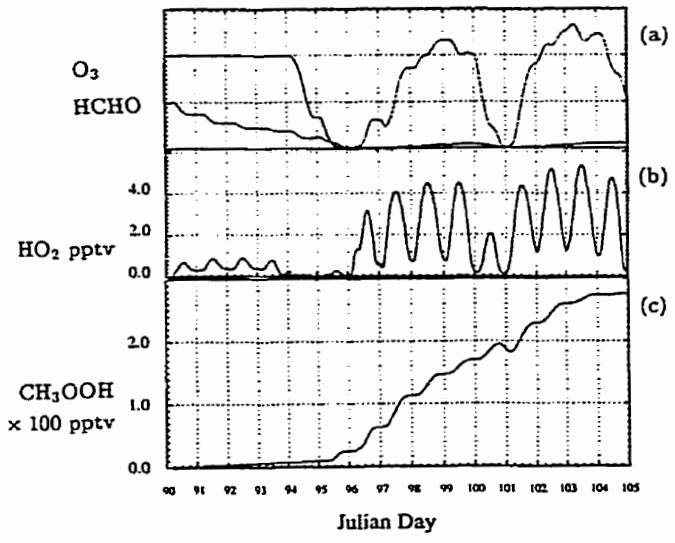

Figure 6.4.6

Panel (a) shows O_3 and HCHO (not to scale). Panel (b) and (c) are the HO_2 and CH_3OOH mixing ratio respectively.

equilibrium for CH_3OOH takes about 10 days to establish. The amount of CH_3OOH accumulated reaches $\sim$ 280 pptv.

Section 6.5 Sensitivity Study With Higher Chlorine Levels

Up to this point, simulation of O_3 depletion has been performed with total chlorine in the model at 10 pptv. To explore a more extreme case, the amount of chlorine in the model was increased to 40 pptv. Figure 6.5.1 compares the results of O_3 depletion. It can be seen, perhaps against one's intuition, that the increase of total chlorine actually increases the time required for O_3 depletion. This happens because the rate of bromine release from the snow

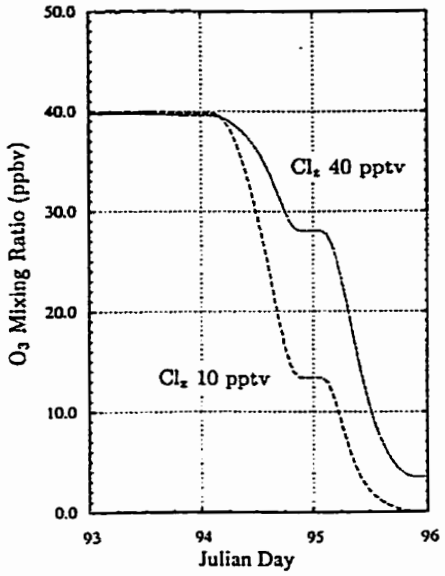

Figure 6.5.1

Time series of O_3 run with 10 pptv (dotted line) and 40 pptv (solid line) of total chlorine. With more chlorine, the rate of O_3 depletion slows down.

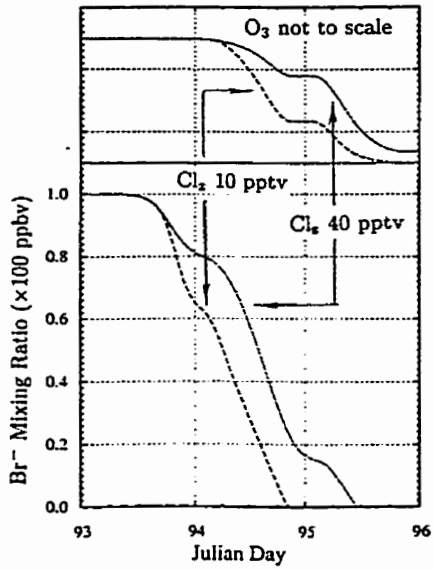

Figure 6.5.2

Time series of Br^- and O_3 with 10 pptv (dotted line) and 40 pptv (solid line) of chlorine. Note that longer times are required for Br^- depletion when chlorine in the model is increased.

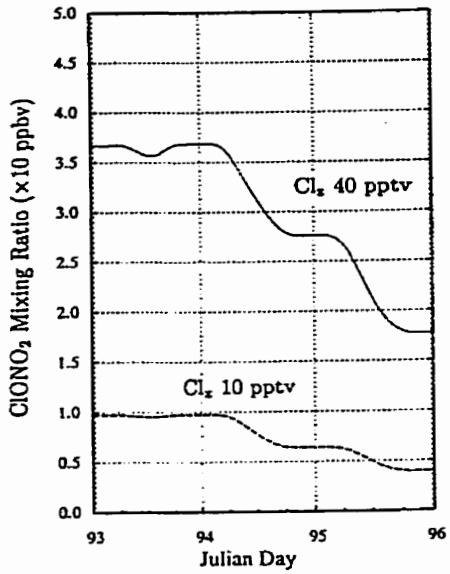

Figure 6.5.3

Time series of inactive nitrogen, $ClONO_2$, at different chlorine level – 10 pptv and 40 pptv (dotted and solid line respectively). With the chlorine amount increased, inactive nitrogen increases.

pack has slowed down (Figure 6.5.2). With more chlorine in the model, more inactive nitrogen ($ClONO_2$) can form (Figure 6.5.3). This reduces the amount of NO_2 available for the formation of $BrONO_2$(aq) and HOBr(aq) production. Figure 6.5.4 compares the rate of $BrONO_2$(aq) being hydrolyzed to HOBr(aq) at different chlorine levels. It can be seen, before JD 95, that the supply rate of HOBr(aq) is smaller for the case with higher chlorine. With smaller supply rates, less HOBr(aq) is available to react with Br^- and the rate of bromine release from the snow-pack slows down. One could argue that the increase of chlorine could increase the amount of HOBr(aq) produced — since more Cl atoms would lead to an increases CH_4 oxidation which produces more HCHO. This would increase the level of HO_2 and the yield of HOBr. However, it can be seen by comparing Figure 6.5.5 and Figure 6.5.4 that the increases of HOBr(aq) supply from HOBr diffusion is not sufficient to compensate for the decrease in HOBr(aq) supplied from $BrONO_2$(aq) hydrolysis under the condition of reduced

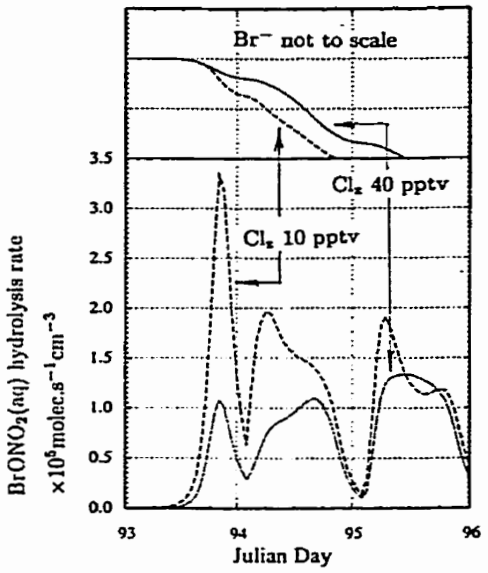

Figure 6.5.4

Time series for the rate at which $BrONO_2(aq)$ hydrolyzes to HOBr(aq). This rate decreases when chlorine in the model is increased. The dotted line is the result with 10 pptv of chlorine and solid line is the result with 40 pptv of chlorine.

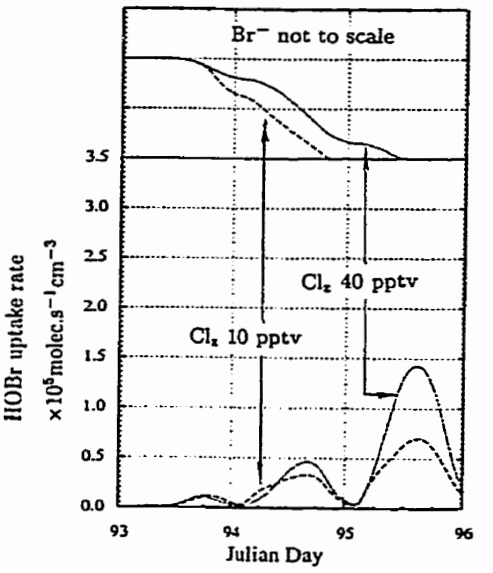

Figure 6.5.5

The gaseous to liquid transfer rate for HOBr. With the amount of chlorine increase from 10 pptv (dotted line) to 40 pptv (solid line), this rate increased. Comparing this with Figure 6.5.4, HOBr(aq) supply by direct gaseous to aqueous diffusion of HOBr is less important than that from hydrolysis of $BrONO_2(aq)$.

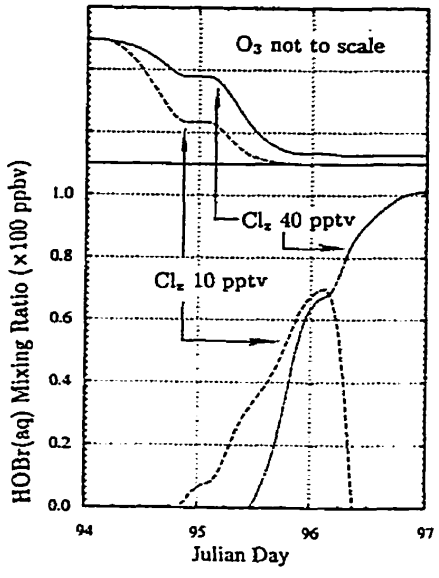

Figure 6.5.6

Time series of O_3 and HOBr(aq) with different chlorine levels. Note that with more chlorine (solid line) O_3 does not deplete because the HOBr(aq) continuously increases until all the active bromine in the model is lost.

atmospheric odd nitrogen.

For the simulation at higher chlorine levels, the O_3 depletion is interrupted twice by the weakening of the solar radiation (Figure 6.5.6, JD 95 and 96). The morning after the second interruption (after JD 96), O_3 depletion does not resume because there is no bromine in the atmosphere. All the bromine is tied up as HOBr(aq) (Figure 6.5.6, after JD 96). Recall in Section 5.7 that while O_3 is being destroyed, bromine in the atmosphere can be lost into the aqueous phase to form HOBr(aq). In this higher chlorine regime, O_3 has a longer depletion time and the atmospheric bromine is transfered to HOBr(aq) before O_3 can be destroyed.

The above situation can be changed to permit complete O_3 destruction if the suggested reaction rate coefficient for HOBr to HOBr(aq) transformation of *Fan & Jacob* [1992] is reduced from 1.4×10^{-4} to $0.5 \times 10^{-4} cm^3 molec^{-1} s^{-1}$. Figure 6.5.7 shows the production rate for HOBr(aq) and Br^- with the two

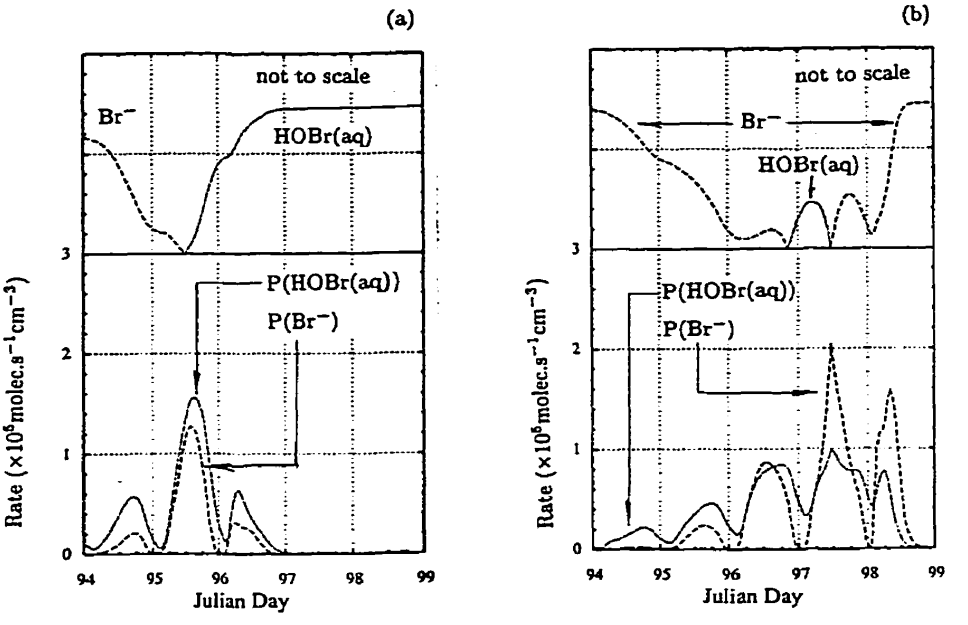

Figure 6.5.7

The upper figure shows the time series of Br^- and HOBr(aq). The lower figure shows the production rate for HOBr(aq) and Br^-. This simulation is run at 40 pptv of chlorine. In Panel (a), the rate coefficient for HOBr to HOBr(aq) transformation follows the suggestion of *Fan & Jacob* [1992]. With this, production of HOBr(aq) is always greater than that of Br^-. In Panel (b), the rate coefficient for HOBr to HOBr(aq) transformation is reduced (see text).

different values for the reaction rate coefficient for HOBr to HOBr(aq) (Panel (a) and (b) respectively). With the faster rate coefficient, the production rate of HOBr(aq) is always greater than that of Br^- (Panel a). Recall the discussion in section 5.5 that in the absence of Br^-, HOBr(aq) can grow if the production rate of HOBr(aq) is greater than that of Br^-. With the slower rate (Figure 6.5.8b), the relative magnitude for both can interchange frequently. This permits bromine to transfer in and out before it is completely lost to the aqueous phase. With this scenario, the atmosphere is not deprived of bromine, and the bromine catalytic cycle is of sufficient strength to sustain O_3 depletion (Figure 6.5.8b).

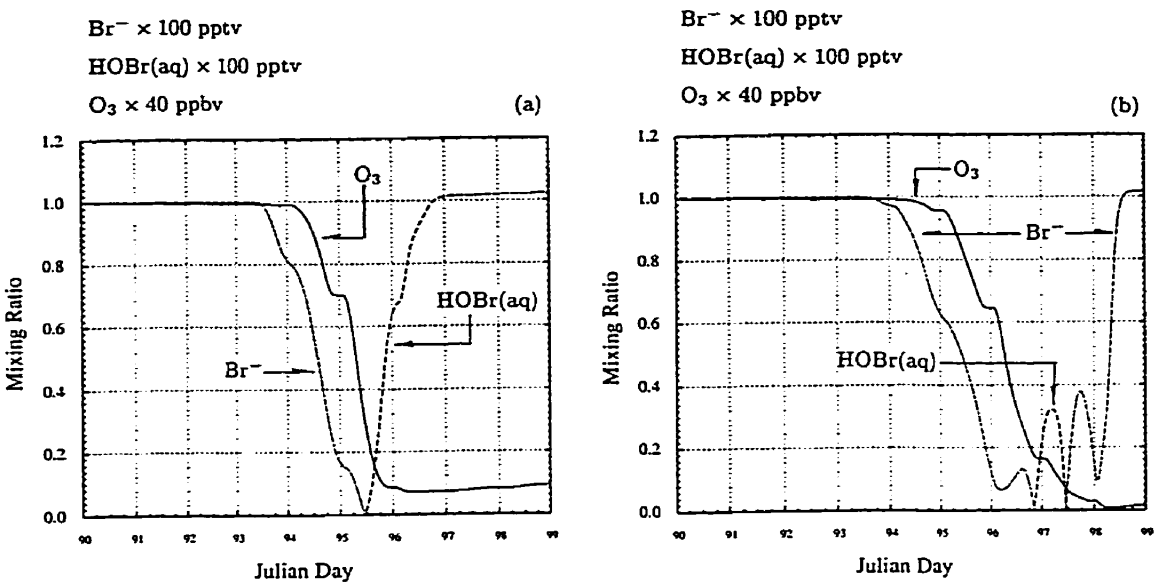

Figure 6.5.8

Time series of Br^-, HOBr(aq) and O_3, simulated with 40 pptv of total chlorine. In Panel (a), the rate coefficient for HOBr to HOBr(aq) transformation of *Fan & Jacob* [1992] is used, and complete O_3 depletion does not occur. In Panel (b), this rate coefficient is reduced to allow longer residence time for bromine in the gaseous phase. This permits complete O_3 depletion.

Chapter VII
Conclusions

This investigation of spring time PBL O_3 depletion has tried to illuminate the geochemical cycling of reactive bromine and chlorine in the Arctic environment. One of the goals of this thesis is to reinforce the idea that the geochemical cycle of bromine in the Arctic is annual and it involves three phases : (1) the winter build up of bromine in the snowpack, (2) spring time bromine release to the PBL, and (3) the dissipation of bromine into the free troposphere at the end of spring when the inversion layer breaks up. As chlorine and bromine are both halogens, one might think that they should undergo similar reactions and exhibit similar behavior. However, the observed geochemical cycle for chlorine is different from that of bromine in that the three stages involving winter time build-up, spring time release and summer time dissipation is not evident. The aerosol content of chlorine is in deficit though out the year. This is in sharp contrast with that for bromine which exhibits a prominent spring time enrichment. The difference suggests the release of bromine from its source (sea salt) is more efficient than that for chlorine. If one were to maintain the premise that sea salt is the source of halogen in the Arctic then the chemical

mechanisms responsible for their geochemical cycling must be different.

In this work, the mechanism of *Fan & Jacobs* [1992] was chosen to be the mechanism responsible for the transference of bromine in the snowpack to the PBL since it appears to be able to explain the observed geochemical cycling of reactive bromine. First of all, the photo-chemical dependence of this mechanism allows winter 'charging' of bromine in the snowpack. And with spring time activation, the amplifying effect of the mechanism can rapidly transfer bromine from the snowpack to the atmosphere. Once the bromine is released, the mechanism can recycle inactive bromine and thus the level of active bromine that is required for O_3 destruction is maintained. After O_3 depletion the mechanism can shut off and bromine returns to the aerosol. For this the bromine content in the aerosol becomes enriched. These model simulations have demonstrated the idea of *Mozurkewich* [1995] that the release of bromine from the snowpack can be triggered by a seed. Although $CHBr_3$ is the seed used in the model, this does not imply that other type of seeds can not be used. *Vogt et al.* [1996] have proposed a mechanism similar to that of *Fan & Jacobs* [1992] for both chlorine and bromine release. This mechanism was not adopted here since it could result in the geochemical cycling of reactive chlorine exhibiting stages like that of bromine. In the search for a mechanism for chlorine, the closest mechanism appears to be that of *Keene et al.* [1990]. This mechanism is still in its hypothetical stage and it lacks detail reactions. For this, it is unlikely that the amount of chlorine and its partitioning in the model is a realistic representation of that in the Arctic atmosphere. The mechanism of *Keene et al.* [1990] was originally proposed to explain the dial cycle of reactive chlorine activities in the MBL. In the polar region, however, this cycle is much longer. A year round field observation to explore this cycle would be useful.

It was learned that the type of recycling mechanism adopted can have a direct effect on the partitioning of halogen. For bromine chemistry, inactive bromine (HOBr, $BrONO_2$ and HBr) is recycled. In chlorine chemistry only HCl is

recycled. This results in more than 50 % of the total bromine being BrO while only 2% of total chlorine is ClO. Given the amount of ClO in the model (less than 1 pptv), the synergistic effect of BrO and ClO as pointed out by *Le Bras & Platt* [1995] contributed a very little to O_3 destruction. It is interesting to note that the presence of chlorine at certain mixing ratios in the model actually decreases the rate of O_3 depletion. It is also seen in the model that the presence of chlorine competes for NO_2 which is required for $BrONO_2$ formation. When $BrONO_2$ formation is reduced, the transfer of bromine from the snowpack to the atmosphere slows down. In addition, based on the observation of NMHC decay by *Ariya et al.*, [1998], this work would argue that elevated reactive chlorine activity is not necessary for the depletion of ethyne and O_3. On the contrary, the process of O_3 depletion by the BrO catalytic cycle can intensify the reactive chlorine cycle of *Keene et al.* [1990]. This results in elevation of Cl atom which increases alkane destruction. The reactive chlorine cycle of *Keene et al.* [1990] can intensify because, while forming $BrONO_2$, considerable amounts of NO_x are deactivated. With less NO_x, the amount of chlorine that can be tie up in $ClONO_2$ is reduced.

As pointed out above, reaction of XlO (X = Cl, Br) with NO_x can deactivate halogen. In the arrangement of this model, chlorine is inactive in $ClONO_2$ until the spring time release of bromine. During spring time, the presence of active bromine adds a new channel by which NO_2 can react. This new channel increases the loss of NO_x by $BrONO_2$ production. And the mechanism of *Fan & Jacobs* [1992] has $BrONO_2$ transferring into the aqueous phase where nitrogen in $BrONO_2$ forms HNO_3(aq). Thus, the total amount of NO_x in the atmosphere is reduced. Although in the model the nitrogen in HNO_3(aq) is converted into HONO and released back to the atmosphere, this rate is slow, resulting in the formation of HNO_3(aq). *Jones et al.* [2000] have measured photo-chemical production of NO_x in the snowpack of Antarctic. The high level of NO_3^- content they measured in the snowpack allowed them to attribute the source for NO_x as NO_3^-. It may not be too early at this point to establish a link between the

event of BrO catalytic destruction of O_3 and the budget of NO_x in the polar environment.

In this model, the removal for $BrONO_2$ and $ClONO_2$ are not treated equally. The loss for the former includes aqueous phase uptake, thus it is more rapid. Over the last decade, due to the impact of O_3 depletion in stratosphere, measurements of $ClONO_2$ in the stratosphere have been made (e.g., *Zander et al.* [1992]). However, direct measurement of $ClONO_2$ in the remote troposphere has not been done. This is partly due to the difficulty in spectroscopic measurement since the level of tropospheric $ClONO_2$ is thought to be low. *Pszenny at al.* [1993] have measured concentrations of HCl^* chemically (HCl^* could include HCl, $ClONO_2$ $ClNO_2$ and NOCl) at 40 to 268 pptv over Virginia Key, Florida. It was not known how much of HCl^* is in the form of $ClONO_2$ in their measurements. It is curious to find out what sort of HCl^* level would be if the similar measurement was done at the polar region. A knowledge of the $ClONO_2$ level would certainly assist the quantification of NO_x budget in the remote troposphere. For instance, if the level of $ClONO_2$ is comparable or greater than that of NO_x ($\sim$ 0.1 to 10 pptv), the recycling of nitrogen from $ClONO_2$ may be important. And if $ClONO_2$ is recycled, one also would have to re-consider the impact on the chlorine budget. In the stratosphere, the reaction

$$ClONO_2(g) + H_2O(s) \rightarrow HOCl(g) + HNO_3(s)$$

reactivates chlorine tied up as $ClONO_2$ and deactivates nitrogen in $HNO_3(s)$ on the PSCs. If this reaction is favorable in tropospheric polar conditions then nitrogen would not be deactivated since, according to *Jones et al.* [2000], NO_3^- in the snow could be the source for NO_x.

This work has studied the non-linear behaviors exhibited in both the BrO catalytic cycle and in the mechanism of *Fan and Jacob* [1992]. *Hausmann & Platt* [1994] first pointed out the non-linear phenomenon of Br atom 'explosion'. That is, the turn over of bromine from BrO to Br atom immedi-

ately before O_3 is depleted. In this work, the *Fan and Jacob* [1992] mechanism adds another layer of complexity to this phenomenon. The model simulation shows that the Br atom 'explosion' is fueled by HOBr(aq) instead of BrO. This is because when O_3 is being depleted, bromine in BrO can transfer gradually to HOBr(aq) and the Br atom 'explosion' is buffered. The explosive release of bromine from HOBr(aq) is triggered when the O_3 has depleted. In addition, the model points out if all the bromine is transfered to HOBr(aq) before O_3 depletion, the mechanism of *Fan and Jacob* [1992] can shut down. However, this can be ameliorated if production of HOBr(aq) in the model is reduced.

The phenomenon of Br atom 'explosion' can possibly explain the behavior of HCHO observed by *Sumner & Shepson* [1999]. Similar to the observation of *de Serves* [1994], they observed a strong inverse correlation between HCHO and O_3 at partial depletion. However, at one episode of complete O_3 destruction, HCHO is exceptionally low. The simulation in this work shows that after the depletion of O_3, the elevated Cl atom density can result in high production of HCHO from CH_4 oxidation. However, immediately after O_3 depletion the Br atom 'explosion' can completely destroy HCHO. If this is true in the real atmosphere, *Sumner & Shepson* [1999] may have seen the effect of the Br atom 'explosion'.

This model is unable to reproduce the level of HCHO see in field observations (> 600 pptv). *Sumner & Shepson* [1999] have measured elevated HCHO in the snowpack at levels exceeding that in the atmosphere. They proposed an aqueous phase photo-chemical source in the snowpack. However, another study by *Hutterli & Röthlisberger* [1999] attributed the elevated HCHO in the snowpack to temperature-dependent degassing of HCHO deposited with snowfall. It is not clear how much HCHO can be produced in gas phase due to elevated Cl atom density. A modeling study for the production of HCHO from NMHC is not available at this point.

References

Abbatt, J.P.D., Heterogeneous Reaction of HOBr and HBr and HCl on ice surfaces at 228 K, *J. Geophys. Res. Lett.*, *21*, 665–668, 1994.

Altshuller, A.P., and McPerson S.P., Spectrophotometric Analysis of Aldehydes in the Los Angeles Atmosphere. *J. Air Pollot. control ass.*, *13*, 109–111, 1961.

Anlauf, K.G., R.E. Mickle, and N.B.A. Trivett. Measurement of Ozone during Polar Sunrise Experiment 1992, *J. Geophys. Res.*, *99*, 25,345–25,353, 1994.

Ariya, P.A., B.T. Jobson, R.sander, H. Niki, and G.W. Harris, Measurement of C_2-C_7 Hydrocarbons During the Polar Sunrise Experiment 1994: Further evidence for halogen chemistry in the troposphere, *J. Geophys. Res.*, *103*, 13,169–13,180, 1999.

Atkinson R., D.L. Baulch, R.A. Cox, R.F. Hampson Jr., J. A. Kerr J. Troe, Evaluatied Kinetic and Photochemical Data for Atmospheric Chemistry: Supplement IV, *Atmos. Environ.*, *7*, 1187–1230, 1992

Barrie, L.A., J.W. Bottenheim, R.C. Schnell, P.J. Crutzen, and R.A. Rasmussen, Ozone Destruction and Photochemical Reactions at Polar Sunrise in the Lower Arctic Atmosphere, *Nature*, *334*, 138–141, 1988.

Barrie, L.A., and J.W. Bottenheim, Sulphur and Nitrogen Pollution in the Arctic Atmosphere, in : *Pollution of the Arctic Atmosphere*, W.T. Sturges, Editor, 155–183, Elsevier Science Publisher, London, 1991.

Behnke, W., & C. Zetzsch, Heterogeneous Formation of Chlorine Atoms From Various Aerosols in the Presence of O_3 and HCl, *J. Aerosol Sci. 20*, 1167–1170, 1989.

Behnke, W., & C. Zetzsch, Production of a Photolytic Precursor of Atomic Cl from Aerosols and Cl^- in the Presence of O_3, in *Naturally-Produced Organohalogens (Environment & Chemistry, Vol 1)*, by Grimvall, A., Ed W.B.De Leer, Kluwer Academic, Norwell, Mass., 1995.

Beine, H.J., D.A. Jaffe, F. Stordal, M. Engardt, S Solberg, N. Schmidbauer, and K. Holmen, NO_x during ozone depletion events in the arctic troposphere at Ny-Ålesund, Svalbard, *Tellus. 49B* 556–565, 1997.

Berg, W.W., P.D. Sperry, K.A. Rahn, and E.S. Gladney, Atmospheric Bromine in the Arctic, *J. Geophys. Res.*, *88*, 6,719–6,736, 1983.

Bottenheim, J. W., A.C. Gallant, and K.A. Brice, Measurements of NO_y Species and O_3 at 82°N Latitude, *J. Geophys. Res. Lett.*, *13*, 113–116, 1986.

Bottenheim, J. W., L. A. Barrie, E. Atlas, L. E. Heidt, H. Niki, R. A. Rasmussen, and P. B. Shepson, Depletion of Lower Troposphere Ozone During Arctic Spring: The Polar Sunrise Experiment 1988, *J. Geophys. Res., 95,* 18,555–18,568, 1990.

Brasseur G. and Soloman S., Aeronomy of the Middle Atmosphere, 2^{nd} edition, *D. Reidel Publishing Company, Dordrecht*, Holland, 1986.

Burden, Richard L. and J. Douglas Faires, Numerical Analysis, 4^{th} edition, *PWS-KENT Publishing Company*, Boston, 1989.

Chance, Kelly, Analysis of BrO Measurements from the Global Ozone Monitoring Experiment. *Geophys. Res. Letters, 25,* 3335–3338, 1998

De Serves, Claes, Gas Phase Formaldehye and Peroxide Measurements in the Arctic Atmosphere, *J. Geophys. Res., 99,* 25,371–25,398, 1994.

DeMore, W. B., Sander, S. P., Golden, D. M., Hampson, R. F., Kurylo, M. j., Howard, C. J., Ravishankara, A. R., Klob, C. E., Molina. M. J., Chemical Kinetics and Photochemical Data for Use in Stratospheric Modelling, Evaluation Number 11, *Jet Propulsion Laboratory Publication*, 94-26, 1994.

Dryssen, E. & E. Fogelqvist, *Oceanologica Acta 4*, 313–317, 1981

Duce, R.A., J.T. Wasson, J.W.Winchester, and F. Burns, Atmospheric Iodine, Bromine and Chlorine, *J. Geophys. Res., 68,* 3,943–3,947, 1993.

Duce, R.A., J.W. Winchester, and T.W. Van Nahl, Iodine, Bromine, and Chlorine in the Hawaiian Atmosphere, *J. Geophys. Res., 70,* 1,775–1,799, 1965.

Duce, R.A., A.H. Woodcock, and J.L. Moyers, Variations of Ratios with Size among Particles in Tropical Oceanic Air, *Tellus, 19,* 369–379, 1967.

Eigen, M. & K, Kustin, The Kinetics of Halogen Hydrolysis, *Am. Chem. Soc., 84,* 1355—1361, 1962.

Eriksson, E., The Yearly Circulation of Chloride and Sulfur in Nature; Meteeorological, Geochemical and Pedogical Implications, *Tellus, 12,* 63–109, 1960.

Fan S. M. and D. J. Jacob, Surface ozone depletion in Arctic spring sustained by bromine reactions on aerosols, *Nature, 359,* 522-524, 1992.

Finlayson-Pitts, B.J., M.J. Ezell, and J.N. Pitts, Jr., Formation of Chemically Active Chlorine Compunds by Reactions of Atmospheric NaCl Particles with Gaseous N_2O_5 and $ClONO_2$, *Nature, 337,* 241–244, 1989.

Finlayson-Pitts, B.J., F.E. Livingston, and H.N. Berko, Ozone Destruction and Bromine Photochemistry at Ground Level in the Arctic Spring, *Nature, 343,* 622–624, 1990.

Finlayson-Pitts, B.J. and Pitts. Jr, J.N., Atmospheric Chemistry: Fundamentals and Experimental Techniques, *A Wiley-Interscience Publication*, N.Y., 961-977, 1986.

Gracdel, T.E., & Keene, W.C., Tropospheric budget of reactive chlorine. *Global Biogeochemical cycle, 9*, 47-77, 1995.

Hausmann, M. and U. Platt. Spectroscopic Measurement of Bromine Oxide and Ozone in the High Arctic During Arctic During Polar Sunrise Experiment 1992. *J. Geophys. Res., 99*, 25,399-25,413. 1994.

Honrath, R.E., M.C. Peterson, and S. Guo, J.E. Dibb, P.B. Shepson and B. Campbell, Evidence of NO_x Production Within or Upon Ice Particles in the Greenland Snowpack, *J. Geophys. Lett., 26*, 695-698. 1999

Hopper, J.F., & W.Hart, Meteorological Aspects of the 1992 Polar Sunrise Experiment. *J. Geophys. Res., 99*, 25,315-25,328, 1994.

Hopper, J.F., B. Peter, Y. Yokouchi, H. Niki, B.T. Jobson, P.B. Shepson, and K. Muthuramu, Chemical and Meteorological Observations at Ice Camp SWAN During Polar Sunrise Experiment 1992, *J. Geophys. Res., 99*, 25,489-25,498. 1994.

Hopper, J.F., L.A. Barrie, A. Silis, W. Hart, A.J. Gallant, and H. Dryfhout, Ozone and Meteorology During the 1994 Polar Sunrise Expeeriment, *J. Geophys. Res., 103*, 1481-1492. 1998.

Hutterli, M.A. & R. Röthlisberger, Atmosphere-to-Snow-to-Firn Transfer Studies of HCHO at Summit, Greenland. *Geophys. Res. Lett., 26*, 1691-1694, 1999.

Impey, G.A., P.B. Shepson, D.R. Hastie, L.A. Barrie, Measurements of Photolyzable Chlorine and Bromine During the Polar Sunrise Experiment 1995, *J. Geophys. Res., 102*, 16,005-16,010, 1997a.

Impey, G.A., P.B. Shepson, D.R. Hastie, L.A. Barrie, Measurements Technique for the Determination of Photolyzable Chlorine and Bromine in the Atmosphere, *J. Geophys. Res., 102*, 15,999-16,004, 1997b.

Jaffe, D., The Relationship Between Anthropogenic Nitrogen Oxides and Ozone Trends in the Arctic Troposphere, in *Tropospheric Chemistry of Ozone in Polar Regions*, eds. H. Niki and K.H. Becker, *NATO ASI Series I*, Global Environmental Change, vol.7, pp 105-115, Springer-Verlag, NY, 1993.

Jobson, B.T., Seassonal Trends of Non Methane Hydro Carbons at Remote Bareal and Hight Arctic Sites, *Ph.D. disssertation*, York Univ., Toronto, Ont. Canada, 1994.

Jobson, B. T., H. Niki, Y. Yokouchi, J. Botenheim, F. Hopper, and R. Leaitch, Measurements of C_2-C_6 hydrocarbons during the Polar Sunrise 1992 Experiment: Evidence for

Cl atom and Br atom chemistry, *J. Geophys. Res.*, *99*, 25,355–25.368, 1994.

Jones, A.E., E.W. Wolff, H-W. Jacobi, Speciation and Rate of Photochemical NO and NO_2 Production in Antarctic Snow. *J. Geophys. Lett.*, *27*. 343–348. 2000.

Kahl, J.D. & E.L. Andreas, Theoretical Heights of Buoyant Convection Above Open Leads in the Winter Arctic Pack Ice Cover, *J. Geophys. Res.*, *97* 9411–9422, 1992.

Keene, W.C., A.A.P. Pszenny, D.J. Jacob, R.A. Duce, J.N. Galloway, J.J. Schultz-Tokos Jr., H. Sievering, and J.F. Boatman, The Geochemical Cycling of Reactive Chlorine Through the Marine Troposphere, *Global Biogeochem. Cycles*, *4*, 407–430, 1990.

Kieser, B.N., J.W. Bottenheim, T. Sideris, and H. Niki. Spring 1989 Obsevations of Lower Tropospheric Chemistry in the Canadian High Arctic, *Atmos. Environ.*, *27A*. 2979–29881, 1993.

Kirchner, U., Th. Benter, and R.N. Schindler, Experimenhtal Verification of Gas Phase Bromine Enrichment in Reactions of HOBr with Sea Salt Doped Ice Surfaces. *Ber. Bunsenges. Phys. Chem.*, *101*. 975–977, 1997.

Kondratyev K. Ya., Radiation Processes in the Atmosphere. Second IMO lecture. *World Meteorological Organization, WMO N0. 309*, p.21, 1972.

Khalil, M.A.K., and R.A.Rasmussen, The Changing Composition of the Earth's Atmosphere, in *Composition, Chemistry, and Climate of the Atmosphere*, Singh, Hanwant B. (ed.), *Van Nostrand Reinhold*. 1995.

Le Bras, G., and U. Platt, A Possible Mechanism for Combined Chlorine and Bromine Catalyzed Destruction of Tropospheric Ozone in the Arctic, *Geophys. Res. Letters*, *21*, 599-602, 1995.

Leaitch W. R., L. A. Barrie, J. W. Botttenheim, S. M. Li, P. B. Shepson, K.Muthuramu, and Y. Yokouchi, Airborne Obeservations Related to Ozone Depletion at Polar Sunrise. *J. Geophys. Res.*, *99*. 25.499–25,517, 1994.

Lelieveld, J., and P.J. Crutzen. The Role of Clouds in Tropospheric Photo Chemistry. *J. Atmos. Chem.*, *12*, 229–267, 1991.

Li, Shao-Ming, Equilibrium of Particle Nitrite with Gas Phase HONO : Tropospheric Measurements in the High Arctic During Polar Sunrise, *J. Geophys. Res.*, *99*, 25.469–25.478, 1994.

Li, S.-M., Y. Yokouchi, L.A.Barrie, K. Muthutamu, P.B. Shepson, J.W. Bottenheim, W.T. Sturges, and S. Landsberger, Organic and in Organic Bromine Compunds and Their Composition in the Arctic Troposphere During Polar Sunrise, *J. Geophys. Res.*, *99*. 25,415–25,428, 1994.

Lightfoot, P.D., R.A. Cox, J.N. Crowley, M. Destriau, G.D. Hayman, M.E. Jenkin, G.K. Moortgat and F. Zabel, Organic Peroxy Radicals: Kinetics, Spectroscopy and Tropospheric Chemistry, *Atmos. Environ.*, *10*, 1805—1961, 1992

Livingston, F.E., and B.H. Finlayson-Pitts, The Reaction of gaseous N_2O_5 with solid NaCl at 298 K: Estimated lower Limit to the Reaction Probablity and its Potential Role in Tropospheric and Stratospheric Chemistry, *Geophys. Res. Lett.*, *18*, 17–20, 1991.

Lowe, D.C. & S. Ulrich, Formaldehyde (HCHO) Measurement in the Nonurban Atmosphere. *J. Geophys. Res.*, *88*, 10,844–10,858, 1983.

McConnell, J.C., and G.S. Henderson, Ozone Depletion During Polar Sunrise, in *Tropospheric Chemistry of Ozone in Polar Regions*, eds. H. Niki and K.H. Becker, *NATO ASI Series I*, Global Environmental Change, vol.7, pp 89–103, Springer-Verlag, NY, 1993.

McConnell, J.C., G.S. Henderson, L. Barrie, J. Bottenheim, H. Niki, C.H. Langford and E.M.J. Templeton, Photochemical Bromine Production Implicated in Arctic Boundary-Layer Ozone Depletion, *Nature*, *355*, 150–152, 1992.

McElroy, M.P., Salawitch, R.J., Wofsy, S.C. and Logan, J.A., Reduction of Antarctic Ozone Due to synergistic Interactions of Chlorine and Bromine, *Nature 321*, 759–762, 1986.

McElroy, C.T., C.A. McLinden, and J.C. McConnell, Evidence for Bromine Monoxide in the Free Troposphere During the Arctic Polar Sunrise, *Nature*, *397*, 338–341, 1999.

Miller, H.L., A. Weaver, R.W. Sanders, K. Arpag, and S. Solomon, Measurements of Arctic Sunrise Surface Ozone Deleption Events at kangeerlussuaq, Greenland (67°N, 51°W) *Tellus*, *49B*, 496-509, 1997.

Molina, L. T. and M. J. Molina, Production of Cl_2O_2 from the self-reaction of the ClO radical, *J.Phys. Chem.*, *91*, pp 433–, 1987.

Moyers, J.C., and R.A. Duce, Gaseous and Particulate Bromine in the Marine Atmosphere, *J. Geophys. Res.*, *77*, 5,330–5,338, 1972.

Mozurkewich M., Mechanisms for the Release of Halogens From Sea-Salt Particles by Free Radical Reactions, *J. Geophys. Res.*, *100*, 14,199–14,207, 1995.

Mulvaney, R., G.F.J.Coulson and H.F.J.Corr, The Fractionation of Sea Salt and Acid During Transport Across an Antarctic Ice Shelf, *Tellus*, *45B*, 179–187, 1993.

Oltmans, S.J., and W.D.Komhyr, Surface Ozone Distributions and Variation from 1973-1984 Measurements at the NOAA Geophysical Monitoring for Climate Change Baseline Observatories, *J. Geophys. Res.*, *91*, 5229, 1996.

Orlando, J. & S. Schauffler, Halogen Compounds, in *Atmospheric Chemistry and Global Change*, eds. G.P. Brasseur, J.J. Orlando, and G.S. Tyndall, *Oxford University Press*. pp.302–316, N.Y. Oxford, 1999.

Press, W.H., B.P. Flannery, S.A. Teukolsky, and W.T. Vetterling et al., Numerical Recipes. The Art of Scientific Computing. *Cambridge University Press*, 1986. 1986

Pszenny, A.A.P., W.C. Keene, D.J. Jacob, S. Fan, J.R. Maben, M.P. Zetwo, M. Springer-Young, and J.N. Galloway, Evidence of Inorganic Chlorine Gases Other Than Hydrogen Chlorine in Marine Surface Air, *Geophys. Res. Lett.*, *20*, 699–702, 1993.

Ramacher, B., J.Rudolph, and R. Koppmann, Hydrocarbon Measurements During Tropospheeric Ozone depletion events: Evidence for Halogen atom chemistry, *J. Geophys. Res.*, *104*, 3633–3653, 1999.

Rogers, R.R., and M.K. Yau, A Short Course in Cloud Physics, 3ed., *International Series in Natural Philosophy*, *113*, Pergamon Press, Oxford, 1989.

Robbins, R.C., R.D. Cadle, and D. L. Eckhardt, The Conversion of Sodium Chloride to Hydrogen Chlorine in the Atmosphere, *J. Meteorol.*, *16*, 53–56, 1956.

Sander, R., R. Vogt., G. Harris, P.J. Grutzen, Modeling the Chemistry of Ozone, Halogen Compounds, and Hydrocarbons in the Arctic Troposphere During Spring. *Tellus*. *49B*. 522-535, 1997.

Schnell, R.C., R.G. Barry, M.W. Miles, E.L. Andreas, L.F. Radke, C.A. Brock, M.P.McCormick, and J.L.Moore, Lidar Detection of Leads in Arctic Sea Ice, *Nature*, *339*, 530–532, 1989.

Schroeder, W.H., & P. Urone, Formation of Nitrosyl Chloride From Sea Particles in Air. *Environ. Sci. Technol.*, *8* 756–758, 1974.

Steinfeld, J.H., Atmospheric Chemistry and Physics of Air, *A Wiley-Interscience publication*, 1986.

Singh, H.B. & F. Kasting, Chlorine-Hydrocarbon Photochemistry in the Marine Troposphere and Lower Stratosphere, *J. Atmos. Chem.* *7*, 261-285, 1988.

Solberg, S., N.Schmidbauer, A.Semb, F.Stordal, and O.Hov, Boundary Layer Ozone depletion as seen in the Norwegian Arctic in Spring. *J. Atmos. Chem.*, *23*, 301-332, 1996.

Spivakovsky, C.M, R. Yevich, J.A. Logan, S.C. Wofsy, and M.B. McElroy, Tropospheric OH in a three-dimensional chemical tracer model: and assessment based on observation of CH_3CCl_3, *J. Feophys. Res.*, *95*, p.18411, 1990.

Stewart, R.W., Multiiple Steady States in Atmospheric Chemistry. *J. Geophys. Res.*, *98*, 20601–20611, 1993.

Sumner, Ann Louise & Paul B. Shepson, Snowpack Production of Formaldehyde and its Effect on the Arctic Troposphere, *Nature 398*, 230–233, 1999.

Tang, T., and J.C. McConnell, Autocatalytic Release of Bromine from Arctic Snow Pack During Polar Sunrise. *Geophys. Res. Lett.*, *23*, 2633-2636, 1996a.

Tang, T., and J.C. McConnell, On the Relative Roles of Bromine and Chlorine During Spring Time Depletion of Ozone in the Arctic Boundary Layer. in *Atmospsheric Ozone. Proceedings of the XVIII Quadrennial Ozone Symposium, L'Aquila, Italy* . eds. Bojkov, R.D. & G., Visconti, *Int. Ozone Commission. L'Aquila*, 427–430. 1996b.

Templeton, E.M. & J.C. McConnell, 1-D Modelling of the Polar Ozone Anomaly and Effect of Halocarbons on the Ozone Layer, *Dept of Earth and Atmospheric Science. York University, Toronto, Canada*, 1991.

Tuckermann, M., R. Ackermann, C. Gölz, H. Loreenzen-Schmidt, T.Senne, J. Stutz, B. Trost, W. Unold, and U. Platt, DOAS Observation of Halogen Radical-Catalysed Arctic Boundary Layer Ozone Destruction During the ARCTOC-campaigns 1995 and 1996 in Ny-Ålesund, Spitsbergen. *Tellus*, *49B*, 533–555. 1997.

Tyndall, Geoffrey & J. Orlando, Chemical and Photochemical Processes, in *Atmospheric Chemistry and Global Change*, eds. G.P. Brasseur, J.J. Orlando, and G.S. Tyndall, *Oxford University Press*, pp. 96–97. N.Y. Oxford, 1999.

Vogt, R., P.J. Crutzen, & Rolf Sander, A Mechanism for Halogen Release From Sea-Salt Aerosol in the Remote Marine Boundary Layer, *Nature. 383*, 327–330. 1996.

Waddington, E.D., J. Cunningham, and S.L. Harder, The Effects of Snow Ventilation on Chemical Concentrations, in *Chemical Exchange Between the Atmosphere and Polar Snow*, eds. Wolff E.W. and R.C. Bales. *NATO ASI Series I*, Global Environmental Change, vol.43, pp 403–450. Springer-Verlag, Berlin, 1996.

Wessel, S., S. Aoki, P. Winkler, R. Weller, A. Herber, H. Gernandt, and O. Schrems, Tropospheric Ozone Depletion in Polar Regions: A Comparison of Observations in the Arctic and Antarctic, *Tellus*, *50B*, 34-50, 1998.

Well, N. *The Atmosphere and Ocean. A Physical Introduction*, p 30, Taylor & Francis, London & Philadelphia, 1986.

Wingenter, O.W., M.K. Kubo, N.J. Blake, T.W. Smith Jr., D.R. Blake, and F.S. Rowland, Hydrocarbon and Halocarbon Measurements as Photochemical and Dynamical Indication of Atmospheric Hydroxyl, Atom Chlorine, and Veritcal Mixing Obtained During Lagrangian Flights, *J. Geophys. Res.*, *101*, 4331–4340. 1996.

Wolff, E.W. and S. Martin, Sea Ice as a Source of Sea Salt Aerosol in Polar Regions. *IGAC Activities, Newsletter of the International Global Atmospheric Chemistry Project 14*, 10 - 11, Sept., 1998.

Yung Y.L., A Numerical Method for Calculation the Mean Intensity in an Inhomogeneous Rayleigh Scattering Atmophere, *J. Quant. Spectrosc. Radiat. Transfer. 16*, 755–761, 1976.

Yokouchi, Y., H. Akimoto, L.A. Barrie, J.W. Bottenheim, K. Anlauf, and B.T. Jobson, Serial Gas Chromatographic/Mass Spectrometric Measurements of Some Volatile Organic Compounds in the Arctic Atmosphere During the 1992 Polar Sunrise Experiment. *J. Geophys. Res., 99*, 25,379–25,389, 1994.

Zander, R., E. Mahieu, M.R. Gunson, M.C. Farmer, C.P. Rinsland, F.W. Irion, and E.Mahieu, The 1985 Chlorine and Fluorine Inventories in the Stratosphere Based on ATMOS Observations at 30° North Latitude, *J. Atmos. Chem.*, *15*, 1992.

Appendix A
Reactions in the Model

Table A.1: O_3, HO_x and NO_x Reactions

	Reaction	Rate[1]	Note
1	$O_3 \xrightarrow{h\nu} O_2 + O^1D$	see Fig B.1a	
2	$O^1D \xrightarrow{O_2,M} O_3$	9.19×10^{8}	2
3	$O^1D + H_2O \rightarrow 2OH$	2.20×10^{-10}	2
4	$OH + H_2 \xrightarrow{O_2} HO_2 + H_2O$	1.57×10^{-15}	2
5	$OH + O_3 \rightarrow HO_2 + O_2$	3.45×10^{-14}	2
6	$HO_2 + O_3 \rightarrow HO_2 + 2O_2$	1.43×10^{-15}	2
7	$OH + HO_2 \rightarrow H_2O + O_2$	1.18×10^{-10}	2
8	$OH + OH \xrightarrow{M} H_2O_2$	5.68×10^{-12}	2
9	$HO_2 + HO_2 \rightarrow H_2O_2 + O_2$	2.66×10^{-12}	2
10	$H_2O_2 + OH \rightarrow HO_2 + H_2O$	1.46×10^{-12}	2
11	$H_2O_2 \xrightarrow{h\nu} 2OH$	see Fig B.1c	
12	$NO + O_3 \rightarrow NO_2 + O_2$	6.60×10^{-15}	2
13	$NO_2 \xrightarrow{h\nu} NO + O_3$	see Fig B.1c	
14	$NO_2 + O_3 \rightarrow NO_3 + O_2$	5.18×10^{-18}	2
15	$NO_3 \xrightarrow{h\nu,O_2} NO_2 + O_3$	1.80×10^{-1}	4
16	$NO_3 \xrightarrow{h\nu} NO + O_2$	2.20×10^{-2}	4
17	$NO_3 + NO \rightarrow 2NO_2$	3.14×10^{-11}	2
18	$NO_3 + NO_2 \xrightarrow{M} N_2O_5$	1.52×10^{-12}	2
19	$N_2O_5 \xrightarrow{M} NO_2 + NO_3$	1.61×10^{-5}	2
20	$N_2O_5 \xrightarrow{h\nu} NO_2 + NO_3$	see Fig B.1d	
21	$NO + HO_2 \rightarrow NO_2 + OH$	9.85×10^{-12}	2
22	$NO + OH \xrightarrow{M} HONO$	7.12×10^{-12}	2
23	$HONO \xrightarrow{h\nu} NO + OH$	see Fig B.1e	
24	$NO_2 + OH \xrightarrow{M} HNO_3$	1.81×10^{-11}	2
25	$HNO_3 + OH \xrightarrow{M} NO_3 + H_2O$	3.06×10^{-13}	2
26	$HNO_3 \xrightarrow{h\nu} NO_2 + OH$	see Fig B.1f	
27	$HO_2 + NO_2 \xrightarrow{M} HNO_4$	2.38×10^{-12}	2
28	$HNO_4 \xrightarrow{M} HO_2 + NO_2$	5.41×10^{-5}	2
29	$HNO_4 + OH \rightarrow NO_2 + H_2O + O_2$	6.13×10^{-12}	2
30	$HNO_4 \xrightarrow{h\nu} HO_2 + NO_2$	see Fig B.1g	

Table A.2: Reactions of Bromine

	Reaction	Rate[1]	Note
1	$CHBr_3 \xrightarrow{h\nu} 3Br + OH + CO$	see Fig B.1h	3
2	$Br + O_3 \rightarrow BrO + O_2$	6.49×10^{-13}	2
3	$BrO \xrightarrow{h\nu,O_2} Br + O_3$	see Fig B.1i	
4	$BrO + BrO \rightarrow 2Br + O_2$	2.58×10^{-12}	2
5	$BrO + BrO \rightarrow Br_2 + O_2$	6.95×10^{-13}	2
6	$Br_2 \xrightarrow{h\nu} 2Br$	see Fig B.1j	
7	$BrO + OH \rightarrow Br + HO_2$	1.63×10^{-11}	2
8	$BrO + NO \rightarrow Br + NO_2$	2.54×10^{-11}	2
9	$BrO + HO_2 \rightarrow HOBR + O_2$	4.77×10^{-11}	2
10	$BrO + NO_2 \xrightarrow{M} BrONO_2$	1.91×10^{-12}	2
11	$HOBR \xrightarrow{h\nu} Br + OH$	see Fig B.1k	
12	$BrONO_2 \xrightarrow{h\nu} Br + NO_3$	see Fig B.1l	
13	$Br + HO_2 \rightarrow HBr + O_2$	1.30×10^{-12}	2
14	$Br + H_2O_2 \rightarrow HBr + HO_2$	4.81×10^{-17}	2
15	$HBr + OH \rightarrow Br + H_2O$	1.10×10^{-11}	2

Table A.3: Reactions of Chlorine

	Reaction	Rate[1]	Note
1	$Cl + O_3 \rightarrow ClO + O_2$	1.00×10^{-11}	2
2	$Cl + HO_2 \rightarrow ClO + OH$	6.53×10^{-12}	2
3	$ClO \xrightarrow{h\nu,O_2} Cl + O_3$	see Fig B.1m	
4	$ClO + ClO \xrightarrow{M} Cl_2O_2$	7.6×10^{-13}	2
5	$ClO + ClO \rightarrow Cl + ClO_2$	2.19×10^{-15}	2
6	$ClO + ClO \rightarrow Cl_2 + O_2$	2.19×10^{-15}	2
7	$ClO + ClO \rightarrow Cl + OClO$	4.87×10^{-16}	2
8	$OClO + Cl \rightarrow 2ClO$	6.53×10^{-11}	2
9	$OClO \xrightarrow{h\nu,O_2} ClO + O_3$	see Fig B.1n	
10	$ClO_2 \xrightarrow{M} Cl + O_2$	7.12×10^{6}	2
11	$Cl_2O_2 \xrightarrow{M} 2ClO$	2.66×10^{-1}	2
12	$Cl_2O_2 \xrightarrow{h\nu} 2Cl + O_2$	see Fig B.1o	
13	$Cl_2 \xrightarrow{h\nu} 2Cl$	see Fig B.1p	
14	$ClO + OH \rightarrow Cl + HO_2$	1.63×10^{-11}	2
15	$ClO + NO \rightarrow Cl + NO_2$	2.09×10^{-11}	2
16	$ClO + HO_2 \rightarrow HOCl + O_2$	8.36×10^{-12}	2
17	$ClO + NO_2 \xrightarrow{M} ClONO_2$	4.52×10^{-12}	2
18	$HOCl \xrightarrow{h\nu} Cl + OH$	see Fig B.1q	
19	$ClONO_2 \xrightarrow{h\nu} Cl + NO_3$	see Fig B.1r	
20	$ClONO_2 + Cl \rightarrow 2Cl + NO_3$	1.31×10^{-11}	2
21	$Cl + HO_2 \rightarrow HCl + O_2$	3.60×10^{-11}	2
22	$Cl + H_2 \xrightarrow{O_2} HCl + HO_2$	3.10×10^{-15}	2
23	$Cl + H_2O_2 \rightarrow HCl + HO_2$	2.01×10^{-13}	2
24	$HCl + OH \rightarrow Cl + H_2O$	6.23×10^{-13}	2

Table A.4: Reaction for Interaction of ClO and BrO

	Reaction	Rate[1]	Note
1	$ClO + BrO \rightarrow OClO + Br$	9.25×10^{-12}	2
2	$ClO + BrO \rightarrow ClO_2 + Br$	7.12×10^{-12}	2
3	$ClO + BrO \rightarrow BrCl + O_2$	1.16×10^{-12}	2
4	$BrCl \xrightarrow{h\nu} Br + Cl$	see Fig B.1s	

Table A.5: Reactions of Methane

	Reaction	Rate[1]	Note
1	$CH_4 + OH \xrightarrow{O_2} CH_3O_2 + H_2O$	1.72×10^{-15}	2
2	$CH_4 + Cl \xrightarrow{O_2} CH_3O_2 + HCl$	3.63×10^{-14}	2
3	$CH_3O_2 + HO_2 \rightarrow CH_3OOH + O_2$	1.03×10^{-11}	8
4	$CH_3O_2 + CH_3O_2 \rightarrow HCHO + CH_3OH + O_2$	4.09×10^{-13}	8
4	$CH_3O_2 + CH_3O_2 \rightarrow 2HCHO + 2HO_2 + O_2$	8.80×10^{-14}	8
5	$CH_3O_2 + NO \xrightarrow{M} HCHO + HO_2 + NO_2$	9.31×10^{-12}	5.8
6	$CH_3O_2 + NO \xrightarrow{M} CH_3ONO_2$	9.32×10^{-15}	5.8
7	$HCHO + OH \xrightarrow{O_2} CO + HO_2 + H_2O$	1.00×10^{-11}	2
8	$HCHO + Br \xrightarrow{O_2} CO + HO_2 + HBr$	6.49×10^{-13}	2
9	$HCHO + Cl \xrightarrow{O_2} CO + HO_2 + HCl$	7.17×10^{-11}	2
11	$HCHO \xrightarrow{h\nu,O_2} CO + 2HO_2$	see Fig B.1t	
12	$HCHO \xrightarrow{h\nu} CO + H_2$	see Fig B.1u	
13	$HCHO + NO_3 \rightarrow HNO_3 + HO_2 + CO$	6.00×10^{-16}	2,6,7
14	$HCHO + HO_2 \rightarrow HOCH_2O_2$	1.24×10^{-13}	9
15	$HOCH_2O_2 \xrightarrow{M} HCHO + HO_2$	9.37×10^{-1}	9
16	$CH_3OOH \xrightarrow{h\nu,O_2} HCHO + HO_2 + OH$	see Fig B.1v	
17	$CH_3OOH + OH \rightarrow CH_3O_2 + H_2O$	6.02×10^{-12}	2
18	$CH_3OOH + OH \rightarrow HCHO + OH + H_2O$	2.58×10^{-12}	2
19	$CH_3OOH + Br \rightarrow CH_3O_2 + HBr$	3.68×10^{-15}	6,10
20	$CH_3OOH + Cl \rightarrow CH_3O_2 + HCl$	8.29×10^{-12}	6,11
21	$CH_3ONO_2 + OH \rightarrow NO_2 + Product$	3.50×10^{-13}	6,9
22	$CH_3ONO_2 + Cl \rightarrow NO_2 + Product$	2.40×10^{-13}	6,9
23	$CO + OH \xrightarrow{O_2} HO_2 + CO_2$	2.40×10^{-13}	9

Table A.6: Recycling Mechanism

	Reaction	Rate[12]	Note
1	$HBr \rightarrow Br^-(aq)$	2.00×10^{-3}	13
2	$HOBr \rightarrow HOBr(aq)$	1.40×10^{-4}	13
3	$BrONO_2 \rightarrow BrONO_2(aq)$	1.30×10^{-4}	13
4	$BrONO_2(aq) \xrightarrow{H_2O} HOBr(aq) + HNO_3(aq)$	4.00×10^{-3}	13
5	$HOBr(aq) + Br^-(aq) \xrightarrow{H+} Br_2 + H_2O$	4.00×10^{-3}	13
6	$HNO_3(aq) \rightarrow HONO$	1.00×10^{-5}	14
7	$HCl \rightarrow Cl^-(aq)$	2.00×10^{-3}	15
8	$Cl^-(aq) \rightarrow \frac{1}{2}Cl_2$	2.00×10^{-3}	15

Note :

[1] All rates unless otherwise indicated are calculated at 245K. Unit: for photolysis rate. s^{-1}; two body rate, $cm^3molec^{-1}s^{-1}$; unimolecular dissociation, s^{-1}. Three body rates are given as equivalent two body rates where the third body [M]=2.99×10^{19}molec·cm^{-3} has been incorporated into the coefficient.

[2] *DeMore et al.*, [1992].

[3] Simplified oxidation scheme.

[4] Estimated.

[5] Upper limit.

[6] Measurement at temperature = 298K.

[7] Products are estimated.

[8] *Lightfoot et al.*, [1992].

[9] *Atkinson et al.*, [1992].

[10] *Osamu and Sidney*, [1984].

[11] *Singh and Kasting*, [1988].

[12] Gas to particle reactions are treated as pseudo first order reactions with unit [s^{-1}]. aqueous phase reaction are treated as pseudo second order reactions with unit [$cm^3molec^{-1}s^{-1}$]. All values are estimated.

[13] Simplified scheme as suggested by *Fan and Jacob*.[1992].

[14] proposed mechanism, based on *Li*, [1994].

[15] proposed mechanism, based on *Keene*, [1990].

Appendix B
Photolysis Rates

1a. O3+hv=O2+O1D

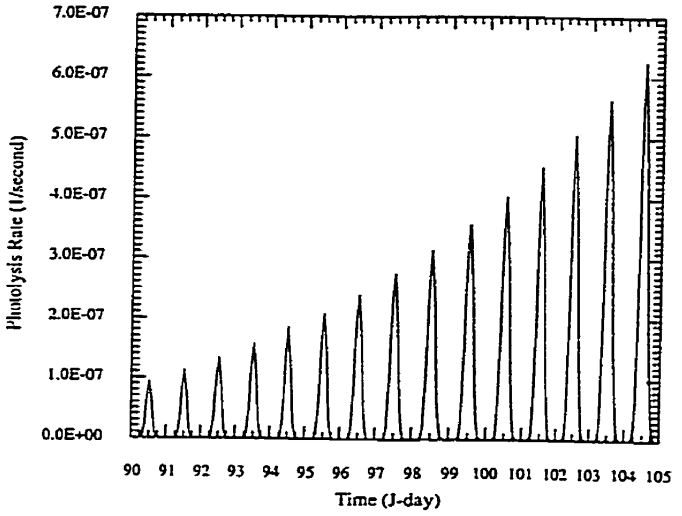

1b. H2O2+hv=2OH

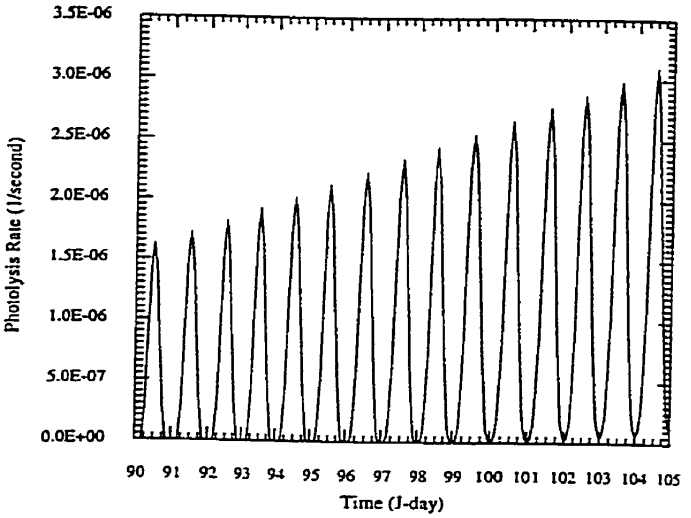

1c. NO2+hv=NO+O3

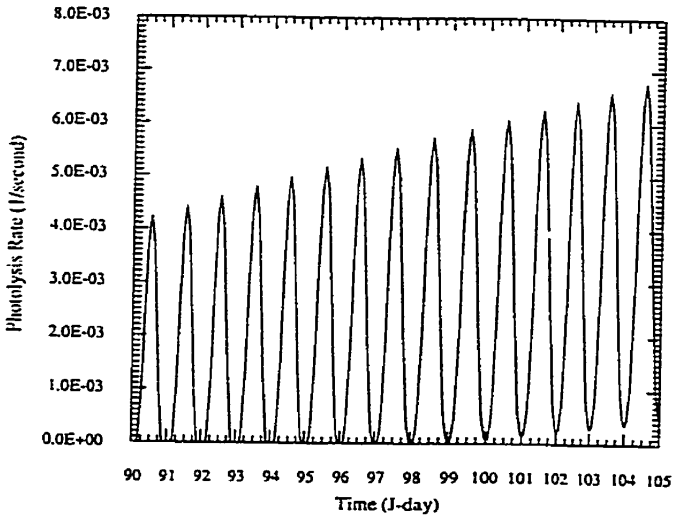

1d. N2O5+hv=NO2+NO3

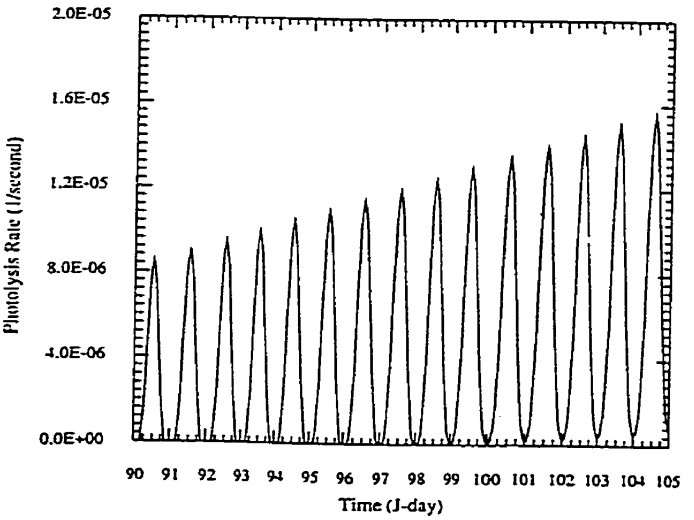

1e. HONO+hv=OH+NO

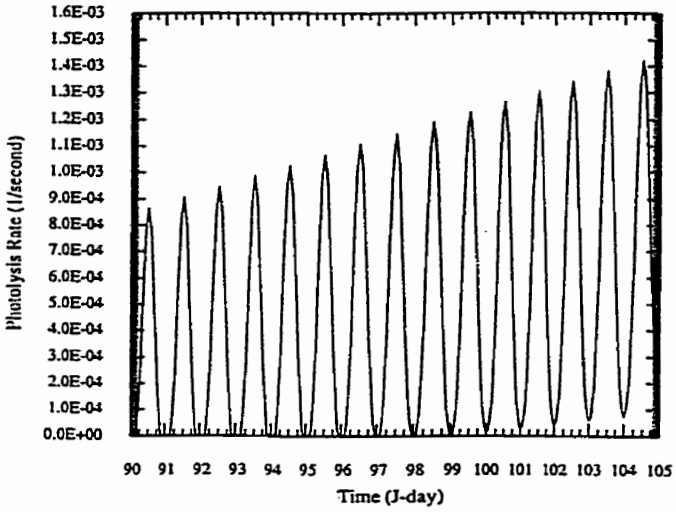

1f. HNO3+hv=NO2+OH

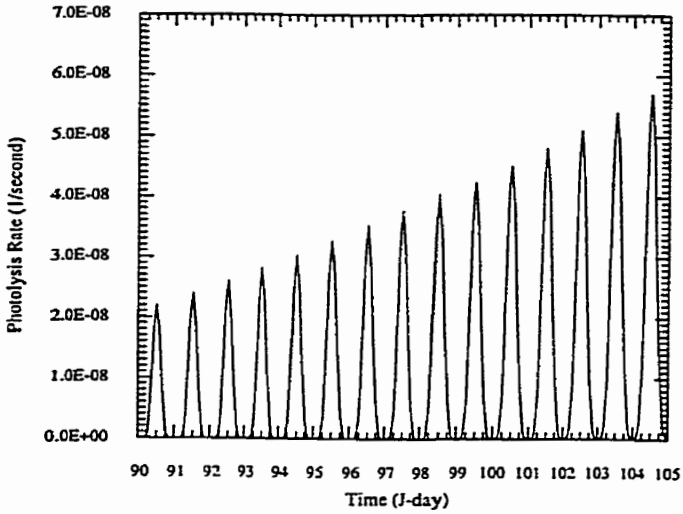

1g. HNO4+hv=HO2+NO2

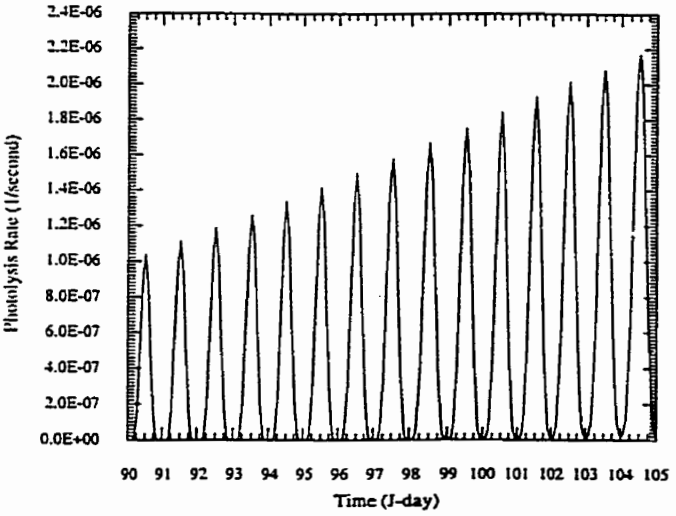

1h. CHBr3+hv=CO+OH+3Br

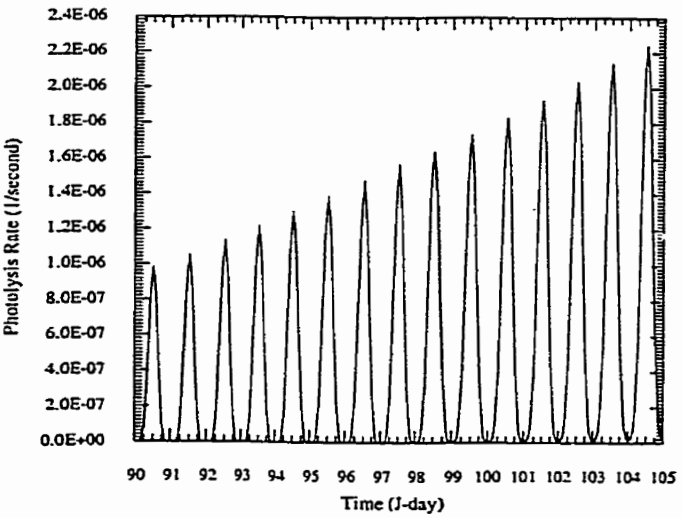

1i. BrO+hv=Br+O3

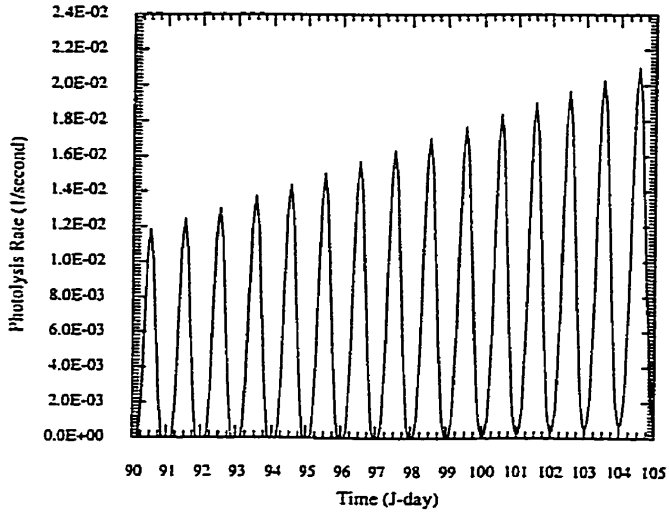

1j. Br2+hv=2Br

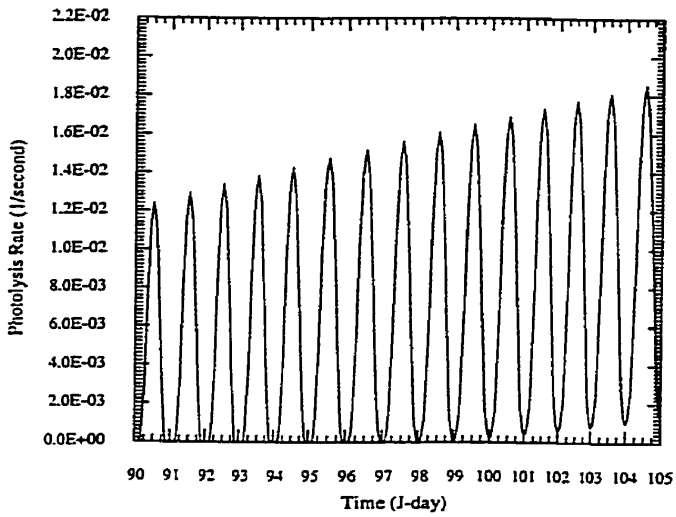

1.k HOBr+hv=Br+OH

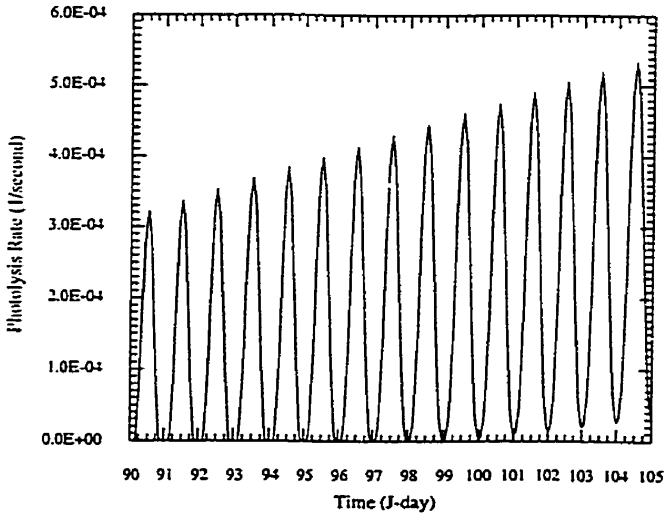

1.l BrNO3+hv=NO3+Br

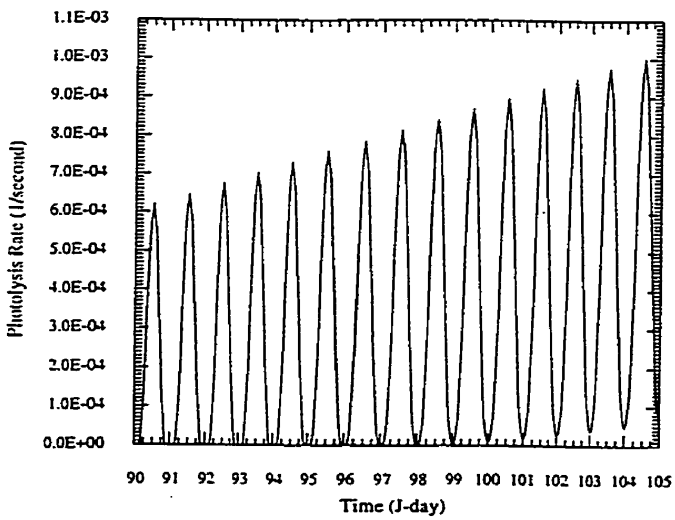

1m. ClO+hv=Cl+O3

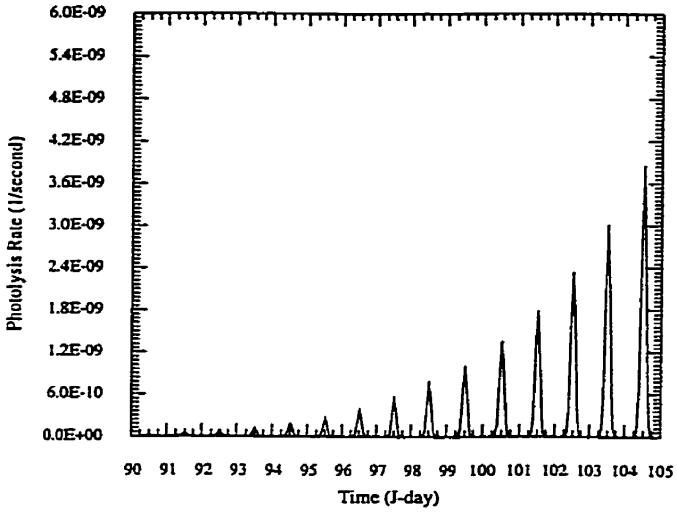

1n. OClO+hv=ClO+O3

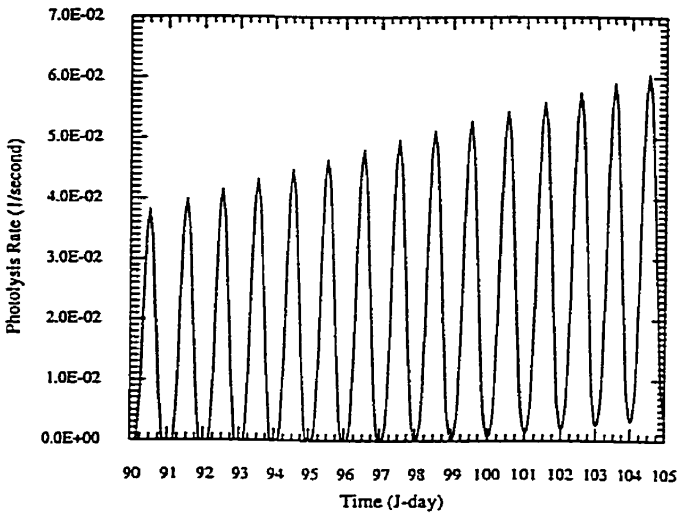

1o. Cl2O2+hv=2Cl+O2

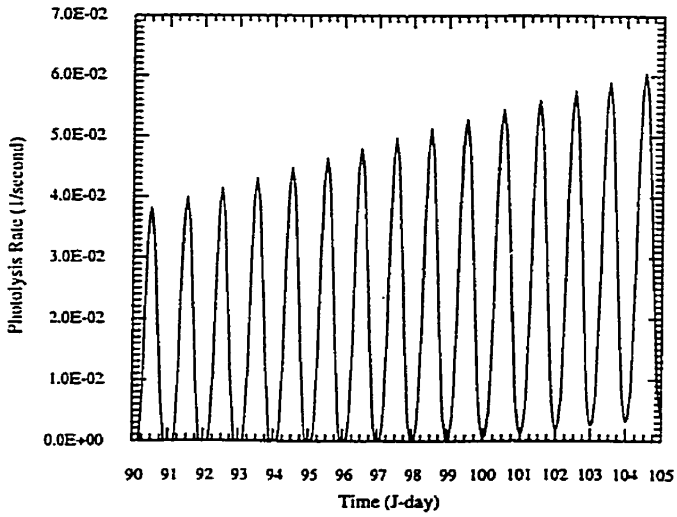

1p. Cl2+hv=2Cl

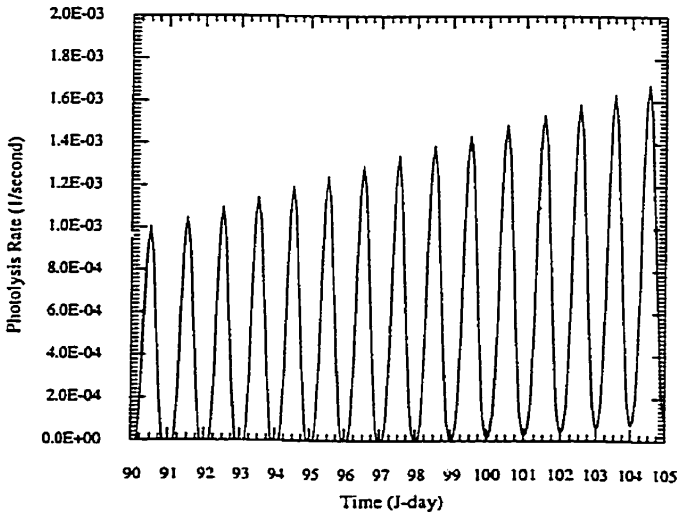

1q. HOCl+hv=OH+Cl

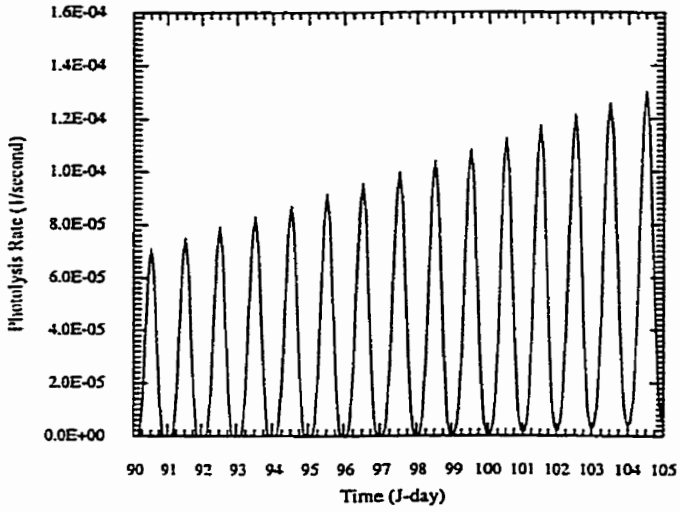

1r. ClNO3+hv=Cl+NO3

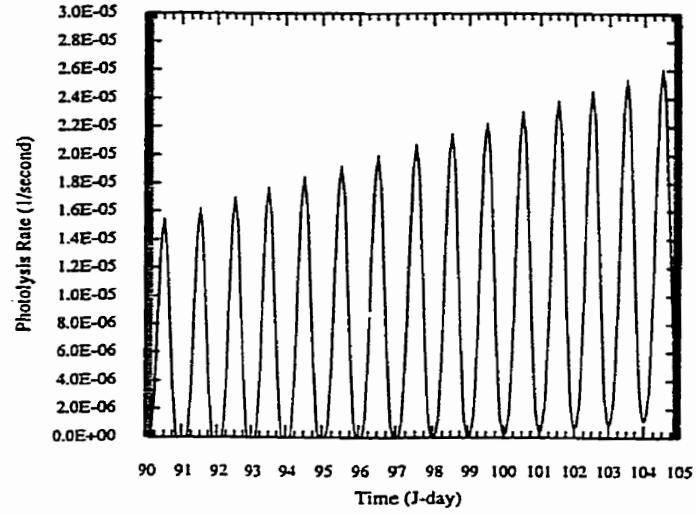

1s. BrCl+hv=Br+Cl

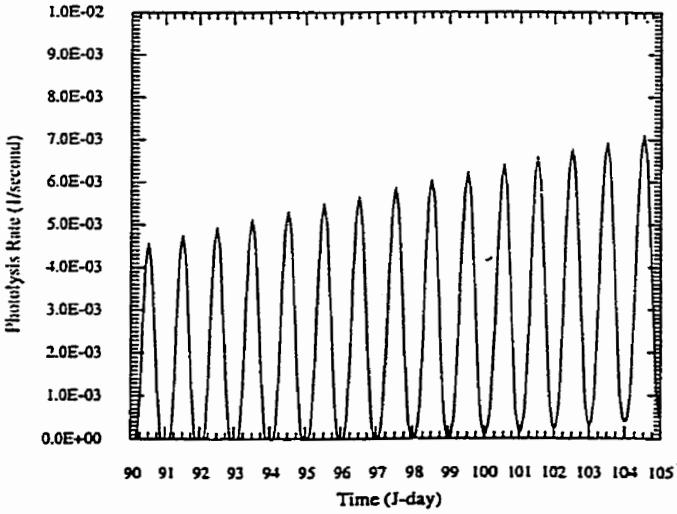

1u. HCHO+hv=CO+H2
1t. HCHO+hv=CO+2HO2

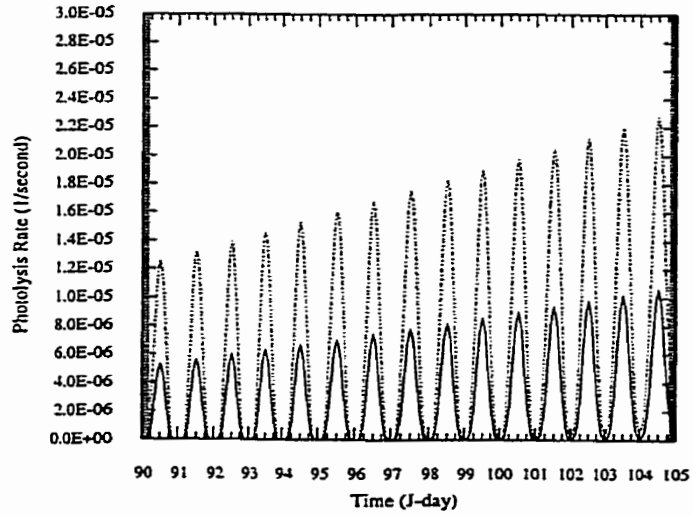

Iv. CH3OOH+hv=HCHO+HO2+OH

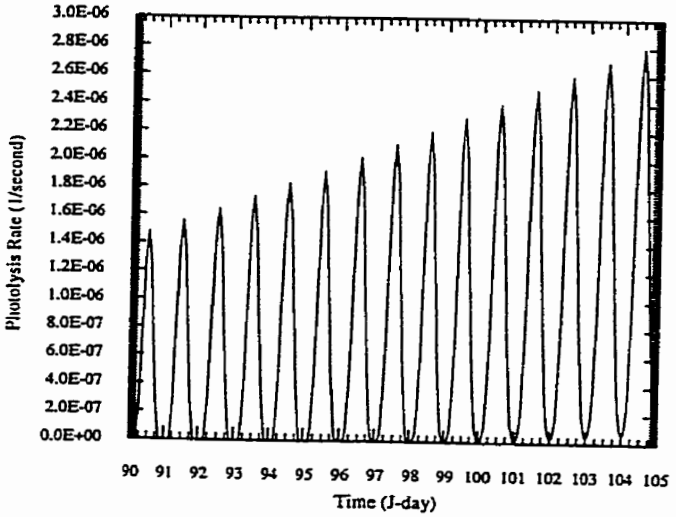

Appendix C
Time Series of the Species

See Chapter IV for initialization of the model

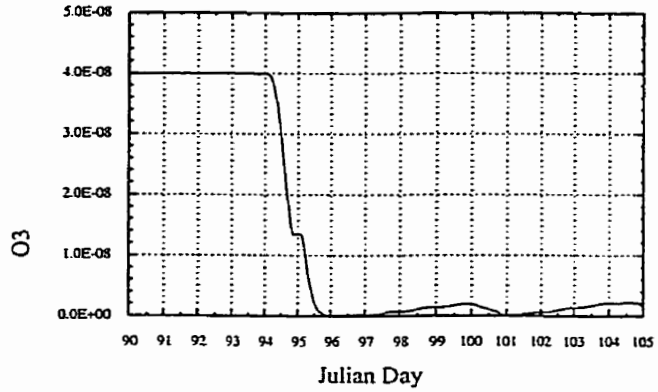
O3
5.0E-08
4.0E-08
3.0E-08
2.0E-08
1.0E-08
0.0E+00
90 91 92 93 94 95 96 97 98 99 100 101 102 103 104 105
Julian Day

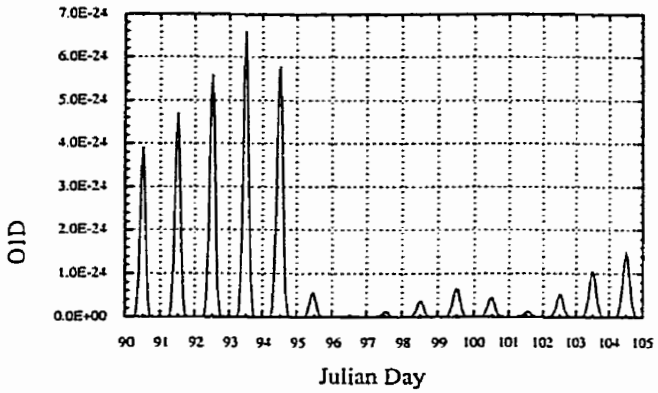
O1D
7.0E-24
6.0E-24
5.0E-24
4.0E-24
3.0E-24
2.0E-24
1.0E-24
0.0E+00
90 91 92 93 94 95 96 97 98 99 100 101 102 103 104 105
Julian Day

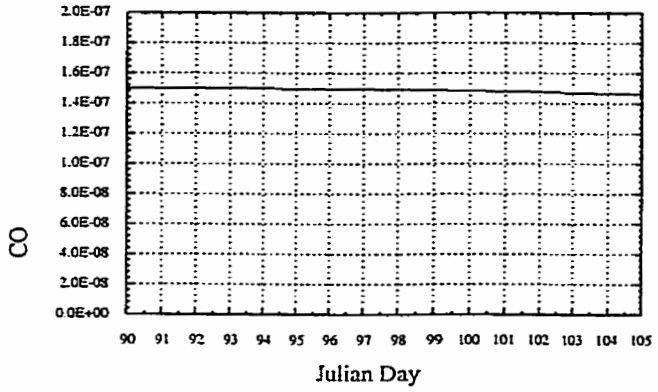
CO
2.0E-07
1.8E-07
1.6E-07
1.4E-07
1.2E-07
1.0E-07
8.0E-08
6.0E-08
4.0E-08
2.0E-08
0.0E+00
90 91 92 93 94 95 96 97 98 99 100 101 102 103 104 105
Julian Day

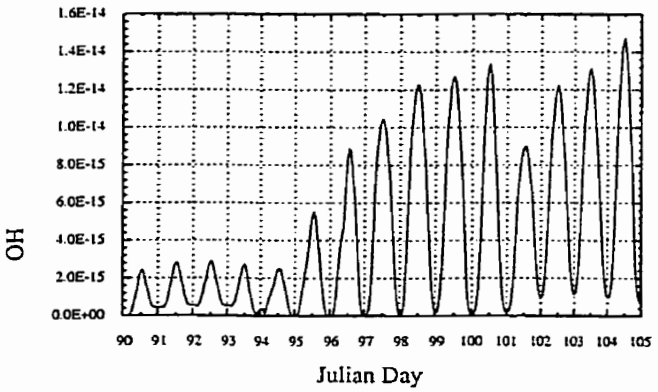
OH
1.6E-14
1.4E-14
1.2E-14
1.0E-14
8.0E-15
6.0E-15
4.0E-15
2.0E-15
0.0E+00
90 91 92 93 94 95 96 97 98 99 100 101 102 103 104 105
Julian Day

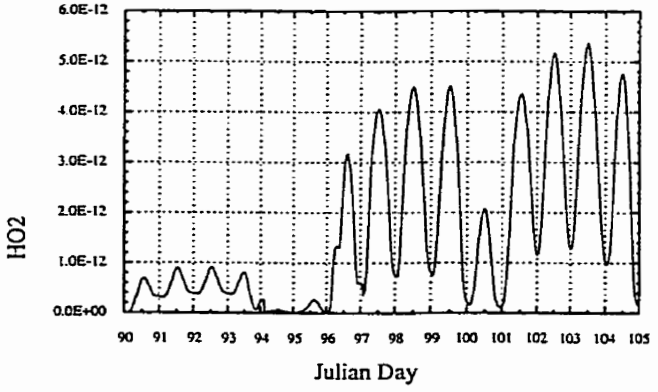
HO2
6.0E-12
5.0E-12
4.0E-12
3.0E-12
2.0E-12
1.0E-12
0.0E+00
90 91 92 93 94 95 96 97 98 99 100 101 102 103 104 105
Julian Day

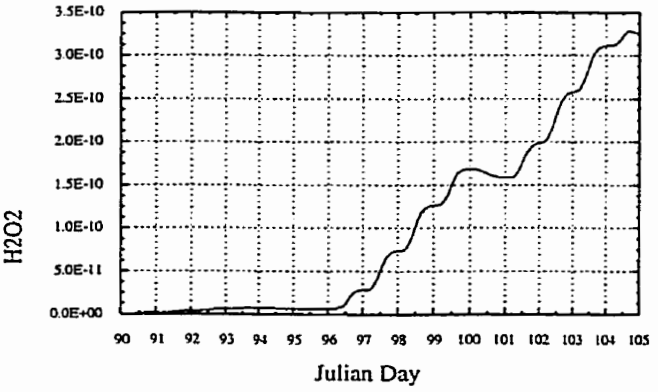
H2O2
3.5E-10
3.0E-10
2.5E-10
2.0E-10
1.5E-10
1.0E-10
5.0E-11
0.0E+00
90 91 92 93 94 95 96 97 98 99 100 101 102 103 104 105
Julian Day

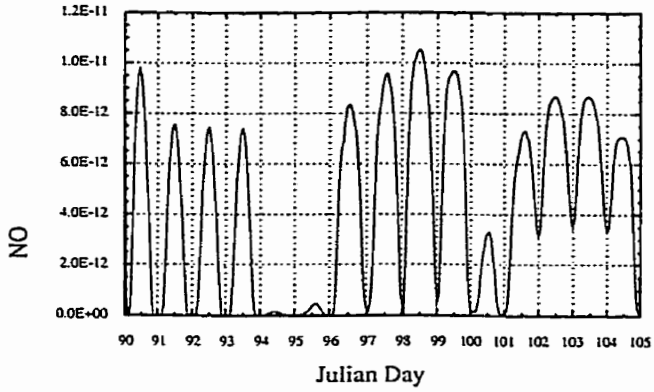
NO
1.2E-11
1.0E-11
8.0E-12
6.0E-12
4.0E-12
2.0E-12
0.0E+00
90 91 92 93 94 95 96 97 98 99 100 101 102 103 104 105
Julian Day

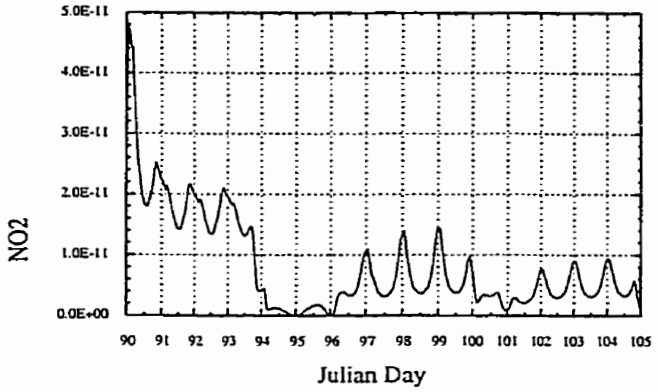
NO2
5.0E-11
4.0E-11
3.0E-11
2.0E-11
1.0E-11
0.0E+00
90 91 92 93 94 95 96 97 98 99 100 101 102 103 104 105
Julian Day

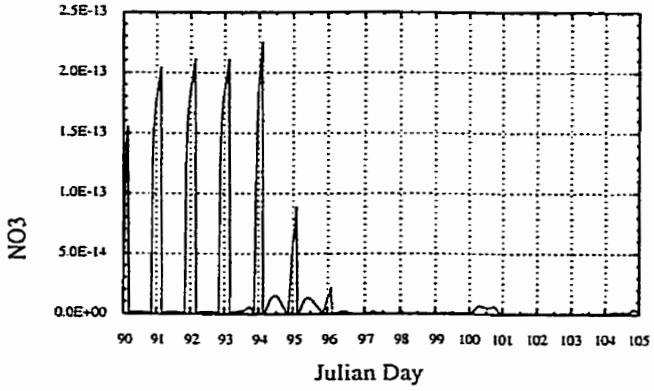
NO3
2.5E-13
2.0E-13
1.5E-13
1.0E-13
5.0E-14
0.0E+00
90 91 92 93 94 95 96 97 98 99 100 101 102 103 104 105
Julian Day

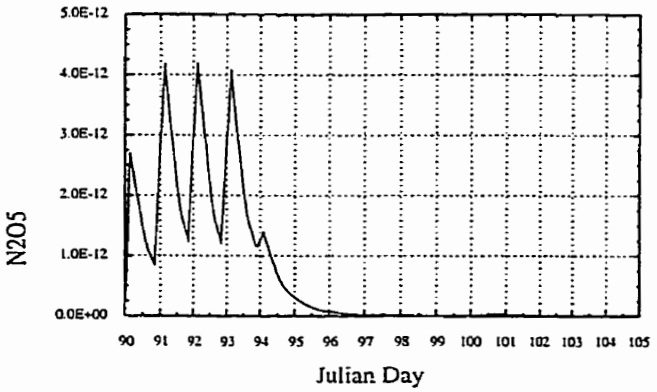
N2O5
5.0E-12
4.0E-12
3.0E-12
2.0E-12
1.0E-12
0.0E+00
90 91 92 93 94 95 96 97 98 99 100 101 102 103 104 105
Julian Day

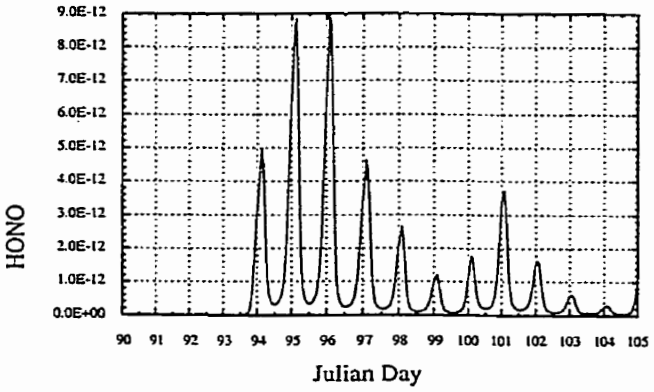
HONO
9.0E-12
8.0E-12
7.0E-12
6.0E-12
5.0E-12
4.0E-12
3.0E-12
2.0E-12
1.0E-12
0.0E+00
90 91 92 93 94 95 96 97 98 99 100 101 102 103 104 105
Julian Day

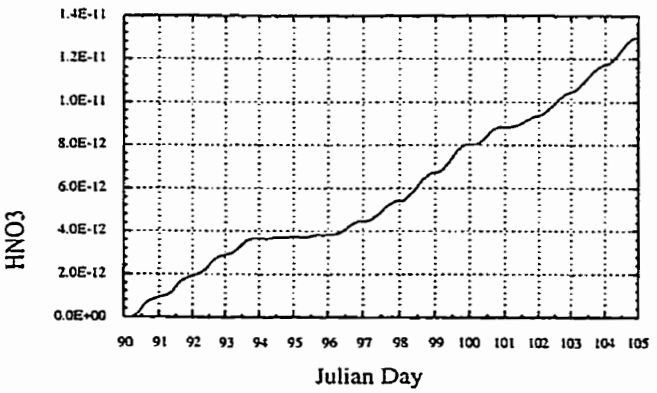
HNO3
1.4E-11
1.2E-11
1.0E-11
8.0E-12
6.0E-12
4.0E-12
2.0E-12
0.0E+00
90 91 92 93 94 95 96 97 98 99 100 101 102 103 104 105
Julian Day

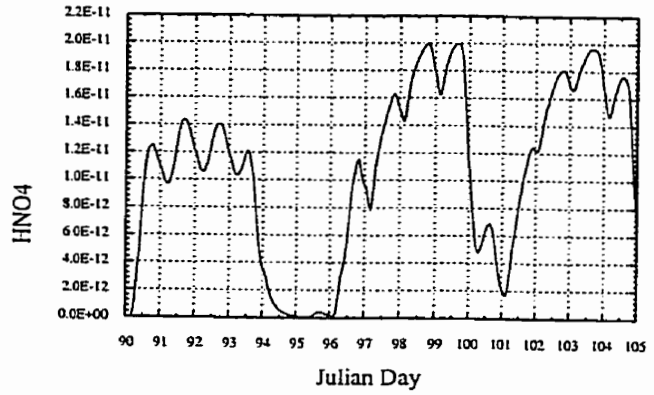
HNO4
2.2E-11
2.0E-11
1.8E-11
1.6E-11
1.4E-11
1.2E-11
1.0E-11
8.0E-12
6.0E-12
4.0E-12
2.0E-12
0.0E+00
90 91 92 93 94 95 96 97 98 99 100 101 102 103 104 105
Julian Day

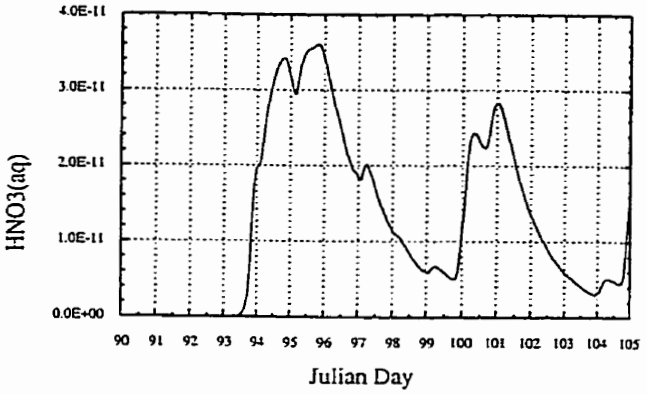
HNO3(aq)
4.0E-11
3.0E-11
2.0E-11
1.0E-11
0.0E+00
90 91 92 93 94 95 96 97 98 99 100 101 102 103 104 105
Julian Day

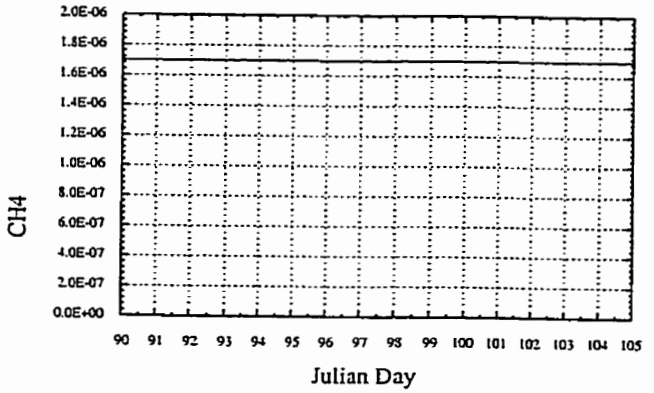
CH4
2.0E-06
1.8E-06
1.6E-06
1.4E-06
1.2E-06
1.0E-06
8.0E-07
6.0E-07
4.0E-07
2.0E-07
0.0E+00
90 91 92 93 94 95 96 97 98 99 100 101 102 103 104 105
Julian Day

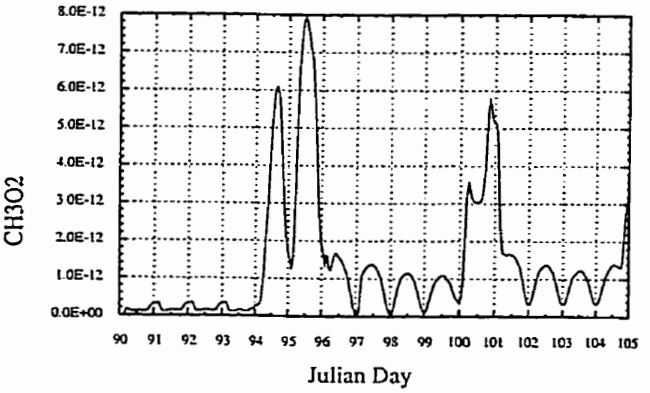
CH3O2
8.0E-12
7.0E-12
6.0E-12
5.0E-12
4.0E-12
3.0E-12
2.0E-12
1.0E-12
0.0E+00
90 91 92 93 94 95 96 97 98 99 100 101 102 103 104 105
Julian Day

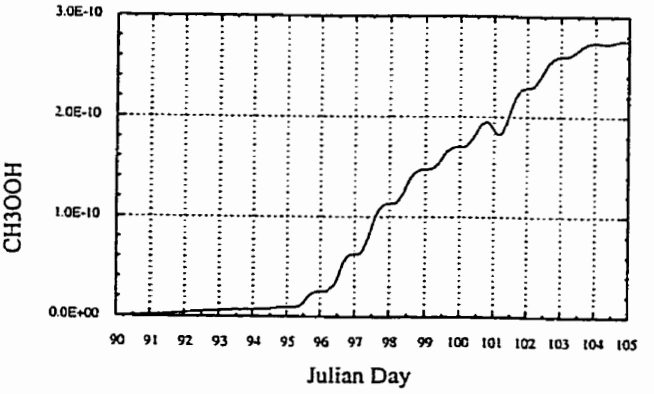
CH3OOH
3.0E-10
2.0E-10
1.0E-10
0.0E+00
90 91 92 93 94 95 96 97 98 99 100 101 102 103 104 105
Julian Day

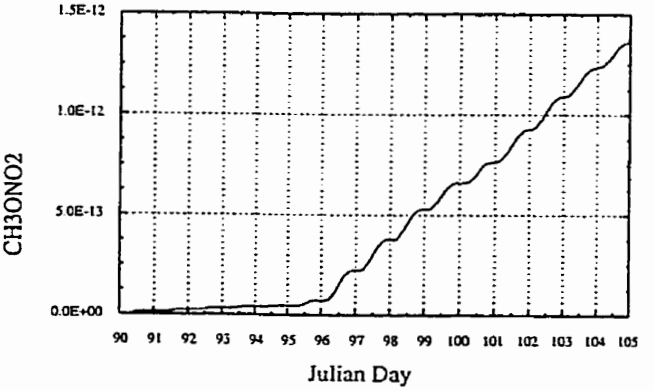
CH3ONO2
1.5E-12
1.0E-12
5.0E-13
0.0E+00
90 91 92 93 94 95 96 97 98 99 100 101 102 103 104 105
Julian Day

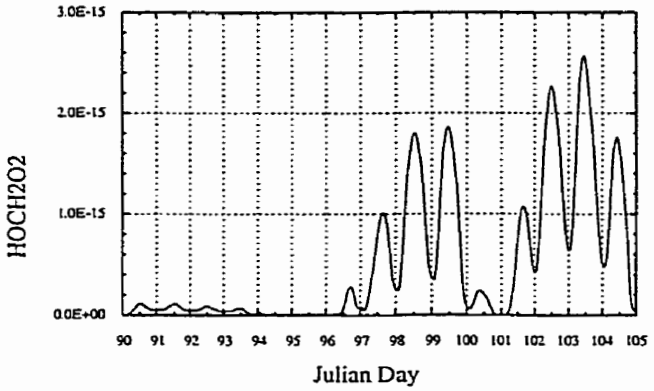
HOCH2O2
3.0E-15
2.0E-15
1.0E-15
0.0E+00
90 91 92 93 94 95 96 97 98 99 100 101 102 103 104 105
Julian Day

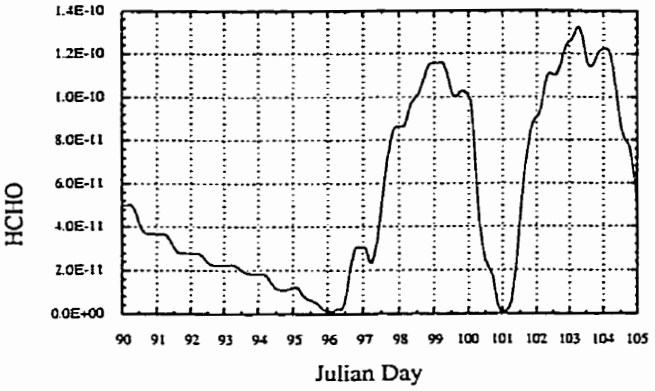
HCHO
1.4E-10
1.2E-10
1.0E-10
8.0E-11
6.0E-11
4.0E-11
2.0E-11
0.0E+00
90 91 92 93 94 95 96 97 98 99 100 101 102 103 104 105
Julian Day

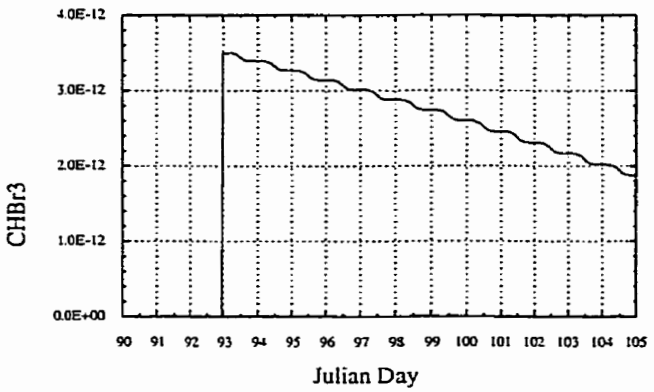
CHBr3
4.0E-12
3.0E-12
2.0E-12
1.0E-12
0.0E+00
90 91 92 93 94 95 96 97 98 99 100 101 102 103 104 105
Julian Day

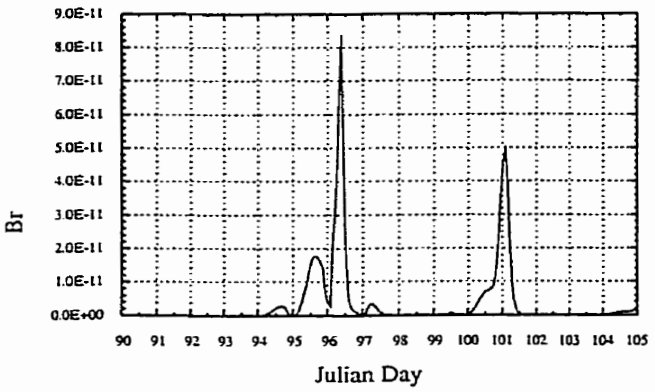
Br
9.0E-11
8.0E-11
7.0E-11
6.0E-11
5.0E-11
4.0E-11
3.0E-11
2.0E-11
1.0E-11
0.0E+00
90 91 92 93 94 95 96 97 98 99 100 101 102 103 104 105
Julian Day

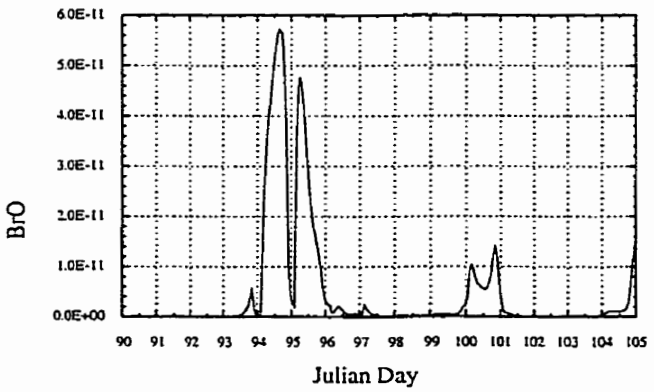
BrO
6.0E-11
5.0E-11
4.0E-11
3.0E-11
2.0E-11
1.0E-11
0.0E+00
90 91 92 93 94 95 96 97 98 99 100 101 102 103 104 105
Julian Day

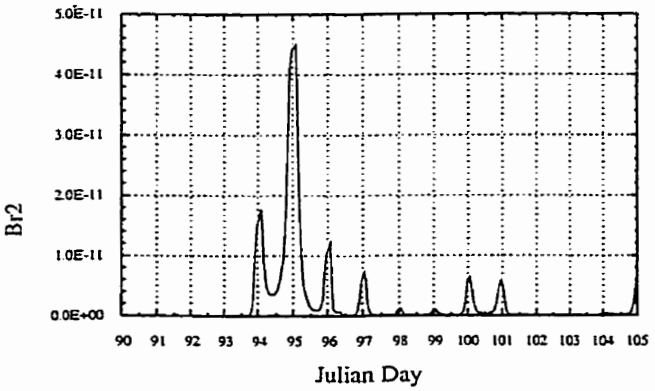
Br2
5.0E-11
4.0E-11
3.0E-11
2.0E-11
1.0E-11
0.0E+00
90 91 92 93 94 95 96 97 98 99 100 101 102 103 104 105
Julian Day

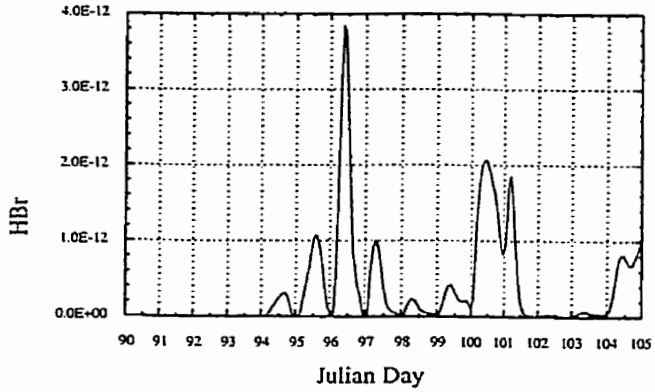
HBr
4.0E-12
3.0E-12
2.0E-12
1.0E-12
0.0E+00
90 91 92 93 94 95 96 97 98 99 100 101 102 103 104 105
Julian Day

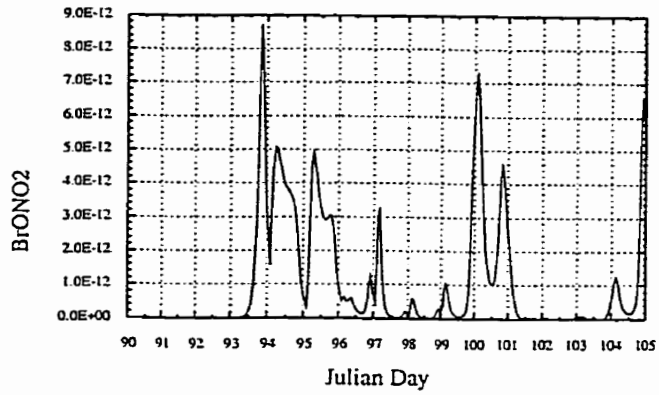
BrONO2
9.0E-12
8.0E-12
7.0E-12
6.0E-12
5.0E-12
4.0E-12
3.0E-12
2.0E-12
1.0E-12
0.0E+00
90 91 92 93 94 95 96 97 98 99 100 101 102 103 104 105
Julian Day

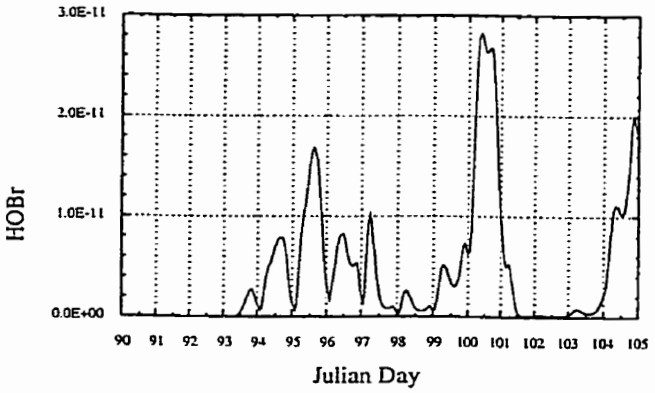
HOBr
3.0E-11
2.0E-11
1.0E-11
0.0E+00
90 91 92 93 94 95 96 97 98 99 100 101 102 103 104 105
Julian Day

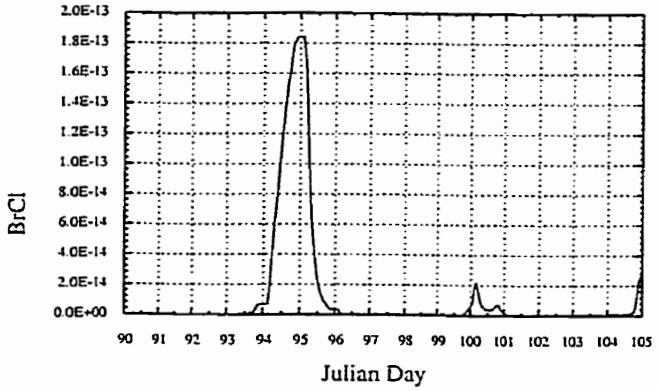
BrCl
2.0E-13
1.8E-13
1.6E-13
1.4E-13
1.2E-13
1.0E-13
8.0E-14
6.0E-14
4.0E-14
2.0E-14
0.0E+00
90 91 92 93 94 95 96 97 98 99 100 101 102 103 104 105
Julian Day

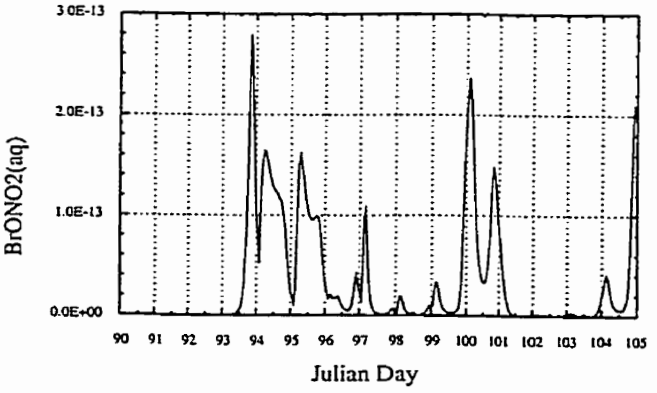
BrONO2(aq)
3.0E-13
2.0E-13
1.0E-13
0.0E+00
90 91 92 93 94 95 96 97 98 99 100 101 102 103 104 105
Julian Day

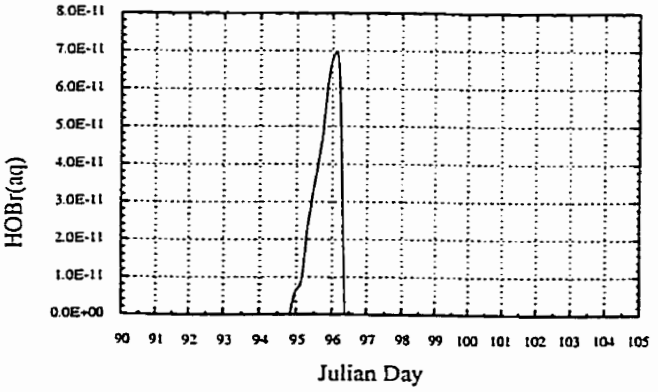
HOBr(aq)
8.0E-11
7.0E-11
6.0E-11
5.0E-11
4.0E-11
3.0E-11
2.0E-11
1.0E-11
0.0E+00
90 91 92 93 94 95 96 97 98 99 100 101 102 103 104 105
Julian Day

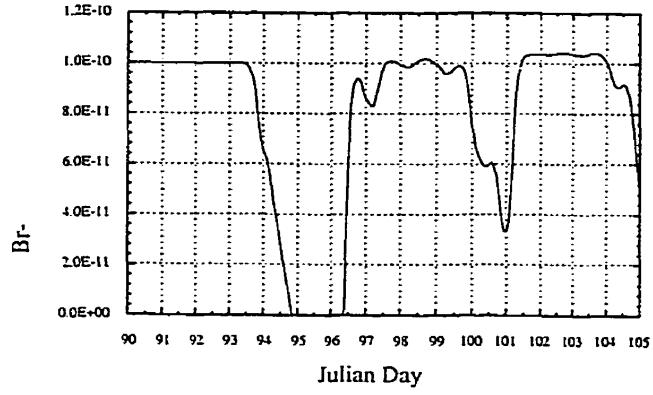
Br-
1.2E-10
1.0E-10
8.0E-11
6.0E-11
4.0E-11
2.0E-11
0.0E+00
90 91 92 93 94 95 96 97 98 99 100 101 102 103 104 105
Julian Day

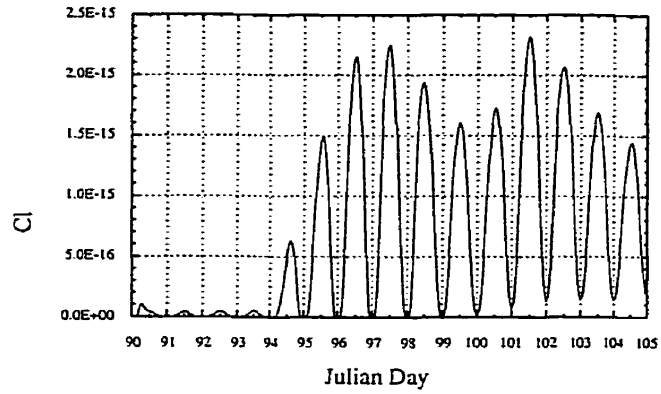
Cl
2.5E-15
2.0E-15
1.5E-15
1.0E-15
5.0E-16
0.0E+00
90 91 92 93 94 95 96 97 98 99 100 101 102 103 104 105
Julian Day

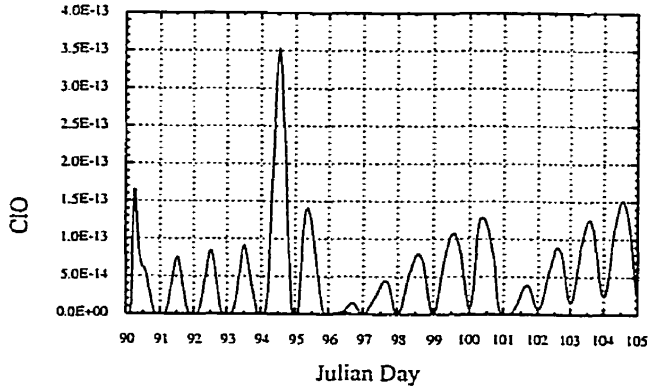
ClO
4.0E-13
3.5E-13
3.0E-13
2.5E-13
2.0E-13
1.5E-13
1.0E-13
5.0E-14
0.0E+00
90 91 92 93 94 95 96 97 98 99 100 101 102 103 104 105
Julian Day

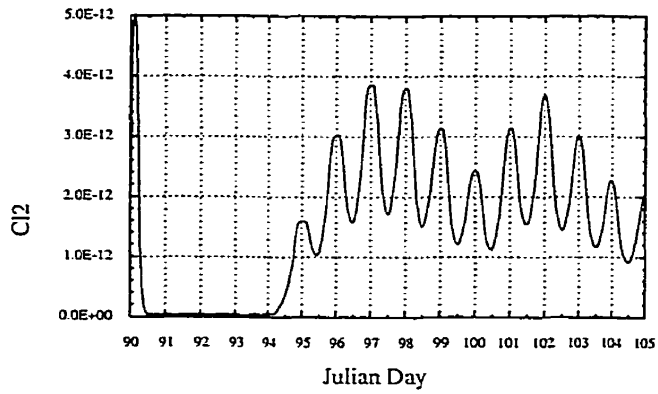
Cl2
5.0E-12
4.0E-12
3.0E-12
2.0E-12
1.0E-12
0.0E+00
90 91 92 93 94 95 96 97 98 99 100 101 102 103 104 105
Julian Day

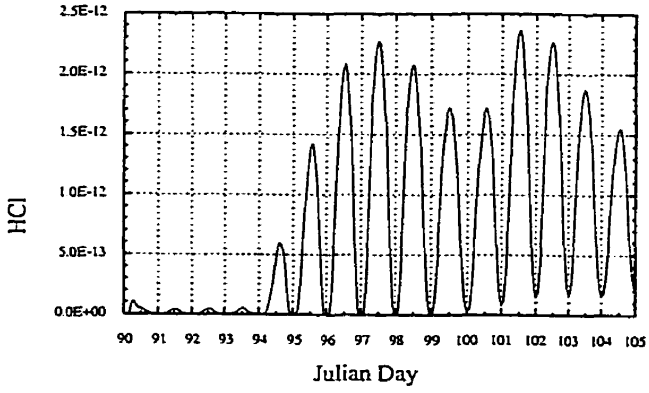
HCl
2.5E-12
2.0E-12
1.5E-12
1.0E-12
5.0E-13
0.0E+00
90 91 92 93 94 95 96 97 98 99 100 101 102 103 104 105
Julian Day

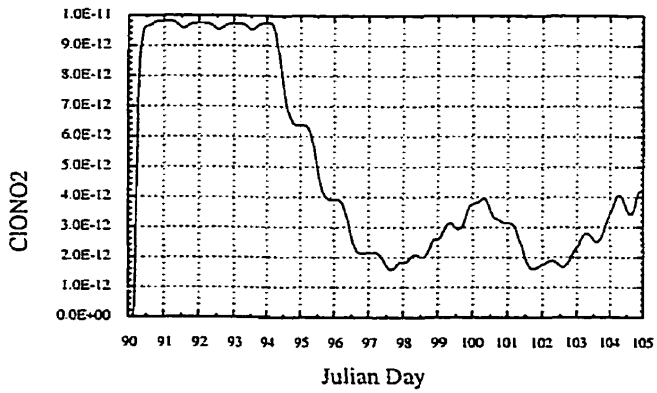
ClONO2
1.0E-11
9.0E-12
8.0E-12
7.0E-12
6.0E-12
5.0E-12
4.0E-12
3.0E-12
2.0E-12
1.0E-12
0.0E+00
90 91 92 93 94 95 96 97 98 99 100 101 102 103 104 105
Julian Day

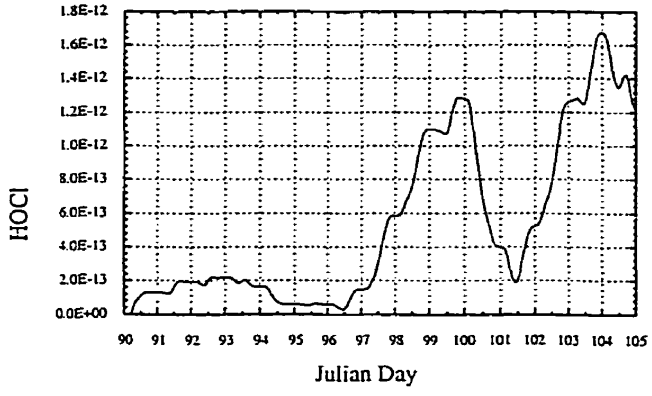
HOCl
1.8E-12
1.6E-12
1.4E-12
1.2E-12
1.0E-12
8.0E-13
6.0E-13
4.0E-13
2.0E-13
0.0E+00
90 91 92 93 94 95 96 97 98 99 100 101 102 103 104 105
Julian Day

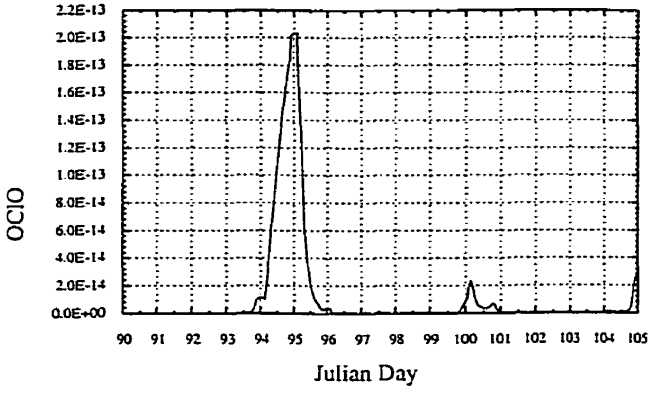
OClO
2.2E-13
2.0E-13
1.8E-13
1.6E-13
1.4E-13
1.2E-13
1.0E-13
8.0E-14
6.0E-14
4.0E-14
2.0E-14
0.0E+00
90 91 92 93 94 95 96 97 98 99 100 101 102 103 104 105
Julian Day

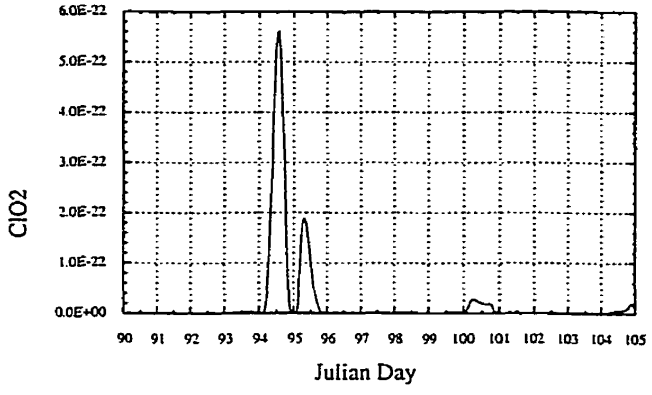
ClO2
6.0E-22
5.0E-22
4.0E-22
3.0E-22
2.0E-22
1.0E-22
0.0E+00
90 91 92 93 94 95 96 97 98 99 100 101 102 103 104 105
Julian Day

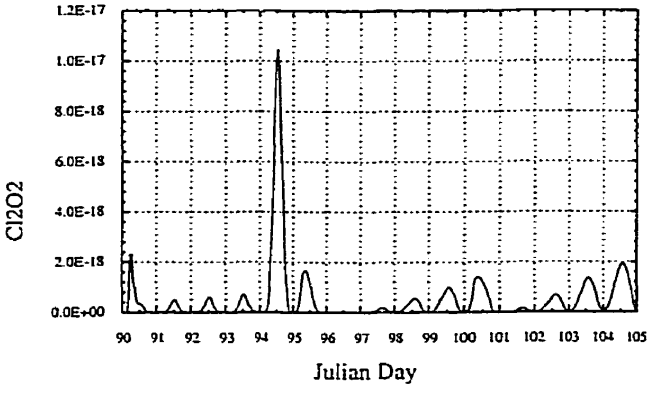
Cl2O2
1.2E-17
1.0E-17
8.0E-18
6.0E-18
4.0E-18
2.0E-18
0.0E+00
90 91 92 93 94 95 96 97 98 99 100 101 102 103 104 105
Julian Day

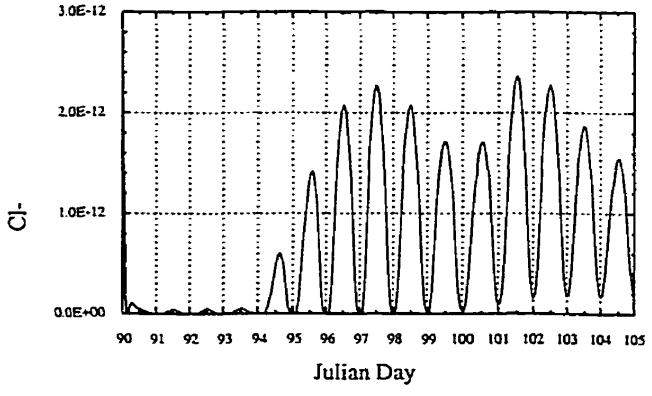
Cl-
3.0E-12
2.0E-12
1.0E-12
0.0E+00
90 91 92 93 94 95 96 97 98 99 100 101 102 103 104 105
Julian Day

Appendix D
Publication 1996a

Tang, T., and J.C. McConnell, Autocatalytic Release of Bromine from Arctic Snow Pack During Polar Sunrise. *Geophys. Res. Lett.*, *23*, 2633-2636, 1996a.

Autocatalytic release of bromine from Arctic snow pack during polar sunrise

T. Tang[1] and J. C. McConnell[2]

Abstract.
Measurements and modeling studies strongly suggest that spring time depletion of ozone in the Arctic planetary boundary layer (PBL) is due to catalytic destruction by bromine atoms. However, the source of the bromine is uncertain. In this note, we propose that the source of the bromine at polar sunrise is the snow pack on the ice covering Arctic ocean and that it is released auto-catalytically, stimulated by a bromine seed from one of the brominated organic compounds, such as $CHBr_3$, by photolysis. In this manner ~ 100 pptv of bromine can be transferred to the atmosphere where it can reside in the gas phase or, by scavenging, be partitioned in the aerosol or ice crystal phase. Moreover, it appears that heterogeneous recycling of bromine may be a process that self-terminates as ozone depletes to low levels. We also have included chlorine chemistry in the model in order to simulate inferred levels of chlorine atoms. This is important as it results in the production of HCHO which acts to convert post ozone depletion active bromine into HBr which is then returned to the snow pack or scavenged by aerosols or ice crystals.

Introduction

During spring, ozone concentrations in the Arctic PBL are often observed to decrease suddenly from about 40 ppbv to the detection limit (~ 0.5 ppbv). Measurements indicate that the sudden decrease in the ozone concentration is accompanied by peaks in particle bromine [e.g., *Barrie et al.*, 1988]. This led *Barrie et al.* [1988] to suggest that a gas phase bromine catalytic cycle could be the process responsible for ozone destruction. *McConnell et al.* [1992] pointed out that the gas phase catalytic cycle would rapidly terminate with the formation of HBr. Thus recycling of the HBr formed is essential in order to maintain a sufficiently high level of BrO necessary for catalytic ozone destruction to occur. Moreover, based on the available non methane hydro carbon (NMHC) measurements, *McConnell and Henderson* [1993] surmised that atomic Cl could also be active and evidence of this has been obtained by [*Jobson et al.*, 1994].

A mechanism for recycling of the HBr was proposed by *Fan and Jacob* [1992] who suggested that HBr will diffuse into an acidified aerosol forming Br^- which can react with HOBr(aq):

$$HOBr(aq) + Br^- + H^+ \rightarrow Br_2(aq) + H_2O \quad (1)$$

The $Br_2(aq)$ produced can subsequently volatilize to yield $Br_2(g)$. The production of $Br_2(aq)$ is limited by the rate of uptake of either HBr(g) or HOBr(g) by aerosol. They further suggested that the reaction:

$$BrONO_2(aq) \xrightarrow{H_2O} HOBr(aq) + HNO_3(aq) \quad (2)$$

can recycle the Br in $BrONO_2$ produced in the gas phase, to supply the HOBr(aq) necessary for the release of $Br_2(g)$ from the aerosol.

O_3 appears to be destroyed with a time constant that may be as short as one day, in which case, BrO levels ~ 30 pptv must be present for the catalytic cycle to be this efficient [*McConnell el al.*, 1993]. Comparable levels of BrO have been observed near Alert [*Hausmann and Platt*, 1994]. One of the unresolved issues with regard to the polar sunrise ozone depletion problem has been the origin of these high levels of Br. *Barrie et al.* [1988] proposed that $CHBr_3$ could be the source. However, photo-dissociation of $CHBr_3$ ($J_{CHBr_3} \sim 10^{-6}s^{-1}$) is too slow and $CHBr_3$ mixing ratios are insufficient. *Finlayson-Pitts et al.* [1990] suggested that N_2O_5 on air-borne sea-salt could be the source of Br. However, using the annual average atmospheric Na mixing ratio of the order of ~ 10^3 ng·m^{-3} [*Berg et al.*, 1983] and $[Br^-/Na^+]_{\text{bulk seawater}} \sim 6.2\times10^{-3}$ by mass we estimate that the atmospheric Br content in newly form sea-salt particles is ~ 2 pptv, which is insufficient.

In this study, we follow the suggestion of *McConnell el al.* [1992] that sea-salt particles originating from the polynyas or the ocean could be carried by the wind to deposit and accumulate on the snow pack throughout the polar night. We are not aware of any pre-sunrise measurements of Br in Arctic snow. However, *Mulvaney et al.* [1993] collected a series of surface snow samples along a traverse of the Antarctic ice shelf. They reported that Na^+ increases from the coast inland, reaching a maximum at ~ 43 km from ice shelf front. The measured snow content of Na^+ is ~ 60 $\mu eq/l$, which is equivalent to a concentration in snow of ~ 3×10^{13}cm^{-3} (using $[Br^-/Na^+]_{\text{bulk seawater}} \sim 1.8\times10^{-3}$ by volume and assuming a conservative snow to liquid volume ra-

[1] Dept. of Phys. & Astron., York Univ., Ont., Canada
[2] Dept. of Earth & Atmos. Sci., York Univ., Ont., Canada

Paper number 96GL02572
0094-8534/96/96GL-02572$05.00

tio of 2). This concentration of Br^- in 30 cm of snow, if released, would yield 3 ppbv of Br in an atmospheric layer 100 m thick. It is likely that Br^- amounts in the Arctic snow are even larger than that in Antarctic since there are other routes to the snow pack such as through cracks in the ice covered ocean [*L.A. Barrie*, 1996 private communication]. We believe that the sea-salt Br residing in the snow pack can be readily accessed by atmospheric air as the specific surface area and porosity for snow is high ($\sim 10^7 cm^2 cm^{-3}$, e.g., *Waddington et al.* [1996]). Assuming that the penetration of air is limited by the molecular diffusion time constant, atmospheric air can diffuse $\sim$ 18 cm into snow pack in $\sim$ 1 hr. The transfer process can be even more rapid as ventilation of the snow pack by other processes such as pressure oscillations associated with turbulence generated by small scale topography can enhance the exchange of air and thus species between the air and snow pack [e.g., *Waddington et al.*, 1996].

Mozurkewich [1995] had suggested that the initial release of Br is from liquid sea-salt particles. He proposed that Caro's acid produced by the free radical chain oxidation of S(IV) could oxidize Br^- to HOBr(aq). Subsequent reaction of HOBr(aq) with Br^- could initiate the release of Br_2(g). Br_2(g) readily photolyzes to yield Br atoms which form BrO on reaction with O_3. In the presence of HO_2, BrO reacts to form HOBr which can be scavenged by the sea-salt particles resulting in the release of additional Br_2 (equation 1). Thus the Br release process is autocatalytic as the conversion of *one* inactive Br^- to a Br seed (HOBr) results in the release of *two* Br atoms (Br_2).

Previous modelling studies have focussed on the simulation of the rapid depletion of ozone assuming that sufficient Br had already been activated. In this study, we attempt a simulation of the release of Br by following the idea of *Mozurkewich* [1995]. However, we propose that the Br seed necessary for the autocatalytic release of Br^- from sea-salt particles accumulated in the snow pack is from the photolysis of brominated organic compounds such as $CHBr_3$.

Model Description

A box model is used to simulate the autocatalytic release of bromine. The chemical module includes standard gas phase HO_x, NO_x, BrO_x and ClO_x chemistry as presented in *DeMore et al.* [1994]. We treat gas-particle reactions as pseudo first order reactions and aqueous phase reactions as pseudo second order reactions. We do not distinguish the snow pack form aerosols or ice crystals. The heterogeneous bromine recycling mechanism is included in the form suggested by *Fan and Jacob* [1992]. We have adopted their suggested time constants for gaseous up take by aerosol or snow pack: 5×10^2 s for HBr; 8×10^3 s for HOBr; and 7×10^3 s for $BrONO_2$. However, this mechanism results in nitrogen rapidly being lost from the gas phase as $BrONO_2$ to the aqueous phase as HNO_3(aq). Levels of NO_x in the Arctic, while small ($\sim$ 30-40 pptv), do contribute to ozone budget (see later) [*Jaffe*, 1994]. To conserve gaseous nitrogen we recycle HNO_3(aq) to HONO(g) with time constant of 10^5 s. The rationale for this transformation is based on the observations of HONO(g) by *Li* [1994] which indicated HONO(g) at concentration of up to $\sim$ 5-10 pptv after polar sunrise.

Without heterogeneous reactions any Cl generated in the model rapidly ends up as HCl which, under these low sun conditions, remains as HCl as the OH levels otherwise remain low. To sustain the gaseous Cl atom mixing ratios in the model we recycle HCl into Cl_2 via the aerosol. We assume the rate of Cl recycling is limited by gaseous diffusion (i.e., $\sim$ 500 s). We initialize the total Cl in our model to 10 pptv such that Cl atom concentrations are comparable to that estimated by *Jobson et al.* [1994]. We are aware of the limitations of our over simplified scheme for Cl recycling. However, a well established set of heterogeneous reaction for Cl in remote troposphere is still lacking at this date.

We initialized our model with 100 pptv of total Br. This is based both on modelling necessities that require $\sim$ 30 pptv BrO for rapid O_3 depletion and the Arctic field studies of *Berg et al.* [1983]. They observed a spring time enrichment of Br^- in the atmosphere and total atmospheric Br level as high as 140 pptv. Our modelling calculation commences with all the Br in the model as Br^- initially, which we anticipate resides on the snow pack. The mixing ratios of various species in the model are initialized to pre-ozone depletion values: O_3 40 ppbv, NO 20 pptv, NO_2 30 pptv, CO 150 ppbv, CH_4 1.7 ppmv and HCHO 50 pptv. The temperature used for the evaluation of the rate constants is 245 K. The model simulates the evolution of a surface air parcel, starting at midnight, Julian day (JD) 90 until the end of JD 105. In order to prime the chain reaction release of Br from the Br^-, at midnight JD 93, we introduce 3.5 pptv of $CHBr_3$ into the air parcel.

Results and Discussion

The mixing ratios of some species from the simulation are shown in Figure 1, panels (a) to (c). In Figure 1a, the O_3 shows no decrease before JD 93. However, when the $CHBr_3$ is introduced into the air parcel on JD 93 (Figure 1c) it slowly photo-dissociates to give Br atoms which act as a seed for the autocatalytic release of Br from the Br^- source as discussed above. Reaction of Br with O_3 leads to the formation of BrO. In the presence of HO_2 and NO_2, BrO can react to form HOBr and $BrONO_2$ (Figure 1b), both of which can then be scavenged onto the Br^- rich snow pack. HOBr(aq) can then react with Br^- to release Br from the snow pack in the form of Br_2(g) (Figure 1c). Thus the slow release of a Br atom from $CHBr_3$ can lead to the rapid release of another Br atom from the snow pack and a chain reaction results until the Br^- source is depleted (Figure 1b, JD 94.5).

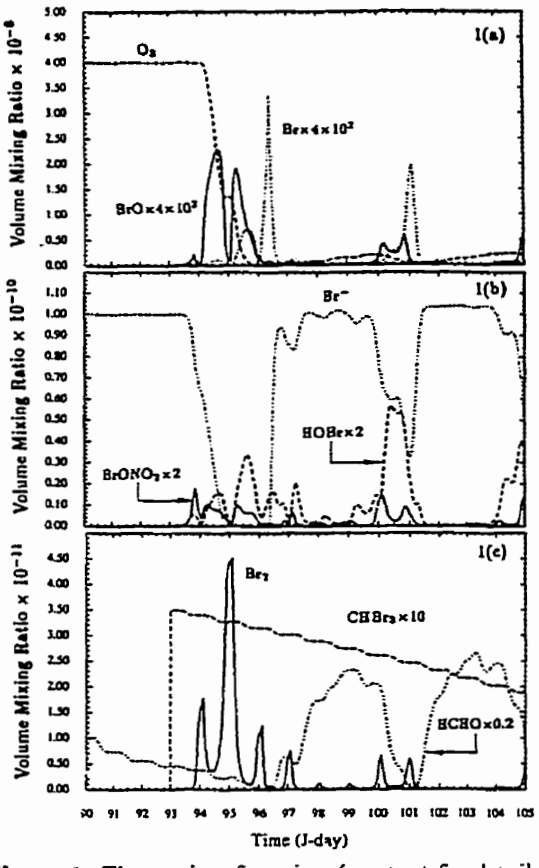

Figure 1. Time series of species. (see text for details)

As long as O_3 is available to react with Br atoms, ~ 60 pptv of Br in the model (peak mixing ratio) is in the form of BrO. However, immediately after O_3 depletion (~ JD 95.5), the principle channel for Br loss, $Br + O_3 \rightarrow BrO + O_2$, ceases. The mixing ratio of Br atoms (Figure 1a), produced by photolysis of BrO and Br_2, reaches a surprisingly high level. (This could be detected by resonance method similar to that used in the stratosphere.) However, the HCHO, generated as a result of the presence of Cl atoms, converts this high concentration of Br atoms to HBr which is scavenged onto the snow pack, the aerosol and the ice crystals. To keep our model simple we have only included CH_4 chemistry. In the real atmosphere, the observed high levels of acetaldehyde produced by oxidation of NMHC [*Shepson et al.*, 1996] will also play a similar role in converting Br to HBr.

After the O_3 has depleted, our simulation shows an increase of HCHO (~ 100 pptv). This occurs because the Cl atom level has increased due to the removal of the largest Cl removal channel. Before the depletion of O_3, the daily average Cl atom density is ~ 10^3 cm^{-3}; after O_3 has depleted Cl atom density increases to ~ 10^4 cm^{-3}. The production of several hundred pptv of HCHO as observed by *Shepson et al.* [1996] and *de Serres* [1994] remains a problem as Cl atom densities must be at least an order of magnitude higher than those estimated by *Jobson et al.* [1994].

We speculate that after the initial release of Br from the snow pack, HBr is scavenged onto the airborne aerosol or ubiquitous ice crystals as well as the snow pack. At this point we assume that the heterogeneous recycling continues on the airborne aerosol or ice crystals. In this manner the effect of the Br catalytic cycle may be rapidly felt throughout the PBL as high as ~ 2 km [*Solberg et al.*, 1996]. Additionally, after the O_3 has depleted, BrO diminishes and HOBr and $BrONO_2$ are no longer available to liberate Br^- from the aerosol. Thus, substantial amounts of Br^- remain on the airborne aerosol or ice crystals and we assume that this is what was measured in the O_3 free air mass. *Bottenheim et al.* [1990] reported that it is the particulate Br instead of inorganic gaseous Br (i.e., HBr) that is anticorrelated with O_3. Furthermore, this could possibly explain the frequently observed spring time enrichment of Br in atmospheric particulate in the Arctic [e.g., *Berg et al.*, 1983].

In our simulation, we find that soon after the depletion of O_3, the small level of NO_x (~ 20 pptv) slowly regenerates O_3. Although the of amounts O_3 involved are small (~ 2 ppbv, ~ JD 100), they are sufficient to form BrO from the Br atoms generated from the photodissociation of $CHBr_3$. This leads to the reformation of HOBr and $BrONO_2$ and so to the re-activation of autocatalytic release of Br. Thus, as long as sufficient Br^- and a Br seed is available, O_3 is continuously suppressed. This can possibly explain the low level of O_3 that last as long as 8 days over the Lincoln sea [*Shepson et al.*, 1996].

Our sensitivity studies show that the efficiency of the recycling scheme of *Fan and Jacob* [1992] is somewhat sensitive to the values of the rates adopted. We found that as total Cl in our model is increased to 30 pptv, the HO_2 generated by photo-dissociation of HCHO leads to an increase in the uptake of HOBr(g) which exceed that of HBr. When this occurs, Br in the model starts to accumulate as HOBr(aq) resulting in the depletion of Br^- in the aerosol. The recycling mechanism of *Fan and Jacob* [1992] requires the presence of both Br^- and HOBr(aq). With all the Br in the aerosol as HOBr(aq), a premature termination of Br recycling occurs prior to a complete destruction of O_3. A similar situation occurs when total Br in our model is decreased to 90 pptv. In this case, with less Br in the model lower levels of HBr result and its uptake is unable to compete with that of HOBr to sustain the Br^- required for recycling. However, we do find that this problem can be ameliorated if the suggested time constant for HOBr → HOBr(aq) is increased to 2×10^4 s. With a slower scavenging rate the range of situations where Br in the aerosol accumulates as HOBr(aq) is reduced.

Acknowledgments. J. C. McConnell wishes to thank the Natural Sciences and Engineering Research Council of Canada and the Atmospheric Environment Service of Canada for continuing support. We wish to thank all our colleagues in the Polar Sunrise Experiment (PSE) in particular P.B. Shepson, M. Mozurkewich, L.A. Barrie, J.W. Bottenheim, S.M. Li, J.F. Hopper, R. Sander, G. Impey, and P. Ariya for useful discussions. We mourn the recent loss of our York colleague Hiromi Niki who played an important role in the PSE..

References

Barrie L.A., J.W. Bottenheim, R.C. Schnell, P.J. Crutzen, and R.A. Rasmussen, Ozone Destruction and Photochemical Reactions at Polar Sunrise in the Lower Arctic Atmosphere, *Nature, 334*, 138–141, 1988.

Berg, W.W., P.D. Sperry, K.A. Rahn, and E.S. Gladney, Atmospheric Bromine in the Arctic, *J. Geophys. Res., 88*, 6719–6736, 1983.

Bottenheim J.W., et al., Depletion of Lower Tropospheric Ozone During Arctic Spring: The PSE 1988, *J. Geophys. Res., 95*, 18,555–18,568, 1990.

DeMore, W. B., et al. Chemical Kinetics and Photochemical Data for Use in Stratospheric Modelling, Evaluation Number 11, *Jet Propulsion Laboratory Publication*, 94–26, 1994.

de Serves, C., Gas Phase Formaldehyde and Peroxide Measurements in the Arctic Atmosphere, *J. Geophys. Res., 99*, 25,391–25,398, 1994.

Fan, S. M. and D. J. Jacob, Surface Ozone Depletion in Arctic Spring Sustained by Bromine Reactions on Aerosols, *Nature, 359*, 522–524, 1992.

Finlayson-Pitts, B.J., F.E. Livingston, and H.N. Berko, Ozone Destruction and Bromine Photochemistry at Ground Level in the Arctic Spring, *Nature, 343*, 622–624, 1990.

Hausmann, M. and U. Platt, Spectroscopic Measurement of Bromine Oxide and Ozone in the High Arctic During Arctic During Polar Sunrise Experiment 1992, *J. Geophys. Res., 99*, 25,399–25,413, 1994.

Jobson, B.T., et al., Measurements of C_2-C_6 Hydrocarbons During the Polar Sunrise 1992 Experiment: Evidence for Cl Atom and Br Atom Chemistry, *J. Geophys. Res., 99*, 25,355–25,368, 1994.

Jaffe, D., The Relationship Between Anthropogenic Nitrogen Oxides and Ozone Trends in the Arctic Troposphere, in *Tropospheric Chemistry of Ozone in Polar Regions*, eds. H. Niki and K.H. Becker, *NATO ASI Series I*, Global Environmental Change, vol.7, pp 105–115, Springer-Verlag, NY, 1993.

Li S.M., Equilibrium of Particle Nitrite with Gas Phase HONO: Tropospheric Measurements in the High Arctic During Polar Sunrise, *J. Geophys. Res., 99*, 25,479–25,488, 1994.

McConnell, J.C., and G.S. Henderson, Ozone Depletion During Polar Sunrise, in *Tropospheric Chemistry of Ozone in Polar Regions*, eds. H. Niki and K.H. Becker, *NATO ASI Series I*, Global Environmental Change, vol.7, pp 89–103, Springer-Verlag, NY, 1993.

McConnell, J.C., et al., Photochemical Bromine Production Implicated in Arctic Boundary-Layer Ozone Depletion. *Nature, 355*, 150–152, 1992.

Mozurkewich M., Mechanisms for the Release of Halogens From Sea-Salt Particles by Free Radical Reactions. *J. Geophys. Res., 100*, 14,199–14,207, 1995.

Mulvaney, R., G.F.J. Coulson and H.F.J. Corr, The Fractionation of Sea Salt and Acid During Transport Across an Antarctic Ice Shelf, *Tellus, 45B*, 179–187, 1993.

Shepson, P.B., et al., Carbonyl Compound Measurements in the Arctic Ocean Boundary Layer, *manuscript submitted to J. Geophys. Res.*, 1996.

Solberg, S., N. Schmidbauer, A. Semb, and F. Stordal, Boundary-Layer Ozone Depletion as Seen in the Norwegian Arctic in Spring, *J. Atmos. Chem., 23*, 301–332, 1996.

Waddington, E.D., J. Cunningham, and S.L. Harder, The Effects of Snow Ventilation on Chemical Concentrations, in *Processes of Chemical Exchange Between the Atmosphere and Polar Snow*, eds. Wolff E.W. and R.C. Bales, *NATO ASI Series I*, Springer-Verlag, Berlin, 1996 (in press).

J.C. McConnell, Dept. of Earth & Atmos. Sci., York Univ., (jack@nimbus.yorku.ca)

T. Tang, Dept. of Phys. and Astron., York Univ., N.York, Ont., Canada. M3J-1P3 (apollo@nimbus.yorku.ca)

(received November 20, 1995; revised June 13, 1996; accepted June 17, 1996.)

Appendix E
Publication 1996b

Tang, T., and J.C. McConnell, On the Relative Roles of Bromine and Chlorine During Spring Time Depletion of Ozone in the Arctic Boundary Layer. in *Atmospsheric Ozone, Proceedings of the XVIII Quadrennial Ozone Symposium, L'Aquila, Italy* , eds. Bojkov, R.D. & G., Visconti, *Int.*

On the Relative Roles of Bromine and Chlorine During Spring Time Depletion of Ozone in the Arctic Boundary Layer

T. Tang[1] and J. C. McConnell[1,2]

Abstract.
We present results of a box model simulation of O_3 destruction, with bromine and chlorine chemistry, in the springtime Arctic planetary boundary layer. To sustain the gas phase mixing ratios of active bromine and chlorine species heterogeneous reactions, both measured and empirical, are used to recycle the halogens which would otherwise terminate in unreactive species. In the model we use estimates of the O_3 loss time constant ($\sim$ days) and the observations of *Jobson et al.* [1994] as constraints on gas phase halogen abundances. We find that the main O_3 loss is due to BrO self reaction with the BrO + ClO reaction accounting for $\leq$ 25%. Our model results are in general agreement with the diagnostic study of *Le Bras and Platt* [1995]. If the time constant for O_3 decay is as rapid as a day, we conclude that bromine species are most likely active only during the depletion period and shortly thereafter, while Cl is more likely to be active for a longer period of 4-5 days after O_3 has been destroyed.

Introduction

Spring time depletion of O_3 in Arctic boundary layer has gained a considerable amount of attention since it was first reported by *Barrie et al.* [1988]. Since then, a significant body of research results have been established [e.g., *Niki and Becker*, 1993; *PSE*, 1994]. It now seems likely that the bromine catalytic cycle

$$\begin{aligned} BrO + BrO &\rightarrow 2Br + O_2 \quad k_{1a}\ 2.6 \times 10^{-12} \\ Br + O_3 &\rightarrow BrO + O_2 \quad k_2\ 6.5 \times 10^{-13} \end{aligned}$$

is the cause of depletion as originally suggested by *Barrie et al.* [1988]. A number of research results support this view: the spectroscopic detection of BrO [*Hausmann and Platt*, 1994]; the measured decay of bromine sensitive hydrocarbons [e.g., *Jobson et al.*, 1994]; detection of photolyzable bromine by *Impey and Shepson* [private communication, 1996]; and modeling studies (eg., *McConnell et al.* [1992], *Fan and Jacob*, [1992]). Furthermore, signatures of chlorine activity have been observed associated with the O_3 depleted airmass, [*Kieser et al.*, 1993; *McConnell and Henderson*, 1993; *Jobson et al.*, 1994]. The latter authors were able to estimate the time integrated chlorine density (i.e., $\int$[Cl]dt) from (apparent) alkane decay in air masses associated with reduced O_3 amounts, and concluded that O_3 destruction by Cl would only contribute $\sim$ 6% to the loss budget.

It seems likely that the gas phase presence of active BrO_x and ClO_x is maintained by heterogeneous recycling although the origin of the halogens is still an unresolved puzzle. *Tang and McConnell* [1996] have suggested that the halogens are inorganic in origin with sea salt on the snowpack as the most likely source. They also modelled autocatalytic release which they considered occurred both via the snowpack and sulphate aerosols and ice crystals.

Most of the discussion to date has focussed on gas phase destruction: nevertheless, heterogeneous destruction remains a possibility. Although O_3 loss to clean surface snow is slow, as evidenced both by laboratory measurements and the stability of measured surface O_3 mixing ratios during the dark winter months, there still remains the possibility that O_3 may be destroyed heterogeneously via the snow pack and/or aerosol in the presence of light, much as is observed in the experiments of *Behnke and Zetzsch* [1988]; with the deposition of many species transported from northern Europe and Siberia during the winter months the snow is far from being pristine.

Le Bras and Platt [1995] pointed out that the synergistic reaction between ClO and BrO that is important in the stratosphere

$$\begin{aligned} ClO + BrO &\rightarrow Br + Cl + O_2 \quad k_{3a}\ 7.0 \times 10^{-12} \\ ClO + BrO &\rightarrow BrCl + O_2. \quad k_{3b}\ 1.2 \times 10^{-12} \end{aligned}$$

could also be important in the Arctic boundary layer at polar sunrise. Because of the high levels of BrO, these reactions increase the rate of ClO to Cl conversion which results in an increased importance for the ClO_x catalytic destruction of O_3 over that deduced from integrated Cl atom amounts [*Jobson et al.*, 1994]. *Le Bras and Platt* [1995] estimated that interaction of BrO and ClO could be responsible for about 10% of the O_3 destruction. The O_3 continuity equation, for no transport, may be written approximately as

$$\frac{d[O_3]}{dt} = -2\left((k_{1a} + k_{1b})[BrO]^2 + (k_{3a} + k_{3b})[BrO][ClO]\right)$$

where $k_{1b} = 7.0 \times 10^{-13}$ is the BrO self reaction channel which forms Br_2.

In this paper we present a continuation of the modelling study of *Tang and McConnell* [1996] which focused on the autocatalytic release of Br^- from the snowpack. Here we present results from a self-consistent

[1]Dept. of Phys. & Astron., York Univ., Ont., Canada

[2]Dept. of Earth & Atmos. Sci., York Univ., Ont., Canada

modelling study of the synergism between BrO_x and ClO_x, using the analysis of *Le Bras and Platt* [1995], that focuses on their relative contribution to O_3 loss. We also draw attention to the different time constants with the context of the polar sunrise O_3 loss that are often assumed to be the same. First and foremost is the time constant for O_3 depletion, τ_{O_3}. There are also the time constants associated with the periods during which active Br and Cl remain elevated, τ_{BrO_x} and τ_{ClO_x}, respectively.

Model Description

The model used in this study is similar to that used in *Tang and McConnell* [1996] with standard gas phase chemistry of methane, bromine, and chlorine [*DeMore et al.*, 1992]. The model is initialized with O_3 40 ppbv, NO 20 pptv, NO_2 30 pptv, CO 150 ppbv, CH_4 1.7 ppmv, HCHO 50 pptv and 100 pptv of bromine, Br_x. We have run various scenarios by varying the total chlorine mixing ratio, Cl_x from 10 pptv to 50 pptv. The heterogeneous bromine recycling mechanism is included in the form suggested by *Fan and Jacob* [1992] but the time constant for HOBr → HOBr(aq) is increased to 2×10^4 s in order to perform our simulation at higher Cl_x (see *Tang and McConnell*, [1996]). Gaseous odd-nitrogen that is lost to HNO_3 via *Fan and Jacob's* [1992] bromine recycling mechanism is replenished via $HNO_3(aq) \rightarrow HONO(g)$. To sustain the gaseous Cl atom mixing ratios in the model, HCl is recycled to Cl_2 via the aerosol. Some of the heterogeneous reactions are rather ad-hoc. However, they do allow us to maintain halogen densities in the gas phase at necessary levels. The alternative is to postulate large sources and sinks of halogens from the surface. We prefer the former approach. The temperature used for the evaluation of the rate constants is 245 K. The model simulates the evolution of a surface air parcel, starting at midnight Julian day (JD) 90 until the end of JD 105. At midnight JD 93, 3.5 pptv of $CHBr_3$ is introduced into the air parcel to prime the autocatalytic release of Br^- from sea-salt particles accumulated in the snow pack.

The process of autocatalytic release of Br^- from the snow pack is described in detail in the study of *Tang and McConnell* [1996]. The process can be summarized as: $CHBr_3$ slowly photolyzes to give Br atoms which react with O_3 to form BrO; the BrO, in turn, reacts with either HO_2 or NO_2 forming HOBr or $BrONO_2$ respectively both of which can be scavenged onto the Br^- rich snow pack to become a HOBr(aq); finally, reaction between a HOBr(aq) and a Br^- results in the formation of Br_2(aq) which volatilizes and is then photolyzed to give *two* bromine atoms thus initiating chain reaction.

Results and Discussion

The simulated mixing ratios of O_3 for various Cl_x mixing ratios are shown in Figure 1a. The O_3 mixing ratios of *Tang and McConnell* [1996] are also included in the Figure (indicated with *T&M*). It can be seen that time scale of the fastest O_3 depletion in the current study is ~ 0.5 day longer than that of *Tang and McConnell* [1996] for the same Cl_x amount. This occurs as a result of the lengthening of the HOBr(aq) scavenging time constant as noted above.

One might expect that the O_3 decay rate would increase with increasing Cl_x, i.e., τ_{O_3} would decrease. However, Figure 1a shows that τ_{O_3} increases with increasing Cl_x. A contributing factor is that ClO in the model can form $ClONO_2$ which acts as a sink for NO_x. With the NO_x reduced, the rate of formation of $BrONO_2$ decreases which reduces its availability for the autocatalytic release of bromine. For example, with $Cl_x = 50$ pptv, $ClONO_2$ can store up to ~ 80% of the

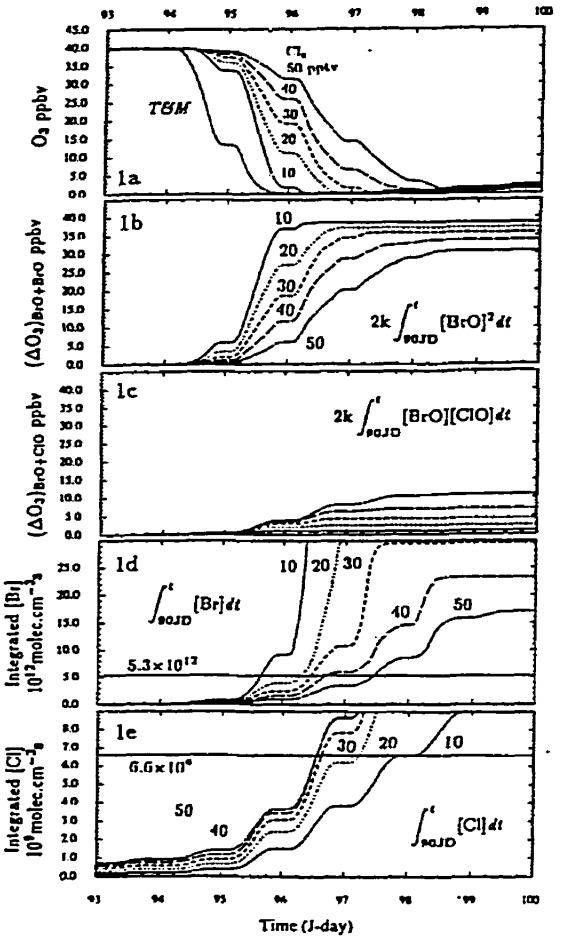

Figure 1. (a) Ozone mixing ratio versus time. (b) The integrated O_3 loss due to BrO self reaction catalytic cycle. (c) The integrated O_3 loss due to the BrO + ClO synergistic catalytic cycle. (d) Time integrated Br densities within the model. (e) Time integrated Cl atom densities within the model. Each panel shows results for 5 levels of Cl_x, 10, 20, 30, 40 and 50 pptv. Panels (d) and (e) also show estimates of the appropriate time integrated halogen densities from Jobson et al. [1994].

available NO_x in the model while for $Cl_x = 10$ pptv only $\sim 20\%$ is tied up. In the model $ClONO_2$ is photolyzed to give Cl and NO_3 with a time constant ~ 1 day. If the NO_x tied up in $ClONO_2$ in the model can be released at faster rate (as in the stratosphere) then the efficiency of Br-release from the snowpack in our model would likely be less effected by the presence of Cl.

Figure 1b shows the amount of O_3 destroyed due to k_1

$$\Delta[O_3]_{BRO+BRO} = 2k_1 \int_{90JD}^{t} [BrO]^2 dt.$$

while Figure 1c shows the amount of O_3 destroyed due to BrO-ClO interaction:

$$\Delta[O_3]_{BrO+ClO} = 2k_3 \int_{90JD}^{t} [BrO][ClO] dt.$$

On each curve, for different Cl_x, a label is placed to denote the time at which O_3 is reduced to ~ 1 ppbv. Figure 2 also shows the time series of both contributions to O_3 loss for $Cl_x = 10$ pptv and 50pptv. With 10 pptv of Cl_x, the BrO self reaction destroys ~ 39 ppbv of O_3 while interaction between BrO and ClO only destroys ~ 1 ppbv of O_3 ($\sim 2\%$). For the highest Cl_x case, 50 pptv, the BrO cycle destroys ~ 31 ppbv of O_3 and interaction between BrO and ClO destroys ~ 11 ppbv ($\sim 25\%$). For our highest Cl_x simulation, 2 ppbv of O_3 more than the initial conditions is destroyed. This 'extra' O_3 is produced from the standard NO_x chemistry.

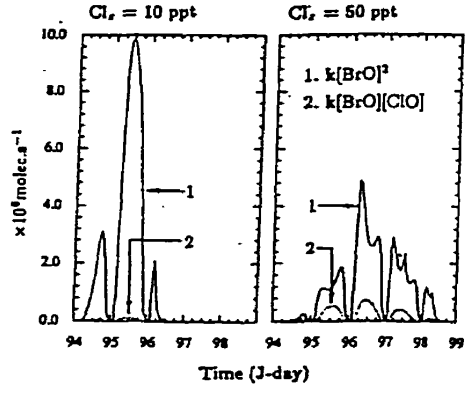

Figure 2. Time series of ozone loss due to (i) the BrO self reaction and (ii) BrO + ClO synergistic catalytic cycles for (a) 10 pptv Cl_x and (b) 50 pptv Cl_x.

Time integrated Br and Cl densities, $\int_{90JD}^{t}[Br]dt$, and $\int_{90JD}^{t}[Cl]dt$, for various Cl_x simulations are plotted in Figure 1d and 1e respectively. The Figures also include the time integrated Br and Cl estimates of *Jobson et al.* [1994] based on the observed hydrocarbon decay during the O_3 depletion episode of April 17-19, 1992. This represents $\int_{t_a}^{t_a+\tau_{Cl}}[Cl]dt = 6.6 \times 10^9$ molecules $cm^{-3}s$ and $\int_{t_b}^{t_b+\tau_{Br}}[Br]dt = 5.3 \times 10^{12}$ molecules $cm^{-3}s$. The time τ_{Cl} is associated with the decay of alkanes, and τ_{Br} is associated with the decay of C_2H_2. Most work has assumed that these time constants, τ_{Cl} and τ_{Br}, and the initial times t_a and t_b, are identical. However, it should be clear from the plots that this may not necessarily so: integrated Cl and Br amounts do not reveal whether or not Cl and Br were active simultaneously or if they were even active in the same location over the Arctic snowpack.

From Figure 1d, it can be seen that the values of $\int[Br]dt$ corresponding to O_3 decreasing to 1 ppbv range from 15×10^{12} to 20×10^{12} molecules $cm^{-3}s^{-1}$. Our simulated values are 3 to 4 times higher than that estimated by *Jobson et al.* [1994]. *Tang and McConnell* [1996] and *Hausmann and Platt* [1994] point out that during the process of O_3 depletion, the Br atom number density is low, suppressed by reaction k_2. However, as O_3 decreases, the impact of k_2 decreases and atomic Br densities increase, to be constrained by loss with HCHO and HO_2. The mixing ratios of Br and O_3, for the case $Cl_x = 20$ pptv, are plotted in Figure 3. It can be seen that, towards the end of O_3 depletion, the Br mixing ratio increases rapidly and then spikes as ozone disappears. A substantial amount of $\int[Br]dt$ calculated in this study includes this spike after the complete destruction of O_3. It would appear that the model actually overestimates the abundance of Br atoms during this period as compared to the measurements. Since our simulation of HCHO (not shown) as compared to measurements (c.f. *Tang and McConnell* [1996]) is also low this could be (partially) ameliorated with a more complete simulation that includes aldehydes.

Figure 3 also shows that as O_3 decreases atomic Cl mixing ratios increase, since O_3 represents the main loss. However, as compared to Br, the increase is not as striking since Cl + CH_4 provides a relatively constant and strong sink for Cl. This latter reaction can produce HCHO which, as noted above, can act as a sink for Br atoms producing HBr which returns to aerosol or ice pack. After the disappearance of O_3 there will be no further recycling since, without O_3 to produce BrO, the recycling mechanism of *Fan and Jacob* [1992] can not release Br from aerosol and ice pack. Thus, the simulated value of $\int[Br]dt$ can be regulated by the amount of Cl_x. This is demonstrated in Figure 1d which shows that the value at which $\int[Br]dt$ plateaus becomes lower as Cl_x is increased. This levelling off corresponds to when all the atmospheric Br is returned to aerosol or ice pack.

If the situation described above can occur in the real atmosphere, then the observed decay of C_2H_2 will be due to the rise of Br atoms toward the end of O_3 depletion. However, this suggests that τ_{Br}, associated with high Br levels and C_2H_2 decay, will not be the same as τ_{O_3} or τ_{BrO_x}. Similarly, τ_{Cl} and so Cl atom densities, associated with alkane decay will be representative of the post-O_3 period. In terms of the period of BrO_x activity, it would appear to be better represented by $\tau_{BrO_x} \approx \tau_{O_3} + \tau_{Br}$.

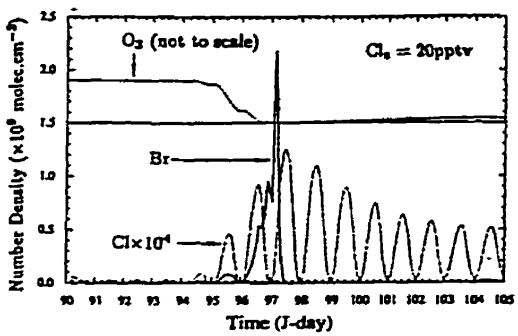

Figure 3. Bromine and Chlorine atom densities with time for the 20 pptv of Cl_x. Also shown is the O_3 time series for this case.

Thus within the context of this model simulation we find that if ozone decays with a time constant $\sim$ 1 day then we need a process to suppress Br atoms and this could be higher levels of HCHO and RCHO in the model. Simultaneously, in order to obtain the integrated Cl densities inferred from the measurements τ_{Cl} $\sim$ 4-5 days after the disappearance of O_3. In fact, the presence of O_3 ensures that Cl atom densities will be low and that any alkane decay is most likely to take place after O_3 has been destroyed. On the other hand if a slower decay of O_3 is indicated as for the case Cl_x = 50 pptv, then our time integrated Br amounts are within the experimental error. However, our time integrated Cl amounts are probably too large and we would require a mechanism to shut off the Cl much earlier during the depletion episode. Clearly, our understanding of the details of the O_3 depletion are still far from resolution but we hope that this study may highlight some of the issues.

Acknowledgments. JMcC would like to thank the Natural Sciences and Engineering Research Council of Canada and the Atmospheric Environment Service of Canada for support.

References

Barrie L.A., J.W. Bottenheim, R.C. Schnell, P.J. Crutzen, and R.A. Rasmussen, Ozone Destruction and Photochemical Reactions at Polar Sunrise in the Lower Arctic Atmosphere, *Nature, 334*, 138–141, 1988.

Behnke W. and C. Zetzsch, Smog Chamber Investigations of The Influence of NaCl Aerosol On the Concentration of O_3 in a Photosmog System, *Proc. Int. Ozone Sympos.* eds. by Bojkov, R., and Fabian. P., *Deepack, Hampton*, 519–523, 1988.

DeMore, W. B., et al. Chemical Kinetics and Photochemical Data for Use in Stratospheric Modelling, Evaluation Number 10, *Jet Propulsion Laboratory Publication*, 92–20, 1992.

de Serves, C., Gas Phase Formaldehyde and Peroxide Measurements in the Arctic Atmosphere, *J. Geophys. Res., 99*, 25,391–25,398, 1994.

Fan, S. M. and D. J. Jacob, Surface Ozone Depletion in Arctic Spring Sustained by Bromine Reactions on Aerosols, *Nature, 359*, 522–524, 1992.

Hausmann, M. and U. Platt, Spectroscopic Measurement of Bromine Oxide and Ozone in the High Arctic During Arctic During Polar Sunrise Experiment 1992, *J. Geophys. Res., 99*, 25,399–25,413, 1994.

Jobson, B.T., et al., Measurements of C_2-C_6 Hydrocarbons During the Polar Sunrise 1992 Experiment: Evidence for Cl Atom and Br Atom Chemistry, *J. Geophys. Res., 99*, 25,355–25,368, 1994.

Kieser, B.N., J.W. Bottenheim, T. Sideris and H. Niki, Spring 1989 Observations of Lower Tropospheric Chemistry in the Canadian High Arctic, *Atmos. Environ., 27A* 2979–2988, 1993.

Le Bras G. and U. Platt, A Possible Mechanism for Combined Chlorine and Bromine Catalyzed Destruction of Tropospheric Ozone in the Arctic, *Geophys. Res. Lett., 22*, 599–602, 1995.

McConnell, J.C., and G.S. Henderson, Ozone Depletion During Polar Sunrise, in *Tropospheric Chemistry of Ozone in Polar Regions*, eds. H. Niki and K.H. Becker, *NATO ASI Series I*, Global Environmental Change, vol.7, pp 89–103, Springer-Verlag, NY, 1993.

McConnell, J.C., et al., Photochemical Bromine Production Implicated in Arctic Boundary-Layer Ozone Depletion, *Nature, 355*, 150–152, 1992.

Niki, H. and K.H. Becker, Eds, *Tropospheric Chemistry of Ozone in Polar Regions, NATO ASI Series I*, Global Environmental Change, vol.7, Springer-Verlag, NY, 1993.

PSE, *Polar Sunrise Experiment (PSE 1992) J. Geophys. Res., 99*, 1994.

Shepson, P.B., et al., Sources and sinks of carbonyl compounds in the Arctic Ocean Boundary Layer, *J. Geophys. Res., 101*, 21,081–21,089, 1996.

Tang, T. and J.C. McConnell, Autocatalytic Release of Bromine from Arctic Snow Pack During Polar Sunrise, *Geophys. Res. Lett., 23*, 2622–2636, 1996.

J.C. McConnell, Dept. of Earth & Atmos. Sci., York Univ., (jack@nimbus.yorku.ca)

T. Tang, Dept. of Phys. and Astron., York Univ., N.York, Ont., Canada. M3J-1P3 (apollo@nimbus.yorku.ca)